CATALYTIC PYROLYSIS OF POLYOLEFINS

A Thesis
Presented to
The Academic Faculty

by

Ifedinma Ofoma

In Partial Fulfillment
of the Requirements for the Degree
Masters of Science in Chemical & Biomolecular Engineering

May 2006

CATALYTIC PYROLYSIS OF POLYOLEFINS

Approved by:

Dr. John Muzzy, Advisor
School of Chemical & Bimolecular Engineering
Georgia Institute of Technology

Dr. Christopher Jones
School of Chemical & Bimolecular Engineering
Georgia Institute of Technology

Dr. Matthew Realff
School of Chemical & Bimolecular Engineering
Georgia Institute of Technology

Date Approved: 11th of January, 2006

ACKNOWLEDGEMENTS

I wish to express my appreciation to my advisor, Dr. John Muzzy for his guidance and assistance during my studies and research endeavor at Georgia Tech. Thank you for your patience and understanding. I must also acknowledge my committee members, Dr. Christopher Jones and Dr. Matthew Realff for their patience, valuable contributions and resources towards my thesis project.

I am also very grateful to Latoya Bryson for assisting me along the way through my time here. Many people assisted me in the various experimental procedures; to them I offer my deepest appreciation: Dr. Beckham's group for their assistance with the thermogravimetry (TG) equipment, especially Chris Hubbell for training me in TG analysis. I would also like to thank John Richardson for assisting me in my catalyst characterization and synthesis.

TABLE OF CONTENTS

LIST OF TABLES

LIST OF FIGURES

SUMMARY

The pyrolysis of Polypropylene (PP), Polyethylene (PE) and PP-Post consumer Carpet (PP-PCC) by various Fluid Catalytic Cracking (FCC) catalysts was studied by thermogravimetry (TG). All the FCC catalysts enhanced the pyrolysis of PP and PE. The reaction rates increased with catalyst fraction and a reduction in the catalyst particle size. On the other hand, the FCC catalysts performed poorly in the degradation of PP-PCC at 92 and 97 wt % of PP-PCC. This may be attributed to the waste composition of the PP-PCC. However, the pyrolysis of the waste PP was achieved at much lower temperatures than the virgin PP. In general, the fresh catalyst (fines) was found to be the most effective in both the polyolefin and PP-PCC pyrolysis.

Furthermore, the rate law parameters, E_a and A, for the pyrolysis reaction were estimated by conventional dynamic TG analysis. Despite the complex nature of polyolefin degradation, a single degradation step involving the solid polymer and the gaseous products was assumed. Although, there are many limitations and assumptions associated with conventional dynamic TG analysis, the derived rate equations for the different catalyzed reactions were used in developing a model for the catalytic pyrolysis of PP in an extruder. Based on the reactor model, basic processing costs were estimated for the catalytic pyrolysis of PP using various FCC catalysts at two screw speeds, 250RPM and 500 RPM. The lowest costs achieved were less than $1 per pound of product with the catalyst.

CHAPTER 1

INTRODUCTION

Due to population increase, the demand for plastic products has steadily increased over the last 40 years. Since plastics are non-biodegradable, they cannot be easily returned to the natural carbon cycle; hence the life cycle of plastic materials ends at waste disposal facilities. In 2003, the Environmental Protection Agency (EPA) reported that plastics constituted a large part of the municipal solid waste (MSW) generated in the US (26.7 million tons or 11.1% of the MSW stream) [1].

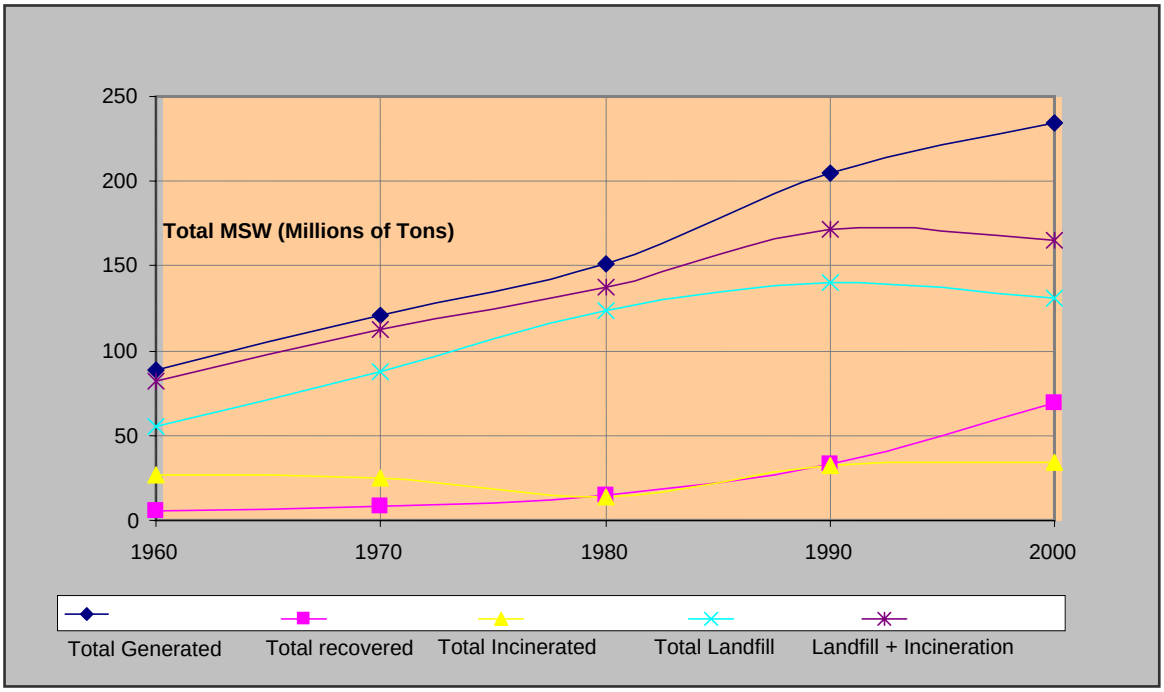

Figure 1.1 Municipal Solid Waste Generation, Recycling, and Disposal in the United States [1]

The current and common MSW management methods used are incineration and landfilling. Figure 1.1 shows the trends for MSW generation and disposal over the last 40 years. Both methods pose negative environmental impact. Although, there are incineration methods in which energy is recovered, incinerators generally produce greenhouse gases which are postulated as sources of global warming [2, 3]. Similarly, landfilling poses the threat of methane emissions [4]. In light of these hazards, the EPA has improved federal regulations for landfilling by normalizing the use of liners in the landfill bed, ground water testing for waste leaks, and post landfill closure care; however, since waste plastics have a high volume to weight ratio, appropriate landfill space is becoming both scare and expensive [5].

Recycling and reuse of plastics has obvious benefits of decreasing the amount of waste plastics that end up in landfills; however, the overall recovery of plastics for recycling is relatively small. In 2003, only 1.4 million tons (3.9 percent of total plastics generated) of plastics were recovered for recycling [1]. The growing awareness in environmental concerns and the reducing landfill space have prompted research in alternative methods such as chemical recycling.

Chemical or feedstock recycling involves processes that convert plastic waste into petroleum feedstock, preferably gasoline range fuel. Although a viable option, this method can be costly. Contributing to the high costs is the fact that waste plastics are indeed mixtures of different materials having different compositions and thus requiring different processing conditions. Moreover, the chemical recycling (or cracking) of plastics has to be combined with other technologies, such as MSW collection, categorization and pretreatment at the upstream end, as well as various separations and product recovery processes on the downstream end. Another prevalent issue with this method is the high energy input required as some post

consumer plastic waste require temperatures as high as 700°C [6]. By using effective catalysts, these temperatures can be significantly reduced, thereby reducing costs. Nonetheless, the catalyst cost can in turn affect the process economy considerably. From an economic perspective, reducing the cost even further will make feedstock recycling an even more attractive option. This option can be optimized by:

- Reuse of catalysts (this is common for reactor design in industry)
- The use of effective catalysts in lesser quantities.

The first goal of this study is to investigate the catalytic decomposition of Polypropylene (PP), Polyethylene (PE) and post consumer carpet (PCC) using thermogravimetry (TG). FCC catalysts have shown great potential in the cracking of polyolefins; however, there is limited kinetic data on catalytic polyolefin pyrolysis using FCC catalysts in literature. Thus, kinetic parameters will be estimated by various methods described in literature for the TG decomposition of PP and PE. Furthermore, the catalytic effect of $CaCO_3$ in the decomposition of polypropylene-post consumer carpet (PP-PCC) will be studied by TG methods. $CaCO_3$ is used as filler in most tufted carpet and any catalytic potential of this carpet backing component may be useful in the recycling of PCC waste.

Next, based on the outcome of the catalysts' screening, kinetic data obtained by TG will be used in generating a reaction model for the cracking of PP in a twin screw, counter-rotating non-intermeshing (CRNI) extruder- reactor. Two key assumptions have been made in the process: (1) The extruder is modeled as a plug flow reactor and (2) the PP cracking products are assumed to be similar to those in literature. In addition to estimating PP conversion, the

model may be used as a cost estimation tool for the decomposition PP to gasoline range fuels using a twin screw CRNI extruder.

An additional goal is to explore the effect of certain processing parameters in the TG degradation of polyolefins. First, the catalyst particle size in the TG degradation of PP and Polyethylene (PE) will be studied. Two particle sizes ('regular' and 'fines') of an FCC catalyst will be investigated in PP and PE pyrolysis.

Furthermore, the mode of catalyst contact with the polymer will be investigated. Marcilla ***et. al.*** dealt with TG (catalytic pyrolysis) of polyolefin, where the polymer(s) and catalyst(s) are finely ground, mixed, and then directly analyzed with TG [3]. This method may not effectively disperse the catalyst(s) and polymer(s) uniformly. Inhomogeneous dispersion could lead to mass transfer limitations that are characteristic of heterogeneous catalysis. Therefore, to ensure that the catalyst(s) are uniformly dispersed within the polymer samples for effective degradation, an alternative mixing method is needed. This problem may be alleviated by mixing the catalyst in the polymer melt phase (melt mixing) prior to the decomposition reactions as is done in this work.

CHAPTER 2

LITERATURE REVIEW

Pyrolysis is generally defined as the controlled burning or heating of a material in the absence of oxygen [7]. In plastics pyrolysis, the macromolecular structures of polymers are broken down into smaller molecules or oligomers and sometimes monomeric units. Further degradation of these subsequent molecules depends on a number of different conditions including (and not limited to) temperature, residence time, and the presence of catalysts as will be discussed in this review.

2.1 Thermal Pyrolysis of Polyolefins

The non-catalytic or thermal pyrolysis of polyolefins is a high energy, endothermic process requiring temperatures of at least 350-500°C [8-10]. In some studies, temperatures as high as 700-900°C are essential in achieving decent product yields [6, 11, 12]. Thermal pyrolysis of both virgin and waste plastics as well as other hydro-carbonaceous sources has been studied extensively in the past. A good number of these thermal cracking studies are on PE [8, 13-27], polystyrene (PS) [10, 13-17], and PP [9, 14, 15, 18-32]. On the other hand, only a few have researched the thermal decomposition of other common plastics such as polyvinylchloride (PVC) ([33, 34]), polymethyl methacrylate [22], polyurethane [35], and polyethylene terephthalate [34].

2.1.1 The HC Cracking Mechanism

A thorough study on the mechanism for the thermal decomposition of polymers is presented by Cullis and Hirschler [36]. The four mechanisms proposed are:

(1) End-chain scission or unzipping: Cracking is targeted at chain ends first, and then successively works down the polymeric length. Unzipping results in the production of the monomer.

(2) Random-chain scission: Random fragmentization of polymer along polymer length. Results in both monomers and oligomers.

(3) Chain-stripping: Side chain reactions involving substituents on the polymer chain.

(4) Cross-linking: Two adjacent 'stripped' polymer chains can form a bond resulting in a higher MW species. An example is char formation.

The thermal pyrolysis of PP and PE is known to follow the random chain scission route, resulting in mainly oligomers and dimers [6]. This mechanism is illustrated for PE and PP in Figures 2.1 and 2.2, respectively. Peterson *et. al.* observed that PE decomposition by thermogravimetry yielded mainly 1-hexene and propene [37].

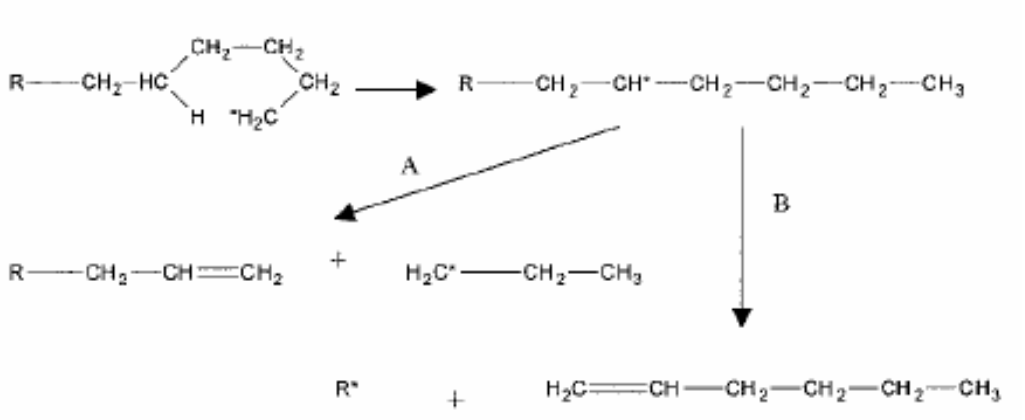

Figure 2.1 Random chain scission in polyethylene [37]

Similarly Peterson *et. al.* observed that in the thermal pyrolysis of PP, the main products were pentane, 2-methyl-1-pentene and 2,4 dimethyl1-heptene [37]. During degradation, methyl, primary and secondary alkyl radicals are formed, and by hydrogen abstractions and recombination of radical units, methane, olefins and monomers are produced [23].

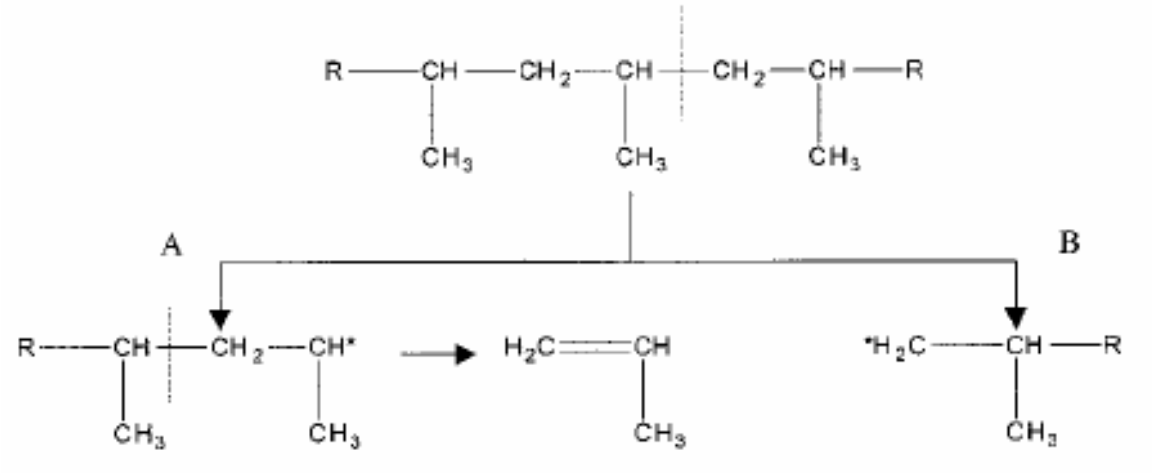

Figure 2.2 Random chain scission in polypropylene [37]

Whereas the pyrolysis of PP and PE is characterized by low monomer yields [2, 33, 38], PS is known to follow an end-chain mechanism or depolymerization steps resulting in mostly monomeric units as the main product, as illustrated in Figure 2.3.

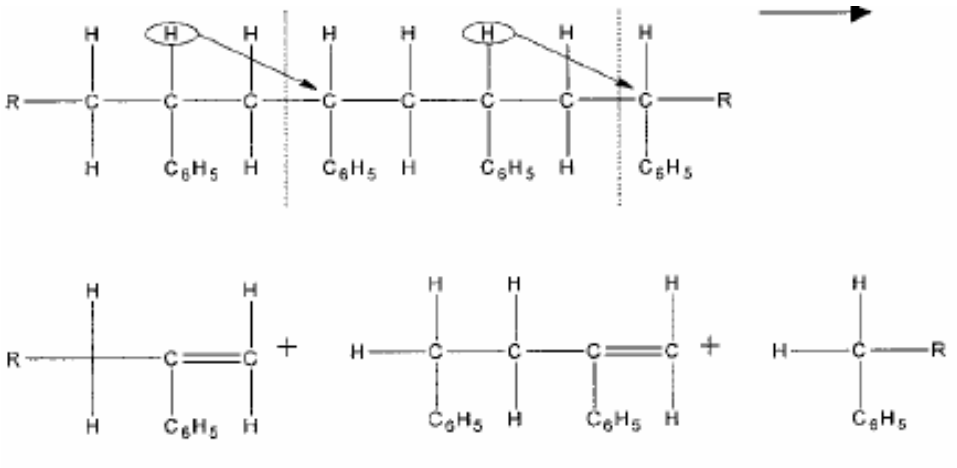

Figure 2.3 Unzipping mechanism in polystyrene [37]

The polyolefin samples are typically degraded in a closed reactor/melting vessel and heated to a reaction temperature at which the polymer decomposes. A reaction time is allowed and over time, the degradation products (gaseous, liquids and solid) are collected and analyzed.

Common methods for liquid products analyses include Infra–Red (IR), Mass Spectroscopy (MS) and gas chromatography (GC). Whereas gaseous products are analyzed typically by Nuclear Magnetic Resonance (NMR), Fourier Transform Infrared Spectroscopy (FTIR), and GC/MS. Solid residues are identified by gel permeation chromatography. Several couplings of the aforementioned analytical methods are available, including FTIR/MS and GC/MS.

2.1.2 Thermal Pyrolysis Product Yields

Liquid product yields greater than 82.5% and as high as 96% have been observed for PE thermal pyrolysis [26, 39]; however, these were obtained at high temperatures (greater than 420°C) and within a reaction time of approximately one hr. Invariably, the gaseous products obtained by thermal cracking are not suitable for use as fuel products, requiring further

refining to be upgraded to useable fuel products [40, 41]. Generally, thermal cracking results in liquids with low octane value and higher residue contents at moderate temperatures, thus making the process an inefficient process for producing gasoline range fuels [15, 29]. A few researchers have sought to improve thermal pyrolysis of waste polyolefins without employing the use of catalysts; however, these changes either yielded insignificant improvements or added another level of complexity and costs to the system [29, 42].

2.2 Catalytic Cracking of Polyolefins

Catalytic degradation of polymers has shown the greatest potential to be developed into a commercialized process. In comparison to the purely thermal pyrolysis, the addition of catalysts in polyolefin pyrolysis:

- Significantly lowers pyrolysis temperatures. A significant reduction in the degradation temperature and reaction time [43] under catalytic conditions results in an increase in the conversion rates for a wide range of polymers at much lower temperatures than with thermal pyrolysis [44-46]. This effect is illustrated in Figure 2.4.
- Narrows and provides better control over the hydrocarbon (HC) products distribution in LDPE [47, 48] , HDPE , PP[49, 50] and PS [51, 52] pyrolysis. While thermal pyrolysis results in a broad range of HCs ranging from C_5 to C_{28} [35], the selectivity of products in the gasoline range (C_5-C_{12}) are much more enhanced by the presence of catalysts [32, 45, 53].
- Increases the gaseous product yields. Under similar temperatures and reaction times, a much higher gaseous product yield is observed in the presence of a catalyst for PE [45, 54].

- Increases the product yield in the gasoline range whereas a purely thermal process will produce more light gas oils [55]. Zeolites in particular are known to enhance the formation of branched hydrocarbons and aromatics [56]. Oils obtained by catalytic pyrolysis contain less olefins and more aromatic content [43].

Table 2.1 summarizes the results obtained by Miskolczi *et. al.* for the batch pyrolysis of HDPE [57]. Results show that both yields and chemical compositions of the resulting products are changed by the catalytic effect. Obviously the extent of the catalytic effect will vary according to the catalysts' inherent properties.

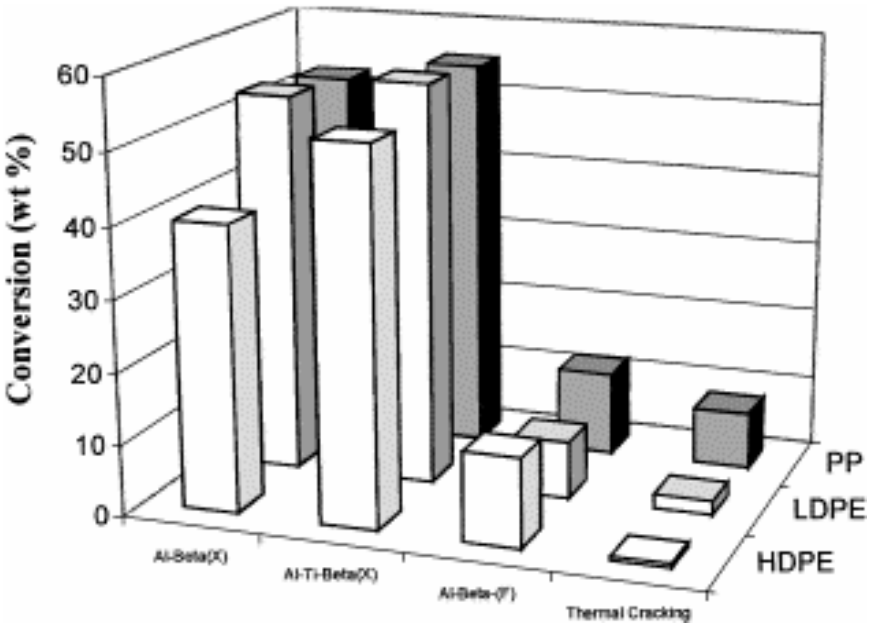

Figure 2.4 Conversion obtained in the thermal and catalytic cracking of HDPE, LDPE and PP (400°C, 0.5 h, plastic/catalyst=50 w/w). Catalysts are Al-Beta and Al-Ti-Beta zeolites [53]

Table 2.1 Thermal versus catalytic pyrolysis of HDPE in a Batch reactor for 1 hr [57]

	Non-Catalytic	*Catalytic*		
		NCM[a]	FCC[b]	HZSM5[c]
Temperature, °C	420	420	420	420
Gases, wt%	2.9	5.8	5.5	15.7
Liquid, wt%	11.5	28.2	30.4	28.9
Coke/residue, wt%	85.6	66	64.1	55.4

[a] A clinoptilolite
[b] Equilibrium fluid catalytic cracking catalyst
[c] Commercial H-formed ZSM-5 catalyst

Thus, the dramatic effect of catalyzed decomposition of polymers has spurred a wave of research in the area of catalysis and polymer degradation. The effect of both novel and traditional catalysts has been extensively investigated. In many of these studies, solid acid catalysts have been widely used and have shown much greater cracking activity over non-acidic catalysts [55]. Solid acids are particularly important in the petroleum industry where many reactions proceed via acid-catalysis e.g. paraffin isomerization, catalytic cracking, reforming and alkylation.

2.2.1 Catalytic cracking pathway

Reaction products are largely determined by carbenium ion chemistry (isomerisation, chain/beta-scission, H-transfer, oligomerisation/alkylation) which is influenced by acid-site strength, density and distribution [58]. The acid strength of solid acids is characterized by both Brønsted and Lewis acid sites; however, the presence of Brønsted acid sites have been observed to favor the cracking of olefinic compounds [43]. A study of the Brønsted and Lewis acid sites in polyolefin cracking has been reviewed by several authors [59-62]. Furthermore, in the case of crystalline solid acids, the majority of the acid sites are believed

to be located within the pores of the material, such as with zeolites [63]. Thus micro-porosity of porous solid acids is an important feature in assessing the level of polyolefin cracking over such catalysts.

Molecular sieves, such as silica alumina [15, 55, 64, 65], zeolites [66-69], and MCM-41 [70-72], are among the most commonly researched solid acids in plastic waste pyrolysis. Other catalytic materials such as clays have been scarcely investigated [73]. Generally, the level of the catalyst activity in polyolefin pyrolysis increases with increasing number of acid sites [43]. Thus it is common knowledge that zeolitic catalysts achieve higher conversion than non-zeolitic acid catalysts [38, 55, 56].

2.2.2 Zeolites in polyolefin pyrolysis

Zeolites are usually described as crystalline aluminosilicate sieves having open pores and ion exchange capabilities [58]. This characteristic makes them useful in common applications, such as water purification, and in catalysis of a wide spectrum of organic reactions with applicability in the petroleum industry [74]. More specifically, a zeolite consists of a rigid tetrahedral network of SiO_4, AlO_4^- or PO_4^+ frameworks [58]. Combinations of the latter two frameworks are found in most common zeolites, resulting in structures that stack in three dimensional shapes forming cavities of varying size and shape as shown in Figure 2.5. The resulting crystal structure and properties depend on the direct synthesis conditions, such as temperature, gel composition, templating agent and the presence of alkaline cations [75]. Cundy and Cox present a thorough review on the hydrothermal synthesis of zeolites [76].

Zeolites were introduced into the refinery about 40 years ago. These molecular sieves combine high acidity with shape selectivity, high surface area and high thermal stability to

catalyze a variety of hydrocarbon reactions including polyolefin cracking [77]. The reactivity and selectivity of zeolites as catalysts are determined by their high number density of active sites which are brought about by a charge imbalance between the silicon and aluminum atoms in the crystals, causing the zeolite to have an overall charge balance of negative one [58].

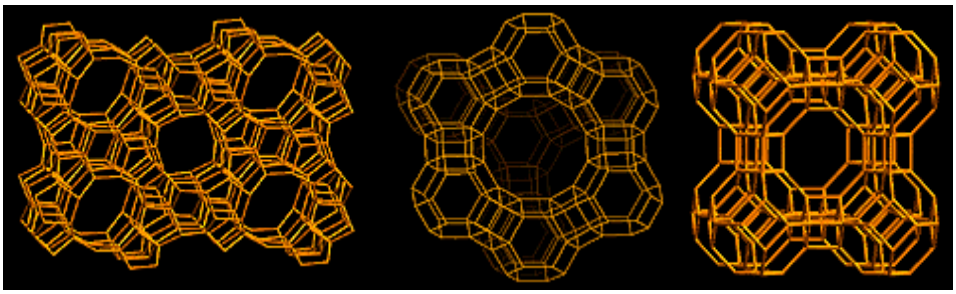

MFI (ZSM-5) FAU (Y-zeolite) LTA (Zeolite A)

Figure 2.5 Structures of some common zeolites used in polyolefin pyrolysis [78].

For this reason, they can catalyze many hydrogen transfer reactions. Moreover, because of their high thermal stability, zeolites can be regenerated by burning off the polymer on the surface and in the pores at very high temperatures. Thus, they are currently used as catalysts in the fluid catalytic cracking (FCC) processes of the petroleum industry [79]. A number of reviews on the different uses of zeolite catalysts in the petroleum refining industry are available in texts [80-84].

Aside from high acidity, the chemistry of zeolite catalyzed reactions is significantly influenced by their pore size, which is typically in the range of 4 - 13 angstroms. Small pore zeolite such as Zeolite A (~ 4 Å) have an 8 member oxygen ring and would typically allow small molecules such as olefins and alcohols to pass through. On the other hand, larger pore

zeolites such as zeolite-Y (~ 7.4 Å) and mordenite (~6.7 Å) will tend to allow larger molecules to pass through their pores (See Figure 2.5).

Therefore, reaction products are influenced by the shape selectivity of the zeolite catalyst [77, 85]. The shape selective mechanisms for diffusion in porous materials are known to fall under four major groups:

- Reactant state selectivity: Only sterically unhindered reactant molecules (reactants with smaller kinetic diameters) are permitted through the catalyst pores for further reaction.
- Product selectivity: Within the intrazeolitic pore system, the exit of certain products is sterically preferred over the other possibilities. A key example is the para-selectivity of HZSM-5 for the alkylation of toluene with ethylene [85].
- Transition state selectivity: The intrazeolitic pore system provides different steric hindrances for the various transition states. It is expected that the transition state with the least resistance will in effect go on to form the main product.
- Molecular traffic control: The pores are important in determining the kinetics of the reactions in zeolites; however, the diffusion of either products or reactants may be improved or hindered by the global zeolite cage system such as the dimensionality of the pore system (1-D, 2-D, 3-D).

The degradation of large olefinic molecules occurs over the surface of these catalysts, forming smaller molecules that can be permitted into the pores of the zeolites for further cracking and selectivity [86, 87]. Diffusion of these 'cracked' molecules within the zeolite is

greatly influenced by pore size constraints and depends on the pore and channel configurations (since the size of the inner channels and HC molecules are about the same). This type of diffusion is commonly referred to as 'configurational" diffusion. Diffusion in the Knudsen regime may also occur in some zeolites; however, it is believed that configurational diffusion dominates [88, 89].

Due to their effectiveness in the cracking of crude oil and petroleum derivatives, they have also been extensively cited in literature as effective catalysts in the study of catalytic polyolefin pyrolysis. Amongst the numerous kinds of zeolites investigated in polyolefin pyrolysis, (Beta [90], USY [91], ZSM-11 [72], REY [40, 92], Mordenite [69, 93]), ZSM-5 is the most commonly used. Conversely, with polystyrene, solid bases are observed to be the most effective [94].

2.2.3 ZSM-5 in Polyolefin Pyrolysis

In literature, ZSM-5 has performed better than most other zeolitic compounds and parent silica alumina catalysts in polyolefin pyrolysis studies [95, 96]. The high catalytic activity of ZSM-5 is attributed to its strong Brønsted acid sites which is closely related to the presence of Al in the framework (a higher concentration of Al denotes increased number of acid sites); hence, the activity of a zeolite sample may be enhanced by varying its gel composition [45]. Other properties of zeolites can also be enhanced by ion-exchange, as well as by molecule impregnation of reactive species into the zeolite framework [72, 97].

It is widely observed that zeolites favor the production of gaseous products and aromatic compounds in fuel feedstock recycling (See Tables A-1, A-2 and A-3 in Appendix A). The high yield of gaseous products could be attributed to the "over-cracking" nature of these

microporous solid acids [73]. Microporous zeolites such as ZSM-5 exhibit high gas yields with higher aromatics and napthenes whereas mesoporous solids such as silica alumina and MCM-41 show high liquid yields with high olefinic content [38]. This is because the diffusion of molecules larger than monomethyl aliphatics into micrporous ZSM-5 is restricted and the reaction of molecules with critical pore diameters greater than 6Å is severely diffusion limited [98]. On the other hand, because of the relatively small pore size of ZSM-5, the interaction between the catalytic surface of ZSM-5 and the reactants is larger resulting in a higher conversion of linear olefins and a higher production of low MW compounds such as ethane. In one study, medium pore zeolites, ZSM-5 and Mordenite, formed significantly more olefins whereas pyrolysis over large-pore zeolites, Y and Beta zeolites, yielded mainly alkanes with less alkene and aromatic content [68]. In addition, significantly more lighter hydrocarbons (C_3-C_6) were formed with ZSM-5 than with larger-pore zeolites such as zeolites-Y [68, 99].

Similar observations were made by Bagri *et. al.* who compared ZSM-5 and Y-zeolite in polystyrene pyrolysis [51]. They found that the former yielded higher gaseous products whereas Y- zeolites resulted in products having a higher aromatic content. A monomolecular and bimolecular cracking mechanism have been proposed to explain the wider product distribution by USY over ZSM-5 respectively [85, 100, 101]. The monomolecular mechanism is based on the assumption that the micropores of ZSM-5 are permissive to only mono-methyl compounds; hence, higher selectivity towards C_1-C_3 species.

In the pyrolysis study of HDPE, Manos *et. al.* observed that the use of US-Y zeolites gave products in the C_3 and C_{15} range [102]. It was also observed that isobutane and isopentane were the main gaseous products whereas the liquid fraction was rich in alkanes [68, 102].

Cardona *et. a*l. studied the catalytic pyrolysis of polypropylene over various US-Y catalysts having different pore sizes [103]. In this study, the selectivity to gases decreased with increasing pore size, unlike the total acidity of the catalysts that seemed unrelated to cracking activity [103]. As such, the pore size of the catalyst is key in controlling the diffusion of the cracked intermediates for the catalytic degradation of waste plastics. Based on these observations, a catalyst with bi-modal pore size distribution such as those found in fluid catalytic cracking (FCC) catalysts may be used to optimize the liquid product distribution [104].

2.2.4 FCC catalysts in Polyolefin Pyrolysis

FCC catalysts have been employed on an industrial scale in the petroleum refining industry and were developed mainly for cracking heavy oil fractions from crude petroleum into lighter and more desirable gasoline and liquid petroleum gas (LPG) fractions [79]. The feedstock products fall under four major classes of HCs: Paraffins, Olefins, Naphthalenes and Aromatics (PONA distribution). Gasoline range fuels consist of paraffin and olefins in the C_5-C_{12} range [41]. Within aromatics, products of polyolefins, especially polystyrene, are grouped as BTX (benzene, toluene, and xylene). Recent reviews on the FCC process can be found in literature [79, 105, 106].

2.2.4.1 The composition of an FCC catalyst

An FCC catalyst is composed of zeolitic crystals and a non-zeolitic acid matrix (commonly silica alumina and a binder) [74]. Zeolite-Y is still the primary component of FCC catalysts for over 40 years because of its high thermal stability and product selectivity [77]. The alumina matrix, clay and binder serve to provide both mechanical and thermal stability

needed for HC cracking in FCC - regeneration unit cycles [74]. FCC catalysts are commercially available in two forms: powder or pellets. FCC powders typically range in the lower microns whereas the fluidizable pellets are typically 60 μm diameter. Various preparation methods for FCCs as well as the interaction between matrix and zeolite on catalytic activity have been investigated [107, 108].

2.2.4.2 Performance of FCC catalysts in polyolefin pyrolysis

Compared to the other common solid acids, FCC catalysts have only been recently studied in the cracking of commodity plastics. Marcilla *et. al.* conducted a thermogravimetric study of PP and PE mixtures in which the FCC catalyst was the most effective over ZSM-5 and Y-zeolite [109]. Similarly, Miscolkzi *et. al.* observed that the yield of gaseous products increased in the order: thermal cracking < clinoptilolite < FCC < HZSM-5 catalyzed cracking, while the yields of liquid products increased in the order of thermal cracking < clinoptilolite < HZSM-5 < FCC catalyzed cracking for the cracking of HDPE [57].

It is generally observed that FCCs result in more gasoline range products than did ZSM-5 and Y-zeolite [57, 110]. In addition, the conversion of C_7^+ n-olefins and the production of ethene is higher in ZSM-5 than with FCCs [51, 100, 110]. This could be attributed to the smaller and thus restrictive micropores found in ZSM-5. On the other hand, the bimodal pore size distribution, and mild acidic properties of FCCs allow for the formation of more parrafins [104].

2.2.4.3 Equilibrium FCC Catalyst (E-CAT)

Equilibrium catalysts are 'used' FCC catalysts with different minute levels of metal contamination but still have value. These metals are typically vanadium, nickel, iron, sodium. Also entrapped in the catalyst pores, is coke (carbon). Before reuse, the spent catalyst typically undergoes a number of burn-offs in regeneration units at temperatures as high as 700°C [103]. This is done to remove some of the entrapped carbon, therefore diminishing ECAT's catalytic activity [111].

Despite their diminished activity, these catalysts are still significantly effective in polyolefin pyrolysis compared to other acid catalysts. De la Puente *et. al.* studied the catalytic pyrolysis of polystyrene over ZSM-5, Mordenite, sulfur promoted zirconia and an equilibrium FCC catalyst [112]. In their study, the spent FCC catalyst resulted in higher yields of desirable products such as ethylbenzene [112]. Lee *et. al.* observed that at 430°C and in a semi batch reactor, the pyrolysis of waste HDPE using an ECAT showed high cracking activity, yielding better liquid gasoline range products than in purely thermal cracking [113]. Cardona *et. al*. compared the gasoline range selectivity of various silica alumina and Y-zeolites with spent FCC over PP and found a comparable gasoline range yield (greater than 70%) [103]. Table 2.2 summarizes the results published by Ali *et. al*., comparing the product selectivity of fresh and equilibrium catalysts [101].

2.2.4.4 Coke Formation in FCC Catalysts

Coke formation is a common problem with FCC catalysts in industry and in polyolefin pyrolysis research. Coke consists mainly of heavy aromatics formed during the polyolefin cracking process.

Table 2.2 Product distribution for degradation of HDPE in a fluidized bed reactor using fresh and equilibrium FCC catalyst at 360°C (C/P loading = 2:1, reaction time = 30 min)

Yield (wt% of feed)	Fresh FCC	E-Cat [a]
Gas	79.8	60.1
Liquid	0	3.3
Coke	9.1	1
Residue	11.1	35.6
Gas & Gasoline breakdown		
C1-C4	42.6	26.7
C5-C8	54.6	73.3
BTX [b]	2.8	0

[a] E-cat has < 50 % BET surface area of fresh sample.

** BTX: Benzene, toluene and xylene content

Due to the strong binding nature of these poly-aromatics, the activity of a catalyst drops with increasing coke content [114, 115]. It is also believed that even at low coke deposition, the strongest acid sites are involved in the coke formation [116, 117].

Catalytic coke is formed when side reactions occur in the larger pores of FCCs forming these high MW poly-aromatics. These molecules tend to be too large to escape through the pore opening of the FCC catalyst resulting in a deactivation of the catalyst over time. Unlike FCCs, microporous catalysts such as ZSM-5 show low coke deposition due to its small pore system which does not accommodate the formation of large molecules such as coke [38, 118, 119]. De la Puente *et. al.* observed that a FCC catalyst yielded more coke than ZSM-5 [112].

On the other hand, coking may be as a result of poisoning of the catalysts by the metals found in the FCC unit such as nickel, iron and vanadium [120]. Bayraktar *et. al.* used analytical methods such as AFM, SEM-EDS, XPS and optical microscopy to show the role of Fe in FCC coking and catalyst deactivation [121].

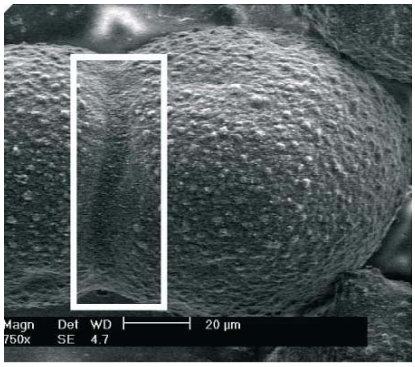

Figure 2-6 Equilibrium FCC sample containing high levels of coke (Ni: 2600; Va: 6700; Fe:7000 ppm. A substantial amount of Fe deposits were found within the white rectangle. Magnification: 750X [122]

Conversely, Guisnet *et.al.* have studied that the entrapped coke, which are themselves active species, can participate in certain catalytic reactions [123].

2.2.5 Effect of Polymer Type on Product distribution

PONA distributions of FCC catalyzed decompositions show that the olefin yield far exceeds the yield of paraffins, naphthenes, or aromatics (PNAs) in the pyrolysis of PP and HDPE [101, 124, 125]. Lee *et. al.* also showed that the catalytic degradation of waste LDPE produced more paraffins and aromatics than those of waste HDPE and PP [125]. Marcilla *et. al.* investigated the pyrolysis of different PE grades (LLDPE, HDPE, LDPE) by thermogravimetry. They observed slight differences in their decomposition behaviors but only in the presence of the catalyst (MCM-41) [126]. Conversely, PS pyrolysis exhibits high yields of aromatics, as high as 97 wt% of liquid product, far exceeding those obtained with

PE or PP (< 20 wt % of liquid yield) [22, 112, 125, 127]. Consequently, very low yields in PNAs are observed. This is attributed to the polycyclic nature of PS and the thermodynamic challenge posed in converting cyclic compounds to aliphatic chains or alkene compounds [112]. A closer look at the aromatic yield in many of these catalyzed reactions reveals that, the product selectivity is higher for benzene, toluene and ethyl benzene unlike in thermal pyrolysis, where the main product is styrene [6, 22, 112, 127, 128]. This clearly indicates the similarity and variance in the cracking mechanisms among these three polyolefins.

2.2.6 Effect of Particle/Crystallite Size on Product Distribution

The effect of catalyst particle size has only been sparsely studied in literature. You *et. al.* investigated the effect of particle size of MFI zeolites on the catalytic degradation of polyethylene wax and found that whereas conversion decreased with particle size, product quality increased [87]. Furthermore, particle sizes in the nano-range have been investigated. Serrano *et. al.* reported conversions as high as 90%, temperatures less than 350°C for the cracking of PP, LDPE and HDPE using nano-crystalline ZSM-5 [129]. Aguado *et. al.* observed similar results in the batch pyrolysis of PP and LDPE mixtures using nano-HZSM5 [99]. Based on these results, it can also be deduced that nano-ZSM-5 catalyzed reactions result in very high gas yields in the range of C_3–C_6 products, and apparently in much higher concentrations than is observed with micron-sized ZSM-5. These nano-sized particles are this effective because of their increased surface area. Conversely, high surface area combined with a very small pore system poses great difficulty in achieving decent amounts of gasoline range products in the C_5-C_{12} range. Moreover, the nano-catalyst selectivity to liquid products is also very limited [99, 129]. This could be resolved by investigating the particle size effect with catalysts that are selective to gasoline range liquid products such as FCC catalysts.

Costa *et. al.* found that a submicron base Y-zeolite for their FCC catalyst formulation showed a reduction in cracking of gas oil but showed a low selectivity for coke [108]. On the other hand, Tonetto *et. al.* observed that the effect of zeolite crystallite size on conversion and product distribution depended on the size of the decomposed hydrocarbon molecules [130]. The processes used in both studies, including the synthesis and embedment of sub-micron into an FCC catalyst seem both labor intensive and costly procedures. Subsequently, one may infer that an easier and economical approach might be to consider varying already formulated FCC catalysts with particle sizes ranging in the sub-microns. The effect of FCC catalyst fines on PP and HDPE pyrolysis will be discussed in this thesis.

2.2.7 Process Design

Thus far, the effects of catalyst and polymer type on the resulting product distribution in polyolefin pyrolysis have been discussed. Literature shows that the distribution can also be affected by other process parameters such as the means of polymer and catalyst contact during degradation, reactor type, feed composition (virgin/waste plastic) and degradation process conditions. To avoid a lengthy bibliography, only the most recent (after 1999) and relevant works will be discussed in this review.

2.2.7.1 Catalyst Contact Mode

One may be able to investigate the catalytic steps involved in polymer degradation by considering different modes of catalyst introduction to the polymer feed. Sakata *et. al.* investigated two modes of contact in the batch pyrolysis of PP using various solid acids: "liquid phase contact" and "vapor phase contact" [55]. For the catalytic degradation in the liquid phase contact, both catalyst and polymer are placed in the reactor and heated to the operating temperature. Whereas, with the vapor phase contact mode, the polymer is first

thermally degraded into HC vapors and then contacted with the catalyst. It was observed the HC vapors underwent further cracking in the vapor phase whereas the product yield in the liquid or melt phase contact did not differ significantly from that obtained by purely thermal degradation of PP [55]. In this study, two contact modes will also be investigated in the TG pyrolysis of PP using various FCC catalysts: melt mix and dry mix.

2.2.7.2 Reactor Type

A wide range of reactors have been used on a lab-scale in polyolefin pyrolysis. The reactor set-ups investigated thus far fall under one of the following categories: Batch, Continuous flow (CFR), modifications or combinations of either of the aforementioned.

2.2.7.2.1 Batch and Semi-Batch Reactors [43, 45]

A common variable in batch and semi-batch operations is nitrogen which is used for the continuous removal of volatiles from the reactor vessel. The products are then collected by passing the vapors through a condensation system. Most are made out of pyrex or stainless steel. Some of these works are tabulated in Table A-1 of Appendix A. A key disadvantage with this is the high reaction times observed. Furthermore, under batch operation, it seems that the potential of a catalyst is minimized with similar product yields to thermal at similar conditions. From an industrial viewpoint, continuous reaction systems are preferred to batch set-ups for operational reasons.

2.2.7.2.2 Fixed Bed Semi-Batch reactor [45, 131]

Polymer and catalysts samples are heated separately and reacted by vapor phase contact. Degraded polymer fragments are carried to the catalyst bed/mesh by a carrier gas, in most cases N_2. Typically the catalyst bed is heated to a higher temperature than the polymer bed.

2.2.7.2.3 Fluidized bed batch reactors [132-134]

Riser simulator reactors are fluidized batch reactors, specifically designed to simulate similar conditions found in a catalytic riser reactor used in the FCC process. It is adapted for liquid phase catalytic reaction, in which heat from the catalysts could vaporize the melt polymer feed while simultaneously cracking the resulting hydrocarbons.

2.2.7.2.4 Continuous Flow Reactors (CFRs) [96, 135]

More recently, researchers have moved focus towards reactors with greater feasibility in the industrial arena such as fluidized bed reactors which mimic the FCC unit in the petroleum industry. Generally, CFRs are characterized by much shorter residence time (less than a few seconds to a few minutes), improved uniformity and dispersion. Most of the more recent works in polyolefin pyrolysis are on fluidized bed reactors (See Table A-2). The use of continuous flow reactors in polyolefin pyrolysis prior to 1998 has been discussed [135].

The University of Hamburg, in particular, has done a lot of research in feedstock recycling from waste plastics using FCCs, and has subsequently developed the 'Hamburg process' which makes use of an indirectly heated fluidized bed [22, 127]. During catalytic cracking, quartz sand is replaced by the respective FCC catalyst as packing material. Amongst the various catalysts investigated, FCCs produced the most decent liquid yields in PE pyrolysis as shown in Table A.2.

Unlike a batch reactor, a fluidized bed reactor is suited for pyrolysis because it provides very good heat and material transfer rates hence generating largely uniform products. However, the disadvantages are many and include:

- Broad residence time distribution of solids due to intense mixing.
- Attrition of bed internals and catalyst particles.
- Difficulty in scale-up.
- Defluidization problems [136].
- Requires large amounts of catalysts.
- Low liquid yields due to 'over cracking' (See to Table A.2)

On the other hand, other continuous systems, such as the three-step continuous flow pyrolysis process involving a pre-heat, cracking reactor and separation zones, have been investigated by a few [26, 35, 42, 47]. In this method the polymer is first pre-heated to a molten state in a CFR such as an extruder and driven into the 'reactor' where it is further 'cracked' at elevated temperatures. Table A.3 summarizes recent and relevant polyolefin pyrolysis works employing CFRs.

2.2.7.3 Effect of Feed Composition

Many have demonstrated that plastics waste can indeed be converted to useful chemical feedstock by both non-catalytic [6, 33, 44, 124, 125, 133, 137, 138] and catalytic pyrolysis [35, 38, 101, 103, 133, 139, 140]. The present issues are the necessary scale up, minimization of waste handing costs and optimization of gasoline range products for a wide range of plastic mixtures or waste. In addition, controlling the product distribution is still an issue with waste and mixtures. Waste contents like PVC [9, 141-143] and biomass [144-146] do have an influence on the pyrolysis products.

In general, the decomposition of polyolefin mixtures occurs roughly in the same range as their virgin counterparts (350 -500°C). However, waste polyolefins may degrade at slightly lower temperatures and achieve higher conversions than the respective virgin polyolefins [44, 113, 139, 147-149]. As with virgin plastics, the addition of catalysts in waste pyrolysis greatly influence product yields and conversion rates; however, the disparities between waste and virgin polyolefin pyrolysis lie mainly in the resulting product compositions [35, 38, 52, 109, 124]. It is clear that during pyrolysis, interactions between the different materials in a waste feed have a significant effect on the selectivity of specific liquid and gaseous product components as shown in Table 2.3 [150].

Typically, PE pyrolysis favors mostly the formation of paraffins; however, upon increasing its PS or PP content, the yield of aromatic and alkenic products is greatly enhanced, thus improving its octane value [124, 140]. Due to the radicals formed during PS decomposition, the conversions of PP and PE are improved by PS addition [52, 149, 151]. Conversely, PS decomposition seems to be immune to effects by either of the other polyolefins.

Table 2.3 Waste versus virgin pyrolysis of HDPE using ZSM-5 and under similar operating conditions. (All experimental parameters are very similar between both references)

Yield (wt% of feed)	Virgin HDPE ([101])	Waste HDPE ([38]) *
Gas	87.1	90.65
Liquid	0	3.71
Coke	1.5	3.43
Residue	11.4	1.69
Gaseous product breakdown		
C1-C4	72.6	56.37
C5-C8	24.6	34.22
BTX	2.7	1.66

Approximate waste composition: 38 wt% HDPE, 24wt% LDPE, 30wt% PP, 7wt% PS, 1wt% PVC

Marcilla *et. al.* found that an FCC catalyst performed better than ZSM-5 and USY in the catalytic pyrolysis of PP-PE mixtures [109]. On the other hand, Lin *et. al.* found that larger pore zeolites (MOR and USY) and non-zeolites (SA, MCM-41) yielded much more coke and residue in comparison to ZSM-5 [38].

2.2.7.4 Effect of other Process Parameters

The effect of other process parameters such as reaction temperature, pressure, reaction time and catalyst loading has been investigated in literature. These are summarized in Table 2-4.

Table 2-4 Influence of certain process conditions in polyolefin pyrolysis

Process Parameter	Results
Temperature [6, 122, 152-154].	• Conversion increases with temperature resulting in decrease of aliphatic content. • Dermibas *et. al.* observed that gaseous products (C2-C4) and liquid products (C5-C9) increased and decreased with temperature respectively [6]. • Effect of the catalysts on the yields and structure of products becomes less significant with increasing temperature [57, 95].
Pressure	• Murata *et. al*. demonstrates the inverse relation of pressure to temperature in the pyrolysis of polyethylene [155].
Residence time [11, 65, 153, 154, 156]	• Key parameter in fluidized bed reactors. Generally conversion increases with residence time. • Miskolczi *et. al* observed that the catalyst activity of HZSM-5 and an FCC catalyst decreased with increasing cracking time in the pyrolysis of HDPE waste. • Effect of residence time on product yield is more pronounced at lower than higher temperatures
Catalyst loading [99, 154, 157]	• Conversion increases with catalyst loading.

2.3 Kinetic Studies in Polyolefin Pyrolysis

Kinetic models are important in the reactor design and scale up of industrial processes. Within the extensive work done in polyolefin pyrolysis, the development of kinetic models describing the cracking process has been narrowly researched. Nevertheless, a wide range of models have been developed. Only the relevant and recent works have been cited in order to portray the current status of this field.

The kinetic models in literature are broadly based on either representing the thermogravimetric method or detailed reaction mechanisms.

2.3.1 Kinetic Models Based on Thermogravimetry (TG)

In addition to the assessment of polymer stability and compositional analysis, thermogravimetry is used to estimate the degradation kinetics of polymers. These kinetic models are based on the analysis of the weight loss curves obtained during thermal gravimetric analysis of the polymeric samples.

The analysis is based on the fact that polymer decompositions are typically heterogeneous (solid state) reactions, and so the rate of conversion or weight loss (X) is a linear function of a temperature dependent rate constant, k, and the weight loss function, f (X), is described as follows:

$$\frac{dX}{dt} = kf(X) = A\exp\left(-\frac{E_a}{RT}\right)f(X) \qquad (1)$$

$$\ln k = \ln A - \left(\frac{E_a}{RT}\right) \qquad (2)$$

$$X = \left(\frac{Wo - W}{Wo - W_f} \right); \qquad [X]_o^f \qquad (3)$$

where A is the pre-exponential factor, Ea is the activation energy, W is the weight of the sample (polymer and catalyst) at time t, and the subscripts 'o' and 'f ' represent times at the beginning and end of the degradation respectively; f (X) is a weight loss function (WLF) which describes the dependence of the rate of conversion to the amount of residual polymer.

For a simple thermal degradation process of polymers, most describe the WLF as the power law function shown in Equation 4. 'n' is the order of the degradation reaction

$$f(X) = (1 - X)^n \qquad (4)$$

Thus, Equation 1 becomes

$$\frac{dX}{dt} = A \exp\left(-\frac{E_a}{RT} \right)(1 - X)^n \qquad (5)$$

The determination of degradation kinetics by TG can be approached in several ways:

2.3.1.1 Isothermal TG measurement

As the name suggests, the temperature is set to a constant during the entire decomposition process. For several measurements, the maximum rate of conversion can be obtained for each temperature and the logarithmic form of Equation 5 can be used to obtain the kinetic parameters (E_a, A and n) as shown in Equation 6 [158].

$$\ln\left(\frac{dX}{dt}\right)_{\max} = \ln A + n\ln\left(1 - X_{\max}\right) - \frac{E_a}{RT} \qquad (6)$$

On the other hand, the kinetic parameters can also be calculated from an integrated form of Equation 5 [159].

$$\ln(t) = \ln\left[\frac{g(a)}{A}\right] + \frac{E_a}{RT} \qquad (7)$$

where $g(a) = \int_0^X \frac{dX}{(1-X)^n} = \left\{-\ln(1-X) \;\; for \;\; n = 1\right\}; \left\{\frac{(1-X)^{n-1} - 1}{n-1} \;\; for \;\; n \neq 1\right\}$

The main problem with this method is that it is time consuming and cumbersome requiring extrapolations for temperatures above the equipment range [160].

2.3.1.2 Dynamic TG measurement

Dynamic (non-isothermal) measurements provide cumulative weight loss data at each linear rising temperature controlled by the chosen heating rate, β (^{o}/min). Many methods that use this concept have been proposed. The most commonly used are the model-free isoconversion methods by Ozawa [161], Flynn and Wall [162], Kissinger [163] and Friedman [158]. The first three are very similar in that they can be used to estimate the kinetic parameters directly from weight loss and temperature data (integral isoconversion methods) whilst the Friedman method is of a differential form (derivative isoconversion method).

Using a change of variables manipulation, Equation 5 can be expressed in terms of β.

$$\frac{dX}{d(1-X)^n} = \frac{A}{\beta}\exp\left(-\frac{E_a}{RT}\right)dT \qquad (8)$$

Therefore, E_a and A can be estimated from TG data collected at different heating rates.

The Ozawa-Flynn-Wall (OFW) method is derived from the integration of Equation 8 and has been incorporated into the American Standard for Testing Materials [164] as well as several commercial software packages [165] on most TG instruments. A detailed critical analysis of all the aforementioned isoconversional methods is discussed in literature [166-168].

Drawbacks with this method lie in the assumptions made. First, it assumes a first order reaction model for thermal pyrolysis of plastics, even though the reaction order changes with conversion [136]. Second, because of an approximation that was made by Doyle in the integration of Equation 8, only conversion values in the low range can be used in the analysis [169].

2.3.1.3 DTG Peak property method (DTG-PPM)

Whereas, OFW is an integral method, Equation 8 may also be used in its differential form, also called a derivative thermogravimetry (DTG) curve. Useful kinetic data can also be obtained indirectly from TG data such as in DTG (derivative thermogravimetry) curves expressed by Equation 8. The DTG peak properties (peak temperature, peak conversion and peak height) are known to have a close relationship with global kinetic parameters, E_a and A [163, 170-174]. Park *et. al.* gives a detailed analysis on the role of peak parameters (peak

temperature, height) in determining kinetic parameters for thermal reactions [172]. In a recent study, Kim *et. al*. estimated 'n' from peak properties of a DTG curve in a HDPE pyrolysis study and showed close similarities to results obtained by other conventional methods [175]. This method is prone to experimental errors during estimation of the exact peak properties, as well as in the choice of a weight loss function, although, $(1-\alpha)^n$ is commonly used [172].

2.3.1.4 Modulated Thermogravimetry (MTG)

This is a relatively new and model-free approach for obtaining TG kinetics. The temperature profile in MTG uses a linear temperature ramp controlled by an oscillatory temperature program that induces an oscillatory mass flow which is proportional to the physical properties of the polymer specimen [160]. The activation energy of a decomposition reaction may be calculated using Equation 9.

$$E_a = (R[T^2_{av} - (0.5T_{amp}]^2 L)/T_{amp} \qquad (9)$$

Mamleev *et. al.* recently presented a critical comparison of the MTG with other model-free methods (OFW, Friedman) as well as a model-fitting method based on MTG [167].

Unlike the model free methods described above, there exist model-fitting methods which require knowledge of the reaction mechanism or input parameters from other forms of analysis, including model free methods. These include the Freeman-Carol [176], Sharp-Wentworth [177], and Coats- Redfern [178] methods.

2.3.1.5 Factors affecting kinetic parameters estimated by TG

While certain kinetics factors, such as the surface area of the reacting sample, do not seem to affect the value of E_a, others, such as the extent of degradation, significantly influences the approximation of E_a [37]. Over a conversion range of 0 - 95%, Peterson *et al.* found that E_a increased by approximately 60 % for PE , 67% for PP and negligibly for PS [37]. A summary of kinetic parameters obtained in more recent literature is displayed in Table 2.5 (Kinetic studies for the non-catalytic pyrolysis of polyolefins in literature prior 1999 has been reviewed [37]).

Table 2.5 Literature values of the activation energy (E_a), reaction order (n) and pre-exponential (A) for degradation of PE, PP, and PS.

Polymer-catalyst	E_a (kJ mol^{-1})	A	n	Method	Refs.
HDPE-					
none	252.78	$2.31*10^{17}$	0.582	DTG- PPM	[175]
none	248.7	$1.75*10^{17}$	0.86-1	Isothermal	[179]
none	345.7	$2.5*10^{24}$	1	OFW	[179]
none	225.5	nd	1	OFW	[180]
alMCM41	184.7	nd	1	OFW	[180]
none	221	nd		Reactor kinetics	[26]
LDPE-					
alMCM-41	174.26	nd	nd	nd	[181]
PP-					
none	96.9 - 99.4	$25.02*10^{2}$	0 - 0.5	Coats-Redfern	[84]
none	208-288	42.08[a]	0.01	Friedman	[15, 182]
none	216	nd	nd	Reactor kinetics	[26]
PS-					
none	164 – 249	60.6[a]	0.32	Friedman	[15]
none	123	$7.62*10^{8}$	1	CSPR	[136]
none	205.2	$5.36*10^{15}$	1	FBR	[13]
none	208			Reactor kinetics	[26]

nd – not determined; [a]may have reported lnA although papers report A

Table 2.5 shows a wide variation between the activation energies and pre-exponential factors found by the various authors. These differences may be due to the different properties and characteristics of the polyolefins used in the various works as well as differences in process conditions from which kinetic data were estimated.

Furthermore, a very wide range of kinetic models have been developed using these methods. Publications before 1999 for the study PE pyrolysis by both isothermal and non-isothermal methods have been documented and their applicability discussed by Ceamanos *et. al*. [179]. More recently, only a few researchers have used one or two of these TG kinetic models in modeling polyolefin pyrolysis [84, 146], comparing results obtained by isothermal and non-isothermal TGA methods. Discrepancies were found amongst the studies due to different reaction definitions [179, 182, 183].

In a fairly recent paper, Marcilla *et. al*. model the thermal and catalytic steps in PE pyrolysis by TG. They included a Michaelis-Menton type constant in their kinetic reactions to describe the 'saturation effect' on catalyst activity commonly observed in polyolefin pyrolysis; however, results from a latter paper deemed this parameter unnecessary [71].

TG is a quick and easy way to obtain the global kinetics of a degradation reaction, however, a critical shortcoming is the heat transfer limitations within the sample, as there is a noticeable influence of heating rates on the activation energy [136, 175]. This problem is typically minimized by using considerably thin and small amounts of sample [164].

2.3.2 Kinetic Models Based on Mechanistic Modeling

2.3.2.1 Kinetic Models based on Reaction Mechanisms and Elementary Reactions

With these models, the reaction rates are expressed in terms of the concentrations of the species involved in the elementary steps [184, 185]. Johannes *et. al.* describe thermal cracking using steps of individual reactions on the basis of well-known kinetic equations and experimental data obtained for the decomposition of LDPE [186]. These kinetic models typically involve a great number of kinetic parameters and does not account for secondary reactions that take place during polyolefin pyrolysis

2.3.2.2 Kinetic Models based on Multi-step Reactions (Lumping System)

These kinetic models involve multi-step reactions accounting for secondary reactions that take place during pyrolysis. Only a few of these mechanistic models are available in literature, especially for catalytic cracking. They are typically complex, consisting of a large numbers of kinetic parameters and reactions that describe and seek to quantify the polyolefin decomposition products [10, 28, 151, 187-189]. These models are based on predictions of a typical free radical chain mechanism including reaction steps such as chain-end and random scissions, inter- and intra-molecular hydrogen abstractions, unzipping, backbiting, radical recombination and disproportionation reactions [85]. They are developed based on population balance equations solved by moment techniques described rigorously in literature [190, 191]. This theory is used to describe molecular weight distributions of species (macromolecules and radicals) in a polymer mixture, also called ‘distribution kinetics’ [191-193]. In addition, most of these models are based on a well known ‘lumping system’ in which individual components of the pyrolysis product stream are grouped into measurable compound classes such as long-chain-olefins, olefins, parrafins, BTX , carbenium ions, coke

and much more [86, 92]. Reactions between these 'kinetic lumps' are also modeled based on experimental data [184].

In a recent study, Lin *et. al.* improved the conventional lumping scheme to account for the catalytic degradation of HDPE and PP over fluidized acidic catalysts in a fluidized bed reactor [86]. In a latter study, Cardona *et. al.* presented a kinetic model for the pyrolysis of PP in a stirred batch reactor and accounted for thermal and catalytic cracking as well as coke formation using decay functions, one as a function of time and the other as a function of coke concentration on catalyst [194].

A common problem with these models is accounting for the immiscibility of the different polyolefins in waste mixtures. Kruse *et. al.* presented a binary model for a PS-PP mixture, consisting of 37000 reactions [195]. This binary model was developed by the combination of two original models, each describing PS and PP degradation respectively. By premixing the two polymers and slightly adjusting the PS to PP diffusion parameter, the model could portray binary interactions in PS- PP pyrolysis, including the enhancement of PP degradation by PS radicals formed during decomposition [195]. On the other hand, Faravelli *et. al.* presented a kinetic model that shows that accounting for binary interactions causes a deviation from experimental data, arguing that binary interactions can only be observed at high macro-mixing levels [151].

TG is a good kinetic estimation tool; however, kinetic information obtained by TG is characterized by errors due to certain restrictions such as heat and mass transfer limitations. Similarly, mechanistic modeling requires a lot of assumptions and is computationally

intensive; therefore, whenever possible, it may be best that kinetic data be estimated directly from experimental data.

As shown, there has been a lot of work done in the pyrolysis of polyolefins. However, the investigations of polyolefin pyrolysis with FCCs are scarce in literature. Furthermore, an estimation of kinetic parameters for the catalytic pyrolysis of polyolefins by TG methods has been scarcely done in literature. Therefore, it is the aim of this study to contribute to the area by investigating the kinectics of polyolefin pyrolysis using FCCs.

CHAPTER 3

EXPERIMENTAL METHODS

This chapter reviews the methods by which the polymer samples were prepared. First, the polymer and catalyst materials are described. Additionally, the various catalyst characterization methods employed are briefly outlined. Next, the various methods by which thermogravimetry (TG) data is used to in the evaluation of the catalysts on polypropylene pyrolysis are explained.

3.1 Polymer Materials

Polypropylene (PP), P4CZ-027, was supplied by Huntsman Corporation from Utah, while high density Polyethylene (PE), DGDA-6944 NT, was supplied by Union Carbide from New Jersey. Polystyrene (PS), MC3600, was supplied by Chevron Phillips Chemical Company. In this study, shredded post consumer carpet (PP-PCC) consisting of PP face yarns was supplied by Wellman, Inc. (Post consumer carpet with nylon face yarns are being evaluated concurrently by Bryson [196].) The composition of this material will be discussed below.

3.1.1 Composition of Polypropylene Post Consumer Carpet (PP-PCC)

Carpet consists of a face yarn with primary and secondary backing fabric/material glued together by a latex rubber product. The face yarns are typically made of nylon, polypropylene, acrylic, or polyester. The primary and secondary backing fabrics are usually PP. The latex adhesive is usually styrene-butadiene rubber (SBR)[197, 198]. Calcium Carbonate ($CaCO_3$) is typically added as filler in the latex adhesive as shown in Figure 3.1.

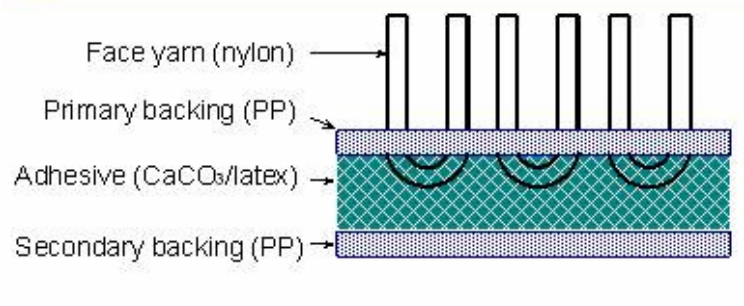

Figure 3.1 Structure of tufted carpet [198]

It was estimated that the shredded carpet material has a weight composition of 84% PP face fiber including backing material and 9% nylon 6 fibers [199]. PP-PCC is also expected to consist of contaminants such as dirt as is commonly observed with post consumer carpets. This is illustrated in Figure 3.2 below.

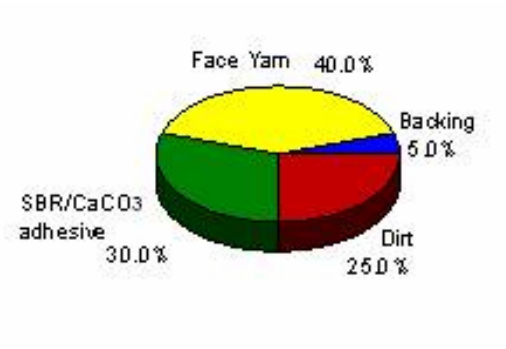

Figure 3.2 Composition of 'post consumer carpet' [198]

3.1.2 Preparation of PP-PCC Pellets

The shredded PP- PCC was converted into pellets using an A-Class type 55 VSP model of a Next Generation Recycling (NGR) repelletizing system. The NGR unit consists of a single screw extruder and a shredder incorporated in the feed section of the extruder. The shredded carpet is melted in the extruder barrel. This melt is filtered through a 20-mesh screen,

extruded as long continuous strands which are cooled in a cold water bath. These strands are collected and cut up into cylindrical shaped pellets using a Reiter pelletizer [199].

3.2 Catalyst Materials

3.2.1 ZSM-5

ZSM-5 was synthesized hydrothermally from clear gel solutions following the general procedure outlined for the synthesis of nanocrystalline ZSM-5 by Van Grieken et. al.[200]. In preparation of the gel solutions, measured amounts of water, sodium hydroxide (NaOH), tetrapropylammonium hydroxide (TPAOH, 40wt% aqueous solution), tetraethyl orthosilicate (silicon source) and aluminium nitrate (aluminum source) were mixed using the following composition:

9TPAOH : 0.16NaOH : Al :25Si :495H20

The hydrothermal treatment was conducted in an autoclave equipped with a rotating sample holder for continuous stirring at 165°C for 116 hours. The resulting solution was a whitish colloidal mixture of crystals and solvent. After three cycles of washing with water and centrifugation, the sample was dried at 120°C for one hour. Subsequently, the dried sample was calcined at 550°C under airflow for 5 hours. The methods of characterization for the synthesized ZSM-5 sample are discussed below.

3.2.1.1 Xray Diffraction

The calcined ZSM-5 crystals were characterized by X-ray diffraction (XRD) using a Cu K alpha target (1.5418740A). XRD patterns were collected between 2θ angles of 0 and 55°. The XRD pattern is shown in Figure 3.3.

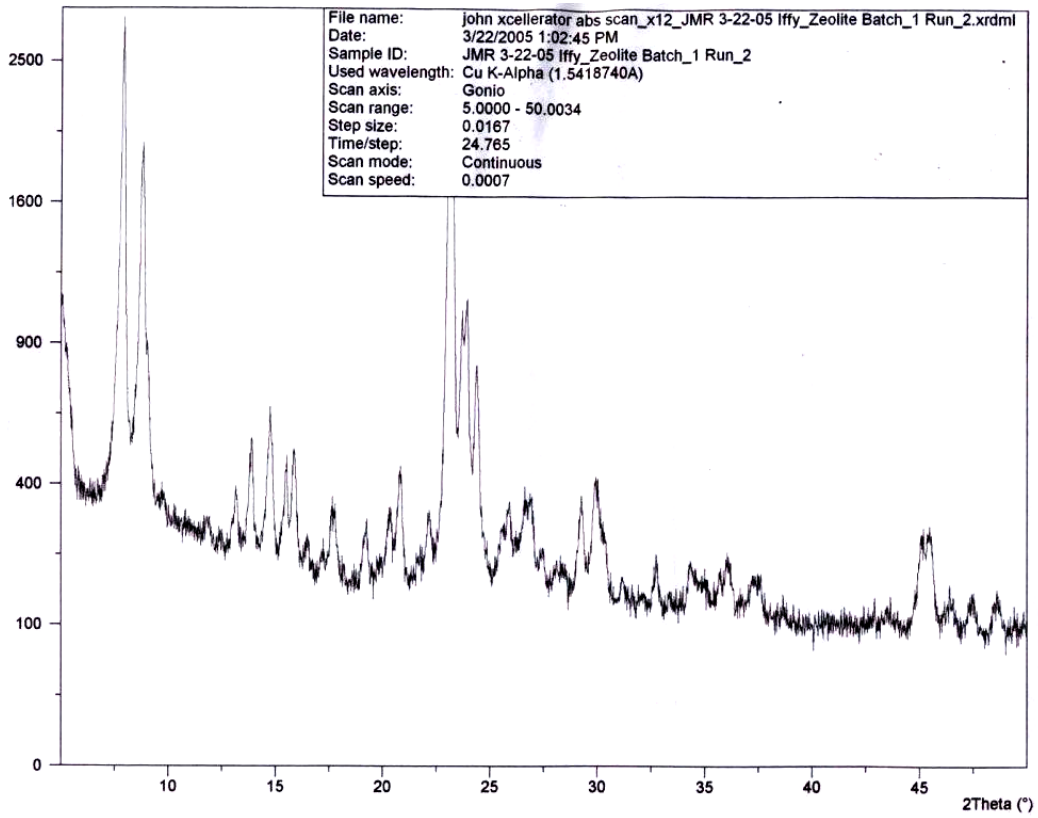

Figure 3.3 XRD patterns of synthesized ZSM-5

The characteristic peaks between 5° and 10° 2θ angles are indicative of a highly crystalline solid and showed a typical MFI-zeolite framework, which is characteristic of ZSM-5. Furthermore, the sharp narrow peaks indicate a high periodicity of the crystalline domains [201].

3.2.1.2 Solid State Magic Angle Spinning (MAS) NMR

^{29}Si and ^{27}Al solid state MAS NMR spectra were obtained using a 7.4 T wide bore magnet (^{1}H frequency at 300 MHz) with 7mm outer diameter rotors MAS probe spinning at 5 kHz and 6.5 kHz, respectively. For ^{29}Si, each single pulse spectrum was acquired for 128 scans

with a 60 seconds pulse repetition delay and calibration with respect to DSS at 0 ppm. For the ^{27}Al spectra, signal averaging of 1024 scans with a 3 seconds pulse delay and calibration with respect to Al^{3+} ions at 0 ppm was used. The results for both spectra are shown in Figures 3.4 (a) and 3.4 (b).

The signal at 53.057 in the ^{27}Al spectrum is characteristic of tetrahedral coordination of Al atoms, whereas the lower signals are typical of calcined ZSM-5 samples.

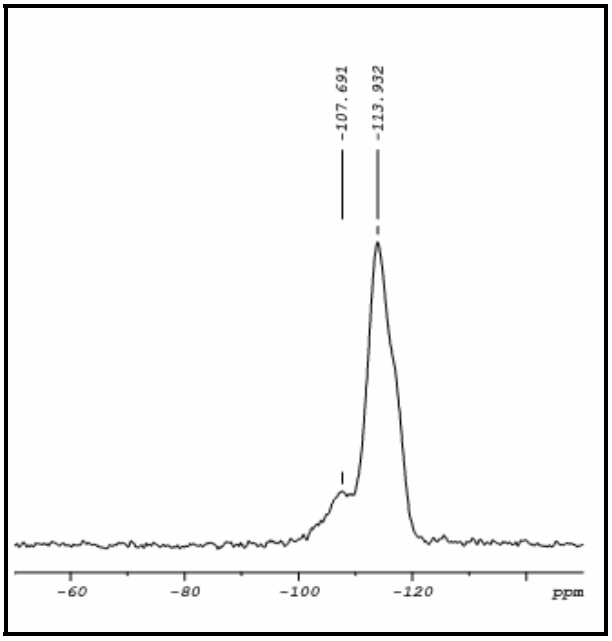

(a)

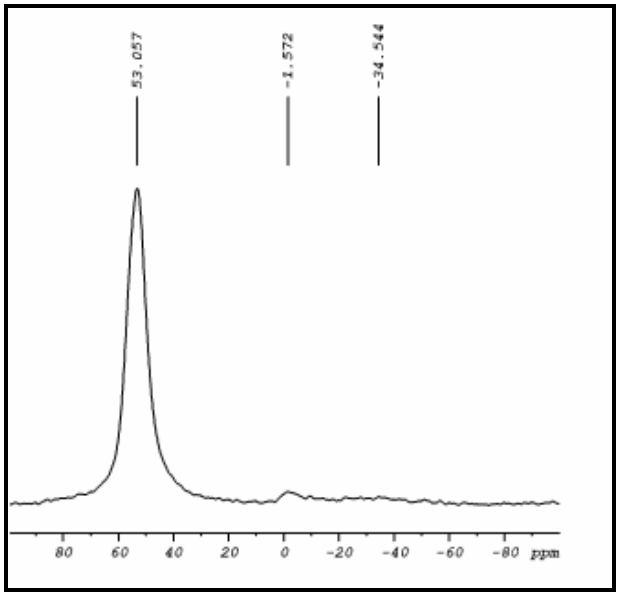

(b)

Figure 3.4 ^{29}Si (a) and ^{27}Al (b) solid state MAS NMR spectrum of calcinated ZSM-5 samples.

3.2.1.3 Scanning Electron Microscopy (SEM)

SEM images of ZSM-5 were obtained using a Hitachi S800 field emission gun (FEG) SEM. Shortly before a SEM image was taken, the sample was coated with gold.

The image of the ZSM-5 crystals shown in Figure 3.5 was taken at a 512 x 512 resolution.

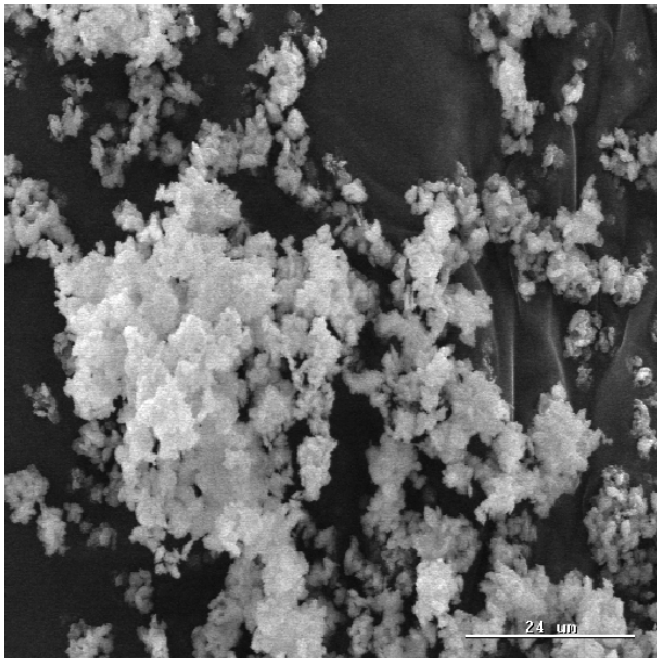

Figure 3.5 SEM image of ZSM-5 at 1000X

Furthermore, SEM was combined with energy dispersive X-ray analysis (EDX) in the detection of the elemental composition of ZSM-5 as reported in Figure 3.6.

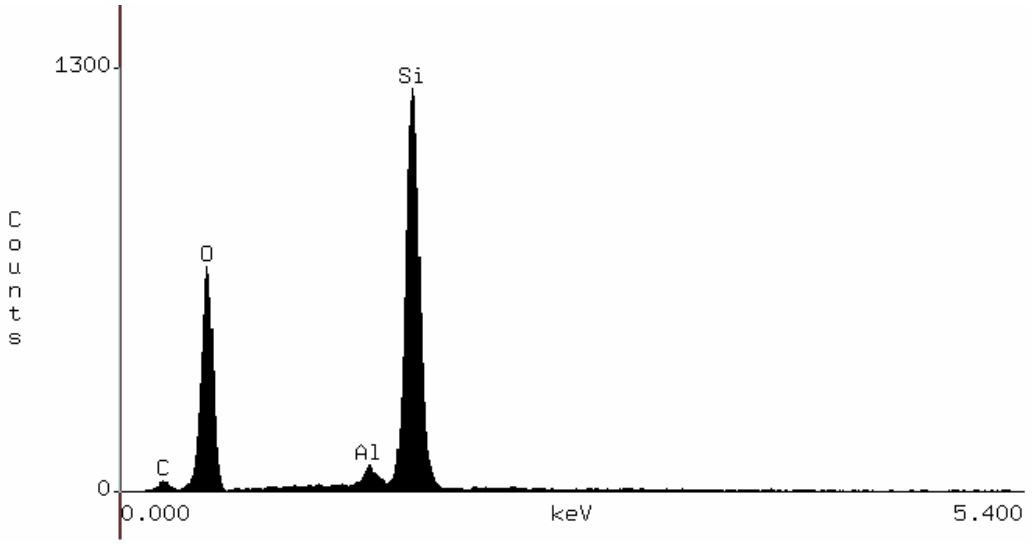

Figure 3.6 EDX bulk plot for synthesized ZSM-5

The results report a Si/Al ratio of 30.4 which is 21% off the original gel composition (Si/Al = 25). This could be attributed to errors in the SEM-EDX analysis, which may not be the paramount method for Si/AL determination. Additionally, errors may also arise from the loss of material during zeolite synthesis.

3.2.1.4 Nitrogen Adsorption Isotherms

Nitrogen adsorption isotherms were obtained on a Micromeritics ASAP 2010 using approximately 0.23g of sample. Prior to nitrogen adsorption, the sample was vacuum degassed for approximately 1 hour at 120°C. The results obtained are shown in Table 3.1 below.

Table 3.1 Nitrogen adsorption isotherm report on ZSM-5 sample

BET surface area, m^2/g	410.82 ± 5.07
Micropore area, m^2/g	230.60
Micropore volume cm^3/g	0.11

Although, a BET surface area was reported here, it should be noted that the BET approximation does not work well with microporous materials. This is because the BET equation is based upon the formation of multiple layers, which are not easily formed in microporous materials [202].

3.2.2 Fluid Catalytic Cracking (FCC) Catalysts

The FCC catalysts employed in this study are believed to be composed of a Y-zeolite. Used (or equilibrium) FCC catalysts were supplied by Shell and Albemarle and are abbreviated as S-ECAT and A-ECAT, respectively. In addition, fresh FCC catalyst samples having two different particles sizes were also supplied by Albemarle and are labeled “Fresh CAT” and “Fresh Fines” for the larger and smaller sizes respectively. The physical properties of these catalysts are displayed in Table 3.2.

Table 3.2 Physical properties of Albemarle catalysts as reported by supplier

	Fresh CAT	Fresh Fines	A-ECAT
Zeolite SA (m^2/gm)	119	115	48
Total SA (m^2/gm)	251	247	114
Particle size distribution (microns)	94	34	81
Nickel (ppmw)			3488
Vanadium (ppmw)			3938
Antimony (ppmw)			1312

It is not clear how the particle size distribution is estimated; however, when such values are reported, they typically represent a peak particle size within a volume based distribution of particle sizes. Additional characterizations were carried out on the FCC catalysts and these are discussed.

3.2.2.1 Scanning Electron Microscopy (SEM) and Energy Dispersive X-ray (EDX)

SEM images of S-ECAT and the Albemarle fresh FCC catalysts are shown in Figures 3.7(a), 3.7(b) and 3.7(c), respectively. These were obtained at magnifications of 200X, 500X and 500X, respectively.

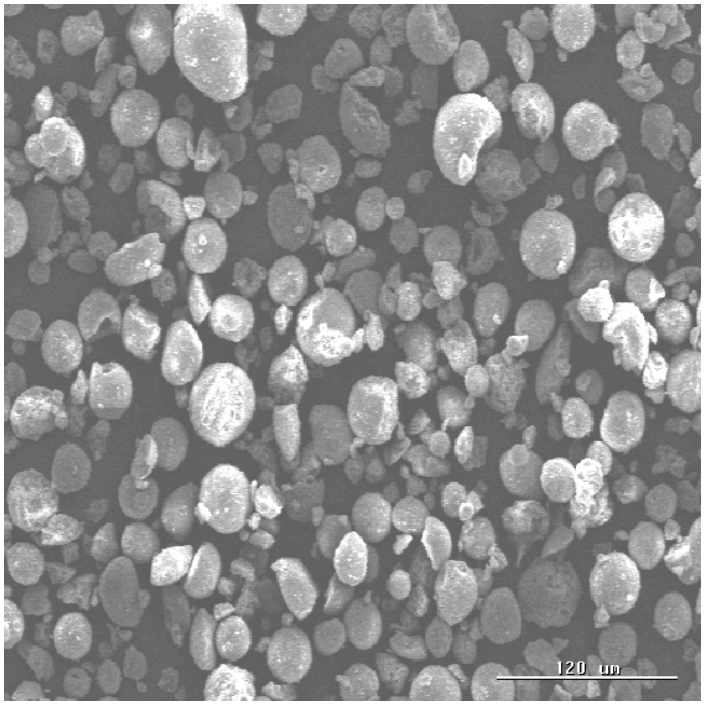

Figure 3.7 (a) SEM image of S-ECAT taken at 200X

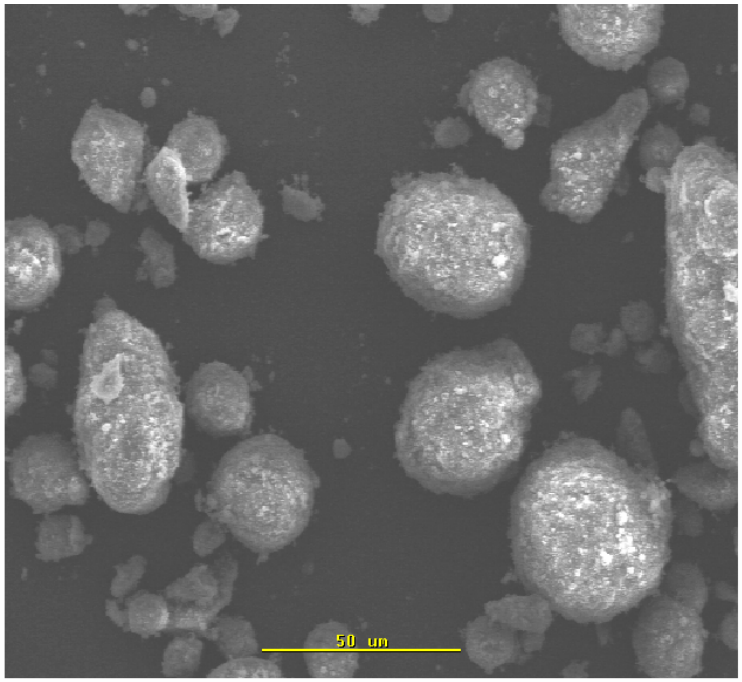

Figure 3.7 (b) SEM image of Fresh FCC Fines taken at 500X

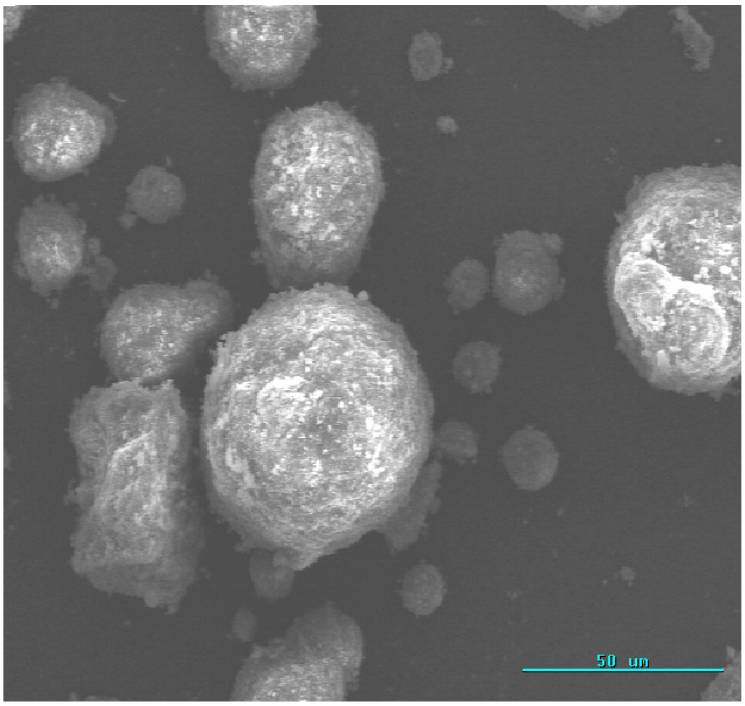

Figure 3.7 (c) SEM image of Fresh CAT (regular) taken at 500 X

From the SEM images, it may be deduced that S-ECAT particles' sizes range within 30-60 μm, whereas the Fresh CAT and Fresh FCC Fines measure 25-65 μm and 12-35 μm, respectively.

In further characterizing S-ECAT, SEM was combined with EDX in the detection of the zeolitic and metal compositions as reported in Figure 3.8.

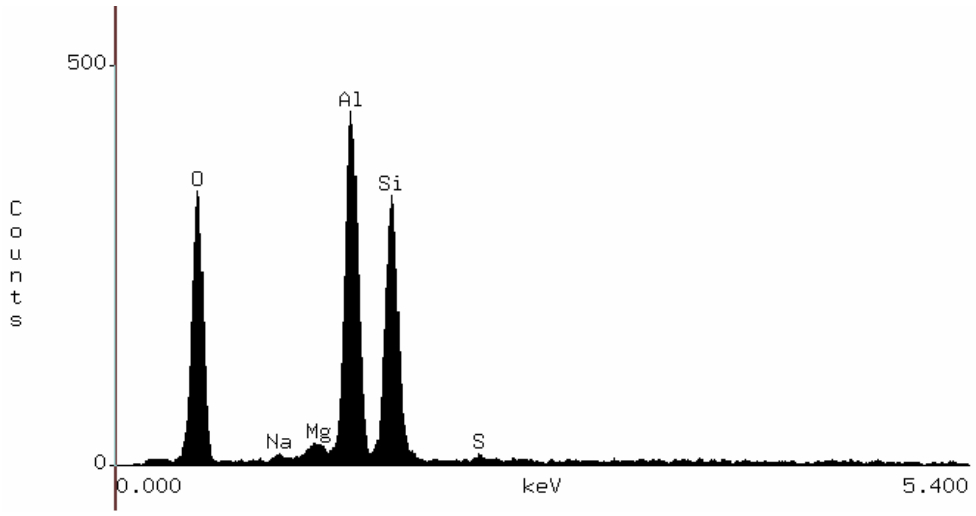

Figure 3.8 EDX bulk plot for S-ECAT

The analysis reports a Si/Al ratio of approximately 1.2 for S-ECAT. This value is very close to that observed in a Y-zeolite (approximately 2).

3.2.2.2 Particle Size Distribution (PSD) by SEM

SEM images of the fresh FCC catalysts were taken and loaded on a Vashall image analyzer where the particle size determinations were performed by analyzing 111 and 102 particles for the Fines and regular sized FCC catalysts, respectively. A plot of the mean diameters observed for the individual particles is shown in Figure 3.9.

The analysis yielded average PSD diameters for the Fines and the regular size particles are 18 ± 11 and 21 ±16 microns, respectively. This is different from the average diameters reported by the supplier (shown in Table 3.2).

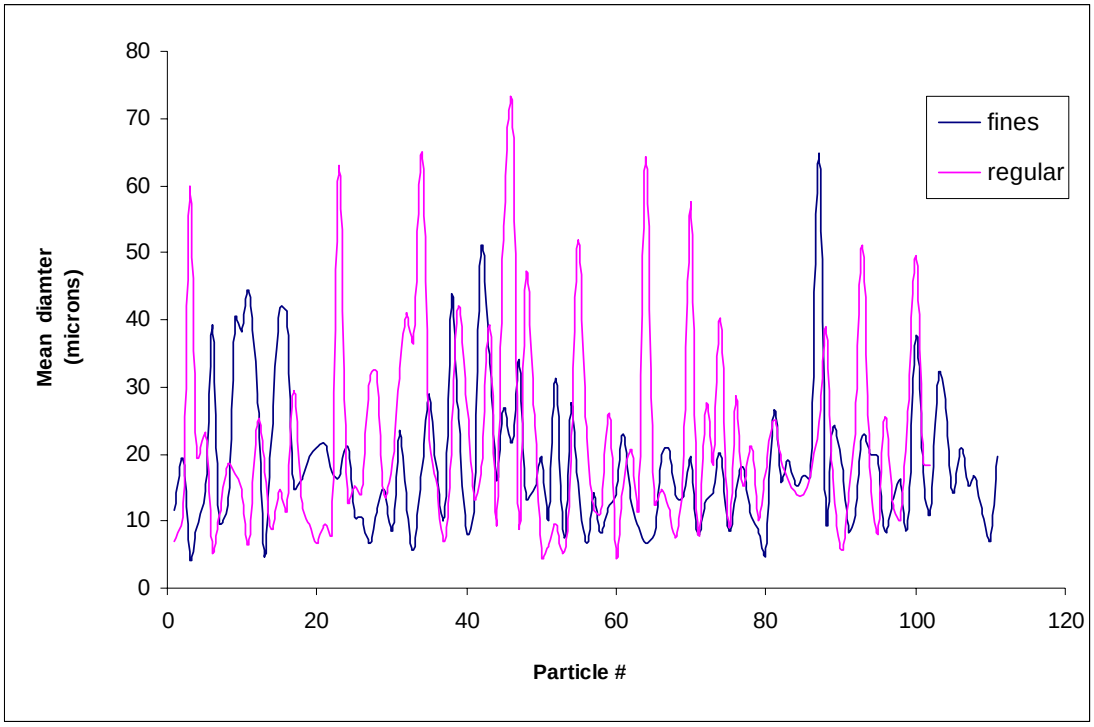

Figure 3.9 PSD analyses by SEM for Fresh FCC catalysts

Figure 3.9 clearly shows much variation of particle mean diameters within both samples.

3.2.3 Calcium Carbonate ($CaCO_3$)

$CaCO_3$ was supplied by Fisher Scientific (CAS: 471-34-1). $CaCO_3$ is typically used as filler in the latex adhesive in carpets. The catalytic effect of $CaCO_3$ in the TG pyrolysis of PP-PCC was assessed and will be discussed in the next chapter.

3.3 Thermogravimetry

TG involves monitoring the weight loss of the sample as a controlled function of temperature. An important application of TG in the study of polymers is the measurement of thermal stability. In this study, this analysis serves primarily as an assessment tool in the

screening of various potential catalysts for polyolefin pyrolysis. An assessment of the catalyst performance prior to use in a reactor reduces costs.

The thermogravimetry analysis (TGA) equipment used in this study is a Seiko TG/DTA 320 running on the EXSTAR6000 software package. An inert atmosphere of high purity nitrogen gas, flowing at 300mL/min was used. The balance can hold a maximum of 15mg; therefore, all sample amounts used in this study averaged approximately 10.2 mg (min: 9.8mg and max: 12.5 mg) and a measurement range of 25° - 550°C was used for all runs. This range was chosen to ensure that all possible decomposition steps are identified for each polymer sample. (Higher temperatures were not attempted because aluminum pans were used and these start to anneal above 600°C.)

Furthermore, this particular TG model allows for the variation of parameters such as the heating rate. In addition, to the mass at each temperature change, the data output also includes time and rate of weight loss (DTG) at each temperature step.
The heating rate feature and time data are particularly important in the kinetic study of the pyrolysis reactions, which will be discussed in Section 3.3.3.

3.3.1 TG Sample Preparation

In the TG study of the catalytic pyrolysis of PE by MCM41, USY and ZSM-5, Marcilla *et al*. prepared their samples by mixing dried proportions of polymer and catalyst ('dry mixing') [25]. In their analysis, they found the amount of catalyst to be different for runs at the same concentration. This makes it difficult to assess the exact performance of the catalysts, especially when the decomposition curves are very similar [25]. This is apparently attributable to the method of sample preparation used. Alternatively, one could mix in the

catalyst into the polymer melt. In this study, the polymer is melted in a Haake Rheomix ® 600. The Rheomix ® 600 has three zones that are heated to set temperatures and mixing is achieved by rotation of the two sigma blades as shown in Figure 3.10.

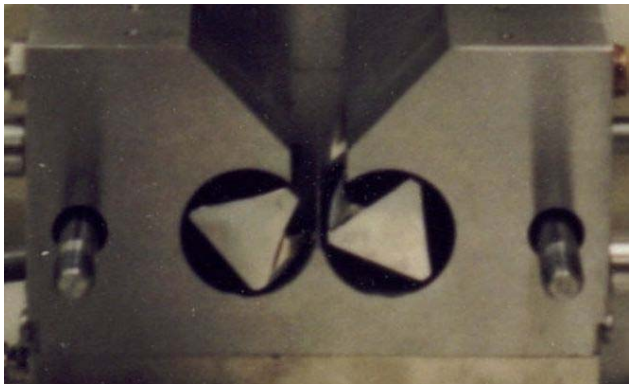

Figure 3.10 Schematic of mixer cross-section showing sigma blade placement in the mixing zone

The operating temperature is set very close to that of the polymer's melting temperature range, T_m. The operating temperatures used to obtain the various mixtures of catalysts and polymer (PP, PS and HDPE) are shown in Table 3.3. Also highlighted in Table 3.3 are the steps taken in obtaining TG samples by melt-mixing.

Table 3.3 TG sample preparation methods

	Dry Mix [25]	Melt Mix
Preparation	Mix proportions of catalyst and polymer in a mortar.	Polymer pellets are melted in pre-heated rheomix at temperature close to T_m. Catalyst is then added to polymer melt. T_m (literature value) PP: 180°C (175 °C) PS: 220°C (240 °C) HDPE: 155°C (137 °C) Rotor speed: 85-90 RPM Mixing time: 10 minutes Cool polymer-catalyst mixture and grind into smaller granular particles using a Wiley mill with a 1mm mesh size screen.
TG sample	Approximately 5 mg of the mortar mixture.	About 10 mg of finely ground sample.

To check that the melt-mixing procedure has no influence on the TG weight loss curves during polymer degradation, virgin PE and virgin PP were each 'melt-mixed' (without catalyst). The resulting weight loss curves were compared to the respective dry sample as shown in Figures 3.11(a) and 3.11 (b) respectively.

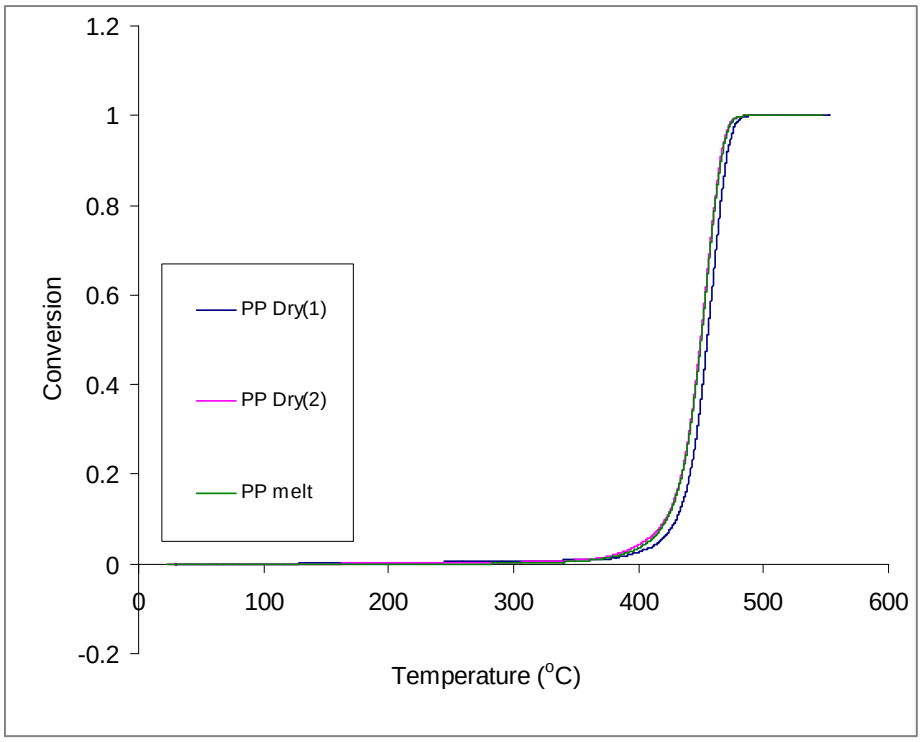

(a)

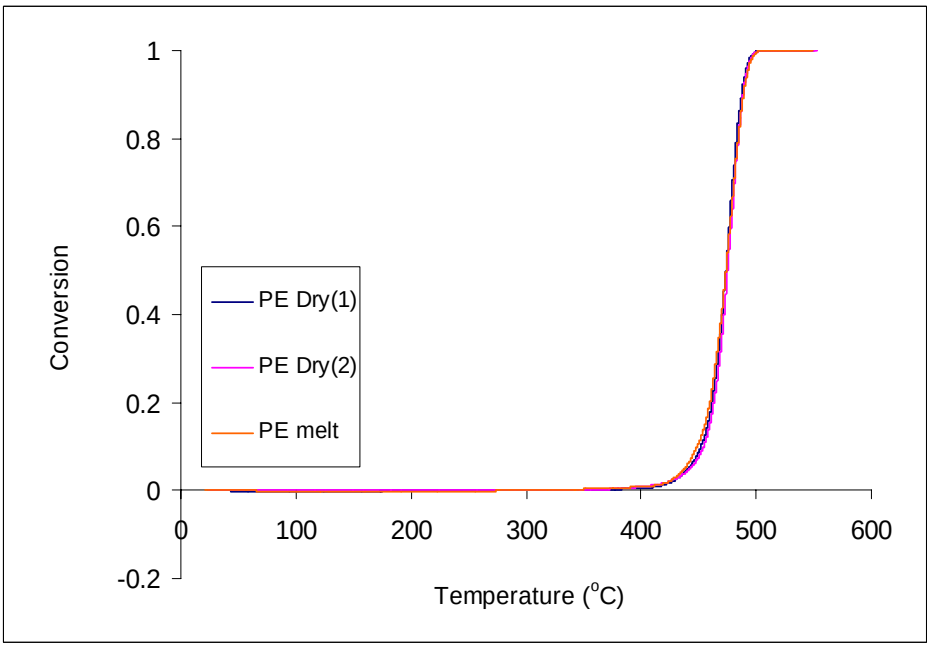

(b)

Figure 3.11 TG plots of dry and melt mixed virgin PP (a) and PE (b). The dry run was repeated (1, 2)

The analysis shows no significant changes observed in weight loss curves, particularly with the temperature at onset and end of sample weight loss for both polymers.

3.3.2 TG Analysis

The shape of the TG curve is merely a qualitative evaluation of the polymer degradation and is typically influenced by certain factors such as particle size, sample amount, sample holder geometry and heating rate [203]. Consequently, an evaluation of the TG curves must be conducted quantitatively by consideration of characteristic temperatures at: (1) the onset of mass loss, (2) the maximum rate of mass loss and (3) the end of mass loss (for the purpose of this study, weight loss will be referred to as conversion (conversion is based on polymer weight only).

In this study, the following measures will be used in assessing the effectiveness of the various FCC catalysts in the PP and PE pyrolysis.

1. Temperature at 1% conversion ($T_{1\%}$).
2. Temperature at maximum rate of conversion (T_{max})
3. Temperature at 99% conversion ($T_{99\%}$).

TG runs at 8wt% of all four FCC catalysts were repeated to check for repeatability of the TG data. It was concluded that the data is repeatable within experimental limits. These results are found in Table A.4 of the Appendix A.

3.3.2.1 Catalyst(s) weight loss

The thermal stability of catalysts was also assessed by TG. Prior to drying, some weight loss was observed as is shown in Figures 3.12.

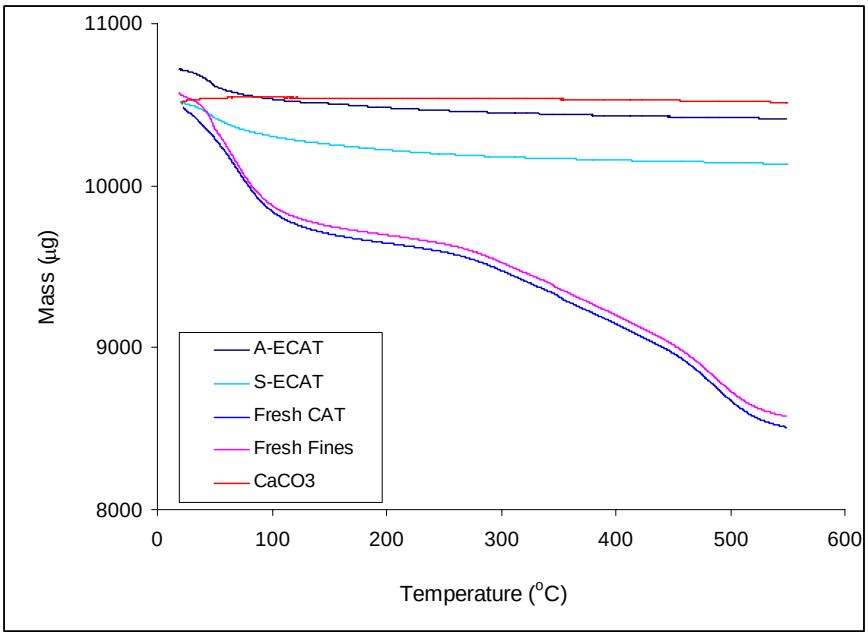

Figure 3.12 TG Plot of FCC catalysts and $CaCO_3$

As expected, $CaCO_3$ showed no weight loss. On the other hand, all FCC catalysts showed weight loss around 100 °C which indicates water loss. The weight change is observed to be more pronounced for the fresh FCC catalysts (Fresh CAT and Fresh Fines) than the equilibrium catalysts (A-ECAT and S-ECAT) as shown in Table 3.4. This may be associated to the reduced pore volume of the spent catalysts due to the presence of metal contaminations.

Table 3.4 Observed weight loss in catalysts prior to and after 100°C

Catalyst (run #)	Weight loss prior to 100°C (%)	Weight loss after 100°C (%)
Fresh CAT (1)	3.57	12.17
Fresh CAT (2)	6.20	12.64
Fresh Fines (1)	3.39	12.32
Fresh Fines (2)	6.79	12.15
A-ECAT (1)	1.50	1.06
A-ECAT (2)	1.71	1.10
S-ECAT (1)	2.07	1.59
$CaCO_3$	-0.37	0.30

Interestingly, there is significant continual weight loss observed with the fresh catalysts compared to the other catalyst materials. After 100°C, Fresh CAT and Fresh Fines on average lost an additional 12% of their total weight. This weight change can be clearly seen in Figure 3.13.

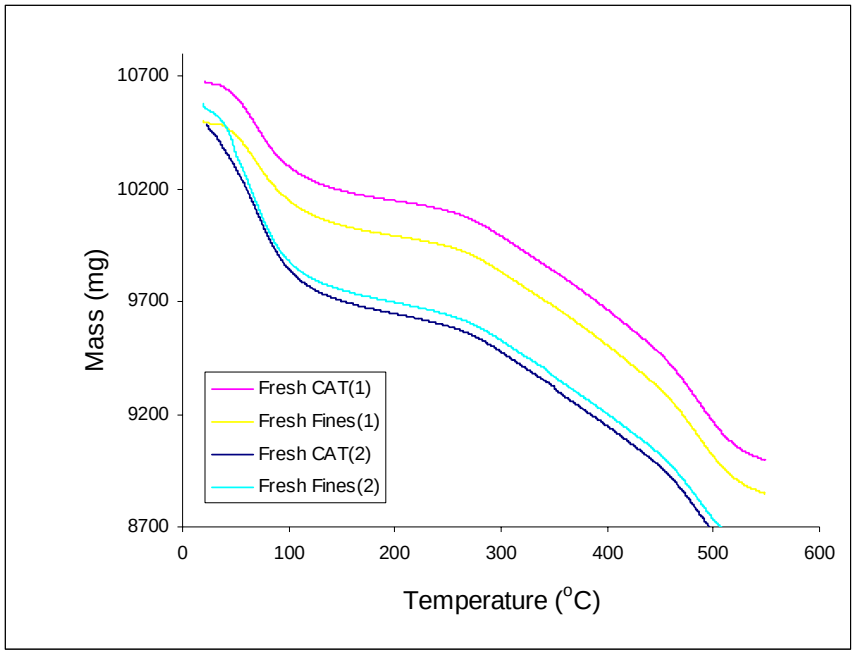

Figure 3.13 TG Plot of Fresh Catalysts

This may be due the loss of more water molecules trapped within the micropores of the catalysts, which eventually are evaporated as the temperature is raised. On the other hand, should this not be water molecules, this continual loss of catalyst may have significant effect in the assessment of the 'dry mix' TG analysis method. This may not be a critical problem with the melt mixed samples as the catalysts are embedded within the polymer melt.

3.3.3 Determination of Kinetic Parameters by TG

The kinetic analysis of TG data for the polymer decomposition process is described by a heterogeneous reaction involving the solid polymer, intermediate decomposition products and the evolution of gaseous products. The overall form of this chemical reaction is illustrated below.

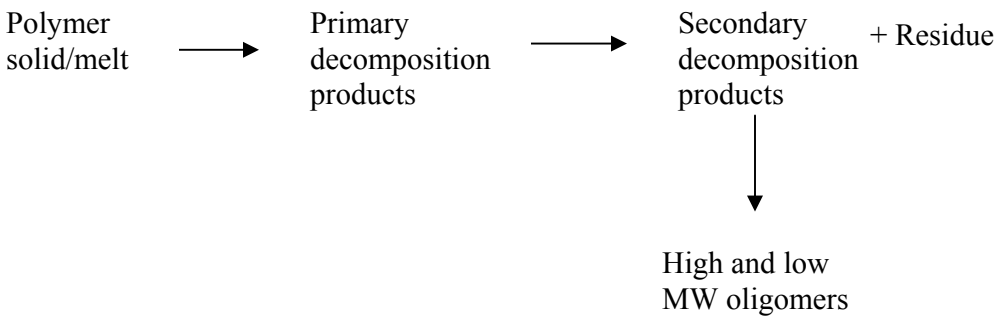

In the TGA equipment, the decomposition reaction takes place in an aluminum pan and the gaseous products are carried off by a sufficient flow of nitrogen gas (300mL/min). Therefore, one can assume that once the gases are formed they immediately leave the reaction volume, resulting in a weight loss. Thus, it is also assumed that the occurrence of secondary reactions between the various decomposition products and the polymer sample is limited. Given that the steps accounting for the rates of formation of the intermediate decomposition products

cannot be monitored by TG, the reaction is assumed to involve the polymer and resulting gases only.

The boundaries of the reaction volume is given by the solid polymer sample and since this varies progressively with the reaction, the reaction can be described as taking place in a constant-pressure, semi-batch reactor. Thus, a mole balance on the decomposition reaction with respect to the polymer (P) can be written as follows:

$$\text{Rate: } in - out + generated = Accumulation$$

$$0 - 0 + r_P V = \frac{d(N_P)}{dt} \qquad (1)$$

where, r_P is the rate of the polymer degradation, V is the voume of the polymer, N_P is the number of moles of the polymer and t is time. By substituting the definition given in equation (2) into equation (1) one ends up with equation (3).

$$N_P = C_P V \qquad (2)$$

where C_P is the concentration of the polymer.

$$r_P V = \frac{d(C_P V)}{dt} = V\frac{dC_P}{dt} + C_P\frac{dV}{dt} \qquad (3)$$

Since the reactant is assumed to be predominantly in the solid state, the concentration of the polymer is assumed to be constant even though the chemical structure of the polymer is changing as the reaction proceeds. This assumption is usually made with other solid reactions such as the degradation of $CaCO_3$. For the unreacted portion, the same proportion of moles of $CaCO_3$ left in remaining volume is equal to that of the initial number of moles contained withing the initial volume. However, for the degration of polymer, the molecular weight of the polymer is constantly changing, so in essence one is looking at a different

compound. It is assumed that the number of moles remaining in the volume with respect to time is similar to to that of the inital moles in the initial volume. With that said, the C_P in equation (3) is assumed a constant with respect to time. This would imply that reaction is zero-order, however the assumption is based on an overall shrinking of the polymer to gaseous products (consequently leading to weight loss) whereas, in reality, the polymer is degraded into both liquid and gaseous products, which should have some dependence on the concentration of the polymer. Thus, in this study, a first-order rate dependence was assumed.

Using the definition of the rate and assuming first order kinetics, $r_P = -kC_P$, equation (3) becomes:

$$-kC_P V = V\frac{dC_P}{dt} + C_P\frac{dV}{dt}$$

$$-kV = \frac{dV}{dt} \qquad (4)$$

where, k is the rate constant. The definition of volume is: $V=M/\rho$ so substituting into equation (4) assuming the density, ρ, is constant, one gets:

$$-k\frac{M}{\rho} = \frac{d\left(M/\rho\right)}{dt}$$

$$-k\frac{M}{\rho} = \frac{1}{\rho}\frac{d(M)}{dt}$$

$$-kM = \frac{dM}{dt} \qquad (5)$$

$$\text{where, } k = A\exp\left(-\frac{E_a}{RT}\right) \qquad (6)$$

Defining the conversion, X, as:

$$X = \left(\frac{Wo - W}{Wo} \right) \qquad (7)$$

Substituting (6) and (7) into (5) to give :

$$\frac{dX}{dt} = A\exp\left(-\frac{E_a}{RT} \right)(1 - X) \qquad (8)$$

where, W is the weight of the sample at time, t, and the subscripts ‘o’ and ‘f ’ represent times at the beginning and end of the degradation respectively.

In this study, the weight loss data is measured by dynamic (non-isothermal) TG measurement where the weight loss data at each linear rising temperature is controlled by the chosen heating rate, β (°C/min). Since both temperature and X change with time, Equation 8 can be rewritten based on manipulation by a change of variable, where,

$$\beta = \frac{dT}{dt} \qquad (9)$$

Thus, the rate of polymer decomposition may be described by

$$\frac{dX}{d(1 - X)} = \frac{A}{\beta}\exp\left(-\frac{E_a}{RT} \right)dT \quad (10)$$

Thus, E_a and A can be estimated from TG data collected at different heating rates. This is important because the heating rate, amongst others parameters, has an effect on the TG curves, thus influencing estimation of the kinetic parameters.

Equations 10 forms the underlying basis for the two TG kinetic analysis methods employed in this study. However, the procedural details differ and are discussed below.

3.3.3.1 Isoconversion Method

The ASTM test method (E 1641-99) is derived from the isoconversion method postulated by Ozawald, Flynn and Wall as was discussed in Chapter 2 [204]. The derivation is based on an integral form of Equation 10 and assumes that the reaction order is 1 [204].

The apparent kinetic parameters E_a and A are estimated by dynamic TG analysis of weight loss measured at various heating rates, β, for given values of conversion (or % cumulative weight loss). Heating rates between 1 and 10 °C/min are recommended; however, in this study the following heating rates are used: 3, 6, 10, 15 °C/min. Even though 15 °C/min is outside the recommendation of the ASTM standard, it was used because the results did not deviate from the linearity of the isoconversion plots. All runs at 10 °C/min were repeated to check for repeatability

The temperatures were obtained at conversions within the 5-15% range and were plotted for the different heating rates. E_a and A are calculated from straight-line plots of the logarithm of heating rate versus the reciprocal of the absolute temperature at each constant conversion.

$$E_a = -(R/b) * slope \qquad (11)$$

$$A = -(\beta / E_a) * R \ln(1-\alpha) * 10^a \qquad (12)$$

where b = 0.457/K for all conversions whereas, 'a' is an integration constant that is read off a table, given in the reference [204, 205].

3.3.3.2 Arrhenius Equation

This method is a differential analysis of weight-loss data and also assumes a reaction order of 1. Unlike the isoconversion method, only a single heating curve is used in this kinetic analysis. Given that the data obtained from TG includes the time interval for each conversion or degradation step, the rate of weight loss at each time interval can be determined from the Arrhenius relationship shown below.

$$k = A\exp\left(-\frac{E_a}{RT}\right) = \frac{1}{(1-X)}\frac{dX}{dt} \qquad (13)$$

where $T = T_r + \beta t$ (T_r is the room temperature) and at each temperature step, 'i', the rate constant is estimated by Equation 14.

$$k_i = \frac{1}{(1-X_i)}\frac{X_{i+1} - X_i}{t_{i+1} - t_i} \qquad (14)$$

Therefore, a linear regression of a plot of ln k versus 1/T yields an estimation of E_a and A from the slope and intercept, respectively.

In this analysis, only data in the range of 4 – 40 % conversion or weight loss was used in generating the Arrhenius plots. The start point of 4 % was chosen because by this stage of the degradation process, water, if present in the TG sample, would have been eliminated, thus removing its effect in the kinetic analysis (although all samples were pre-dried). A cut off at 40% was chosen in order to account for the early stages of the weight-loss reaction, prior to the point of maximum conversion, when most of the polymer is converted to gaseous hydrocarbons.

It should be noted that both the Arrhenius Equation and Isoconversion Methods which are used in this analysis are controversial in the scientific community [206]. The controversy occurs because the basic for these methods is the application of homogenous kinetics to a heterogeneous process. Some researchers are concerned about the fact that the kinetics measured is a function of experimental conditions such as the shape of the crucible and the arrangement of the powder. Also these methods give overall kinetic constants which may not reflect the complex reactions that are occurring. They are based on a simplified approach that does not take into account whether or not if the reaction is sequential, competitive or both at the same time. However, over 90% of the work in literature does use conventional TG analysis. This was used in this work since a more accepted form of thermal analysis, Sample Controlled Thermal Analysis (SCTA), was not available. With SCTA, the heating rate is not held constant at all times. Instead, upon detection of a change in the sample's mass, temperature is held constant. When a change in mass is no longer detected, heating resumes and this is repeated during the entire degradation process. In essence, this method is a quasi-isothermal thermogravimetric analysis that will allow for the determination of the dominant mechanisms that occur during polymer degradation. This is why it is accepted as a more reliable method than conventional dynamic TG.

As mentioned earlier, the use of the Arrhenius Equation and Isoconversion Methods have limitations in terms of analysis. For both methods, the values of the kinetic parameters found for the different heating rates or conversions will be averaged. In the case of isoconversion, the kinetic parameters are averaged over the chosen conversion values whereas with the differential method, the parameters are averaged over the different heating rates. This will add an error in the kinetic analysis. In addition, since kinetic analysis by TG takes into

account only the reaction steps involving volatile products, the conditions under which the analysis could be applied to a non-isothermal reactor must adjust accordingly.

Furthermore, the Arrhenius method assumes that the E_a is constant over a specific temperature range which may not be true since the reaction mechanism is complex in itself. Also, the dynamic change in the TG temperature constitutes an additional variation in the estimation of E_a.

CHAPTER 4

RESULTS AND DISCUSSION:

PERFORMANCE OF CATALYSTS

In Chapter 4, the evaluation of the various fluid catalytic cracking (FCC) catalysts in the decomposition of Polypropylene (PP), Polyethylene (PE) and post consumer carpet (PCC) by TG is presented. The weight loss curves are analyzed for samples prepared by melt-mixing and at a heating rate of 10°C/min. Rate constants for the catalytic pyrolysis of PP and PE are obtained from the TG curves at different heating rates and are presented in Section 4.5. The effect of catalyst contact mode on the weight loss properties is presented in Section 4.6.

4.1 Catalytic Degradation of Polypropylene and Polystyrene (PS) with ZSM-5.

A TG analysis on the performance of ZSM-5 in the catalytic pyrolysis of PP was carried out using 3 and 8 wt% ZSM-5. These results were compared to the spent catalyst from Shell (S-ECAT) as shown in Figure 4.1.

Both ZSM-5 and S-ECAT were effective in reducing the onset temperature (T_{onset}) for degradation. Although S-ECAT is a spent catalyst, it is more effective than ZSM-5 in its catalyzing the pyrolysis of PP at both 3 and 8 wt%. As discussed in Chapter 2, the number of acid sites on a solid catalyst plays a key role in the catalytic degradation rate of polyolefins. This number increases with increasing aluminum incorporation into the zeolite crystal. This may explain ZSM-5's reduced catalytic activity (Si/Al = 25) in comparison to the spent catalyst (Si/Al = 2).

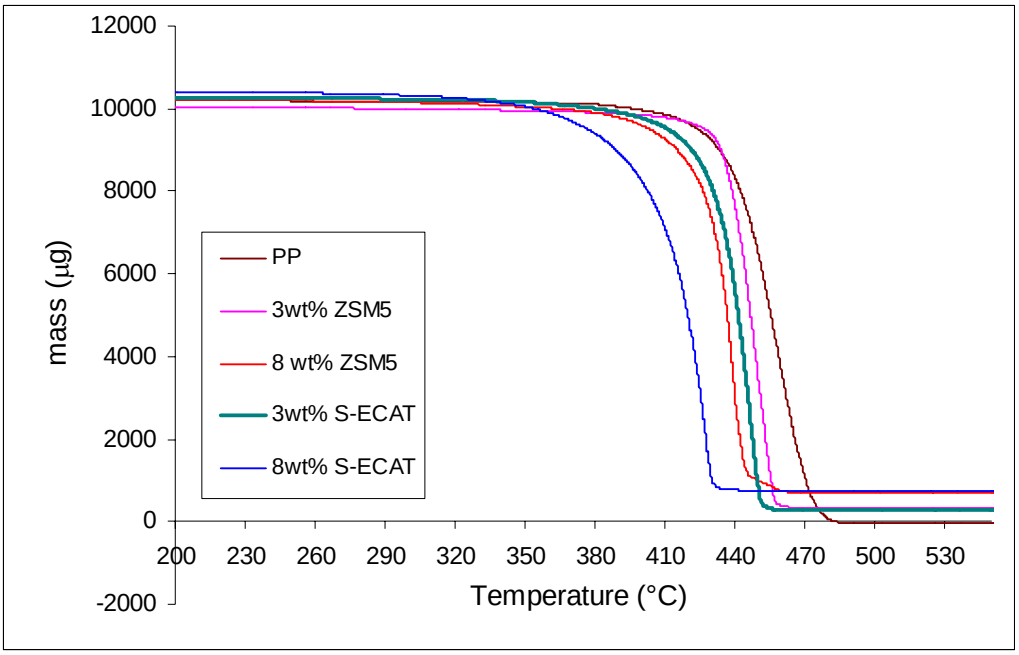

Figure 4.1 TG plot of PP degradation using 3 and 8 wt% of ZSM-5 and S-ECAT catalysts

Another influence on polyolefin degradation using microporous materials is the catalyst pore size. ZSM-5 is a medium-pore zeolite (0.54nm), whereas the base-zeolite of FCC catalysts (Y-zeolite) is characterized by larger pores (0.74nm). Given that PP molecules are much larger than the pore size of zeolites, the degradation of the primary decomposition products (large olefinic molecules) occurs over the surface of these catalysts, forming smaller molecules that can be permitted into the pores of the zeolites for further cracking. Thus, larger pore S-ECAT will permit for further degradation of PP within its pore, unlike medium pore ZSM-5. This direct influence of catalyst acidity and pore size on the catalytic degradation of PP was also observed in literature [207].

The same catalysts were employed in PS pyrolysis. The results are shown in Figure 4.2. Unlike in the case with PP, ZSM-5 and S-ECAT were found to be ineffective in enhancing

the degradation process. Similarly, in literature, solid acids were found to be less effective in PS degradation [94]. As a result, it was decided in this study to focus on PP and PE.

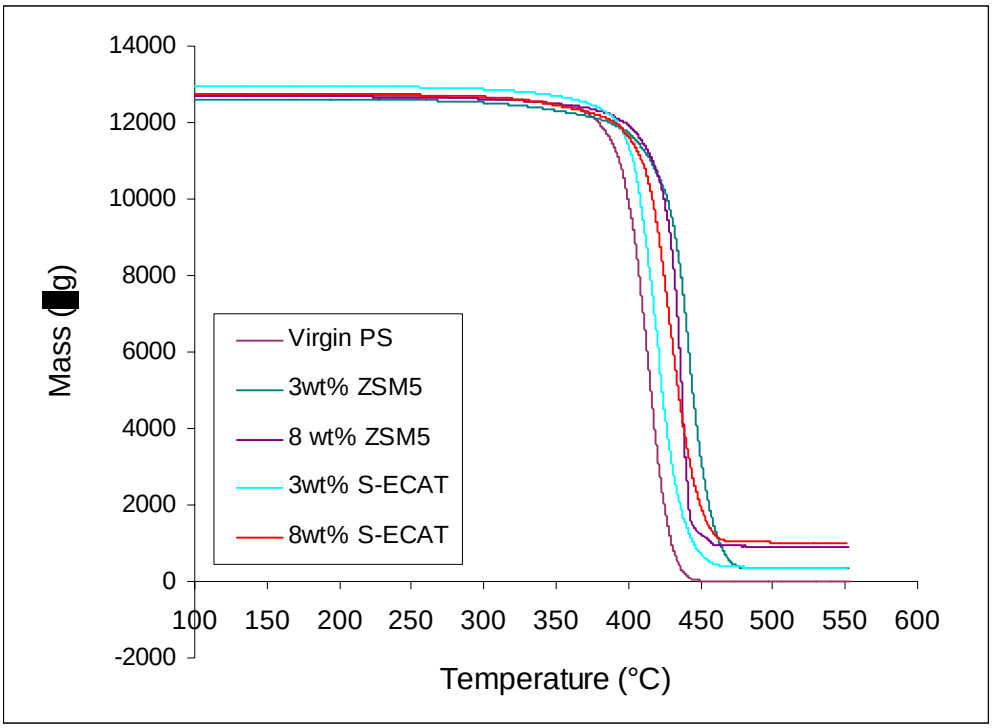

Figure 4.2 TG plot of PS degradation using 3 and 8 wt% ZSM-5 and S-ECAT

4.2 Evaluation of FCC Catalysts in PP Pyrolysis

TG analysis for the degradation of PP using 3, 8 and 13 wt% of all four FCC catalysts (S-ECAT, A-ECAT, Fresh Fines and Fresh CAT) was carried out. The conversions of PP with respect to temperature for each sample are shown in Figures 4.3 (a) – (c)

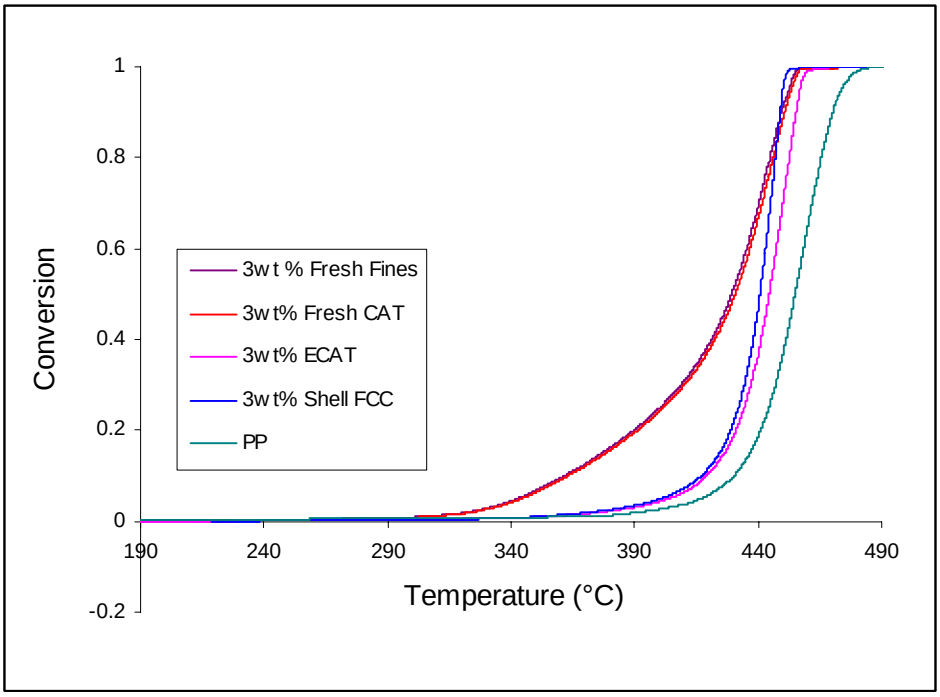

Figure 4.3 (a) TG analyses of FCC catalysts in the PP pyrolysis at 97 wt% of polymer

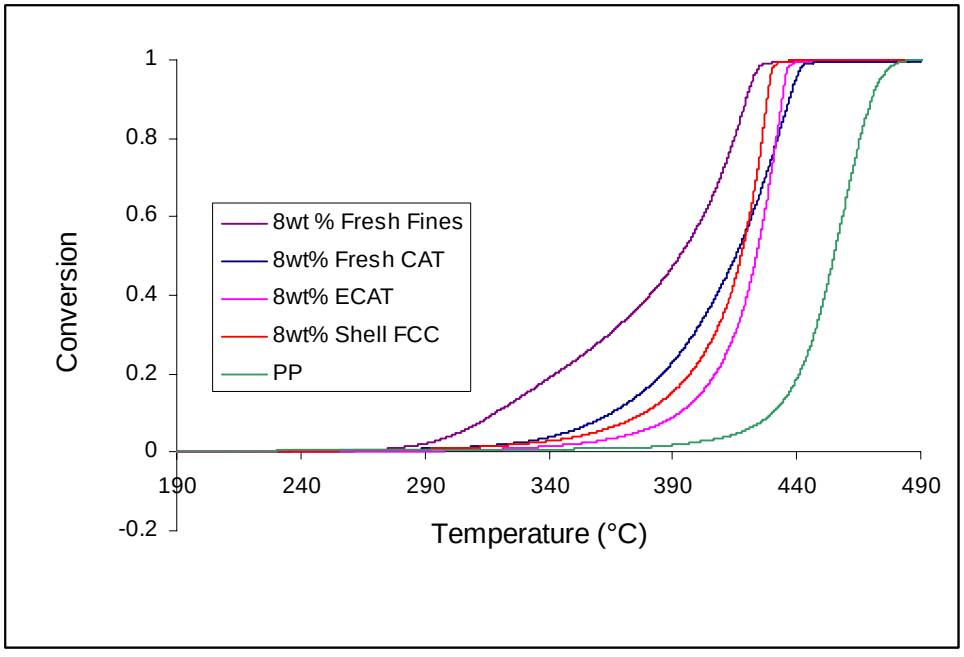

Figure 4.3 (b) TG analyses of FCC catalysts in the PP pyrolysis at 92 wt% of polymer

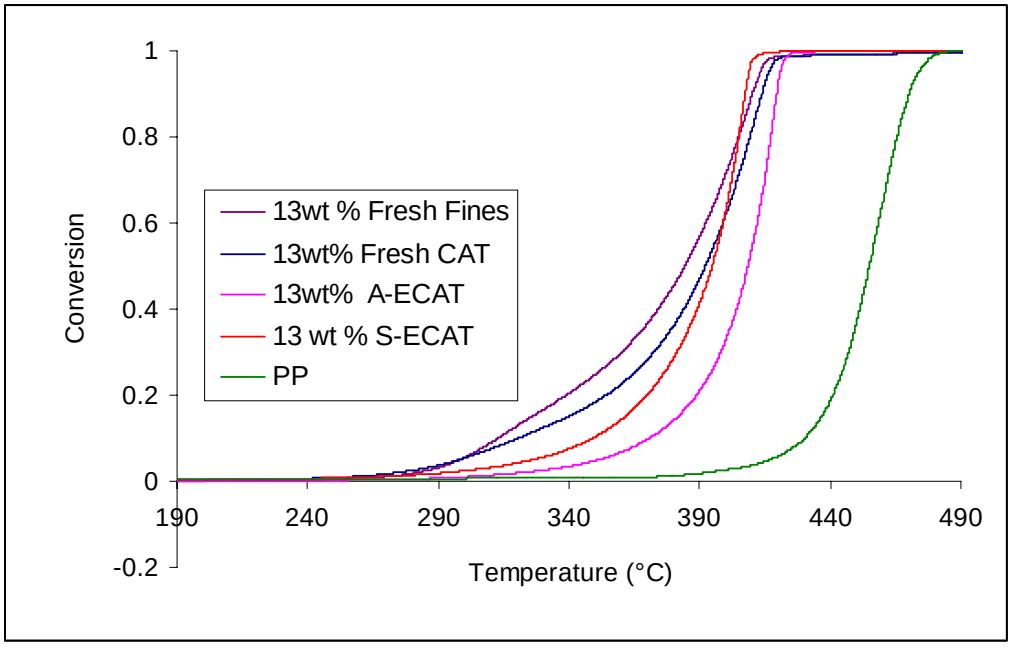

Figure 4.3 (c) TG analyses of FCC catalysts in the PP pyrolysis at 87 wt% of polymer

From the plots it is evident that all the FCC catalysts enhanced the degradation of PP. Moreover, T_{onset} is lowered with increasing catalyst weight for all the catalysts employed. The number of acid sites that are available for hydrocarbon cracking increases with the catalyst amount, thereby, enhancing the decomposition reaction. In addition, the fresh FCC catalysts improve degradation at lower temperatures best. This is expected, as they have not yet been subjected to thermal aging that occurs when used in commercial FCC units. On the other hand, with equilibrium catalysts, dealumination may have occurred, where the aluminum in the zeolite framework is extracted at elevated temperatures, eliminating the Bronstead acid sites and thus reducing catalyst activity [208].

Furthermore, it appears that the fresh FCC fines are the most effective. A reduction of the particle size increases the external surface area of the catalyst thus improving the cracking of PP. A more quantitative view of this analysis, considering the temperatures at 1 % ($T_{1\%}$), and

99 % ($T_{99\%}$) conversion, is presented in Tables 4.1. Also shown are the % decreases (-ΔT) in the PP pyrolysis temperatures as a result of the respective catalysts.

Table 4.1 Performance of FCC catalysts at 1% and 99% conversion of PP

Sample	*1% Conversion*		*99% Conversion*	
	$T_{1\%}$ (°C)	-ΔT (%)	$T_{99\%}$ (°C)	-ΔT (%)
Virgin PP	370	0	480	0
3 wt% S- ECAT	350	5	452	6
8 wt% S- ECAT	300	19	432	10
13 wt% S- ECAT	265	28	412	14
3 wt% Fresh CAT	307	17	459	4
8wt% Fresh CAT	295	20	444	8
13 wt% Fresh CAT	256	31	436	9
3wt% Fresh Fines	304	18	456	5
8wt % Fresh Fines	277	25	427	11
13wt% Fresh Fines	268	28	434	10
3wt% A-ECAT	353	5	460	4
8wt% A-ECAT	325	12	439	9
13wt% A-ECAT	300	19	424	12

Table 4.1 shows that the fresh FCC catalysts performed better than the equilibrium catalysts in lowering the onset of degradation, more so at the lower weight fractions. At 3 wt% catalyst, Fresh CAT and Fresh Fines lowered $T_{1\%}$ by approximately 17 and 18 %, respectively, whereas A-ECAT and S-ECAT both lowered $T_{1\%}$ by only 5%. Similarly, $T_{99\%}$ decreased with increasing catalyst weight fraction for all the catalysts. Thus, the degradation temperature range is significantly reduced with the addition of the FCC catalysts.

The results also show the fresh catalysts were the most effective at decreasing the overall degradation range. Between both spent catalysts, it seems that S-ECAT performed better than A-ECAT. At all three weight fractions, S-ECAT reduced both $T_{1\%}$ and $T_{99\%}$ better than A-ECAT. This may imply that A-ECAT is more acidic than S-ECAT (although this was not validated in the lab). Another factor is the particle size data. SEM pictures show that S-ECAT has a lower particle size range (30 -60μm) than the average particle size (81μm) reported for A-ECAT. It was already observed that a reduction in particle size enhances the activity of a catalyst in PP degradation and this may be the reason for the difference in activity between the two spent catalysts.

The effect of catalyst weight at the maximum rate of degradation on the conversion (α_{max}) and temperature (T_{max}) is reported in Table 4.2. Also shown are the % decreases ($-\Delta T_{max}$) in the PP pyrolysis temperatures as a result of the respective catalysts. The results show that at 461°C, α_{max} is 67% for the non-catalytic degradation of PP. This value is lower than the values reported in literature (78%) at a similar heating rate of 10°C/min [207, 209]. This could be attributed to the different experimental conditions under which the TG experiments were conducted, as well as the varying intrinsic characteristics of the PP sample such as the grade and molecular weight distribution.

Table 4.2 also shows that PP conversion at maximum weight loss increases with the addition of the various catalysts and more so with increasing catalyst weight fractions. However, there was not a significant correlation between α_{max} and the amount of catalyst present, although an indistinct stabilizing effect on conversion may occur with increasing catalyst weight fraction.

Table 4.2 Temperature and conversion at maximum rate of degradation of PP

Sample	T_{max} (^oC)	$-\Delta T_{max}$ (%)	α_{max} (%)
Virgin PP	461	0	67
3 wt% S-ECAT	448	3	85
8 wt% S-ECAT	419	9	79
13 wt% S-ECAT	406	12	84
3 wt% Fresh CAT	447	3	77
8wt% Fresh CAT	438	5	90
13 wt% Fresh CAT	410	11	82
3wt% Fresh Fines	441	4	73
8wt % Fresh Fines	421	9	90
13wt% Fresh Fines	411	11	92
3wt% A-ECAT	451	2	72
8wt% A-ECAT	432	6	82
13wt% A-ECAT	418	9	83

On the other hand, T_{max} clearly decreases with increasing catalyst weight fraction for all four FCC catalysts, as the pyrolytic decomposition of PP into volatile hydrocarbons is enhanced at much lower temperatures by the addition of catalysts. Figure 4.4 shows a linear relationship exists between T_{max} and catalyst weight fraction for PP degradation.

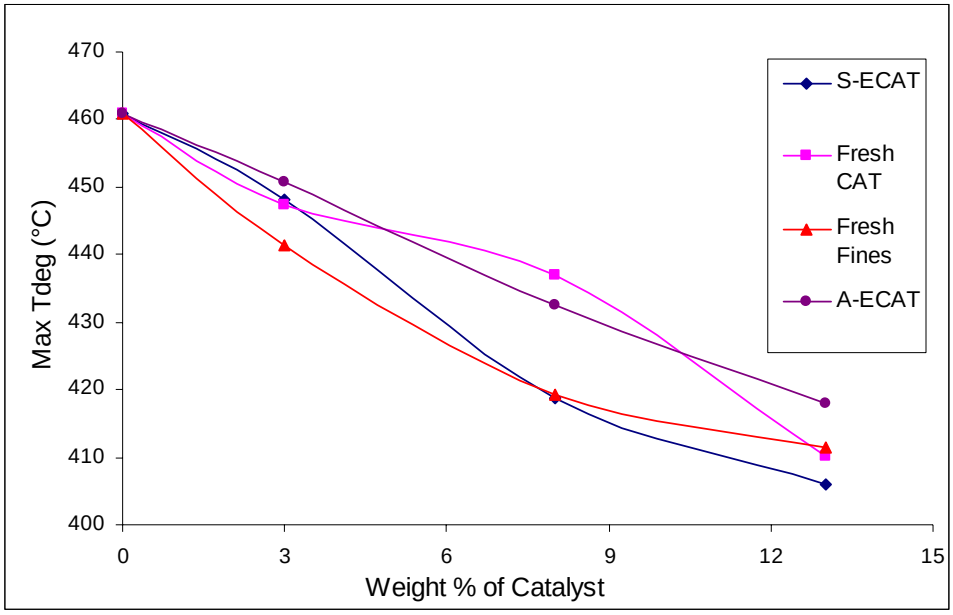

Figure 4.4 Effect of catalyst weight fraction on T_{max} in PP degradation

The spent catalysts showed better correlations then the fresh catalysts, as shown in Table 4.3

Table 4.3 Linear correlation of maximum degradation temperature with catalyst weight ratio

Catalyst	r[a]	Linear Equation
S-ECAT	0.976	-4.3984x + 459.81
Fresh CAT	0.968	-3.6995x + 461.06
Fresh Fines	0.935	-3.7918x + 456.01
A-ECAT	0.997	-3.3289x + 460.51

[a] correlation coefficient

Furthermore, at each catalyst weight amount, there is only a slight variation in T_{max} amongst the different catalysts, however, α_{max} varies significantly. This is because at higher temperatures (above 400 °C), the rate of vaporization of decomposition products is increased

[179]. Of course this range will shift with T_{onset}, which also varies with catalyst weight fraction. Thus, for 0 and 3wt% of catalyst, this temperature is approximately 460 and 450 °C, respectively, and is reduced to a range of 410-420 °C at 13 wt% of catalyst. The variation in α_{max}, accounts for the difference in activity and reaction mechanism amongst the FCC catalysts.

Additionally, above T_{max}, the rate of weight loss gradually decreases and this allows for the total conversions of a less active catalyst such as S-ECAT to approach that of the more active catalyst such as the Fresh fines. This is the reason for crossing of some TG curves in Figures 4.3 (a) – (c).

4.2.1 Enhancing A-ECAT Performance in PP Pyrolysis

In order to reduce costs, and optimize commercial FCC processes, fresh FCC catalyst is commonly mixed with equilibrium catalyst [208]. The same idea was applied to this study. The performance of A-ECAT in PP pyrolysis has been discussed. At 97 wt% PP, A-ECAT showed minimal catalytic effect on PP degradation. Overall, it showed the least catalytic effect on the polymer degradation, whereas, the Fresh Fines performed the best. Thus, in enhancing the performance of A-ECAT, catalyst mixtures consisting of varying amounts of Fresh Fines and A-ECAT were mixed to yield a constant amount of catalyst (the total catalyst weight was kept at 3wt % for all samples). The results are shown in Figure 4.5.

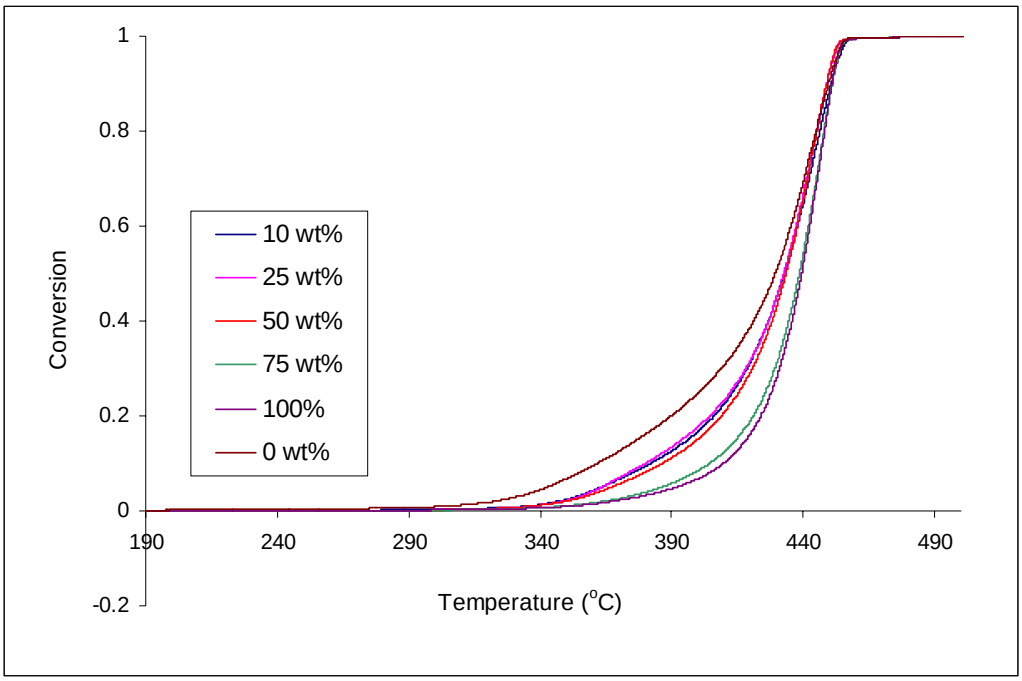

Figure 4.5 Degradation of 97 wt % PP with 3 wt % mixed catalyst where 0 wt % is all Fresh Fines and 100 % is all A-ECAT

Figure 4.5 shows an improvement in the degradation of PP by A-ECAT achieved by the increasing addition of Fresh Fines in the polymer sample.

4.3 Evaluation of FCC Catalysts in PE Pyrolysis

TG analysis for the degradation of PE using 3, 8 and 13 wt % of all four FCC catalysts (S-ECAT, A-ECAT, Fresh Fines and Fresh CAT) was carried out. The conversions of the PE with respect to temperature for each sample are shown in Figures 4.6 (a) – (c)

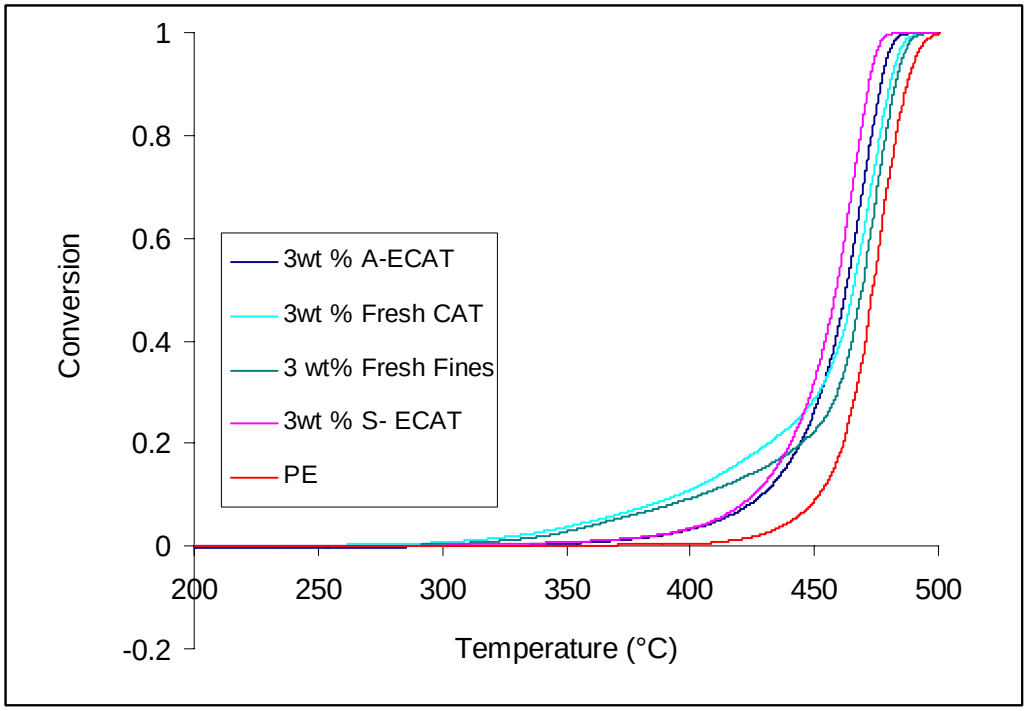

Figure 4.6 (a) TG analyses of FCC catalysts in the PE pyrolysis at 97 wt% of polymer

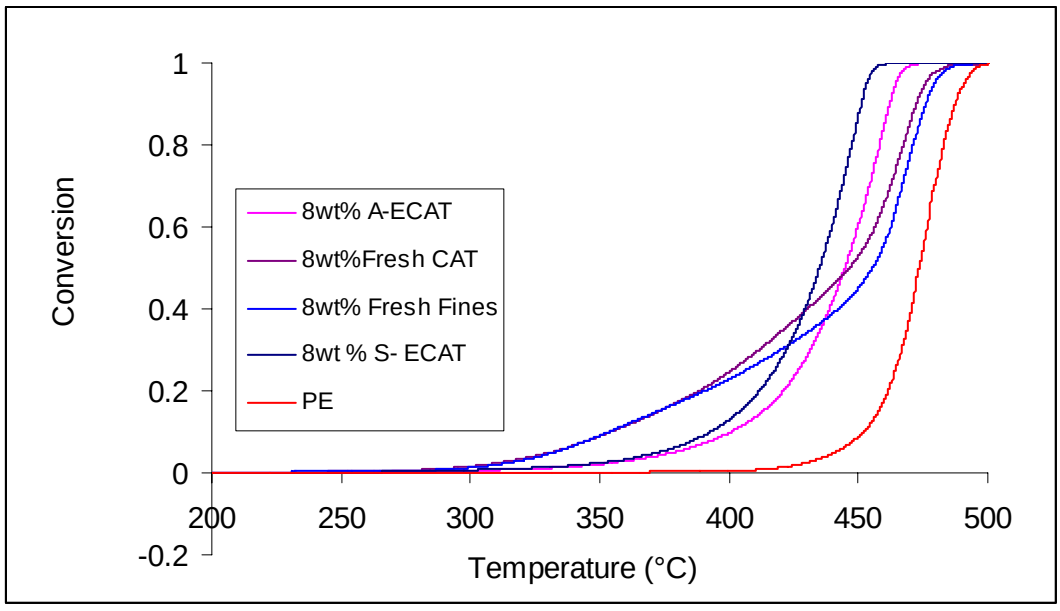

Figure 4.6 (b) TG analyses of FCC catalysts in the PE pyrolysis at 92 wt% of polymer

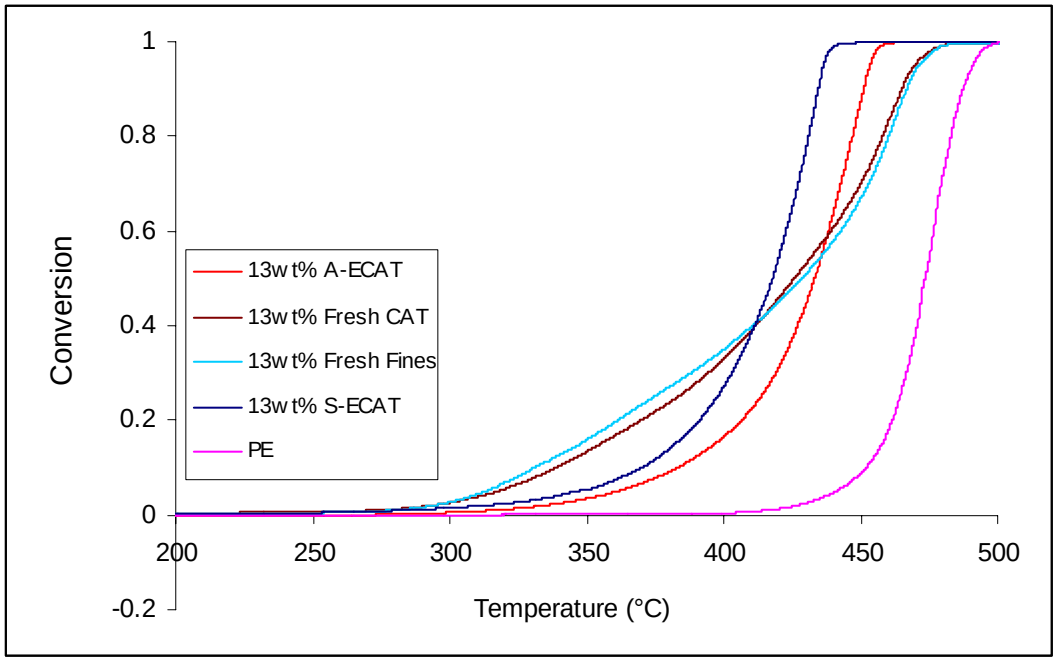

Figure 4.6 (c) TG analyses of FCC catalysts in the PE pyrolysis at 87 wt% of polymer

The TG plots show that all the FCC catalysts enhanced the degradation of PE. Moreover, it is observed that T_{onset} in PE degradation is lowered with increasing catalyst weight fraction for all catalysts employed. However, at all catalyst weight fractions, the TG curves are relatively close, indicating similar cracking activities among the catalysts. This is a very different observation from PP pyrolysis, where the respective cracking activities of the catalysts are both consistent and distinguishable over most to the degradation range.

A more quantitative view of this analysis, considering the temperatures at 1 % and 99 % conversion is presented in Table 4.4. Also shown are the % decreases ($-\Delta T$) in the PE pyrolysis temperatures as a result of the respective catalysts.

At 3wt% catalyst, Fresh CAT and Fresh fines lowered $T_{1\%}$ by approximately 26 and 22 %, respectively, whereas A-ECAT and S-ECAT lowered $T_{1\%}$ by approximately 12 and 14%, respectively. However, at higher catalyst weight fractions the performance of the fresh catalysts is similar to the equilibrium catalysts. Additionally, $T_{99\%}$ decreased with increasing catalyst weight fraction for all the catalysts.

Table 4.4 Performance of FCC catalysts at onset and end of PE degradation.

Sample	1% Conversion		99% Conversion	
	$T_{1\%}$	-ΔT (%)	$T_{99\%}$ (°C)	-ΔT (%)
Virgin HDPE	416	0	497	0
3 wt% S-ECAT	359	14	478	4
8 wt% S-ECAT	316	24	457	8
13 wt% S-ECAT	282	32	441	11
3 wt% Fresh CAT	308	26	488	2
8wt% Fresh CAT	289	31	484	3
13 wt% Fresh CAT	273	34	479	4
3wt% Fresh Fines	323	22	490	1
8wt % Fresh Fines	294	29	486	2
13wt% Fresh Fines	279	33	479	3
3wt% A- ECAT	368	12	483	3
8wt% A- ECAT	324	22	469	6
13wt% A- ECAT	316	24	457	8

The results also show the degradation temperature range did not significantly decrease for the fresh catalysts, unlike with the spent catalysts. Amongst the used catalysts, it seems that S-ECAT performs better than A-ECAT in PE pyrolysis, most likely for the same reason that it does with PP pyrolysis.

As expected, the fresh FCC catalysts enhance degradation at lower temperatures in comparison to the spent catalysts. Interestingly, this is not the case at higher temperatures, where the spent catalysts exhibit higher conversion, evidenced by the apparent crossing of the TG curves at temperatures between 400 and 450°C. This may be explained by different conversion rates observed for the various catalysts. The effect of catalyst weight on the maximum rate of conversion (α_{max}) and degradation temperature (T_{max}) is reported in Table 4.5. Also shown are the changes in the PE pyrolysis temperatures ($-\Delta T_{max}$) as a result of the respective catalysts.

Table 4.5 Temperature and conversion at maximum rate of degradation of PE

Sample	T_{max} (^{o}C)	$-\Delta T_{max}$	α_{max} (%)
Virgin HDPE	478	0.0	64
3 wt% S-ECAT	463	3.0	63
8 wt% S-ECAT	448	6.2	81
13 wt% S-ECAT	435	9.0	90
3 wt% Fresh CAT	472	1.2	67
8wt% Fresh CAT	465	2.7	75
13 wt% Fresh CAT	463	3.2	87
3wt% Fresh Fines	471	1.4	56
8wt % Fresh Fines	469	1.7	76
13wt% Fresh Fines	458	4.0	77
3wt% A-ECAT	468	2.1	64
8wt% A-ECAT	459	3.8	83
13wt% A-ECAT	450	5.8	87

Table 4.5 shows that T_{max} decreases with catalyst weight, as was observed with PP; however, it does not change significantly with increasing catalyst weight fraction for the fresh catalysts. Unlike with PP, a clearer trend is observed between α_{max} and the catalyst weight fraction. By increasing the amount of catalyst in the sample, the rate of conversion to

volatiles is increased. However, when compared to PP pyrolysis, the values of α_{max} observed here are relatively lower. As discussed in Chapter 2, radical chain mechanism is widely accepted as the reaction mechanism for polyolefin pyrolysis. Among the steps postulated, hydrogen abstractions, followed by beta scissions are the important steps in the generation of volatiles [31, 210]. Due to the presence of methyl groups, the intra-molecular transfer of hydrogen is preferred in PP over PE [211].Thus, higher conversions to volatiles can be achieved in PP pyrolysis.

A linear relationship between T_{max} and catalyst weight fraction was also observed with all four FCC catalysts as shown in Figure 4.7 and Table 4.6. S-ECAT data shows the most linearity.

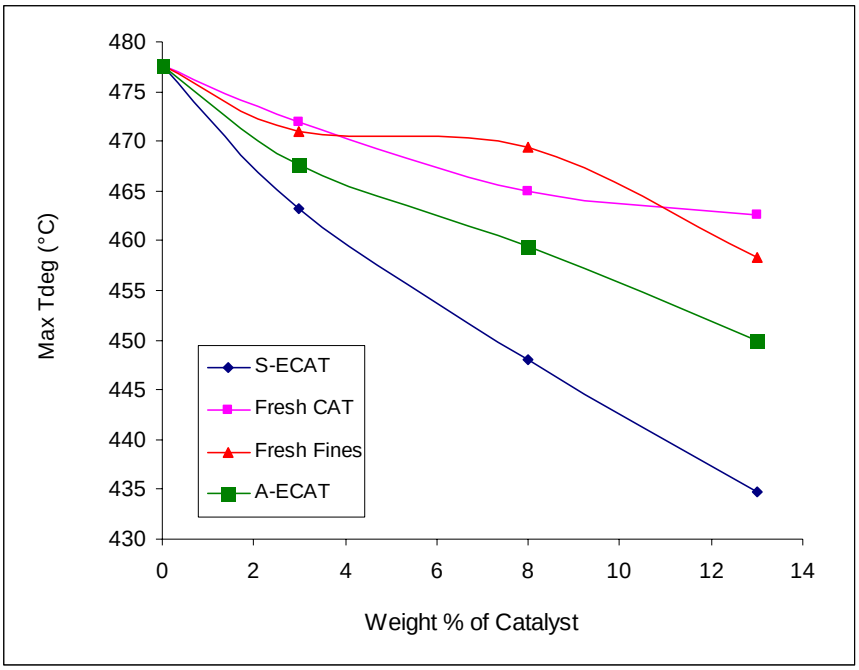

Figure 4.7 Effect of catalyst weight fraction on T_{max} in PE degradation

Table 4.6 Linear correlation of maximum degradation temperature with catalyst weight fraction

Catalyst	r[a]	Linear Equation
S-ECAT	0.9853	-3.2294x + 475.29
Fresh CAT	0.9385	-1.1611x + 476.27
Fresh Fines	0.9209	-1.3453x + 477.17
A-ECAT	0.9814	-2.0522x + 475.96

[a] correlation coefficient

4.4 Performance of FCC Catalysts and $CaCO_3$ in PP-PCC Degradation

The performance of the FCC catalysts, as well as $CaCO_3$, a filler component in the carpet adhesives, was assessed in the TG degradation of polypropylene post-consumer carpet, PP-PCC, at 97 and 92 wt% of PP-PCC. Results are shown in Figures 4.8 (a) and 4.8 (b) for 97 and 92 wt% PP-PCC respectively.

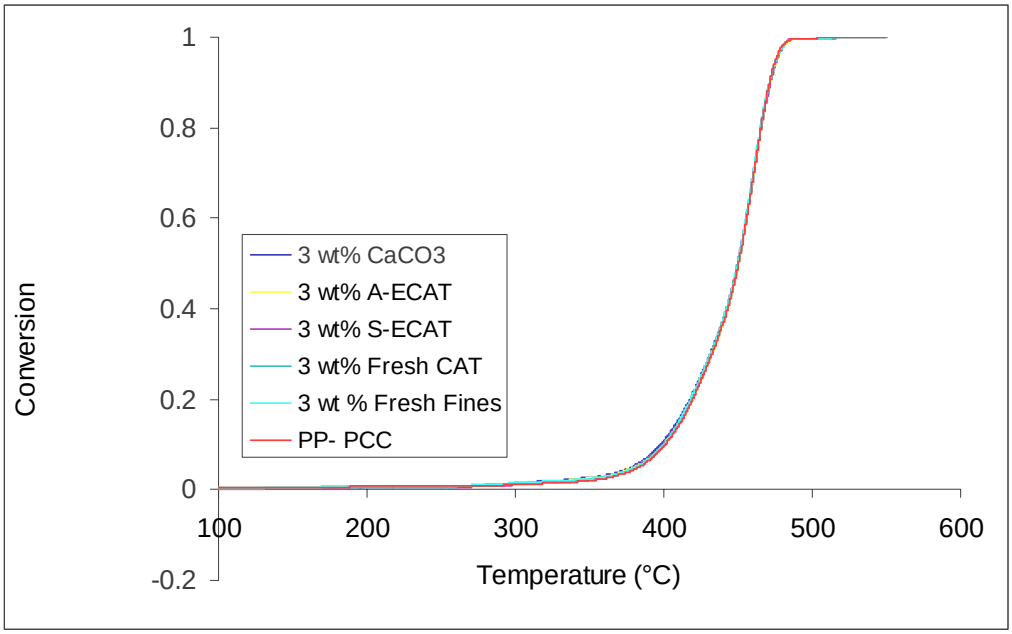

Figure 4.8 (a) TG plot of FCC catalysts and $CaCO_3$ in the PP-PCC pyrolysis at 97 wt% of PP- PCC

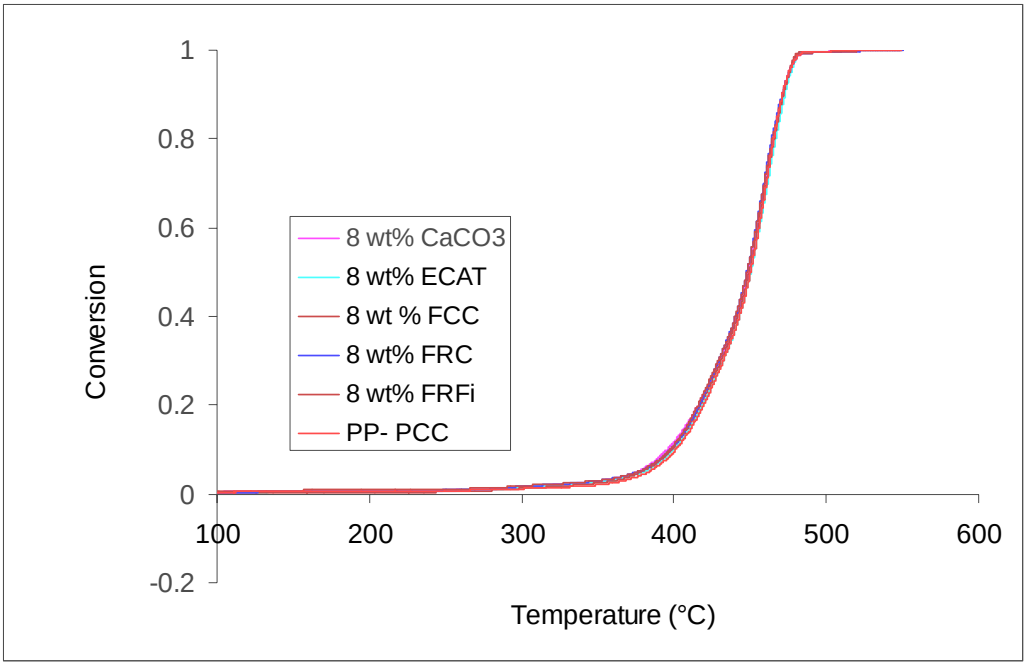

Figure 4.8b TG plot of FCC catalysts and $CaCO_3$ in PP-PCC pyrolysis at 92 wt% of PP-PCC

The TG plots in Figures 4.8 (a) and 4.8 (b) show a slight reduction in T_{onset} amongst the various catalysts. The individual effect of the catalysts on PCC degradation is not clear. Consequently, a better analysis would be to observe quantitative data. Thus, temperatures at 1% conversion and % decrease from the pure PCC are shown in Table 4.7

At 3wt %, all the catalysts including $CaCO_3$ showed minimal catalytic effect in thermal degradation of PP-PCC. However, at 8 wt%, T_{onset} was further decreased. Although $CaCO_3$ is a solid base, it was found to be more effective than the equilibrium catalysts in lowering $T_{onset.}$ S-ECAT did not enhance the PCC pyrolysis at 3 and 8 wt% at all. The decreased activity of the acidic catalysts may be caused by the neutralization of the acidic sites by the original $CaCO_3$ content in the PP-PCC.

Table 4.7 Performance of FCC catalysts and $CaCO_3$ on the onset of PP PCC degradation.

Sample	$T_{1\%}$ (°C)	-ΔT (%)
PP PCC	288	0
Pure PP	370	-62
3wt% $CaCO_3$	275	5
8wt% $CaCO_3$	271	6
3wt% S-ECAT	294	-2
8wt% S-ECAT	289	-1
3 wt% Fresh CAT	286	1
8wt% Fresh CAT	265	8
3wt% Fresh Fines	263	8
8wt% Fresh Fines	235	19
3wt% A-ECAT	284	1
8wt% A-ECAT	275	5

Furthermore, since the PP-PCC is waste, it could be contaminated with unknown materials that could deactivate the acidic sites on the FCC catalysts. Overall, the Fresh FCC Fines were the most effective, particularly at 3 wt%; however, its activity on the waste PP was reduced by half compared to the pure PP. It is possible that at much higher catalyst fractions, increased rates of degradation of PP-PCC may be observed.

On the other hand, the overall degradation temperature range for PP-PCC pyrolysis is similar to the ranges observed for the catalytic pyrolysis of PP. T_{onset} for the PP PCC waste was found to be significantly lower than the value observed with the pyrolysis of pure PP (see Table 4.7). This is an indication that waste polymers can be pyrolyzed at relatively lower temperatures than the virgin polymer.

4.5. Estimation of Rate Equations for PP and PE Degradation

4.5.1 Rate Equation for PP Degradation

The kinetic parameters, activation energy (E_a) and the pre-exponential factor (A), were estimated for the catalytic pyrolysis of PP by the various FCC catalysts. On this basis, a comparison of the activities amongst the FCC catalysts was performed. The methods used in this kinetic analysis are the dynamic isoconversion method (an integral method) and the Arrhenius relationship (a differential method), which were described in Chapter 3.

4.5.1.1 Estimating E_a and A by the Arrhenius Equation

The kinetic parameters were estimated for the samples containing 8 wt % of FCC catalysts (S-ECAT, Fresh Fines, Fresh CAT and A-ECAT). Similarly, E_a and A were also estimated for samples containing 3, 8 and 13 wt% of S-ECAT. The latter was done to compare the effect of catalyst weight on the kinetics as well as to compare the Arrhenius method parameters obtained with those obtained by the isoconversion method. As was discussed in Chapter 3, only data in the range of 4 - 40% conversion was utilized in this analysis

Figures 4.9 and 4.10 are plots of ln k versus T^{-1} for virgin PP and Fresh Fines (k is the rate constant estimated at each weight loss step). The plots show data at four different heating rates (β = 3, 6, 10 and 15°C/min) and the run at 10°C/min was repeated to check for repeatability of the data. Similar plots were generated for the other samples (See Figures B.1 – B.5 in Appendix B).

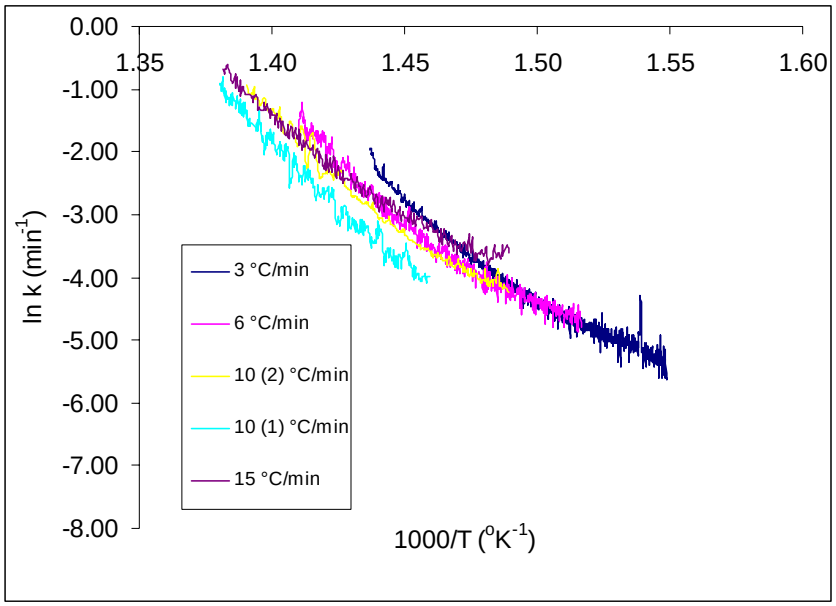

Figure 4.9 Arrhenius plot for the degradation of virgin PP

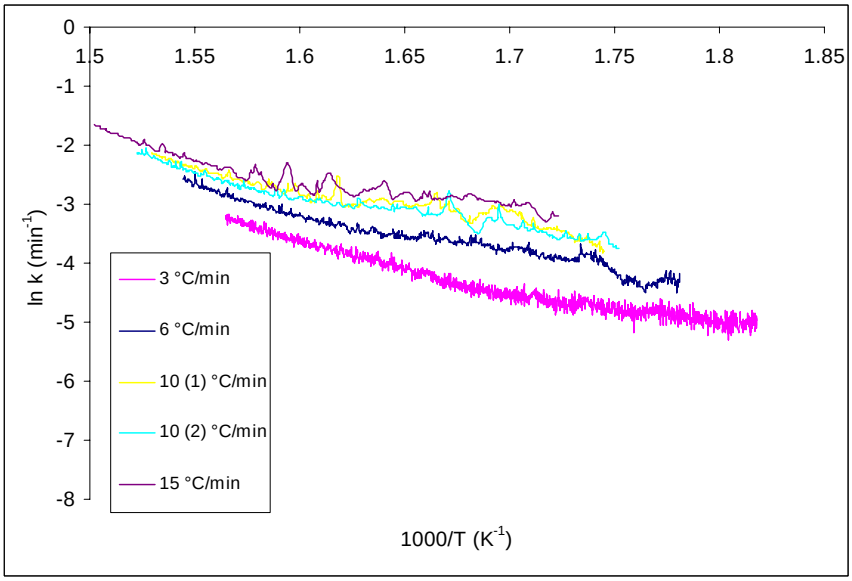

Figure 4.10 Arrhenius plot for the catalytic degradation of PP using 8 wt% Fresh Fines

The irregularity in the plotted data is partly attributed to the dynamic measurement of TG data. Also, the plots do not appear smooth because the noise in the data becomes pronounced when the derivatives are considered. (In addition, it was found the best linear fits were

obtained for the range of 4-40% conversion). Linear correlation coefficients of 0.92 and better were observed (except for 8 wt% Fresh Fines at 15°C/min, r = 0.894) for all the Arrhenius plots. Nevertheless, the plots were presumed to be linear for this kinetic analysis.

Table 4.8 summarizes the results obtained for PP degradation at 8 wt% of the FCC catalysts. These have reported values have been averaged over the different heating rates. The kinetic parameters, including correlation coefficients for the Arrhenius plots at each heating rate can be found in Table B.1 of Appendix B.

Table 4.8 Average kinetic parameters for PP degradation using 8 wt % of FCC catalysts. The Arrhenius equation method was applied for conversion range of 4- 40%

Catalyst	Catalyst[a] (% w/w)	E_a (kJ/mol)	ln A (min^{-1})
Virgin PP	0	250 ± 18	40 ± 3
Fresh CAT	8	120 ± 17	19 ± 4
Fresh Fines	8	53 ± 4	7 ± 0.4
A-ECAT	8	215 ± 16	36 ± 3
S-ECAT	8	173 ± 18	29 ± 3

[a] Measured weight fraction

Literature reports an E_a within the range of 170-250 kJ/mol for thermal pyrolysis of virgin PP, as was summarized in Table of 2.5. This range is attributed to the different kinetic analysis methods applied as well as the variance in the PP material properties. Nevertheless, Table 4.8 shows that a value within this range was obtained for the non-catalytic pyrolysis of PP.

An additional observation is the sharp lowering of the activation energy by employing the FCC catalysts, more so for the fresh catalysts than the E-CATs. The lowering of E_a with increasing catalytic activity of solid acids catalysts (ZSM-5, BEA) was also observed by Durmus et. al. [207].

It was also found that the apparent E_a increased with β.This occurs because when β is increased, degradation onset is shifted to a higher temperature range (see Figures B.6 – B.10 in Appendix B). This increased temperature range is needed to overcome the higher activation energy observed. This observation is common with dynamic TG measurements in literature [179, 209]. Furthermore, it was found that an increase in E_a was followed by a concurrent increase in A. This is a common observation with dynamic TG analysis of polymer degradation and is generally attributed to the 'compensation effect' (change in E_a may be compensated by a change in A) [212].

Using the average kinetic parameters, rate constants were derived at temperatures between 200-375°C using Equation 1.

$$k = A\exp\left(-\frac{E_a}{RT}\right) \qquad (1)$$

This range was chosen based on the observed catalytic degradation range in the weight loss curves for PP pyrolysis seen earlier. A plot of the derived rate constants for all the FCC catalysts in PP pyrolysis is shown in Figure 4.11.

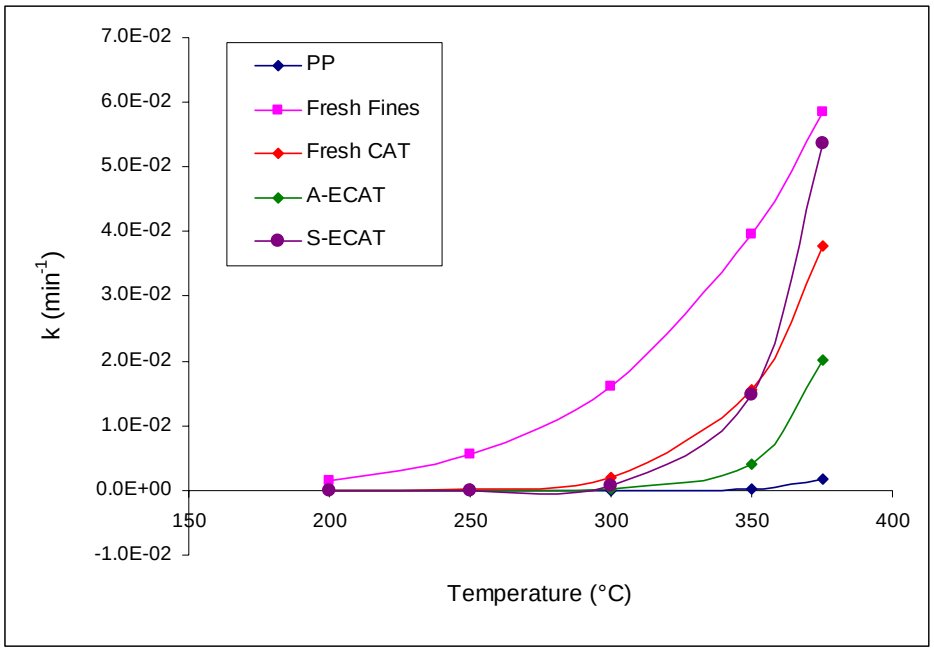

Figure 4.11 Plot of the rate constant, k, versus temperature for the catalytic pyrolysis of PP by FCC catalysts. The kinetic parameters were derived by the Arrhenius method.

Figure 4.11 clearly indicates Fresh Fines as the most active fresh catalyst and S-ECAT as the most active equilibrium catalyst in PP pyrolysis within the specified temperature range. Conversely, at higher temperatures (above 400°C), the rates of reactions for the used catalyst (A-ECAT) seems to surpass that of the fresh catalysts. This is shown by the values listed in Table 4.9, which describes relationship between catalyst activity and temperature, by comparing k/k_{PP} amongst the different catalysts (where, k and k_{PP} are the rate constants for the catalyzed and pure PP sample).

Table 4.9 Rate constant ratios at temperatures between 200 and 400°C

T (°C)	k/k_{PP}			
	8 wt % Fresh Fines	8 wt % Fresh CAT	8 wt % A-ECAT	8 wt % S-ECAT
200	2.7E+07	1.7E+05	1.3E+02	3.4E+02
250	2.2E+05	7.3E+03	5.7E+01	5.1E+01
300	4.2E+03	5.4E+02	2.8E+01	1.1E+01
350	1.5E+02	6.0E+01	1.6E+01	2.9E+00
375	3.5E+01	2.3E+01	1.2E+01	1.6E+00
400	9.1E+00	9.3E+00	9.5E+00	9.4E-01

The higher rates observed for the equilibrium catalysts above 400°C may be attributed to the variation of the estimated kinetic parameters and the use of a respective average value. Also, since a conversion range of only 4 – 40% conversion was used in the analysis, an extrapolation of the data over a larger temperature/conversion range may lead to a propagation of error.

Based on a first order kinetic model, the half-life of PP at 400°C was estimated to be 75 minutes. This value is reduced to approximately 8 minutes for both Fresh FCC catalysts, and 8 and 5 minutes for the A-ECAT and S-ECAT, respectively.

Similarly, the average kinetic parameters for PP degradation using varying weight fractions of S-ECAT are summarized in Table 4.10. The kinetic parameters, including correlation coefficients for the Arrhenius plots at each heating rate, can be found in Table B.2 of Appendix B.

Table 4.10 Average kinetic parameters for PP degradation using varying weight fractions of S-ECAT. The Arrhenius equation method was applied for a conversion range of 4- 40%

Catalyst[a] (% w/w)	E_a (kJ/mol)	ln A (min^{-1})	r[b]
0	250 ± 18	41 ± 3	0.97 ± 0.007
3	300 ± 15	49 ± 3	0.97 ± 0.004
8	172 ± 18	29 ± 3	0.98 ± 0 .007
13	142 ± 12	24 ± 2	0.98 ± 0.004

[a] Measured weight fraction
[b] Linear correlation coefficient

The results also show a lowering of E_a and ln A, most significantly at 8 and 13 wt % of S-ECAT. However, it shows a higher E_a value for 3 wt% than with the pure polymer, even though S-ECAT at 3wt% showed a reduction in the onset of degradation. On the other hand, the change is compensated by a subsequent increase in A, which should ultimately affect the rate of the pyrolysis reaction, as shown by the degradation curves presented in Section 4.2.

Similarly, a plot of the rate constants for the reaction at different weight fractions of S-ECAT is shown in Figure 4.12. A significant increase in the rate constants commences around 300°C for 8 and 13 wt % of S-ECAT. This observation was also made in Section 4.5. It was shown that the temperatures at 1% conversion for both weight fractions begins at approximately 300°C; whereas, at 3 wt% of S-ECAT, degradation commences at 350 °C, which also coincides with the rates shown in Figure 4.12.

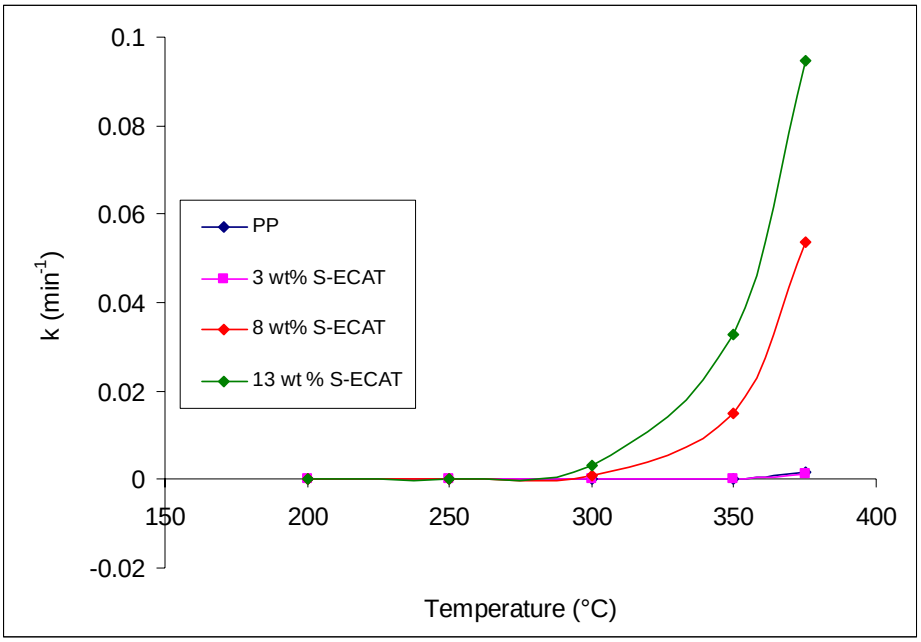

Figure 4.12 A plot of the rate constant, k versus temperature for PP pyrolysis using S-ECAT. The kinetic parameters were derived by the Arrhenius method

At 400°C, the 3 wt % showed comparable rates to the non-catalytic ($k/k_{PP} = 1$); whereas, rates for 8 wt% and 13 wt% of S-ECAT were calculated to be 19 and 27 times faster, respectively.

The half-life of PP pyrolysis at 400°C was estimated to be approximately 70 minutes for a 3wt % fraction versus, 4 and 3 minutes for 8 wt% and 13 wt% of the fresh FCC catalysts. The value at 3wt % is very similar to that obtained for the pure PP sample (75 minutes). Nevertheless, PP pyrolysis rate seems to increase with increasing catalyst concentration.

4.5.1.2 Estimating E_a and A by the Isoconversion method

Estimation of kinetic parameters for the catalytic pyrolysis of PP was carried out using the isoconversion method within a range of 5 – 15% conversion and at heating rates of 3, 6, 10

and 15 °C/min. The TG plots at different heating rates can be found in Figures B.6 – B.11 of Appendix B. All runs at 10°C/min were repeated.

The isoconversion plots obtained for virgin PP and Fresh Fines are shown in Figures 4.13 and 4.14, respectively. Similar plots were generated for the other samples (See Figures B.12 – B.16 Appendix B). In generating the isoconversion plot for virgin PP, the values at 15°C/min were omitted because these data points generated non-linear fits.

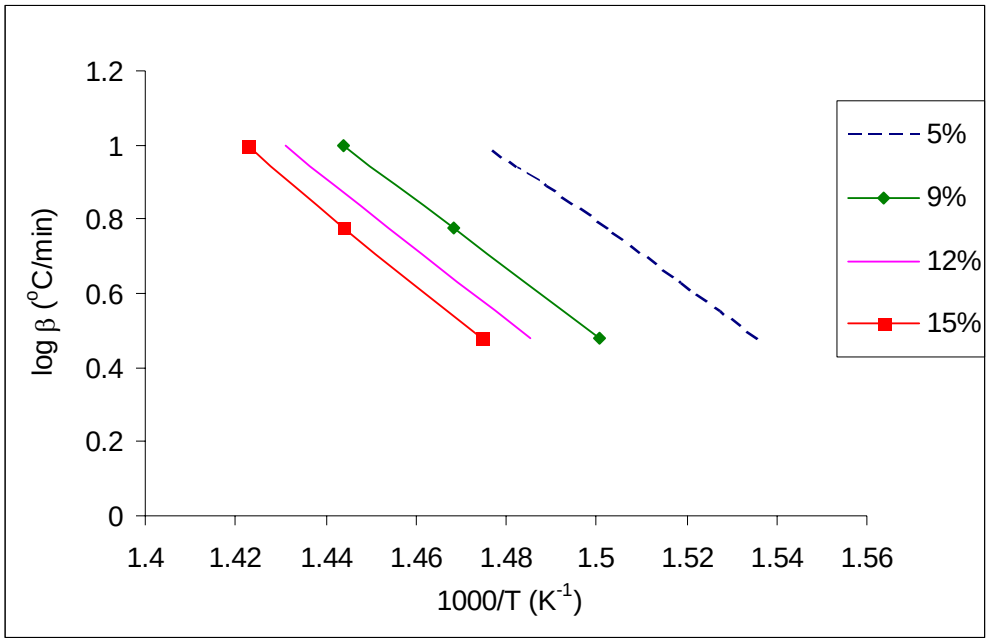

Figure 4.13 Isoconversion TG data analysis method. Plot of log β versus T^{-1} for Virgin PP.

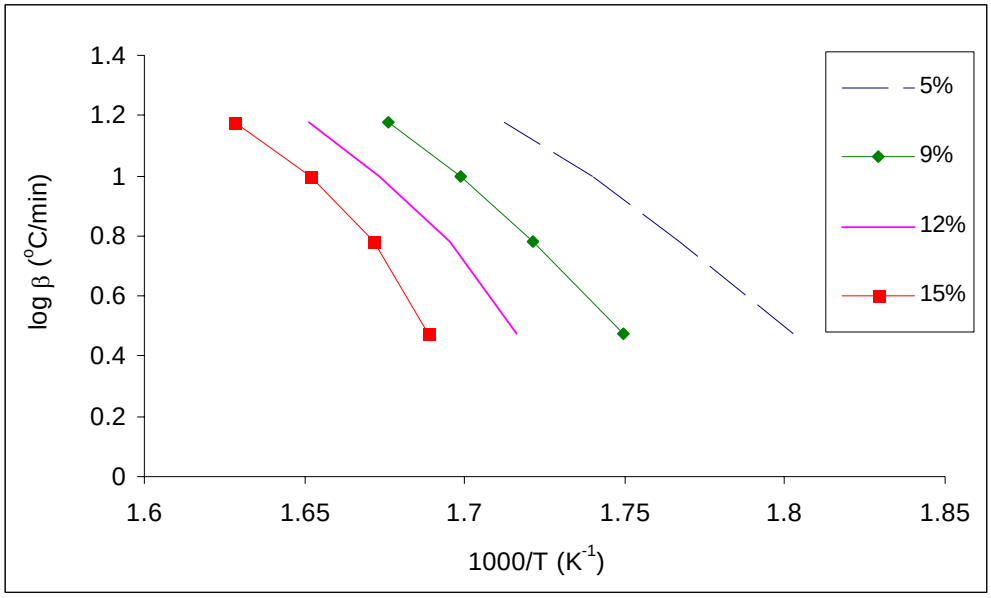

Figure 4.14 Isoconversion TG data analysis method. Plot of log β versus T^{-1} for 8 wt % Fresh fines.

For all samples, both E_a and ln A increased with conversion. Again, this is as a result of the dynamic measurement of TG. Based on the isoconversion TG analysis, averaged values of the kinetic parameters were obtained at 92 wt % of polymer using the FCC catalysts are summarized in Tables 4.11. Literature reports an E_a within the range 170 - 250 kJ/mol for the pyrolysis of virgin PP, as was indicated in Chapter 2. The value of E_a estimated in this case falls within that range.

The rate constants were derived using Equation 1 for the catalytic pyrolysis of PP. The results are plotted in Figure 4.15 for temperatures between 200 – 375°C.

Table 4.11 Apparent kinetic parameters estimated by the isoconversion method for the catalytic pyrolysis of PP using 8 wt % FCC Catalysts.

	E_a (kJ/mol)	ln A (min^{-1})
Virgin PP[a]	170 ± 8	27 ± 3
8 wt % Fresh CAT	150 ± 6	25 ± 1
8 wt % Fresh Fines	180 ± 30	34 ± 5
8 wt% A-ECAT	154 ± 5	25 ± 1
8 wt % S-ECAT	108 ± 8	17 ± 1

[a] conversions at 15 °C/min were omitted

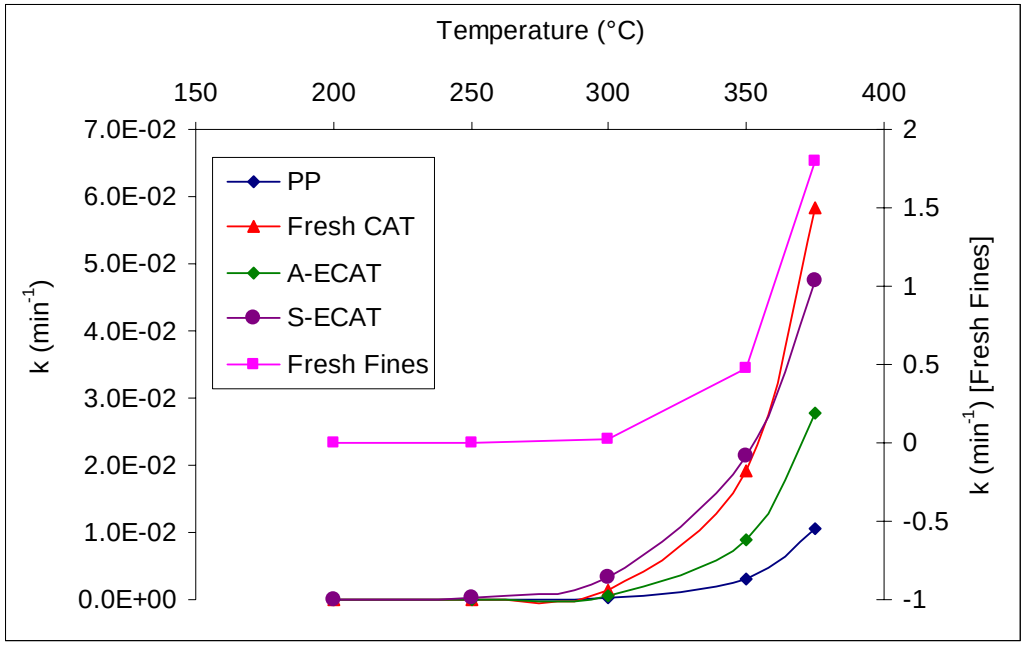

Figure 4.15 Plot of the rate constant, k versus temperature for the TG pyrolysis of PP using FCC catalysts. The kinetic parameters were obtained by the Isoconversion method.

As with the Arrhenius method, Figure 4.15 shows the Fresh Fines as the most active fresh catalyst and S-ECAT as the most active equilibrium catalyst in PP pyrolysis within the specified temperature range. Furthermore, the activity of the various catalysts is further

compared in Table 4.12, which compares k/k_{PP} amongst the different catalysts (where k and k_{PP} are the rate constants for the catalyzed and pure PP sample).

Table 4.12 Rate constant ratios between 200 and 400°C

T (°C)	Rate Constant Ratios, k/k_{PP}			
	Fresh Fines	Fresh CAT	A-ECAT	S-ECAT
200	8.6E+01	2.2E+01	7.9E+00	3.2E+02
250	1.1E+02	1.3E+01	5.4E+00	7.1E+01
300	1.3E+02	9.0E+00	3.9E+00	2.0E+01
350	1.6E+02	6.4E+00	3.0E+00	7.2E+00
375	1.7E+02	5.5E+00	2.6E+00	4.5E+00
400	1.8E+02	4.8E+00	2.4E+00	2.9E+00

Table 4.12 shows that at 400°C, the PP degradation rate with the Fresh Fines was approximately 180 times faster than the non-catalytic path. Moreover, the rates the reactions using Fresh CAT and the spent catalysts were observed to be comparable. Although, the Fresh Fines have been identified as the most active, the results of this analysis seem to amplify the rates of the Fresh Fines.

Similar trends were observed in assessing the effect of catalyst weight on the pyrolysis kinetics. The average kinetic parameters for PP degradation using varying weight fraction of S-ECAT is summarized in Table 4.13. Similar to the Arrhenius method, the results showed a lowering of E_a and ln A, most significantly at 8 and 13 wt % of S-ECAT. Both E_a and A are higher at 3 wt% of catalyst than at 0 wt %, however, this is compensated by a concurrent increase in A. Thus the rates at 3 wt% may actually be higher than the virgin PP.

Table 4.13 Apparent kinetic parameters for variation of S-ECAT in PP sample by the isoconversion method

	Ea (kJ/mol)	ln A (min^{-1})
Virgin PP[a]	170 ± 8	27 ± 3
3 wt % S-ECAT	203 ± 4	33 ± 1
8 wt % S-ECAT	108 ± 8	17 ± 1
13 wt % S-ECAT	119 ± 9	20 ± 1

[a] conversions at 15 °C/min were omitted for Virgin PP

Likewise, although E_a is lower at 8wt% than 13wt% of S-ECAT, the calculated rate constants indicate that the reaction rate increase with increasing catalyst weight fraction. A plot of the derived rate constants for all the varying weight fractions of S-ECAT in PP pyrolysis is shown in Figure 4.16.

Figure 4.16 shows a significant increase in the rate constants commencing around 300°C for 8 and 13 wt % of S-ECAT. At 400°C, the 3 wt % showed comparable rates to the non-catalytic ($k/k_{PP} = 1$), whereas, rates for 8 wt% and 13 wt% of S-ECAT were calculated to be 3 and 8 times faster, respectively. The half-life of PP pyrolysis at 400°C was estimated to be approximately 18 minutes for a 3wt % fraction versus, 7 and 3 minutes for 8 wt% and 13 wt% of the fresh FCC catalysts. The value at 3wt % is very similar to that obtained for the pure PP sample (20 minutes). Nevertheless, PP pyrolysis rate clearly increases with increasing catalyst concentration.

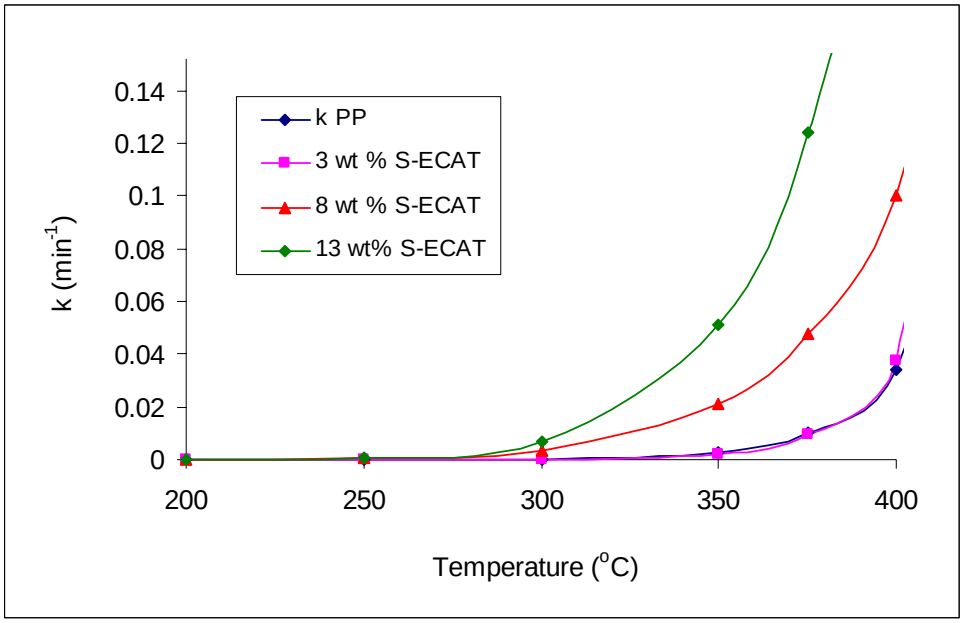

Figure 4.16 A plot of the rate constant, k versus temperature for PP pyrolysis using S-ECAT. The kinetic parameters were derived by the Isoconversion method

The observations made with the Fresh Fines and Fresh CAT may indicate that the isoconversion method may not be appropriate for describing the kinetics for catalyzed polyolefin pyrolysis at a suitable temperature range. This may be due to the use of an approximation to the time-dependent - temperature integral [204]**.** This implies that while certain permissible assumptions could be made in the kinetic analysis of dynamic TG data, the application of the resulting rate equations to a reactor design must be carefully considered.

4.5.1.3 Simulation of weight loss plots

In further assessing the applicability of the calculated kinetic parameters in PP pyrolysis, TG plots were simulated based on the average parameters and then compared with the actual weight loss curves. Equation 2 and 3 were utilized in generating the simulated curve,

$$\frac{dX}{dt} = A\exp\left(-\frac{E_a}{RT}\right)(1-X)^n \qquad (2)$$

where X is the conversion with respect to the polymer, t is the time period of degradation in minutes, $T = T_r + \beta t$ (T_r is the room temperature and β is the heating rate), n is assumed to be 1 and R is the gas constant (kJ/molK).

Assuming first order integration of Equation 2 gives an equation for the conversion as shown in Equation 3

$$X = 1 - \exp\left[At\exp\left(-\frac{E_a}{RT}\right)\right] \qquad (3)$$

Since both conversion and temperature vary with time, the actual TG data was used in simulating the weight loss curves for PP pyrolysis. A comparison of the real and calculated data is shown in Figures 4.17 - 4.20 for PP, and samples at 3 wt%, 8 wt% and 13 wt% S-ECAT, respectively. These were measured at 10 °C/min. Conversion of PP at other heating rates (3, 6 and 15 °C/min) were also simulated, and only small differences in the fittings were observed for each sample at the different heating rates, thus only the data measured at 10 °C/min are reported.

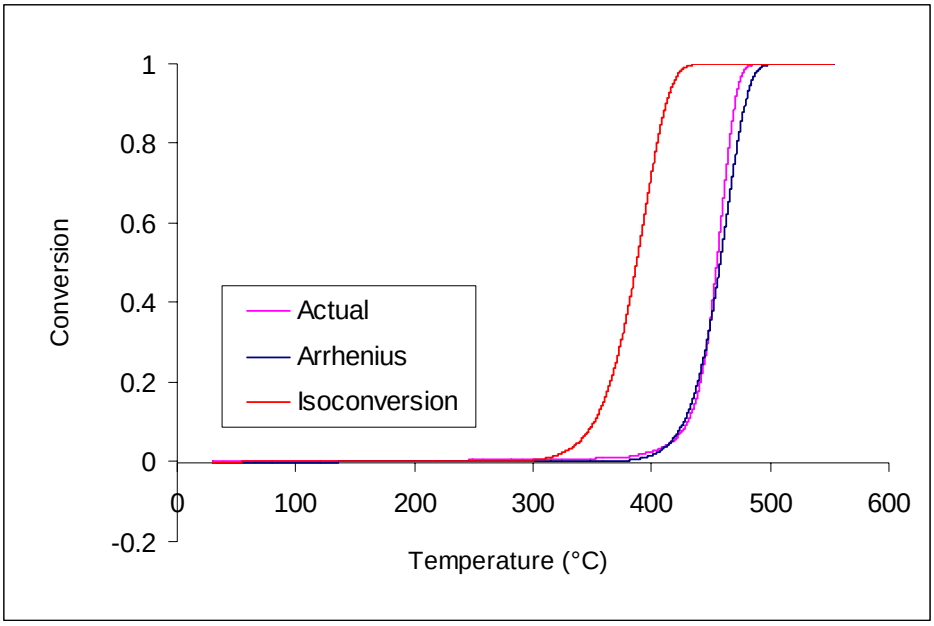

Figure 4.17 TGA simulation of PP measured at 10 °C/min. Arrhenius parameters: E_a = 250 kJ/mol and ln A = 37 min^{-1}. Isoconversion parameters: E_a = 170 kJ/mol and ln A = 27 min^{-1}

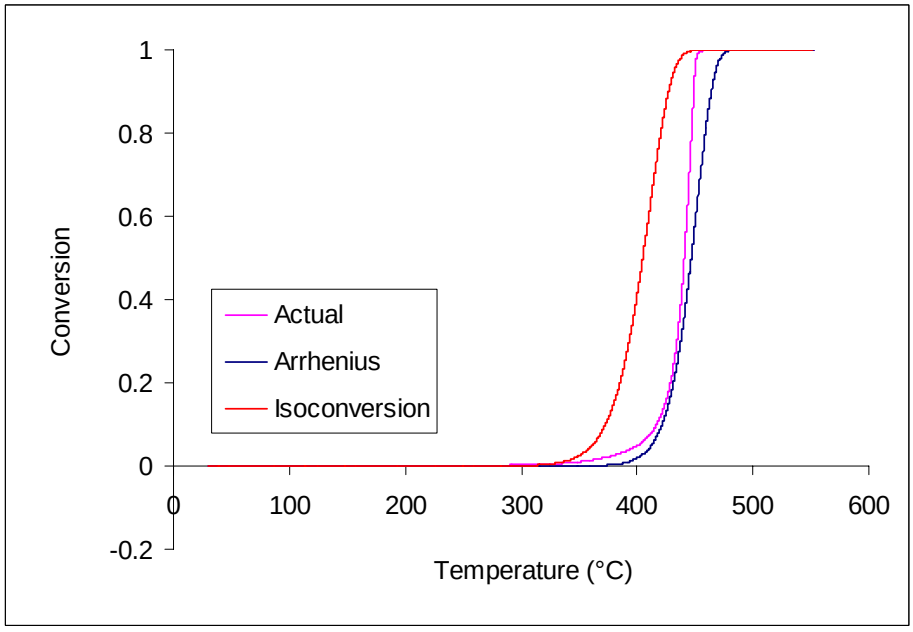

Figure 4.18 TGA simulation of PP sample containing 3 wt% of S-ECAT measured at 10 °C/min. Arrhenius parameters: E_a = 300 kJ/mol and ln A = 46 min^{-1}. Isoconversion parameters: E_a = 203 kJ/mol and ln A = 33 min^{-1}

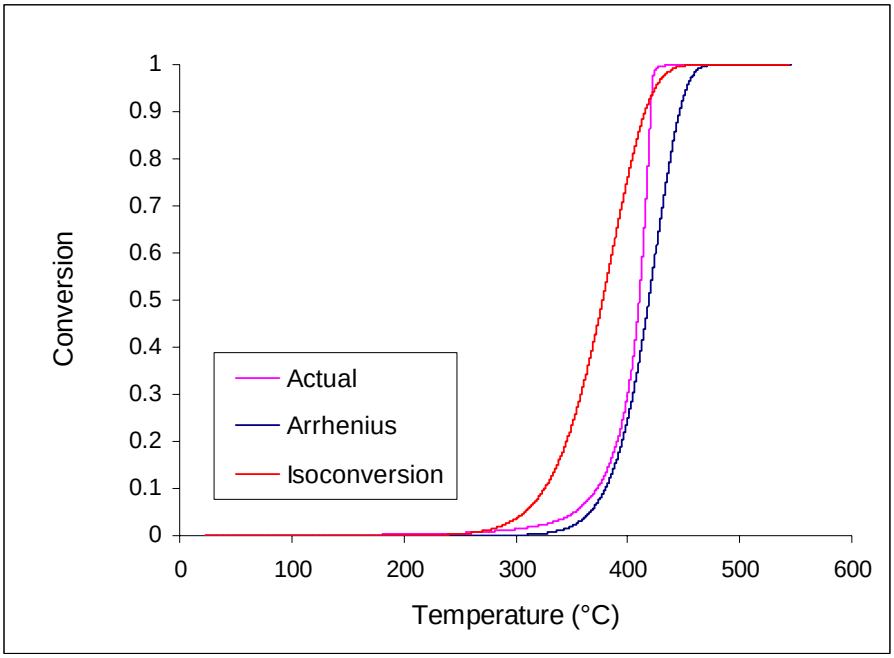

Figure 4.19 TGA simulation of PP sample containing 8 wt% of S-ECAT measured at 10 °C/min. Arrhenius parameters: E_a = 172 kJ/mol and ln A = 26 min^{-1}. Isoconversion parameters: E_a = 108 kJ/mol and ln A = 17 min^{-1}

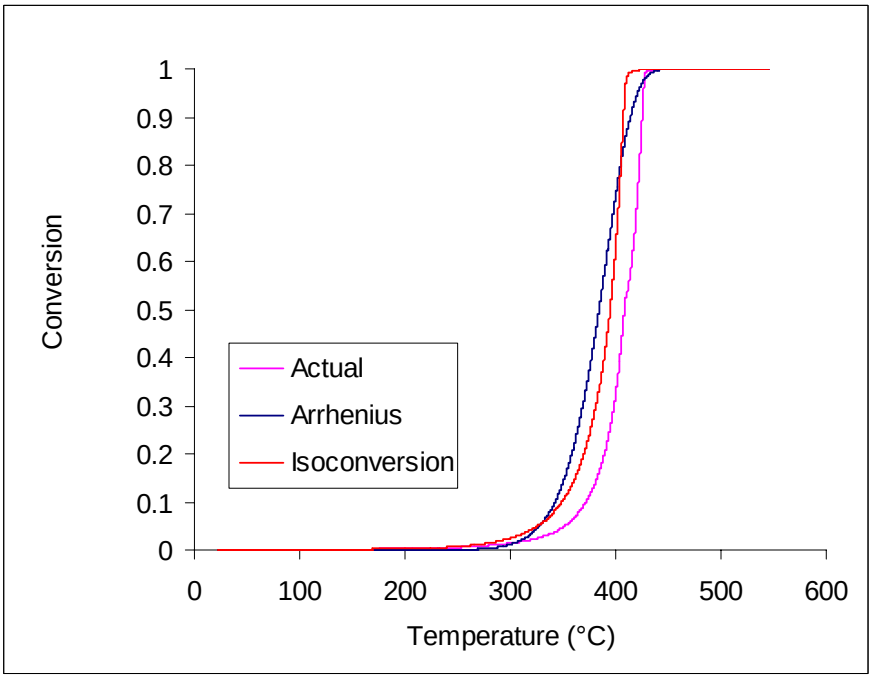

Figure 4.20 TGA simulation of PP sample containing 13 wt% of S-ECAT measured at 10 °C/min. Arrhenius parameters: E_a = 142 kJ/mol and ln A = 22 min^{-1}. Isoconversion parameters: E_a = 119 kJ/mol and ln A = 20 min^{-1}

Figures 4.17-4.20 shows a closer fit with the actual data for the curves simulated on the basis of the Arrhenius method compared to the isoconversion analysis. This may be attributed to shorter analysis range used with the isoconversion analysis, as well as the systematic error in the isoconversion method as was already mentioned. However, it is observed that deviation from the real data occurs with increasing catalyst fraction in the PP. The degradation of PP will proceed by a different pathway upon addition of catalyst. These pathways account for the increasing complexity of the degradation mechanism.

The same analysis was applied to pyrolysis data using the Fresh Fines, Fresh CAT and A-ECAT at 92 wt% of PP. The results are plotted in Figures 4.21 – 4.23 below. The plots also indicate a deviation from the real data with increasing catalytic activity.

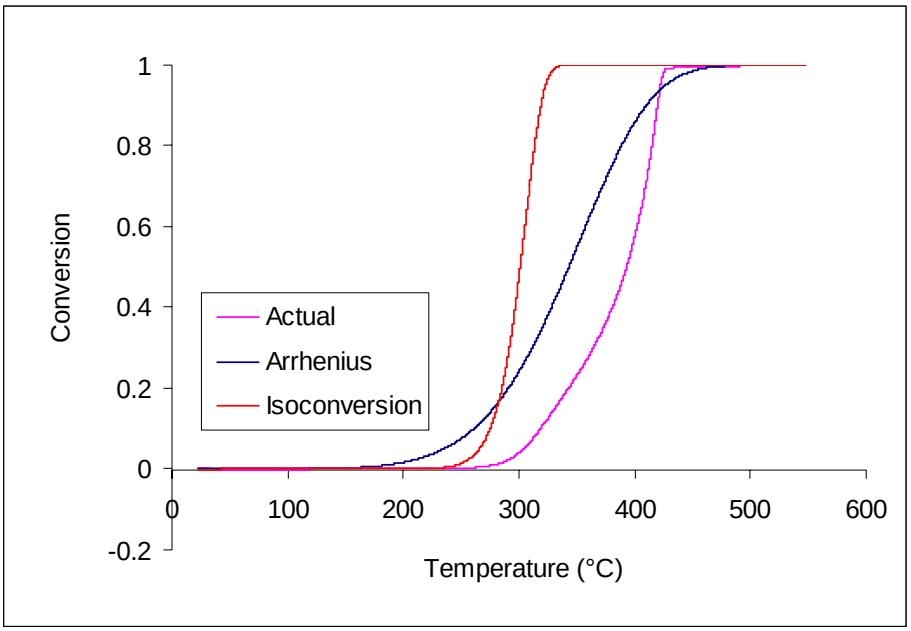

Figure 4.21 TGA simulation of PP sample containing 8 wt% of Fresh Fines measured at 10 °C/min. Arrhenius parameters: E_a = 53 kJ/mol and ln A = 6.5 min^{-1}. Isoconversion parameters: E_a = 180 kJ/mol and ln A = 34 min^{-1}

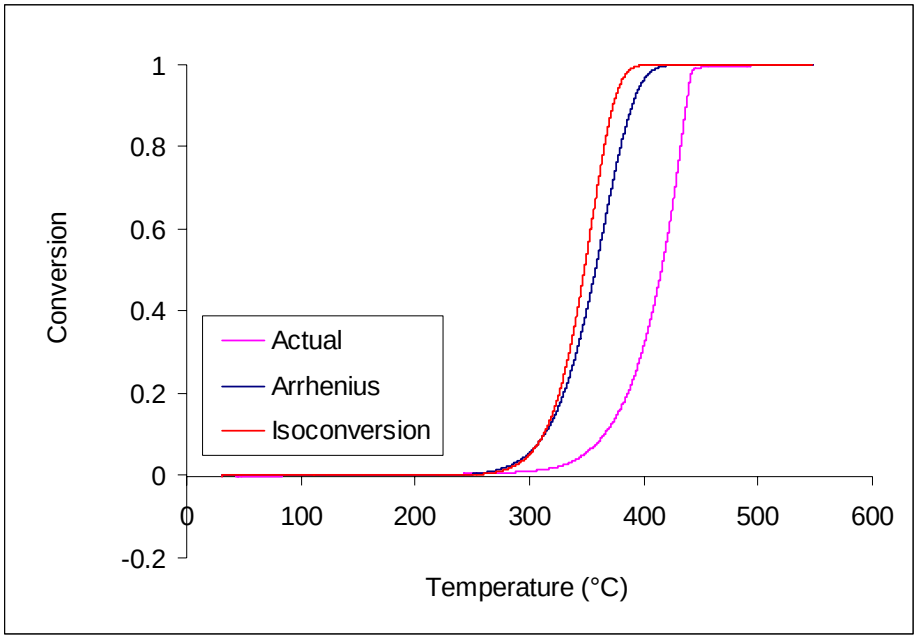

Figure 4.22 TGA simulation of PP sample containing 8 wt% of Fresh CAT measured at 10 °C/min. Arrhenius parameters: E_a = 120 kJ/mol and ln A = 19 min^{-1}. Isoconversion parameters: E_a = 150 kJ/mol and ln A = 25 min^{-1}

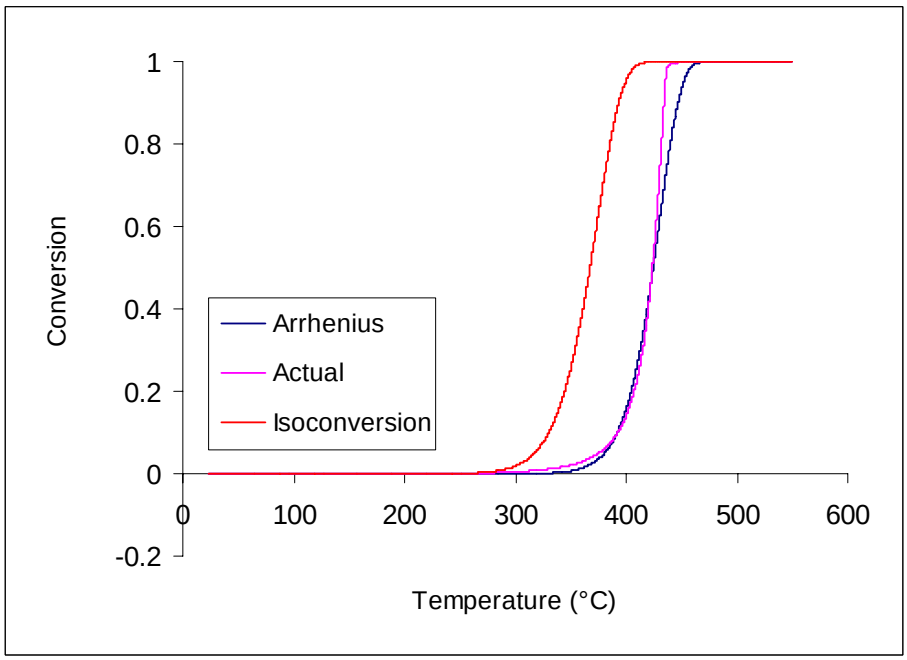

Figure 4.23 TGA simulation of PP sample containing 8 wt% of A-ECAT measured at 10 °C/min. Arrhenius parameters: E_a = 215 kJ/mol and ln A = 33 min^{-1}. Isoconversion parameters: E_a = 154kJ/mol and ln A = 25 min^{-1}

The deviation observed with the highly active catalysts may be attributed to increasing complexity of the degradation mechanism due to the addition of catalysts. Overall, the parameters estimated by the Arrhenius data, provide the best fit to the TG data, thus for the purposes of this study, it was presumed to be a more accurate estimation of catalytic PP pyrolysis over the isoconversion method.

4.5.2 Rate Equation for PE Degradation

Only the Arrhenius method was applied in the kinetic analysis for the catalytic pyrolysis of PE. Arrhenius plots were generated for samples containing 8 wt % of all four FCC catalysts. The Arrhenius plots for virgin PE and Fresh Fines samples are shown in Figures 4.24 and 4.25. Similar plots were obtained for the other samples. (Please see Figures B.17 –B.19 in Appendix B).

Table 4.14 summarizes the kinetic parameters obtained for the catalytic degradation of PE using the Arrhenius Equation including the linear regression coefficients. Table B.3 in Appendix B presents each kinetic parameter obtained at each heating rate.

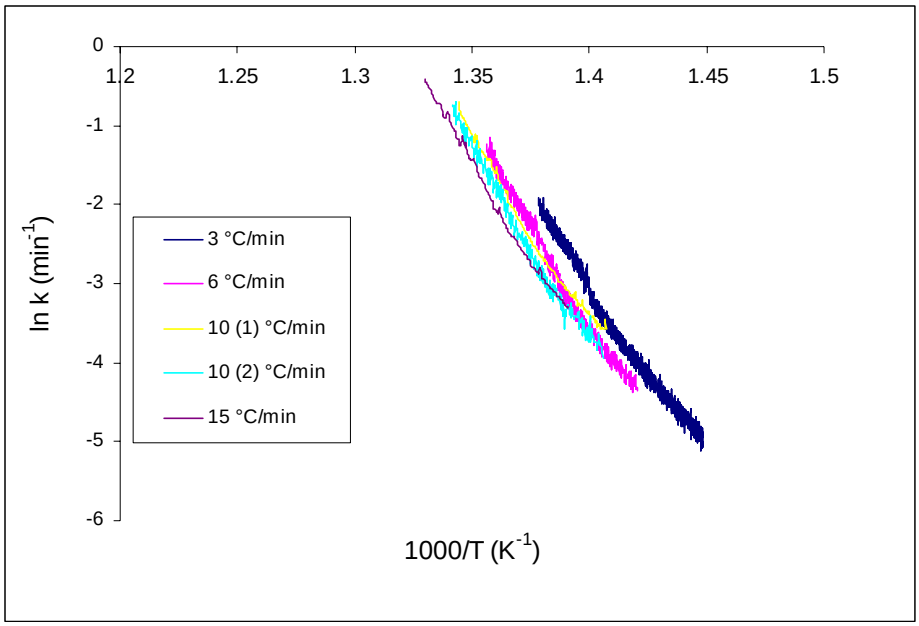

Figure 4.24 Arrhenius plot for the degradation of virgin PE

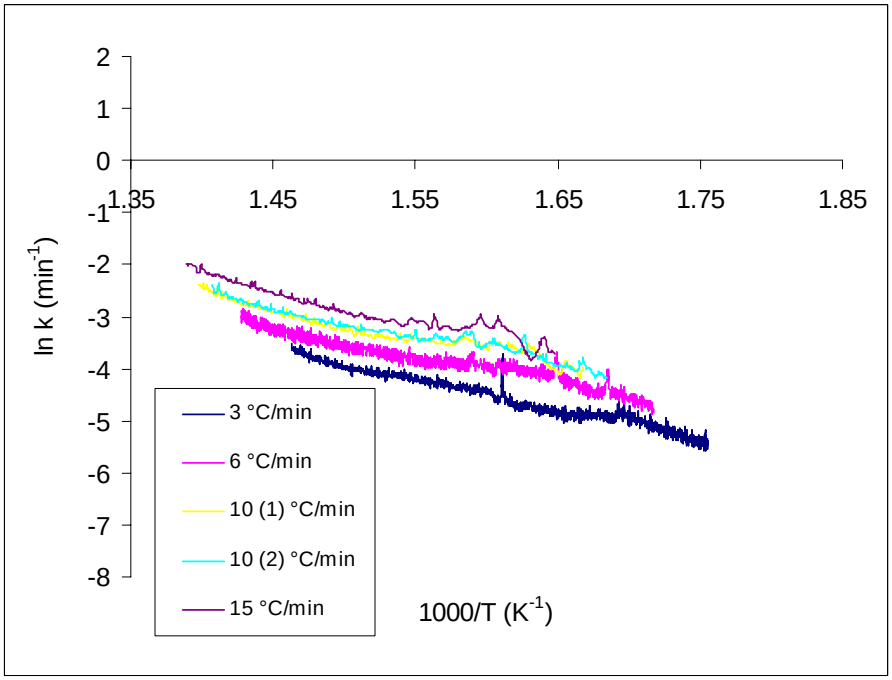

Figure 4.25 Arrhenius plot for the catalytic degradation of PE using 8 wt% Fresh Fines

Table 4.14 Estimation of kinetic parameters for the catalytic pyrolysis of PE at 8 wt % catalyst using the Arrhenius equation within a conversion range of 4- 40%

Catalyst	Catalyst[a] (% w/w)	E_a (kJ/mol)	ln A (min^{-1})	r[b]
Virgin HDPE	0	393 ± 21	56.3 ± 3	0.99 ± 0.004
Fresh CAT	8	59 ± 8	8 ± 1	0.94 ± 0.01
Fresh Fines	8	44 ± 2	8 ± 0.6	0.94 ± 0.02
ECAT	8	163 ± 9	26 ± 2	0.97 ± 0.001
Shell ECAT	8	159 ± 14	26 ± 3	0.98 ± 0.004

E_a and A varied with heating rates, with the most variation arising for the Virgin and E-CAT samples. This is because as with PP, a variation of the heating rate shifts the degradation temperature range, so that the calculated E_a values also change. This variation in E_a has also been observed in literature and similar values for both kinetic parameters were also obtained in literature for the thermal pyrolysis of PE [179]. Using the kinetic parameters, rate constants were derived at temperatures between 200-375 °C. A plot of the derived rate constants for all the FCC catalysts in PE pyrolysis is shown in Figure 4.26.

As shown in Figure 4.26, the Fresh Fines is observed as the most active fresh catalyst sample and S-ECAT as the most active equilibrium catalyst in PE pyrolysis. This can also be seen in Table 4.15, which describes this relationship between catalyst activity and temperature by comparing k/k_{PE} amongst the different catalysts (where, k and k_{PE} are the rate constants for the catalyzed and pure PE sample).

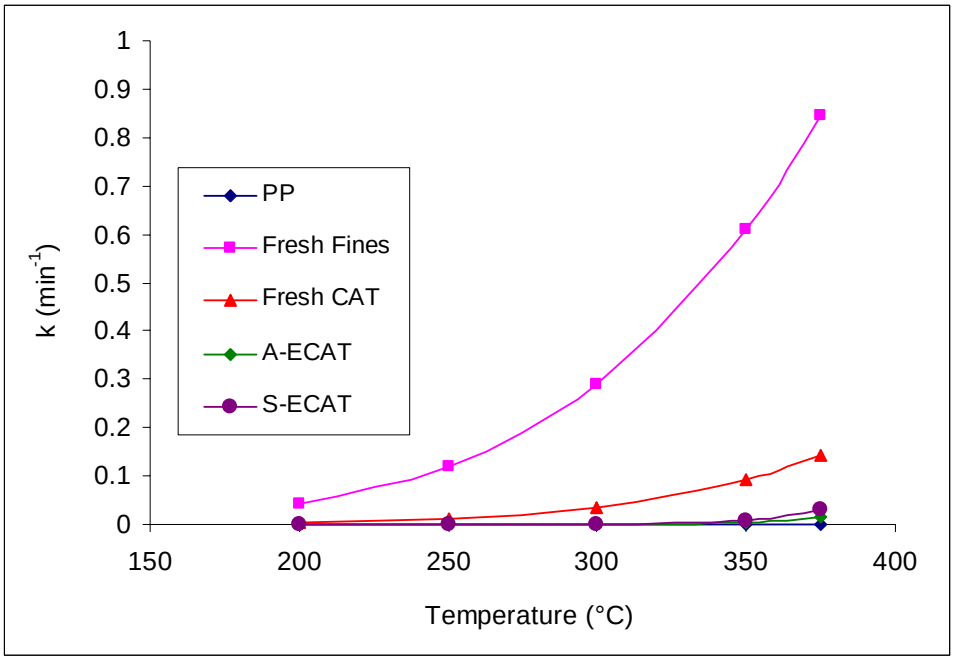

Figure 4.26 A plot of the rate constant, k versus temperature using the kinetic parameters derived by the Isoconversion method in the TG pyrolysis of PE using FCC catalysts

Table 4.15 Rate constant ratios at temperatures between 200 and 375°C

	Rate Constant Ratios, k/k_{PE}			
T(°C)	Fresh Fines	Fresh CAT	A-ECAT	S-ECAT
200	6.7E+16	1.5E+15	8.7E+11	6.5E+12
250	1.4E+13	4.4E+11	3.2E+09	2.2E+10
300	1.3E+10	5.4E+08	3.2E+07	2.0E+08
350	3.5E+07	2.0E+06	6.6E+05	3.9E+06
375	2.6E+06	1.6E+05	1.2E+05	6.8E+05

Overall, the rate equations show that the Fresh Fines as the most active catalyst in PE pyrolysis as was observed in Section 4.3.

4.6 Effect of Catalyst Contact Mode in TG Analysis of Polypropylene Degradation

Blends of PP and each of the four FCC catalysts (S-ECAT, A-ECAT, Fresh Fines and Fresh CAT) were prepared by both 'melt-mix' and 'dry- mix' methods. The procedures for each method are outlined in Chapter 3.

4.6.1 Dry Mixing: Performance of FCC catalysts

Dry mixing was carried out at 3 and 8 wt % of catalyst and each run was repeated twice. Figures 4.27 and 4.28 show the TG plots at 3 and 8 wt % of catalyst, respectively. The (1) and (2) represent a first and repeated run, respectively.

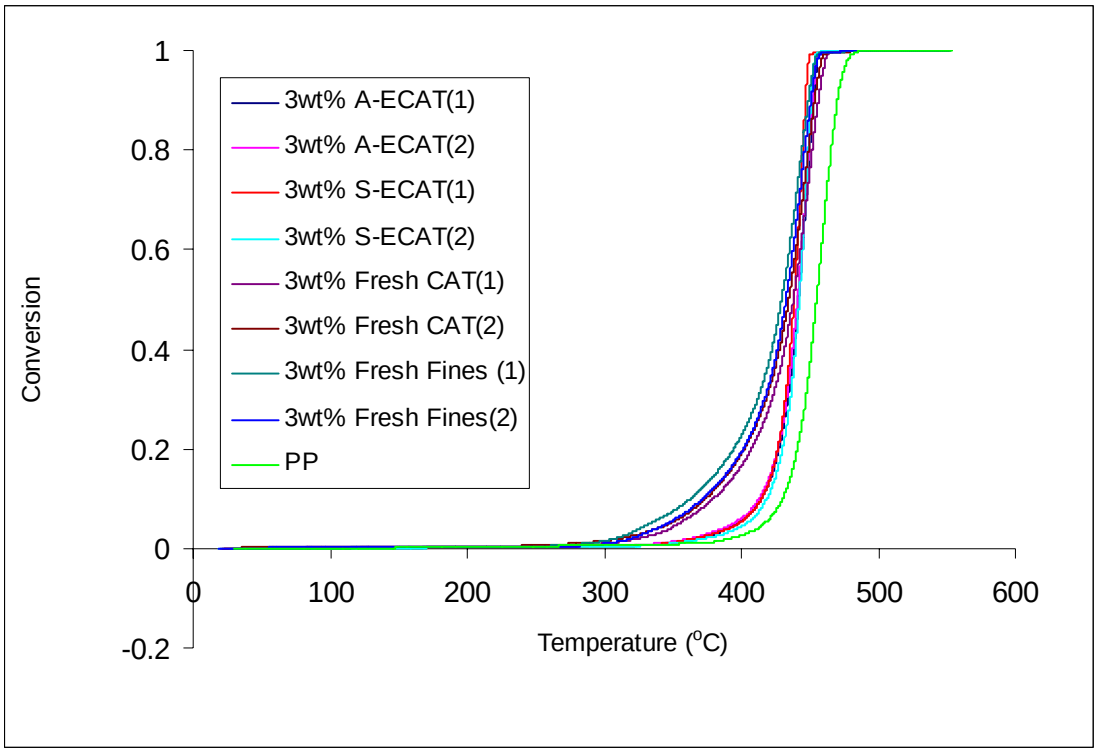

Figure 4.27 Conversion of PP at 3 wt% of various FCC catalysts. Dry mixing

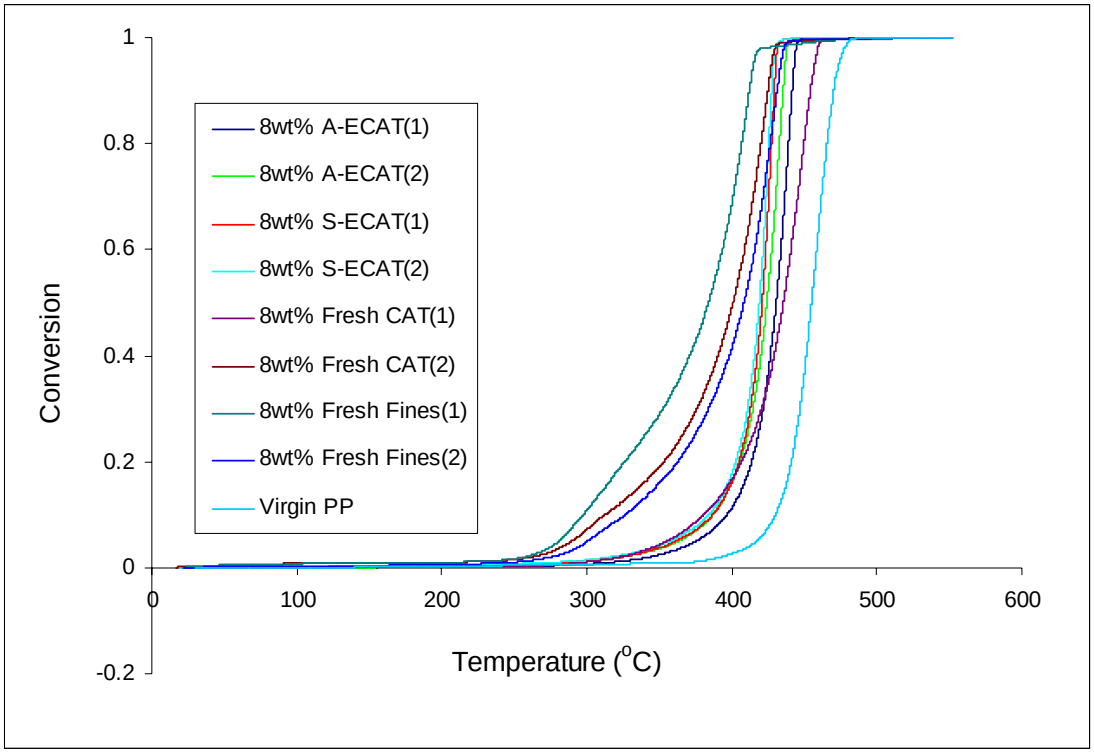

Figure 4.28 Conversion of PP at 8 wt% of various FCC catalysts by Dry mixing

As with the melt-mix samples, the effectiveness of the catalyst in degrading PP varied similarly:

Fresh fines > Fresh CAT> S-ECAT>A-ECAT.

However, there might be some variance in the repeatability of the TG curves, particularly at the higher catalyst weight fraction. Furthermore, this variance is observed more in the dry mix than melt mix samples. This justified why melt mixing was preferred and used for most of this study since there is less deviation. This is more evident in the TG plots for Fresh CAT and Fresh Fines shown in Figures 4.31 and 4.32.

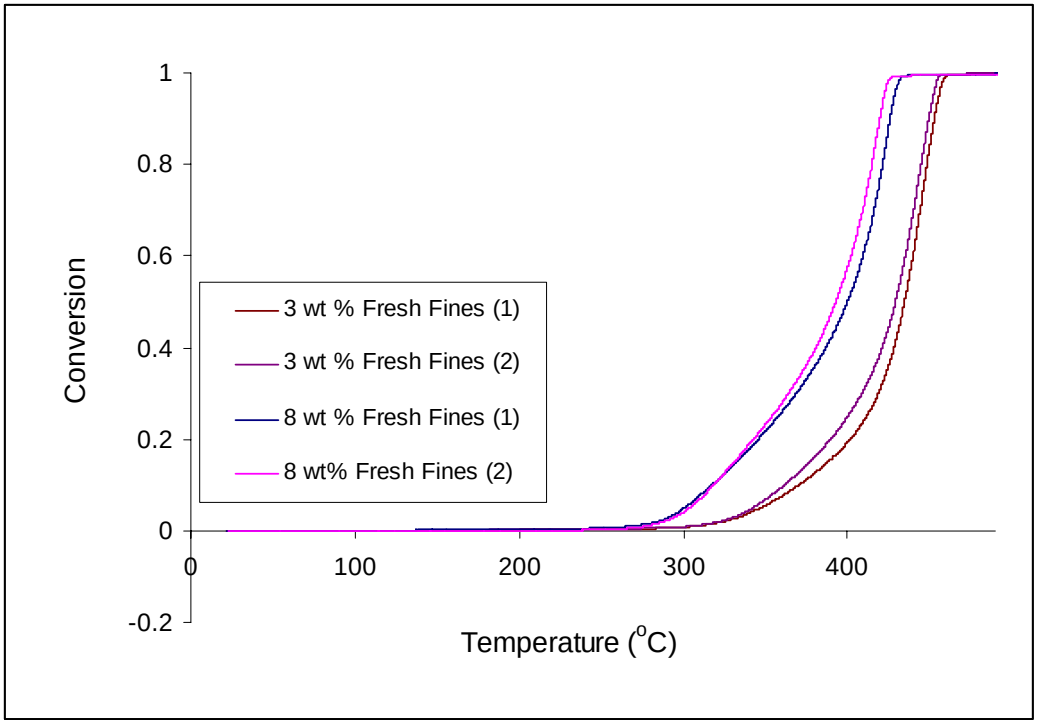

Figure 4.31 Repeated melt-mixing for 3 wt% and 8 wt% Fresh FCC Fines

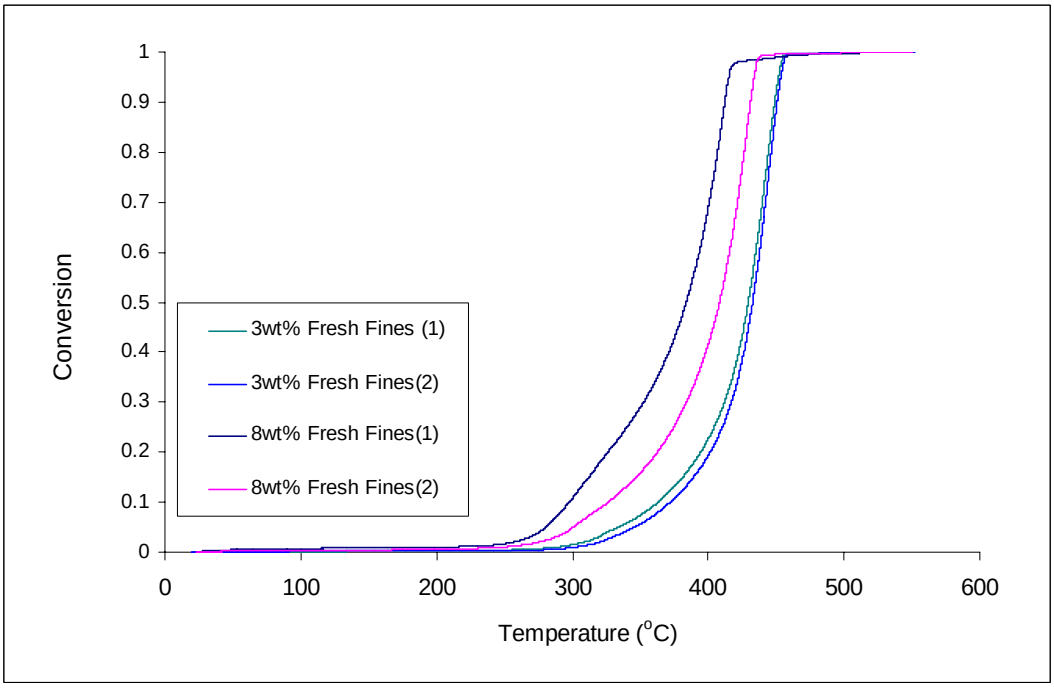

Figure 4.32 Repeated Dry-Mixing for 3 wt% and 8 wt% Fresh FCC Fines

4.6.2 Dry Mixing and Melt Mixing: Comparison of TG analysis

Figure 4.33 shows a comparison of the melt mixing and dry mixing TG plots measured for 3 wt % Fresh CAT in PP. There is not a significant difference between the results of the two methods.

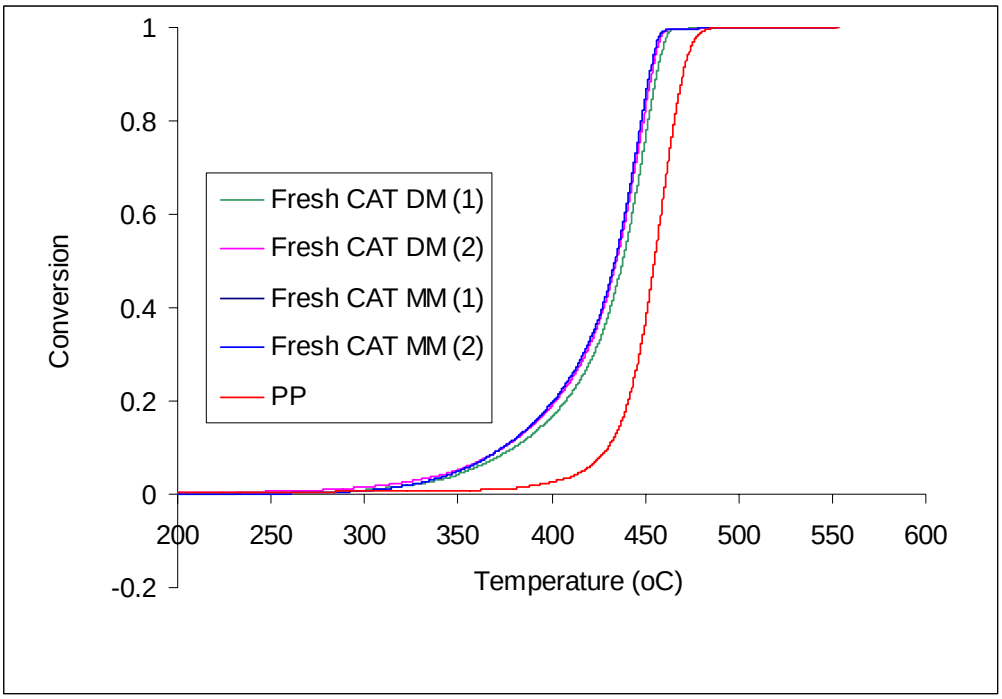

Figure 4.33 Comparison of the Melt mixing (MM) and Dry mixing (DM) TG analysis of PP degradation at 3 wt% of Fresh CAT

On the other hand, with samples containing 3 wt% of Fresh Fines (as shown in Figure 4.34), there is a repeated, though small, deviation from dry and melt mixing TG plots. Overall, no significant differences in the TG plots were observed between the dry and melt mixing methods

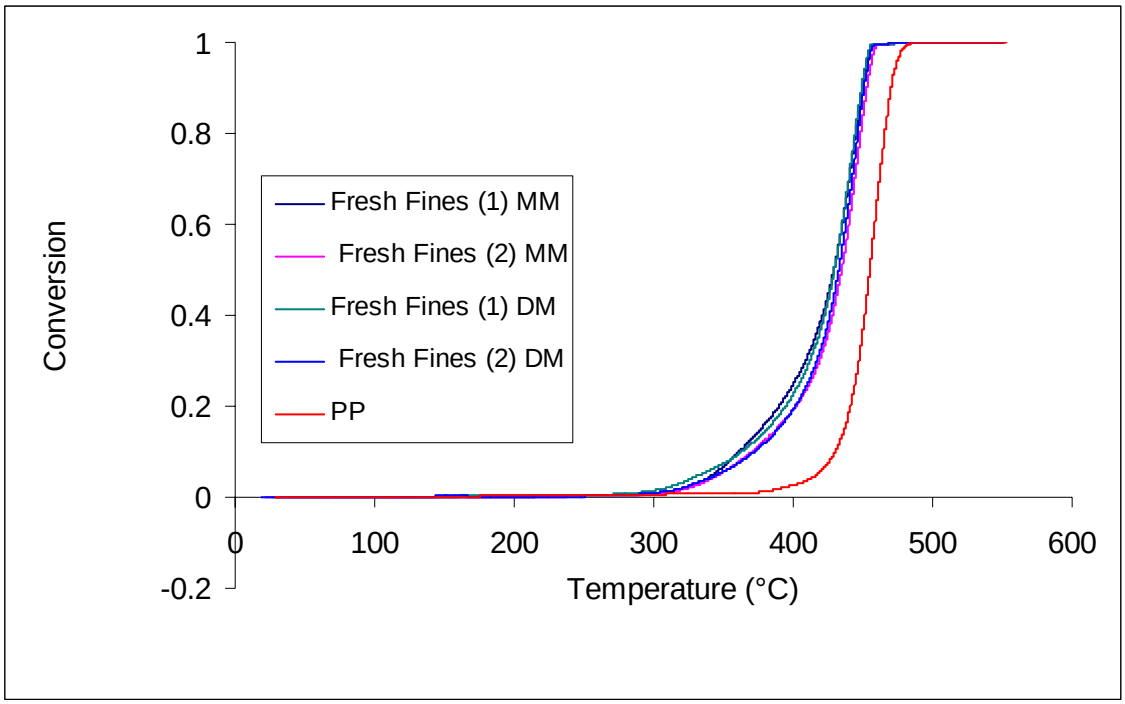

Figure 4.34 Comparison of the Melt mixing (MM) and Dry mixing (DM) TG analysis of PP degradation at 3 wt% of Fresh Fines

On the other hand, at a higher catalyst weight fraction, the difference is more pronounced as shown in Figures 4.35-4.36. With 8wt% Fresh CAT, in Figure 4.35, only the 2nd dry mixing run was close (within the error) to both the melt mixing runs; the 1st dry mixing run had a substantial deviation. Similarly, with the 8wt% Fresh Fines (Fig 4.36), the most deviation was observed for dry mixing plots.

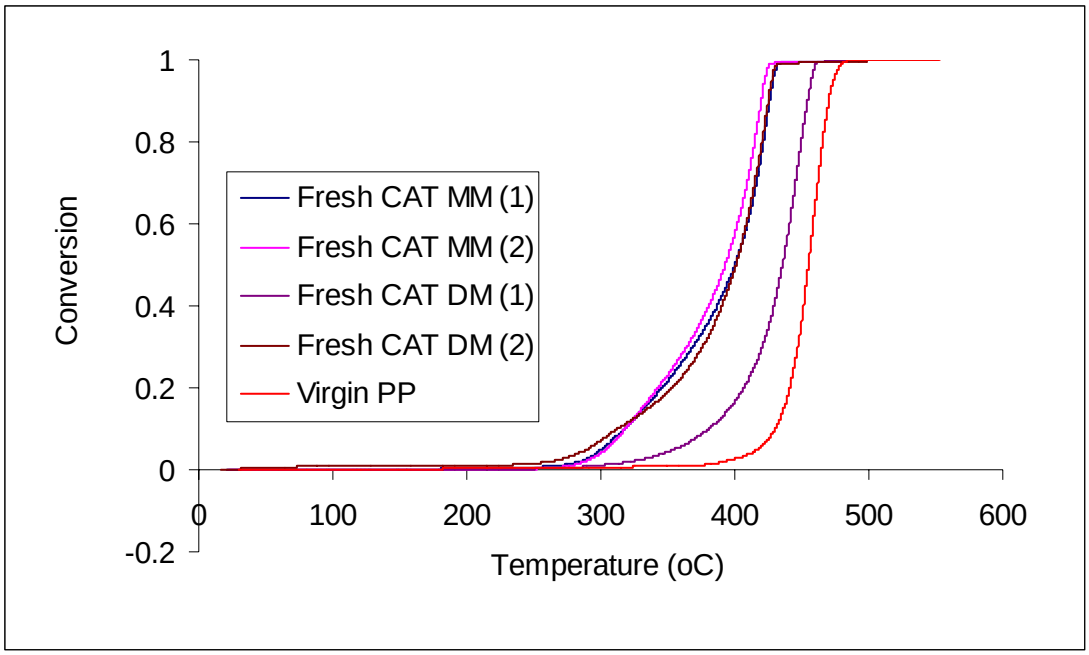

Figure 4.35 Comparison of the Melt mixing (MM) and Dry mixing (DM) TG analysis of PP degradation at 8 wt% of Fresh CAT

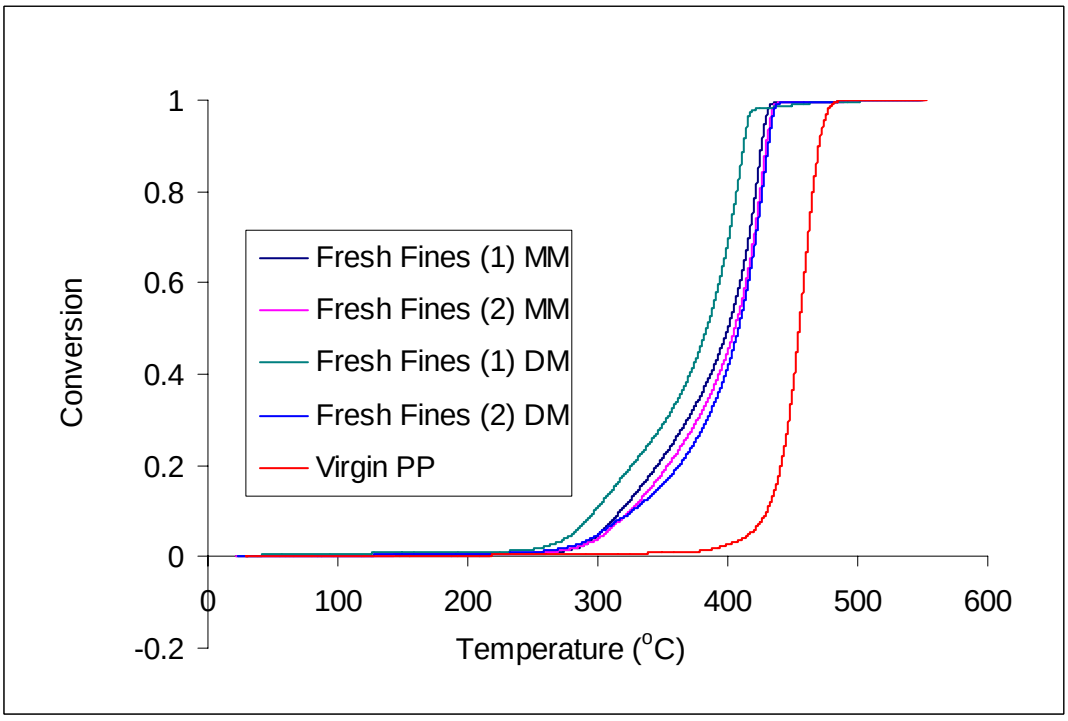

Figure 4.36 Comparison of the Melt mixing (MM) and Dry mixing (DM) TG analysis of PP degradation at 8 wt% of Fresh Fines

A more quantitative analysis of the data was performed. This looked at the variances of T_{max}, $T_{1\%}$ and $T_{99\%}$ between both mixing methods. These results are shown in Table 4.11 for 3wt% of Fresh CAT, Fresh FCC Fines and A-ECAT.

Table 4.16 Comparing the repeatability of TGA properties between the melt mix and dry mix method of TG sample preparation at 97 wt% of PP

Sample	Average TG properties				
	$T_{1\%}$ (^oC)	$T_{99\%}$ (^oC)	T_{max} (^oC)	α_{max} (%)	Residue (%)
3 wt% Fresh CAT-DM	290 ± 11	462 ± 1	449 ± 0	77 ± 3	3 ± 0
3 wt% Fresh CAT- MM	300 ± 7	459 ± 0	447 ± 0	77 ± 0	3 ± 0
3 wt% Fresh Fines- DM	295 ± 7	456 ± 1	442 ± 1	72 ± 5	3 ± 0
3 wt% Fresh Fines- MM	306 ± 1	458 ± 2	445 ± 3	75 ± 3	3 ± 1
3 wt% A-ECAT-DM	344 ± 4	457 ± 0	449 ± 0	75 ± 0	3 ± 0
3 wt% A-ECAT-MM	355 ± 2	460 ± 1	451 ± 0	77 ± 4	2 ± 0

DM- Dry mixed sample
MM – Melt mixed sample

Similarly, the repeatability of both methods at 92 wt% of PP was observed for the Fresh FCC catalysts: Fresh CAT and Fresh Fines. The results are displayed in Table 4.14

Table 4.17 Comparing the repeatability of TGA properties between the melt mix and dry mix method of TG sample preparation at 8 wt% of catalyst

Sample	Average TG properties				
	$T_{1\%}$ (^oC)	$T_{99\%}$ (^oC)	T_{max} (^oC)	α_{max} (%)	Residue (%)
8 wt% Fresh CAT-DM	243 ± 54	448 ± 13	436 ± 12	82 ± 5	6 ± 4
8 wt% Fresh CAT- MM	313 ± 2	468 ± 1	452 ± 2	68 ± 4	6 ± 0
8 wt% Fresh Fines- DM	211 ± 37	445 ± 7	420 ± 8	86 ± 2	8 ± 2
8 wt% Fresh Fines- MM	264 ± 3	435 ± 2	428 ± 4	89 ± 5	6 ± 0

DM- Dry mixed sample
MM – Melt mixed sample

Deviations in the TG characteristics were observed for both the dry mixing and melt mixing methods. However, a greater deviation from the mean is observed more for the dry mixing method, especially with increasing catalyst fraction.

Although, the average values of T_{onset} are lower for the dry mix runs, the repeatability of the results is questionable. The results obtained with the melt mix method are more consistent.

CHAPTER 5

REACTOR MODEL

In Chapter 5, a reactor model was developed to simulate the catalytic pyrolysis of PP in a continuous flow pyrolysis reactor. The model estimates the rate of conversion of PP, using the kinetics obtained by TGA. Based on the results, a simple economic analysis on the degradation operation is performed.

5.1 The Reactor

Numerous studies in polyolefin pyrolysis were conducted in batch systems, resulting in low polymer conversions and increased char formation [43, 45, 135]. On the other hand, with continuous flow reactors, volatiles are continuously removed, thus a higher conversion of the polymer to desirable products is achieved in a shorter amount of time.

In this study, the selected continuous flow reactor is a counter-rotating non-intermeshing (CRNI) twin screw extruder design. A schematic of a basic twin screw extruder is shown in Figure 5.1. Control parameters for extruders such as this one include the feed rate, screw-speed and temperatures along the various process zones.

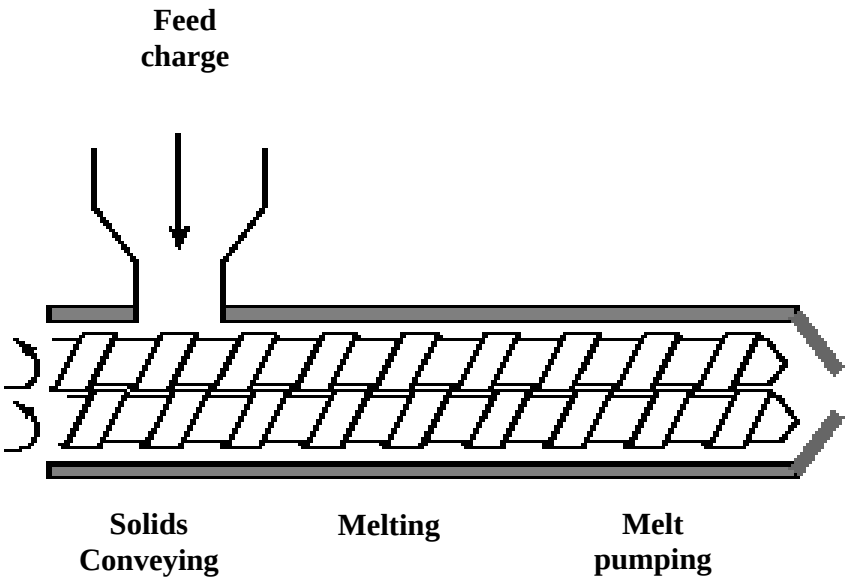

Figure 5.1 Schematic of twin-screw extruder [213].

Attached to the extruder, is a motor that drives the twin-screws, enhancing the proper mixing of the polymer feed. In addition to mixing, the mechanical action of the screws also inputs energy into the process by the interaction of the twin screws and shearing of the polymer melt. Typically, higher screw speeds result in increased shear heating. Additional heating to the extruder zones is also supplied electrically; whereas, cooling to the extruder is supplied either by water or air, depending on the barrel heat-transfer configuration.

The reactive extrusion process begins with polymer pellets being fed through the hopper into the 'solids conveying zone'. Next, they are pumped into the 'melting zone', where they are melted by the twin screw action. The exiting polymer melt immediately flows into the 'melt pumping zone' (in this case the 'reaction zone') where the catalytic pyrolysis occurs. A catalyst injection port, placed at the beginning of the reaction zone, feeds the preferred catalyst into the reactor to be mixed with the polymer melt. Vent ports stationed along the

extruder barrel remove the generated volatile products whereas un-reacted polymer, catalyst and char exit at the extruder die end. This process is illustrated in Figure 5.2 below.

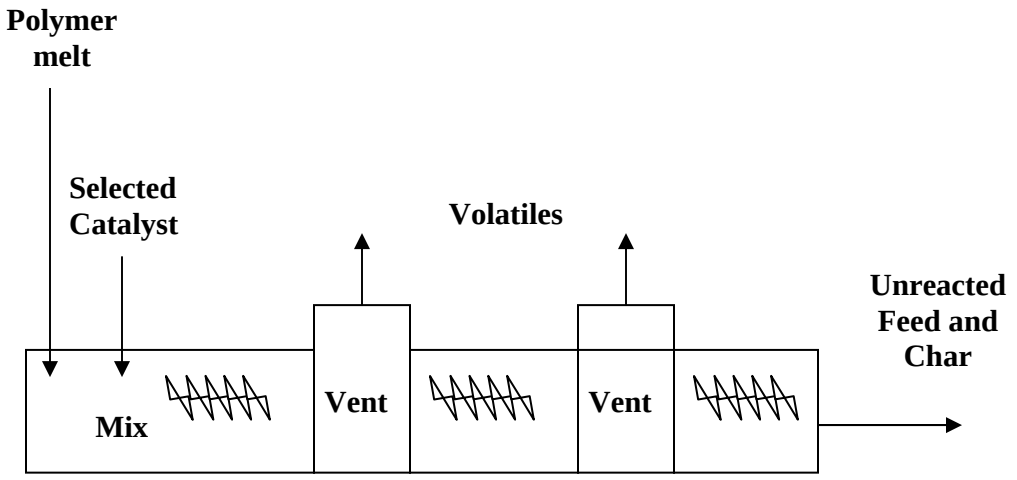

Figure 5.2 Schematic of the twin-screw reactor for the catalytic pyrolysis of polyolefin waste (melt zone not shown).

5.2 Critical Assumptions in Process Modeling

Several assumptions were made in modeling the polypropylene pyrolysis and these could be critical in our economic analysis. These are discussed below.

5.2.1 Reactor Design

The 'reaction zone' of the extruder was modeled as a non-isothermal plug flow reactor (PFR). Thus, the mass and energy balances are integrated along the reactor length; consequently, both composition and reaction temperature changes down the length of the reactor. Heat and mass transfer in the radial direction was assumed to be negligible. With the short residence times exhibited by these reactors, most of the energy and mass transfer occurs axially in the direction of feed flow.

Another critical assumption made in the reactor design is that the throughput is constant. Twin-screw extruders are typically operated by 'starve feeding', meaning that the feed is metered into the reactor hopper and the actual throughput is determined by a feeder and not the screw speed [214]. However, this model allows for the variance of screw speed. With larger sized extruders, it is desirable to operate the extruder at a lower screw speed, thereby increasing the residence time, however, a disadvantage is the lower throughput that results.

Moreover, the PFR was modified to vent products at three equidistant points down the reactor length in which the first vent is placed at 1/4 the total length of the extruder (in practice, more vents are required). This devolatilization of products, in addition to starve feeding operation, further reduces the pressure build in the system, thus it was assumed that the pressure buildup in the extruder is low. In simulating the venting process, it was assumed that the products are volatized at the vent location, thus they are immediately removed from the reaction zone. Possible back flow of the vapor products was assumed negligible.

5.2.2 Rate Equation

In developing the reactor model, several simplifications to the rate equation were made. First, global kinetic parameters derived by TGA were employed in deriving the rate equation. Ideally, the rate equation should reflect a distinct cracking mechanism, consisting of the probable reaction steps that result in the formation of assorted volatile products. However, due to limited information on the pyrolysis mechanism of PP in literature, only an overall degradation step was assumed (polymer to gaseous hydrocarbons).

Secondly, a common assumption in pyrolysis studies of polyolefins is that the reaction follows first order kinetics. This assumption was also made in our study. In addition, kinetic

parameters (E_a and A) estimated by TG analysis (using the Arrhenius equation) were used in the rate equation describing the degradation reaction. Although, it was determined that a lower data range than was used in this study may be a more accurate estimation of the rate equation by differential TG data analysis, the current parameters were still used in developing this reaction model.

5.2.3 Heat and Mass Transfer Limitations

There are two sources of heat input in this model. Firstly, part of the energy generated by the drive unit (mechanical screw action) is converted directly into heat by internal friction, resulting in a temperature rise of the reaction materials. In developing this model, it was assumed that all of the mechanical energy input is dissipated as heat [214]. All of this energy was used to compensate for the endothermic reaction. Since polyolefin pyrolysis is an endothermic reaction, cooling is not a critical issue.

Another external heat source is that supplied by electrical heating. The heat resistance between the polymer and the barrel wall is the most critical in describing heat transfer in an extruder. Models describing the heat transfer coefficient in an extruder are sparse. In calculating the heat transfer coefficient at the extruder barrel wall, a model described by Todd ***et. al.*** was used [215]. This model shows a dependence on rotational speed, screw diameter and bulk properties of the material such as the Reynolds and Prandtl numbers. Subsequently, the overall heat flux was calculated based on an estimation of the overall heat transfer coefficient. A detailed description of the calculations will be presented later.

Furthermore, with heterogeneous reactions involving porous materials, such as the zeolitic catalyst employed in this study, there is often the issue with mass transfer within the pores of

the catalysts. Nevertheless, with these microporous catalysts, there still exists a high density of acid sites on the surface; therefore, mass transfer limitations in the catalyst were assumed to be negligible. In addition, the catalyst was assumed to be well dispersed in the polymer melt immediately following its addition to the reactor. Temperature effects due to this addition were neglected since only very small amounts are used.

5.2.4 Reaction and Product Distribution

Gasoline quality fuels consist of hydrocarbons in the $C_5 – C_8$ range. Moreover, most studies observe that the main products obtained in polyolefin pyrolysis are hydrocarbon gases (C_1-C_4) and liquid gasoline range (C_5-C_{12}) products composed of mainly olefins and paraffins [216-218]. Based on this information, it was assumed that the reaction products would consist of various hydrocarbon compounds in the $C_1 – C_{12}$ range. Selected compounds within this range are listed in Tables C.1, C.2a and C.2b of Appendix C. Also shown, are the physical properties of each compound, including heat capacities and boiling point temperatures obtained from Lange's handbook of chemistry [219]. Utilizing data from each contributing compound, the mean heat capacity of the reaction mixture was estimated.

5.2.5 Extruder Geometry

An advantage of a CRNI twin screw extruder is that each screw can be configured using the same design of a single screw [220]. Therefore, in modeling the twin screw reactor, the cross sectional area was calculated by assuming that it was twice that of a single screw extruder. This single screw extruder would have all the intended geometric dimensions of one barrel in a twin screw extruder. In which case, the screw diameter was assumed to be 70 % of the barrel diameter.

On the other hand, in a twin screw non–intermeshing configuration, a nip is formed due to the truncation of the two barrel apices, as shown in Figure 5.3. This nip was neglected in calculating the twin screw cross sectional area.

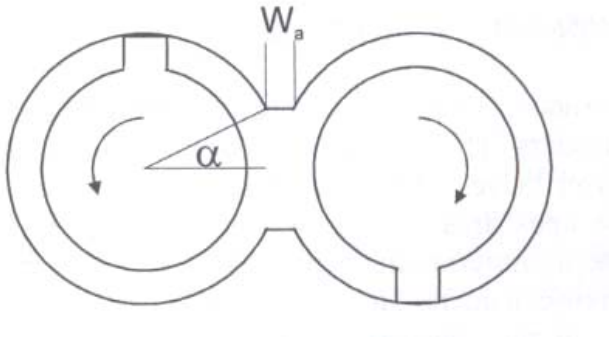

Figure 5.3 Cross section of a CRNI twin-screw extruder showing the apex width (w_a) and angle (α) [221].

Furthermore, the barrel diameter is calculated by assuming a L/D ratio. A typical range of screw diameters for a CRNI twin-screw system is 20 to 250 mm, having L/D ratios in the range of 30-54 [220]. For starve feeding to be efficient, an L/D of at least 30 is recommended [214]. In choosing L/D, the melt zone was not included because it constitutes only a small part of the entire extruder length (typically around 2-3 D) [214].

5.2.6 Estimation of the Heat of Reaction

The heat of reaction, ΔH_{rxn} (degradation of PP) was estimated by Differential Thermal Analysis (DTA) of PP. This technique measures the difference in temperature between a sample and a reference material as a function of temperature [222]. Thus, a thermal change in a sample will result in a change in the recorded temperature, producing endothermic (- ΔT) or exothermic (+ ΔT) peaks. DTA measurements were carried out simultaneously with TGA

using a Seiko TG/DTA 320. Figures 5.4 - 5.6 show endothermic DTA peaks obtained for a virgin PP and samples containing 3 and 8 wt% of S-ECAT, respectively.

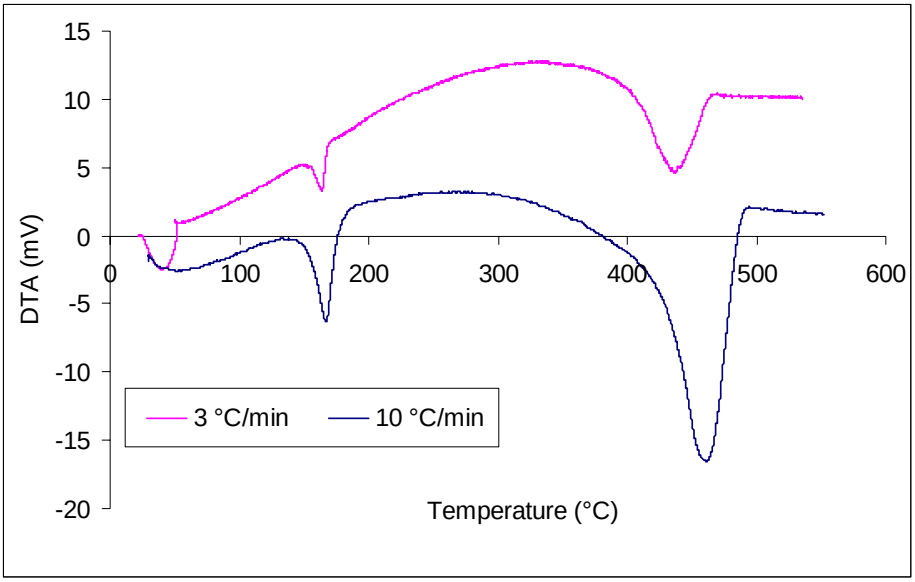

Figure 5.4 DTA plot for the non-catalytic pyrolysis of PP

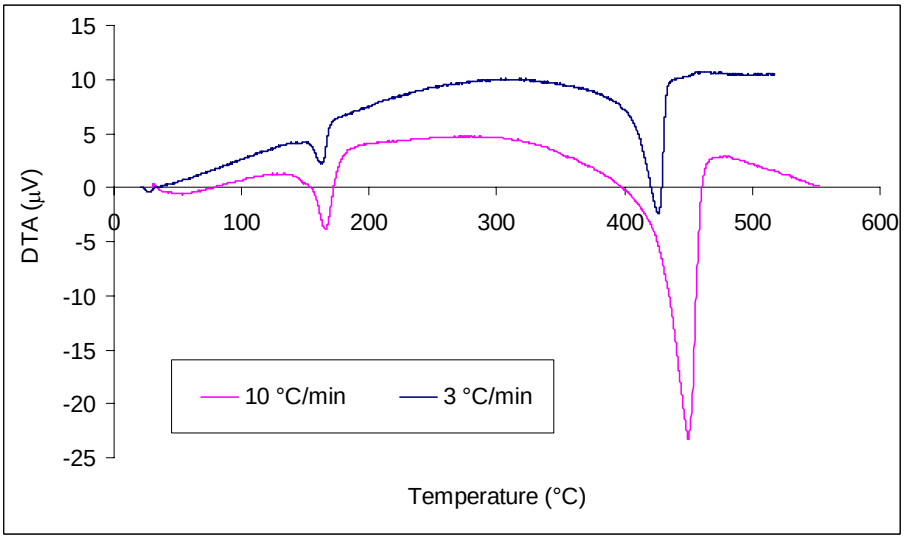

Figure 5.5 DTA plot for PP pyrolysis at 3 wt % S-ECAT

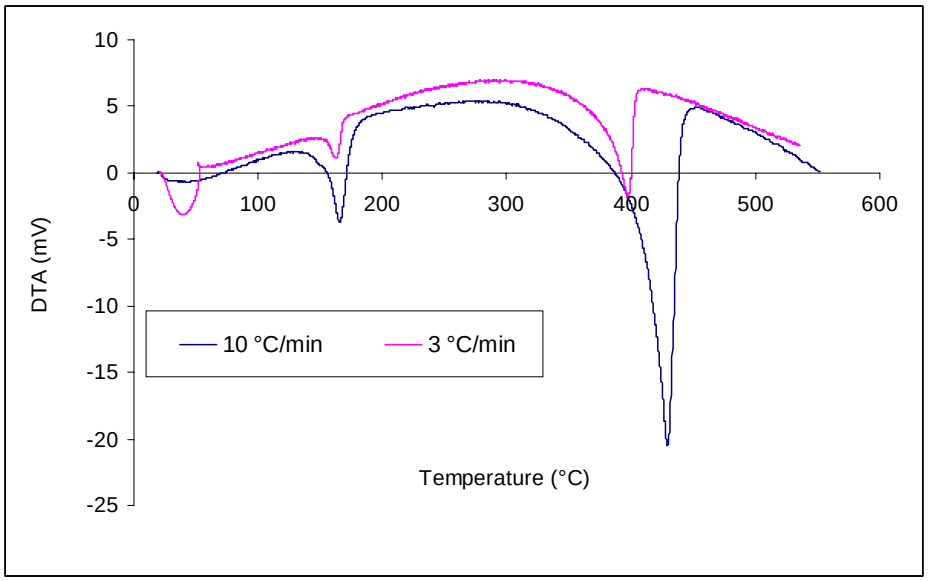

Figure 5.6 DTA plot for PP pyrolysis at 8 wt % S-ECAT

The DTA plots each show two endothermic peaks. The earlier peaks denote the temperature range where the melting transition occurs. The DTA plots show melting curves that peak at very similar temperatures for all the samples (approximately 163 °C) as well as similar peak areas. Therefore, the melting transition is not influenced in the catalytic pyrolysis of PP.

The latter peaks represent the change in temperature during the pyrolysis reactions. This is an endothermic change as expected with polymers. The area under the pyrolysis reaction curve may be used to estimate ΔH_{rxn}. The peak area was estimated for different heating rates and was found to be fairly similar. The averaged values were then converted to units of heat change (kJ/kg) using software on the Seiko TG/DTA equipment. The estimated values for virgin PP, 3, 8 and 13 wt% of S-ECAT, as well as 8 wt% of Fresh Fines, A-ECAT and Fresh CAT are shown in Table 5.1. Also shown are the peak temperatures of the degradation curve,

which are considered as reference temperatures for the estimation of the heat of reaction at a specified temperature.

Table 5.1 Estimated heat of reactions for selected samples

Sample	ΔH_{rxn} (kJ/kg)	T_{peak} (°C)
PP	420	460
3 wt% S-ECAT	420	444
8 wt% S-ECAT	380	417
13 wt% S-ECAT	328	402
8 wt % Fresh Fines	200	426
8 wt% Fresh CAT	273	457
8wt% A-ECAT	307	436

Table 5.1 shows that the heat of reaction decreases with catalyst addition in PP pyrolysis.

In the TG analyzer, the PP sample is essentially converted to gaseous products, thus these values also account for the heat of vaporization. There is an obvious variance in the estimated heat of reaction amongst the different catalysts. This implies that for the different catalysts the mechanisms for the pyrolysis of PP differs.

Differential Scanning Calorimetry (DSC) monitors the changes in heat flow as a function of temperature and is mostly used to observe the heat of melting (ΔH_m) of materials during thermal analysis [222]. DSC is regarded as a more accurate method of measuring heat effects than DTA, however, the temperature range on these instruments are limited. Therefore, degradation reactions are not usually observed by DSC. On the other hand, in this study, DSC analysis was performed on virgin PP and samples containing 3 and 8 wt% of S-ECAT. ΔH_m

obtained by DSC was compared to the values acquired by DTA and was found to be very similar. Both values are shown in Table 5.2. The DSC plots of all three samples also show melting temperatures of 163 °C and can be found in Figures C.1 – C.3 of the Appendix C.

Table 5.2 A comparison of ΔH_m estimated by DSC and DTA

Sample	ΔH_m (kJ/kg of PP)	
	DTA	DSC
PP	57	56
3 wt% S-ECAT	60	61
8 wt% S-ECAT	61	63

The similarity between the two methods indicates that our estimation of ΔH_{rxn} by DTA may be suitable.

5.3 Development of the Reactor Model

5.3.1 Mass and Energy Balances

The general form of the mass balance described by this reactor is defined in terms of conversion as shown in Equation 1 [223].

$$\frac{dX}{dL} = \frac{-r_P}{F_{po}} A_c \qquad (1)$$

where,

X = Polymer conversion

r_P = Rate of the reaction ($kg/m^3/s$)

A_c = Cross sectional area (m^2)

L = Reactor length (m)

F_{po} = Initial polymer feed rate (kg/s) or (lb/hr)

The individual parameters of Equation 1 are discussed below.

The general expression for a first order, single reactant reaction is,

$$r_A = kC_A$$

where, r_A is the rate of reaction with respect to reactant, A; k is the rate constant and C_A is the concentration of A at any point during the reaction [223].

On the other hand, in the decomposition of polymers, the reaction rates are calculated based on a weight loss basis and is described in terms of a weight loss function as shown in Equation 2.

$$r_P = kC_{po}(1 - X) \qquad (2)$$

where,

k = Rate constant (s^{-1})

C_{po} = Initial polymer concentration. Given that calculations made in developing the model are on a mass basis, C_{po} is also the density of the polymer melt = 0.769kg/m^3 [224].

F_{po} is feed rate of the polymer given by Equation 3.

$$F_{po} = w_p F_f \qquad (3)$$

where, F_f is the total feed rate and ω_p is the weight fraction of polymer in the feed.

The other parameter in Equation 1 is the cross-sectional area defining the reactor volume.

$$Ac = 2\pi\left(\frac{D_b{}^2 - D_s{}^2}{4}\right) \qquad (4)$$

where, D_b and D_s are the diameters of the barrel and screw respectively and $D_s/D_b = 0.7$. The dimensions are based on a single screw extruder, thus the factor of 2 is present for the twin screw basis as discussed in section 5.2.5.

Thus the mean residence time in seconds may be calculated by,

$$residence\ time = \frac{A_c L_t}{F_f \diagup C_{po}} \qquad (4b)$$

where, L_t is the total length of the reactor.

Similarly, the energy balance is defined by a differential equation describing the change of temperature with distance down the reactor length [223].

$$\frac{dT}{dL} = \frac{Q_{in}(2\pi D_b) + E_L + \left[(-r_P)(-\Delta H_{rxn})A_c\right]}{F_{po}\left(\sum \Theta i C_{pi} + X\Delta C_p\right)} \qquad (5)$$

where,

T = reaction temperature (K)

Cp_i , Θi = heat capacity and fraction of each feed component, in this case, catalyst and polymer (kJ/mol/K). Cp of the catalyst was assumed to be 1 kJ/kg/K.

ΔCp = mean heat capacity (kJ/kg/K). This was estimated from the heat capacities of light weight hydrocarbons listed in Tables C.1, C.2a and C.2b of Appendix C.

ΔH_{rxn} (kJ/mol) is the heat of the decomposition reaction. Polymer decomposition is an endothermic reaction. Polypropylene's heat of reaction (degradation) was determined by DTA as explained earlier.

E_L (kilowatts/m) is the mechanical energy input across the length of the screw and Q_{in} (kilowatts/m^2) is the required heat input through the wall of the extruder, supplied by electrical heaters. This term constitutes the energy input required to drive the reaction and is estimated by Equation 6.

$$Q_{in} = U\left(Tw - T\right) \qquad (6)$$

where U is the overall heat transfer coefficient (kW/m^2K), T_w is the temperature at the barrel wall and T is the temperature of the polymer [215]. The desired operating temperature is 500°C. In order to estimate the required heating to achieve this temperature, T_w was set to this temperature.

U is calculated based on two local heat transfer processes: heat transfer through the barrel wall and heat transfer between the wall and the polymer. Therefore, U is given by Equation 7.

$$U = \frac{1}{\left[\frac{(D_b/2)*\ln(D_o/D_b)}{\lambda_b}\right] + \frac{1}{h_i}} \qquad (7)$$

where, λ_b is the heat conductivity of the barrel (W/mK). The barrel material chosen was stainless steel, which has λ_b value of 19 W/mK [225]. The inverse of h_i is the estimated heat

resistance between the polymer and the barrel wall. D_o and D_b are the outer and inner diameters of the barrel, respectively. The barrel thickness was estimated as one-quarter of an inch. Using the Todd model, the value of h_i was estimated by Equation 8.

$$h_i = \frac{\lambda}{D_s}\left[0.94\,\mathrm{Re}^{0.28}\,\mathrm{Pr}^{0.33}\left(\frac{\mu_p}{\mu_w}\right)^{0.14}\right] \qquad (8)$$

where, λ is the thermal conductivity of the material (PP), Re and Pr are the Reynolds and Prandtl numbers, respectively, μ_p and μ_b are the viscosities of the polymer in the bulk and at the wall, respectively. (This ratio was assumed as one, because the viscosity is a function of temperature and the temperature at the wall is assumed to be that of the bulk polymer. Also, even if the temperatures where not assumed to be the same, the values of the viscosity would have to be determined at the different temperature which time did not permit for this study.) The units of h_i are W/m^2K.

Equation 8 can also be written as

$$h_i = \frac{\lambda}{D_s}\left[0.94\left(\frac{\rho N D_s^{\,2}}{\mu}\right)^{0.28}\left(\frac{C_p\mu}{\lambda}\right)^{0.33}\right] \qquad (9)$$

where, ρ is the density of the polymer, N is the rotational speed of the screw (1/s), μ is the viscosity of the polymer melt in units of Pa.s [215].

The heat required for melting the initial polymer feed at 25°C to a melt temperature is calculated by Equation 10.

$$Q_{melt} = F_f * C_p * (T_m - 298) + \Delta H_m \qquad (10)$$

where, ΔH_m is the heat of melting is approximately 60 kJ/kg as estimated by DSC and DTA.

In addition to the Ordinary Differential Equations (ODEs) that define the reaction temperature and conversion, the polymer and product flow were also calculated and are defined by Equations 11 and 12.

$$\frac{dF}{dL} = r_P A_c \qquad (11)$$

$$\frac{dP}{dL} = -r_P A_c \qquad (12)$$

5.3.2 Calculation of E, Energy input from extruder drive

The power (E) needed to drive the screw was found using Equation 13 [226, 227], which describes the power input for a single screw extruder based on the barrel geometry and screw configuration of a CRNI twin-screw extruder sold to Georgia Tech by NFM Welding Engineers, Inc. In estimating the power required to drive twin screws, the results were multiplied by a factor of 2 (for 2 screws). (This model does not account for one of the screws being shorter than the other.)

$$E = p\mu N^2 (\pi D_b)^2 \frac{W}{H} \frac{L}{\sin\theta_b} f \qquad (13)$$

where,

p = Number of flights in parallel

μ = Viscosity of PP = 500 kg/ms (determined from lab data, using a parallel plate rheometer)

N = Screw speed (RPM), assumed maximum for NFM extruder at GA Tech (500 RPM)

D_b = Inside Barrel diameter

W = Channel width

H = Channel depth

L = Length of screw (axial distance)

θ_b = barrel helix angle

θ = screw helix angle (given by NFM)

f = geometrically determined factor.

These variables are found by using Equations 14-17 [226, 228].

$$f = 4 - 3\cos^2\theta\left(\frac{Q}{Q_d}\right) + \frac{\mu_f}{\mu}\frac{H}{W}\frac{e}{\delta_f} \qquad (14)$$

$\frac{\mu_f}{\mu}$ is assumed to be equal to 1 reasons described above.

where

Q = volumetric throughput, (based on capacity) cm^3/sec

Q_d = volumetric drag flow, cm^3/sec found by using Equation 17

μ_f = average viscosity in flight clearance, dyne sec/cm^3

e = width of the flight, cm

δ_f = flight clearance, cm

$$W = S * \cos(\theta) - e \qquad (15)$$

where, S = pitch, cm

$$\theta_b = \tan^{-1}\frac{S}{\pi D_b} \qquad (16)$$

$$Q_d = \frac{pV_{bz}WH}{2}\left(1 - \frac{\delta_f}{H}\right)^2 \qquad (17)$$

where, V_{bz} = velocity in the down channel direction (cm/s) found by Equation 18 [215].

$$V_{bz} = pND_b \cos(\theta_b) \qquad (18)$$

The NFM CRNI twin-screw extruder has a barrel diameter of 30mm, much smaller than the typical industrial sizes. Consequently, E was scaled up to the extruder size defined by the present study, by employing Equation 16 [227].

$$E_E = E_b \left(\frac{D_E}{D_b} \right)^{1.5} \left(\frac{N_E}{N_b} \right) \qquad (19)$$

where, E_E, D_E and N_E are the mechanical energy input, barrel diameter and screw speed of the current extruder, respectively; whereas E_b, D_b and N_b are the mechanical energy input, barrel diameter and screw speed of the base extruder (NFM CRNI extruder), respectively. For scaling purposes, N_E is equal to N_b. An exponent of 2.5 is specified for scale-up of the extruder; however, 1.5 was used because, in scaling up from 20 - 30mm extruders to larger capacity industrial sizes, there is usually an exaggeration in the commercial size capacity [227].

The estimation for E_E is solved by the MATLAB file 'screw' attached in Appendix C.

5.4 MATLAB simulation

The MATLAB software function, ODE23s was used in solving the ODEs (Equations 1 and 5). This function integrates stiff ODEs with a low-order method. This function was chosen because it is specifically designed to solve very stiff ODEs and can be more efficient than most of the other MATLAB ODE solvers at crude tolerances.

The ODE solver works on three requirements: an 'odefile', a set of integration limits for the independent variable, (the reaction zone length-L), and a set of initial conditions for the dependent variables (conversion-X, temperature of melt at reactor zone inlet -Tin, feed flow rate-F). At L = 0, the initial values for X was set to zero. The polymer's initial temperature in the reactor is assumed to be equal to that of the polymer melt exiting the 'melt zone'. This is calculated by the MATLAB file, 'meltzone' whereas the 'odefile' is defined by 'Diff' (See Appendix C). All four ODEs (Equations 1, 5, 11 and 12) are solved by the ODE solver defined in the 'extruder' function.

5.5 Economic Analysis

The annual conversion cost for the PP pyrolysis was estimated by summing all required capital and manufacturing costs. The calculations of the individual costs are discussed below.

5.5.1 Base Extruder Costs

The maximum capacity and cost (A_b and C_b, respectively) of the counter-rotating non-intermeshing twin screw extruder sold to GA Tech by NFM Welding Engineers, Inc in 2004 was employed with the six-tenths- rule to determine the base cost of the extruder (C_E). C_E was found using Equation 20 [229]. (The cost was not adjusted for inflation because the index didn't change by much over the past few years).

$$C_E = C_b \left(\frac{A_E}{A_b} \right)^{0.6} \qquad (20)$$

Similarly, the cost of the vacuum pump system bought by GA Tech from NFM in 2005 was used to estimate the cost of the vacuum pump system required for product collection.

The total capital cost was found by multiplying the sum of vacuum system and the extruder by a Lang factor of 3.63 by considering the processing in a solid-fluid plant [229]. A 3-yr capital recovery period was assumed.

5.5.2 Raw materials

The cost of the fresh FCC catalyst fines was estimated to be $0.05/lb (sold at $100/USton) [230]. It was assumed that the cost of equilibrium catalysts was sold at half price ($0.025/lb). The value of the polymer was assigned $0/lb based on the assumption of end of life PP. Moreover, since the goal of the study is to determine the conversion costs of PP using catalysts, it seems more reasonable to assign no value to the polymer.

5.5.2 Utility Costs

5.5.2.1 Electricity

To calculate the electricity costs needed to heat the extruder, the total drive power input and electrical input were summed [231]. The current cost of electricity ($0.0475/kWhr) was taken from www.doe.gov for August 2005.

5.5.2.1 Cooling Water Costs

The cooling water requirements for the NFM vacuum system at GA Tech was used to estimate the cost of cooling required for the process. The cost of cooling water cost of $6.7/1000$m^3$ was taken from reference [229] and then scaled-up based on the throughput.

5.5.2.1 Labor Costs

Labor cost was estimated at $46,000/yr for each operator, and it is estimated that 2 operators per shift will be required. It was assumed that operation is carried out as three shifts per day**.** All costs are estimated by the MATLAB 'cost' function.

5.6 Results and Discussion

This simplified extruder design models the catalytic pyrolysis of PP using the catalysts supplied by Albemarle (Fresh CAT, Fresh Fines and A-ECAT) at 8 wt% of PP feed. Simulations were also generated for PP. The rate equation for the respective feed materials was determined by the Arrhenius method as discussed in Chapter 4. These are shown in Table 5.3.

Table 5.3 Rate law parameters for pyrolysis reaction

Feed	E_a (kJ/mol)	ln A (min^{-1})
PP	250	37
8 wt% Fresh Fines	53	7
8 wt% Fresh CAT	120	19
8 wt% A-ECAT	215	36

The reactor throughput and geometry are based on the capabilities of commercial twin-screw extruders sold by NFM Welding Engineers (NFM/WE)[232]. The reactor model tested for

throughputs (15,000 and 7,500 lb/hr) using an L/D of 52 and a reaction zone length (L) of 12 meters. The vents are located at the 3, 6 and 9m positions along the reaction zone length.

The power (E) produced by the drive unit is based on the barrel diameter and was estimated using Equation 19. It was assumed that all of E is dissipated energy and is used to heat the feed. For the electrical heating, Q_{in} was calculated by fixing the outer barrel wall temperature at 500°C. Although a desired temperature between 350-400°C is preferred in catalytic pyrolysis, 500°C was used to account for any set-backs in the Todd model, which estimates the overall heat transfer through the barrel wall. This ensures that adequate heating is supplied to the reactor. A summary of the reaction zone specifications is shown in Table 5.4.

Table 5.4 Reaction zone specifications

	500 RPM	250 RPM
Residence time (min)	3.5	7
L/D	52	52
L (m)	12	12
D (mm)	230	230
E (kW)	1300	326
Throughput (lb/hr)	15000	7500

5.6.1 Results: Run at 250 RPM

At 250 RPM, the extruder temperature, conversion, and material flow profiles were generated. Table 5.5 gives a summary of these results.

Table 5.5 Modeling results for the catalytic pyrolysis of PP at 250 RPM

	PP	A-ECAT	Fresh CAT	Fresh Fines
Temperature profile (°C)	175-400	175-380	175-350	175-300
Conversion	0.0004	0.0435	0.0431	0.0657
Product Flow (lb/hr)	2.38	301	298	454

At this screw speed, the inlet temperature to the reaction zone is 175 °C, slightly above the melting temperature of the polymer (163°C). This inlet temperature is low because at this screw speed, the mechanical energy input supplied to the melt feed is low (326kW). However, upon entering the reaction zone, the temperature profiles differ between the respective feed. The temperature profile for virgin polypropylene spans to about 400°C. On the other hand, with the addition of catalysts, the range is significantly lowered to values at approximately 300°C and 350°C for Fresh Fines and Fresh CAT respectively. Conversely, the A-ECAT is slightly reduced at 380°C. The operating temperatures reflect the activity of the various FCC catalysts, with the Fresh Fines showing the most reduction in the operating temperature range.

Overall, the conversion of PP achieved at this screw speed was minimal, which resulted in very low production of volatile products. Whereas virgin PP was hardly degraded, the conversion of PP achieved by the addition of Fresh Fines was calculated as approximately 7%. Similarly, a low yield of approximately 4 % was achieved by the Fresh CAT and A-ECAT catalysts. This low yield is as a result of the low operating temperature profiles in the reactor.

The final conversion calculated for A-ECAT is slightly higher than that of the Fresh CAT. This occurs because the reaction using A-ECAT achieves a much higher temperature range than the fresh catalysts, thus the rate of the reactions increases with temperature. However, it was clear from TG analysis that the activity of Fresh Fines surpasses that of A-ECAT in PP pyrolysis, hence the observance of higher conversions with the Fresh Fines. This may also result because of the limitations that were identified with the estimation of these kinetic parameters.

In general, the production of volatiles is enhanced with increasing catalytic activity, with the Fresh Fines yielding the most pyrolysis products at 454 lb/hr. Furthermore, based on these results, it is inferred that the operation of this particular extruder at 250RPM, is not an economical option for the catalytic pyrolysis of PP. In essence, one may further investigate into the redesign of the screw elements to increase shearing at specific positions along the extruder, thus increasing conversion. However, due to limited time resources, this was not investigated in this study. Instead, the pyrolysis reaction was carried out at a higher screw speed of 500RPM.

5.6.2 Results: Run at 500 RPM

Similarly, the temperature, conversion, and material flow profiles were also generated at 500RPM. Figure 5.7 shows the temperature profile for this run. While the temperature profiles for the catalyzed reactions are maintained below 400°C, the non-catalytic reaction occurs at a higher temperature range (360 – 470°C). This is mainly because there is less endothermic reaction in the case of the non-catalyzed reaction, allowing the PP to heat more (see Table 5.1). Overall, the temperatures achieved at 500RPM are higher than that at 250RPM because the drive energy input is increased (1300kW).

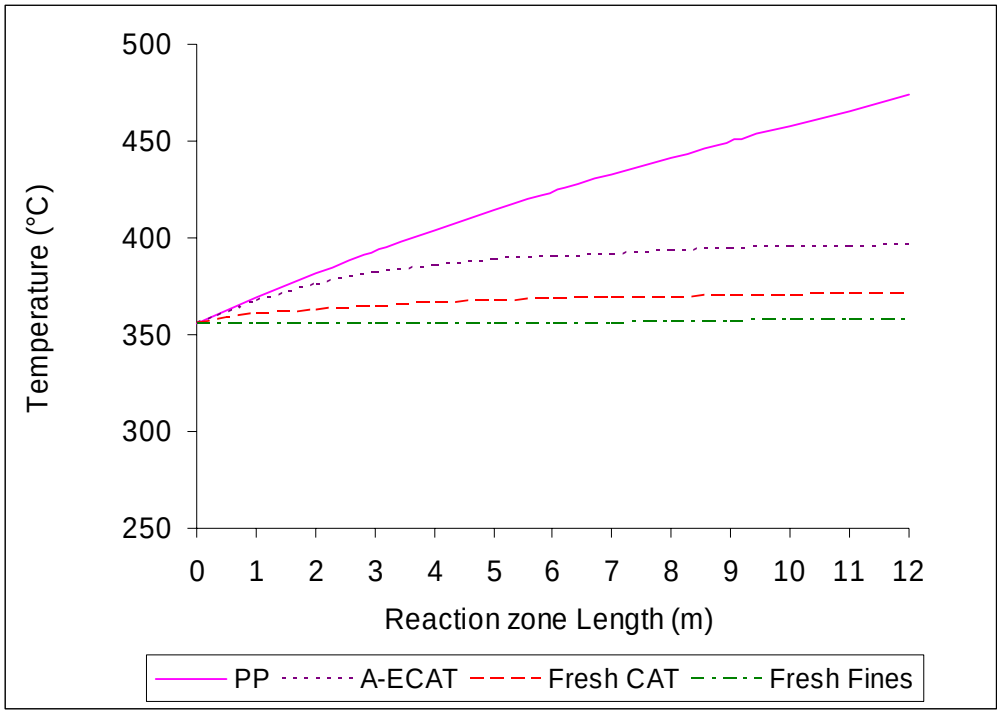

Figure 5.7 Extruder temperature profile at 500 RPM

At these temperatures, the catalyzed reactions commences quickly as is shown by the steady conversion profiles in Figure 5.8. For the non-catalyzed reaction, only 2% conversion is achieved. On the other hand, with the Fresh Fines and Fresh CAT catalyzed reactions, 15% and 10% of the polymer is reacted. Interestingly, the final conversion for A-ECAT (16%) was higher than that of Fresh CAT. This occurs because, further down the reaction zone length, the reaction using A-ECAT achieves a much higher temperature range than the Fresh CAT and only slightly higher than the Fresh Fines, thus the rate of the reactions increases with temperature. However, it was clear from TG analysis that the activity of Fresh Fines surpasses that of A-ECAT in PP pyrolysis, hence the observance of higher conversions with the Fresh Fines.

Similar observations were made with the product flow profile as shown in Figure 5.9.

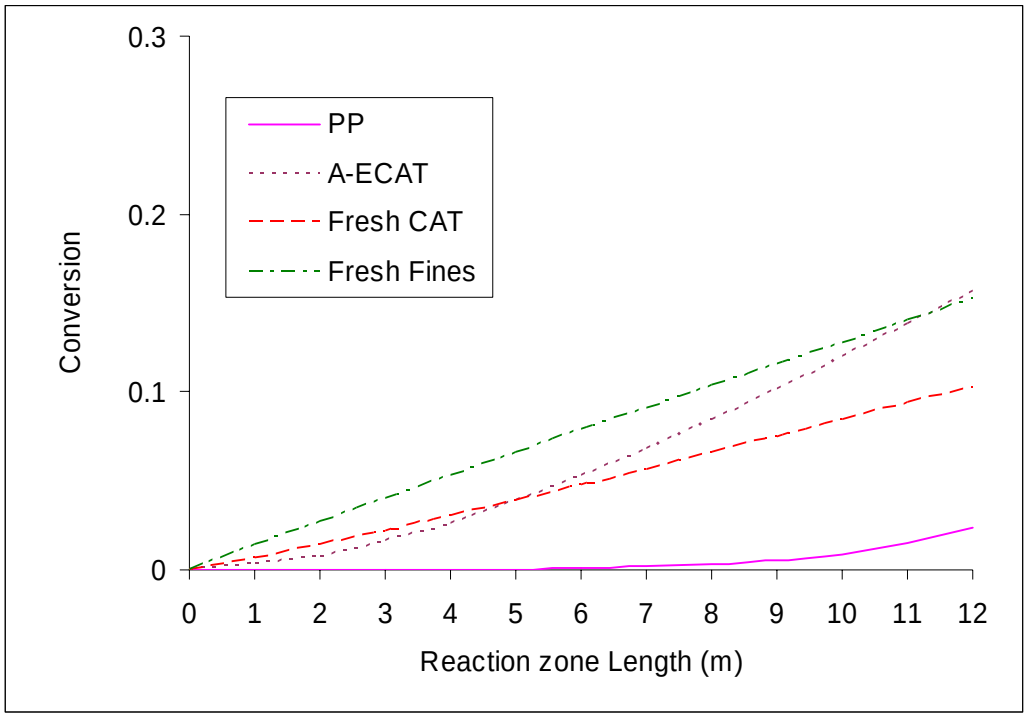

Figure 5.8 PP conversion profile at 500 RPM

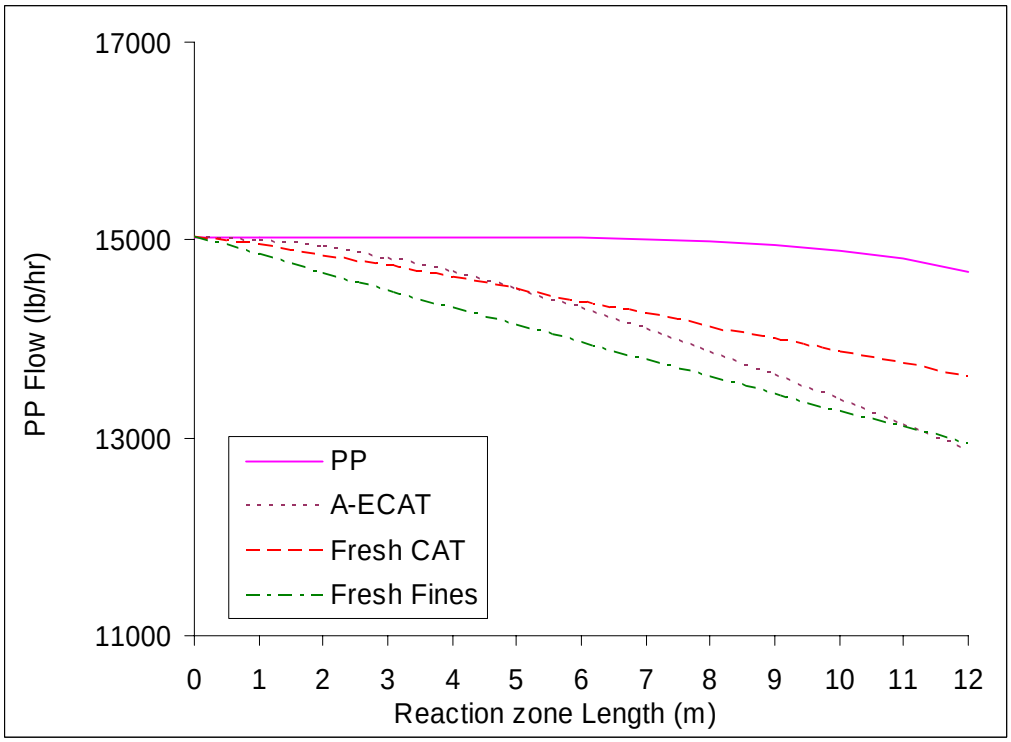

Figure 5.9 PP flow profile at 500 RPM

Similarly, the production of the hydrocarbon volatiles is profiled for the different catalyzed reactions at 500 RPM and is enhanced with increasing catalytic activity as shown in Figure 5.10. The peaks represent the points of venting in the extruder model. The total flowrate of gaseous products formed was estimated by summing up the flows at each vent, prior to being vented.

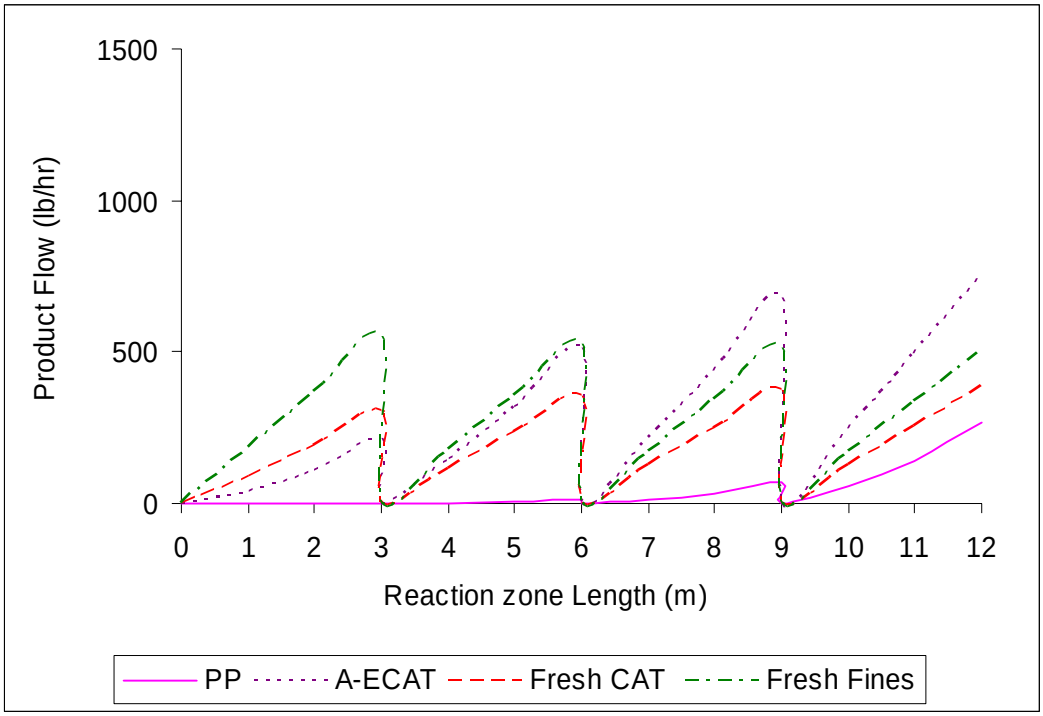

Figure 5.10 Extruder product flow profile at 500 RPM

The A-ECAT catalyst run exhibits very low yields in the front end of the reaction zone, however, towards the end of the reactor, the product yields are increased and exceeds that of the Fresh catalysts due to the higher temperature achieved (360-400°C).

Based on these results, basic costs were estimated for PP pyrolysis at a screw speed of 500 RPM. These are summarized in Table 5.6. Also shown are the total conversion achieved, total product flow and required overall heat input through the barrel wall.

Table 5.6 Estimated costs for the catalytic pyrolysis of PP at 500 RPM

RESULTS	PP	A-ECAT	Fresh CAT	Fresh Fines
Conversion	2.33E-02	1.57E-01	1.03E-01	1.52E-01
Product Flow (lb/hr)	3.50E+02	2.16E+03	1.42E+03	2.10E+03
Qin (kW)	5.52E+04	8.77E+04	9.31E+04	1.00E+05
CAPITAL COSTS				
Cost of Extruders ($)	4.05E+06	4.05E+06	4.05E+06	4.05E+06
Capital Cost (3 yr capital recovery) ($/yr)	5.78E+06	5.78E+06	5.78E+06	5.78E+06
MANUFACTURING COSTS ($/yr)				
Utilities				
Electricity	2.23E+07	3.52E+07	3.73E+07	4.02E+07
Cooling water	3.98E+03	3.98E+03	3.98E+03	3.98E+03
Total cost of utilities	2.23E+07	3.52E+07	3.73E+07	4.02E+07
Raw Materials ($/yr)				
PP	0.00E+00	0.00E+00	0.00E+00	0.00E+00
Catalyst	0.00E+00	2.50E+05	5.00E+05	5.00E+05
Total cost of raw materials	0.00E+00	2.50E+05	5.00E+05	5.00E+05
Labor costs ($/yr)	2.76E+05	2.76E+05	2.76E+05	2.76E+05
Total Costs ($/yr)	2.84E+07	4.15E+07	4.39E+07	4.67E+07
Cost per lb of Feed ($/lb)	0.23	0.33	0.35	0.37
Cost per lb of Product ($/lb)	9.75	2.12	3.41	2.46

The cost per pound of feed was only slightly different for the catalyzed and non-catalyzed pyrolysis runs mainly because of their difference in the catalyst cost. On the other hand, the conversion costs are very different. These conversion costs are this high because of the very low conversions that are also achieved from running the extruder at 500 RPM.

Under both processing conditions described above, the unreacted polymer and catalyst could be recycled in with fresh polymer to increase yields. Another option is to increase the energy input into the reaction. Despite setting the barrel temperature to 500°C, the temperature of the melt either didn't reach 500°C or maintain that temperature for a significant amount of time. In Chapter 4, it was observed by TG analysis that the temperatures at the maximum rate of conversion for both the catalyzed and non-catalyzed reactions were in the range of 450 °C and above. Like the extruder model, the TG analyzer is also a non-isothermal reactor, although the change in temperature is controlled for the latter. Nevertheless, this implies that although the reactions catalyzed by the Fresh Fines and Fresh CAT begin at temperatures below 300°C, high conversions were not achieved until above 450°C. Thus, an adjustment was made to the extruder model. The current pyrolysis set-up was tailored to incorporate multiple extruders in series.

By incorporating an additional two extruders of similar geometry and design in series with the original extruder described earlier, both the temperatures and conversions can be increased as the PP is pyrolyzed progressively through all three reaction zones. Thus, the output variables for the preceding reactor were used as input variables for the following extruder.

Furthermore, certain assumptions were made in this case. First, since the polymer feed is already melted after the run through the first extruder, it was assumed that for the second and third extruders, all of the mechanical energy input is contributed towards the pyrolysis reaction. Second, it was presumed that the additional extruders would require more labor, thus the number of operators per shift was increased to 4 operators. Based on these modifications, basic costs were estimated for the catalytic pyrolysis of PP using the Fresh

catalysts and are shown in Table 5.7. Also shown are the temperature ranges achieved for both catalysts, using this extruder set-up. In calculating the total costs for the respective PP feed, the utitlity costs for each extruder in the series set-up was added whereas, the costs of the raw materials remain the same.

Table 5.7 Estimated costs for the catalytic pyrolysis of PP using multiple extruders at 500 RPM

RESULTS	Fresh CAT	Fresh Fines
Conversion	9.57E-01	8.46E-01
Product Flow (lb/hr)	1.26E+04	1.12E+04
Qin (kW)	1.93E+05	1.12E+05
Temperature range (°C)	360-530	360-480
CAPITAL COSTS		
Cost of the three Extruders ($)	1.21E+07	1.21E+07
Capital Cost (3 yr capital recovery) ($/yr)	1.73E+07	1.73E+07
MANUFACTURING COSTS ($/yr)		
Utilities		
Electricity	7.78E+07	4.58E+07
Cooling water	1.19E+04	1.19E+04
Total cost of utilities	7.79E+07	4.58E+07
Raw Materials		
PP	0.00E+00	0.00E+00
Catalyst	5.00E+05	5.00E+05
Total cost of raw materials	5.00E+05	5.00E+05
Labor costs	5.52E+05	5.52E+05
Total Costs ($/yr)	9.63E+07	6.42E+07
Cost per lb of Feed ($/lb)	0.77	0.51
Cost per lb of Product ($/lb)	0.80	0.61

The results show an increase in the final conversion of PP feed. At these processing conditions, about 96 and 85% of PP was reacted, respectively. This is much higher that the

results obtained using a single extruder. Therefore, the conversion costs are significantly reduced to less than one dollar per pound.

Considering the temperature range and profile, it is presumed that the volatile mixture consists of both light and heavy weight hydrocarbon compounds in the C_1-C_{12} range. This model does not account for the downstream processing and separation of these products. In addition, char production was not accounted for in this model, although its formation is expected during the degradation process. The char amount will obviously build up with increasing residence times, and slower reaction.

Overall, the reactor model shows the effectiveness of FCC catalysts in the pyrolysis of PP with fresh catalysts showing the most potential at the specified operating conditions.

CHAPTER 6

CONCLUSIONS AND RECOMMENDATIONS

The catalytic pyrolysis of PE and PP was studied by TGA. For this study, the pyrolysis of PE and PP was enhanced by the use of both fresh and equilibrium FCC catalysts. The catalytic activity of a specific FCC formulation was found to increase with reduction in catalyst particle size. The increased surface area of the finer catalyst sample was found to significantly enhance the pyrolysis of PP and PE. While equilibrium catalysts were less effective than the fresh catalysts at desired temperatures, their catalytic activity may be improved by the addition of small amounts of Fresh Fines.

In spite of the complex nature of polyolefin degradation, as well as the limitations and assumptions made in kinetic analyses used in this study, the kinetic parameters, E_a and A for the catalysis of PP pyrolysis were obtained from TG data. However, the kinetics estimation by the two different approaches (Isoconversion analysis and the Arrhenius equation) led to some key observations.

First, significant deviations were observed in the values of E_a at the different heating rates. Averaging the estimated kinetic parameters over the different heating rates propagates error in both analyses.

Secondly, in simulating the TG plots, it was evident that the best fits favored lower weight fractions of catalysts and more so for the non-catalytic reaction, which may be attributed to

the simplified mechanism assumed for the complex degradation scheme in polyolefin pyrolysis. Based on these observations, it is recommended that an unconventional approach be used in the kinetic analysis of polyolefin pyrolysis by TG, such as the sample controlled thermal analysis (SCTA) method described in Chapter 3.

Although, deviations in the TG characteristics were observed for both the dry mixing and melt mixing methods, the melt-mixing method may still be a more accurate method for TG sample preparation in polyolefin pyrolysis.

In this study, the pyrolysis of PP-PCC was achieved at much lower temperatures than the virgin PP. Furthermore, the pyrolysis of the waste PP was only slightly influenced by the FCC catalysts. The decreased activity of the acidic catalysts may be caused by the neutralization of the acidic sites by the original $CaCO_3$ content in the PP-PCC. $CaCO_3$ was found to be more effective than the equilibrium catalysts in lowering $T_{onset.}$ Overall, the Fresh FCC Fines were the most effective, particularly at 3 wt%; however, its activity on the waste PP was reduced by half compared to the pure PP. It is possible that at much higher catalyst fractions, increased rates of degradation of PP-PCC may be observed.

The catalytic pyrolysis of PP in an extruder was modeled using a non-isothermal plug flow reactor model. Based on the kinetic parameters obtained in this study, the reactor model suggests that optimum operating conditions required by the various catalyzed reactions are different. As was shown, the rate of the catalytic reaction is driven by the temperature achieved in the extruder, thus higher yields can be achieved by additional energy input into the system. This may be achieved by the redesign of the screw elements to increase shearing at specific positions along the extruder, consequently increasing conversion of the polymer.

Furthermore, the assumptions made in estimating the rate equation may have also contributed in the low yields that were observed. This reactor model may be further investigated using a different estimation of the rate equation.

APPENDICES

APPENDIX A

Table A.1: Recent lab-scale experiments on polyolefin pyrolysis using other reactor set ups.

Researcher	Experimental set-up	Polyolefin feed	Catalysts	T_{op} (°C)	Main HC yield	Refs.
Akpanudoh et. al.	Infra red heating of polymer-catalyst charge in semi-batch Pyrex reactor in N_2 flow.	PE	USY- based commercial cracking catalysts	317-414	Liquid	[233]
Zhou et. al.	Batch operation on dry mixture of catalyst and polymer charged in SS vessel under N_2 flow.	PP	Modified ZSM-5 (MZ)	380	C_4-$C_{9\ w/MZ}$ C_4-$C_{13\ w/o\ MZ}$	[97]
Lee et. al.	Semi-batch reactor containing polymer + catalyst dynamically heated to degradation temperature at atmospheric pressure. Studied effect of varying HDPE: PS amount.	PP + HDPE mixture	Spent FCC	400	C_{13}^- Aromatics (> 80 wt% liquid yield at > 50% PS content)	[124]
Ukei et al.	Vapor phase. Pyrolysis in a fixed bed reactor where polymer is heated to degradation temperature HC vapors carried to catalyst bed by N_2	PS	Solid bases Solid acids Active carbon Metal oxides	350	Liquid (oil) w/high styrene selectivity. B>A>C>MO??	[234]
Takuma et. al.	Down flow tubular fixed bed reactor (catalyst in a reactor located below polymer bed). Helium gas drives polymer melt into reactor below.	PP HDPE LDPE	H-gallosilicate ——	375-550 550	Liquid; BTX aromatics C_1-C_{21}^+	[235]
Williams et. al.	Fixed bed reactor consisting of a pyrolysis section and a catalyst section, both heated separately.	PS	HZSM-5 US- Y	*500, 500	Ethene, propene Propane, ethene isobutane	[236]

Table A.2. Product distribution of polyethylene in fluidized bed reactors

Refs.	[101]	[218]	[218]	[11]	[11]	[127]	[127]
Reactor parameters							
Packing material	ZSM-5	HZSM-5	USY	Silica Sand	Silica sand	FCC	Quartz sand
Temp (°C)	360	360	360	645	850	450	515
C: P loading (wt/wt %)	2 : 1	0.25:1	0.25:1	----	----		
Reaction time (min)	30	30	30	25	25	100	315
Residence time (s)						12	1-2
N_2 flow rate (ml min^{-1})	40-500	570	570	0.72 – 7	0.72 – 7		
PE type	HDPE	Waste PE [a]	Waste PE	HDPE	HDPE	LDPE	LDPE
Product distribution							
Wt % of feed							
Gas	87.1	90.65	87.51	17.5	72.5	48.3	2.4
Liquid	0	3.71	4.03	79.7	16.2	37.6	97.4
Coke	1.5	1.69	3.75	nd	Nd	14.1	0.2
Residue	11.4	3.43	4.27	neg	neg	0	0
HC range				C1-C30	C1-C30		
Product breakdown (wt%)	0	nd	nd	0	1.5	0.1	< 0.05
H_2	72.6	56.37	31.64	13.5	69.1	48.2	2.4
C1-C4	24.6	34.28	50.84	Nd	Nd	17.2	4.4
C5-C9	2.7	1.66	0.82	Nd	Nd	Nd	
BTX							
PONA distribution[b]							
Olefins		C_3-C_5	$C_4 – C_5$	C_1-C_5	$C_1 – C_3$	C_3-C_5	Waxes
Paraffins		$C_4 – C_5$	C_3-C_6			C_3-C_4	C_{11}^+
Naphthenes							
Aromatics							

[a] 38% HDPE, 24% LDPE. [b] Only the main products are reported

Table A.3: Recent lab-scale experiments on polyolefin pyrolysis using CFRs and modified CFRs/CFR combos.

Researcher	Experimental set-up	Polyolefin feed	Catalysts	T_{deg} (°C)	Main HC yield	Refs.
Schirmer et. al.	Granular plastic was melted in extruder and fed into a cycled-spheres-reactor containing catalysts.	PE	HZSM-5 H-Y	440	Wax: C_{15}^{+}	[233]
Serrano et. al.	Liquid phase catalytic cracking in a continuous screw kiln reactor w/ two heating zones.	LDPE oil	Al-MCM-41 Nano-ZSM-5	420-450	C_5-C_{12} C_3-C_5	[42, 47]
Murata et. al.	Polymer pellets are melted in extruder and further reacted in stirred tank reactor	PE PP PS	____	420 380 350	Liquid: C_6^{+} Liquid: C_{10}^{-} Liquid: C_{10}^{-}	[26, 155]
Lin et. al.	Catalytic fluidized bed reactor for 30 min and 40 w/w polymer to catalyst. Fluidizing gas: High purity N_2.	PC waste	MCM-41, HUSY SA ZSM HMOR	360	C_5-C_9 C_5-C_9 C_5-C_9 C_1-C_4 C_1-C_4	[38]
Miskolczi et. al.	3-stage continuous set-up Extruder: polymer preheating Reactor: polymer decomposition Separator: products collection	PE/PP/PS/EPC/PA/PUR MSW	_____	500-550	C_5-C_{24}	[35]
Vasile et. al.	Studied effect of temperature, reaction time and MSW content.	HDPE/LDPE/PS/PP/PET MSW	HZSM-5 _____	420-450	C_5^{-} Olefins Wax : C_{13}^{+}	[237]
Hernandez et. al.	Fluidized bed reactor. Fluidizing gas: High purity N_2.	HDPE	HZSM-5	200, 300	C_5^{-} Olefins	[95]

Table A.4 Repeatability of TGA runs for PE

PE sample	$T_{1\%}$	$T_{99\%}$	T_{max}
8wt% A-ECAT (1)	324	469	459
8wt% A-ECAT (2)	319	469	459
8wt% Fresh CAT(1)	289	484	465
8wt% Fresh CAT(2)	284	483	467
8wt% Fresh Fines (1)	294	486	469
8wt% Fresh Fines (2)	283	485	470
8wt% S-ECAT(1)	316	457	448
8wt% S-ECAT(2)	303	455	448

APPENDIX B

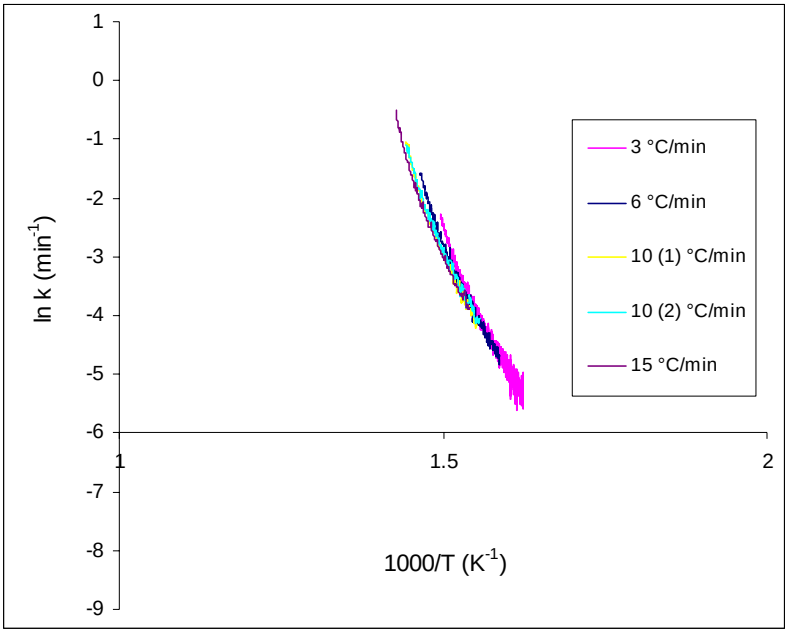

Figure B.1 Arrhenius plot for the degradation of 8 wt % A-ECAT

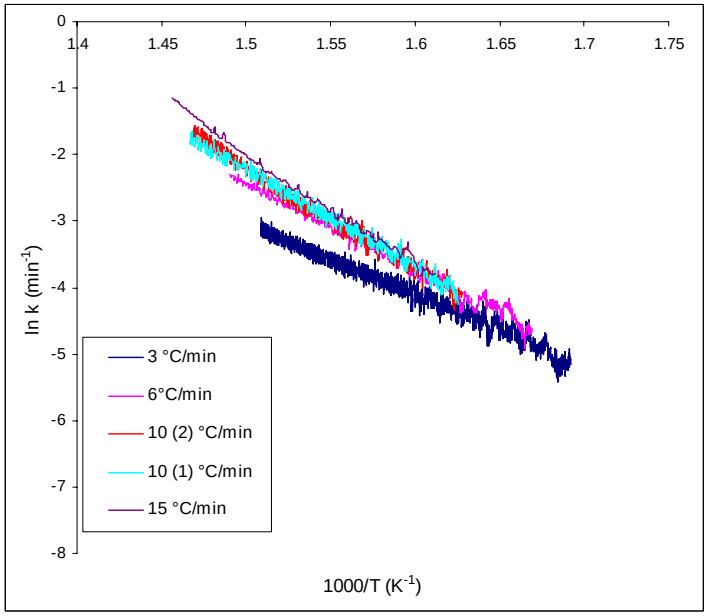

Figure B.2 Arrhenius plot for the degradation of 8 wt % Fresh CAT

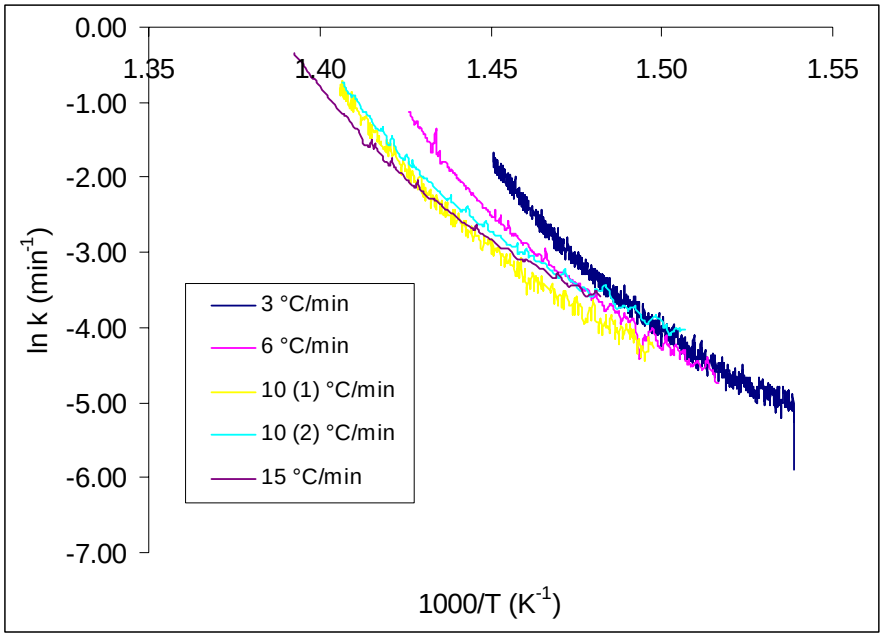

Figure B.3 Arrhenius plot for the catalytic degradation of PP using 3 wt% S-ECAT

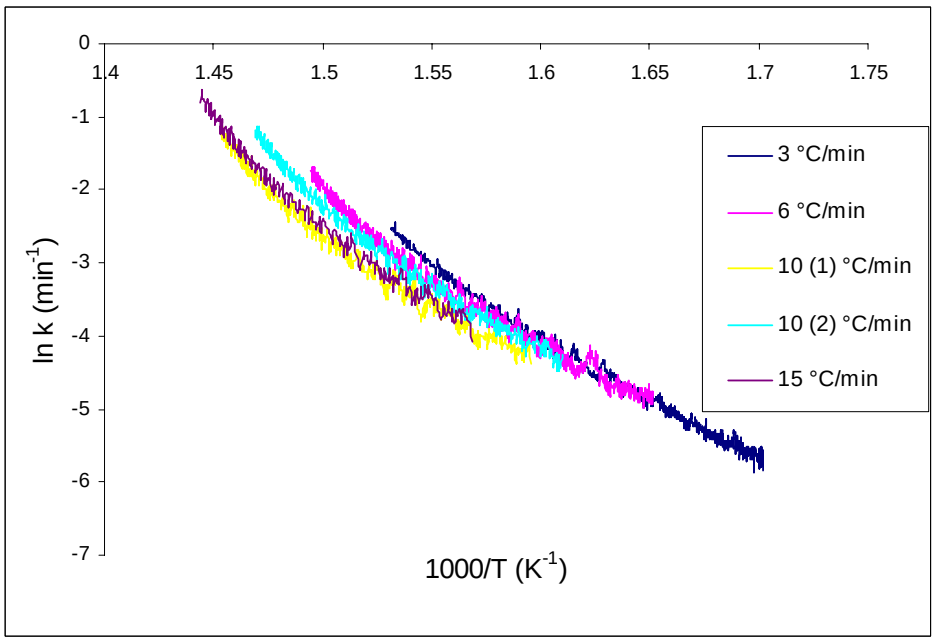

Figure B.4 Arrhenius plot for the catalytic degradation of PP using 8 wt% S-ECAT

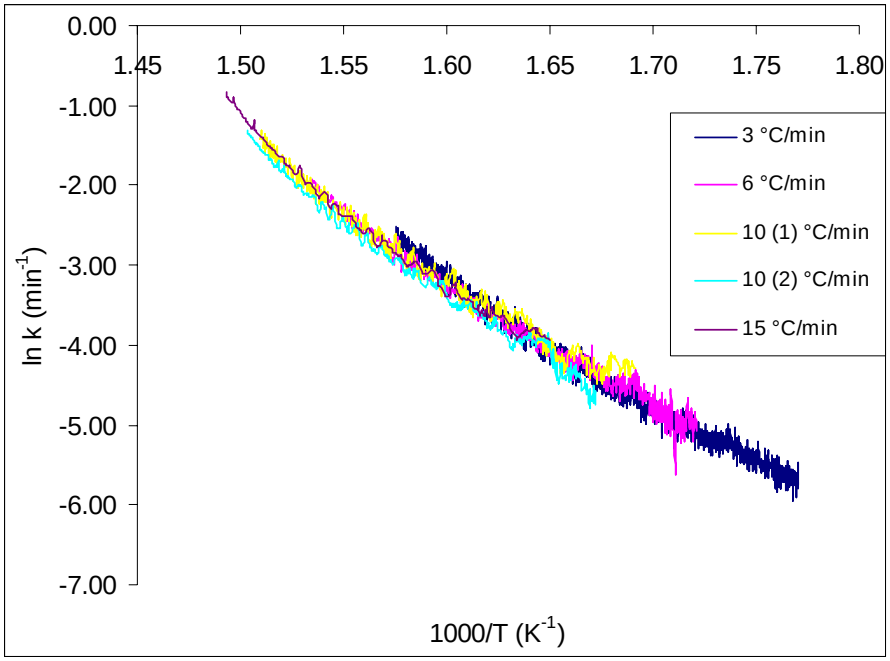

Figure B.5 Arrhenius plot for the catalytic degradation of PP using 13 wt% S-ECAT

Table B.1 Estimation of kinetic parameters for PP degradation using 8wt % of FCC catalysts. The Arrhenius equation method was applied for conversion range of 4- 40%
(Some heating rates were repeated)

Catalyst	Catalyst (% w/w)	β (^{o}C/min)	E_a (kJ/mol)	ln A (min^{-1})	r^b
Virgin PP	0	3	230	37	0.96
		6	251	41	0.96
		10-1	279	46	0.97
		15-1	239	39	0.97
		15-2	227	41	0.97
Average			251 ± 19	41 ± 3	
Fresh CAT	8	3	89	13	0.97
		6	107	17	0.98
		10-1	121	20	0.98
		10-2	127	21	0.99
		15	139	23	0.99
Average			120 ± 17	19 ± 4	
Fresh Fines	8	3	60	8	0.95
		6	55	8	0.96
		10-1	49	7	0.92
		10-2	50	7	0.94
		15	49	7	0.89
Average			53 ± 4	7 ± 0.5	
ECAT	8	3	190	32	0.98
		6	207	35	0.99
		10-1	229	38	0.99
		10-2	216	36	0.99
		15	233	39	0.98
Average			215 ± 16	36 ± 3	
Shell ECAT	8	3	150	25	0.99
		6	159	26	0.97
		10-1	172	29	0.97
		10-2	179	30	0.98
		15	202	34	0.97
Average			173 ± 18	29 ± 3	

[a] Measured weight fraction
[b] linear correlation coefficient

Table B.2 Estimation of kinetic parameters for PP degradation using S-ECAT. The Arrhenius equation method was applied for conversion range of 4- 40%
(Some heating rates were repeated)

Catalyst[a] (% w/w)	β (°C/min)	E_a (kJ/mol)	ln A (min^{-1})	r[b]
0	3	230	37	0.96
	6	251	41	0.96
	10-2	279	46	0.97
	15-1	239	39	0.97
	15-2	227	41	0.97
	Average	251 ± 19	41 ± 3	
3	3	303	51	0.972
	6	314	52	0.980
	10-1	295	52	0.972
	10-2	268	44	0.970
	15	298	49	0.976
	Average	300 ± 15	49 ± 3	
8	3	150	25	0.99
	6	159	26	0.97
	10-1	172	29	0.97
	10-2	179	30	0.98
	15	202	34	0.97
	Average	172 ± 18	29 ± 3	
13	3	129	22	0.98
	6	133	22	0.98
	10-1	136	23	0.97
	10-2	150	26	0.99
	15	162	28	0.98
	Average	142 ± 12	24 ± 2	

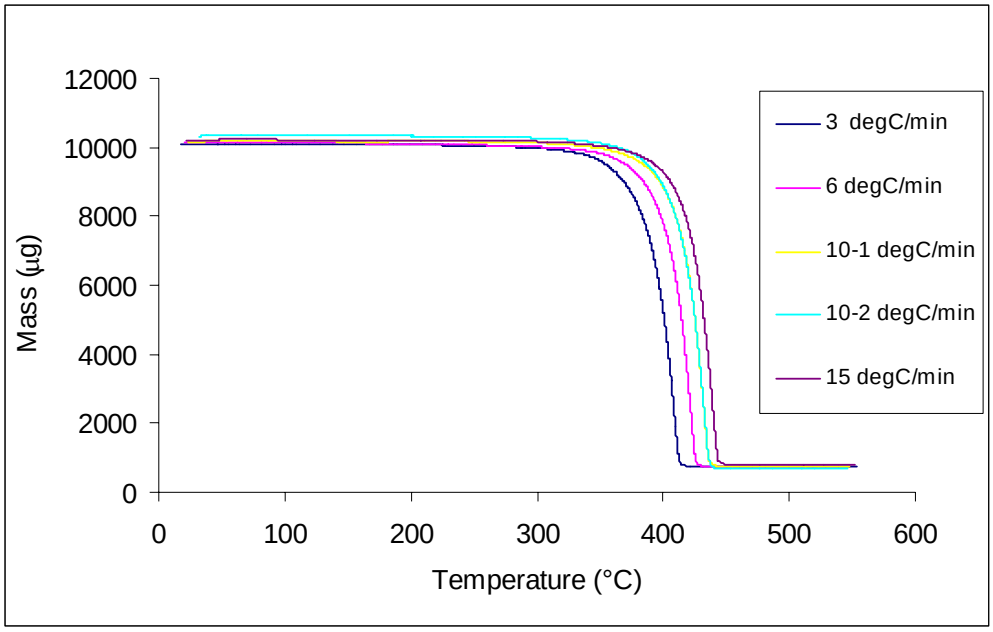

Figure B.6 TG plot for the degradation of PP using 8 wt % A-ECAT

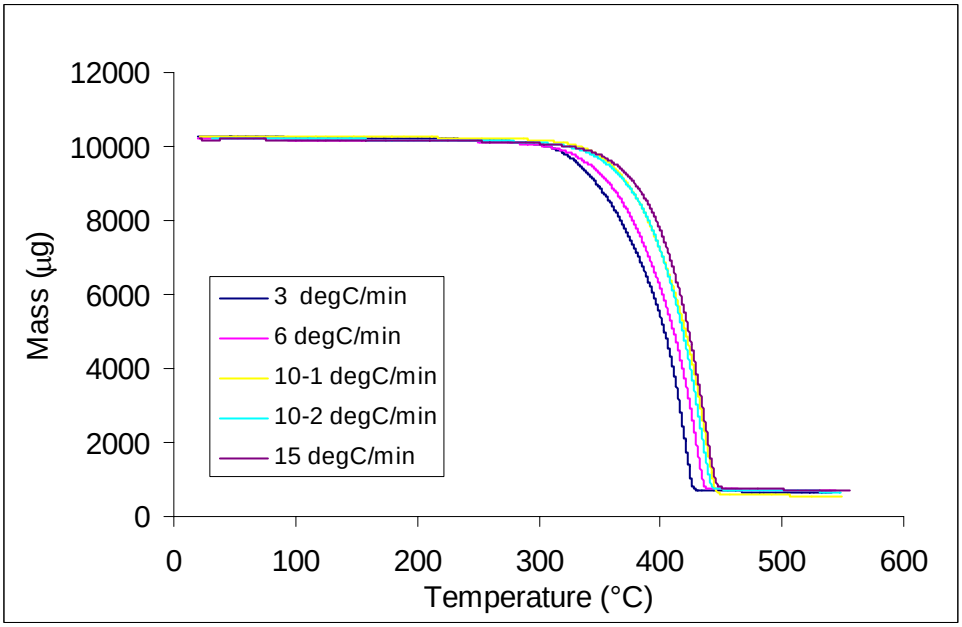

Figure B.7 TG plot for the degradation of PP using of 8 wt % Fresh CAT

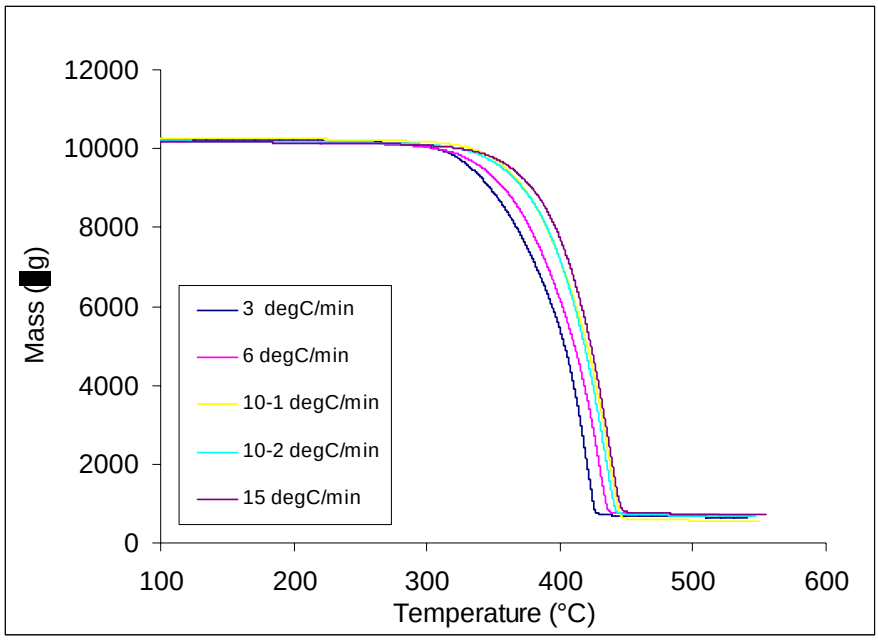

Figure B.8 TG plot for the degradation of PP using 8 wt % Fresh Fines

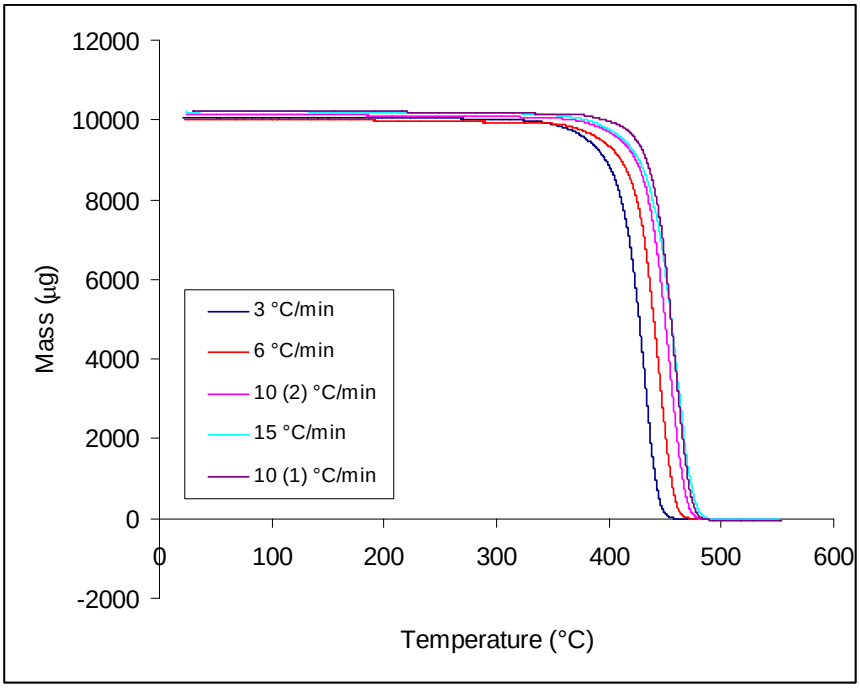

Figure B.9 TG plot for the degradation of Virgin PP

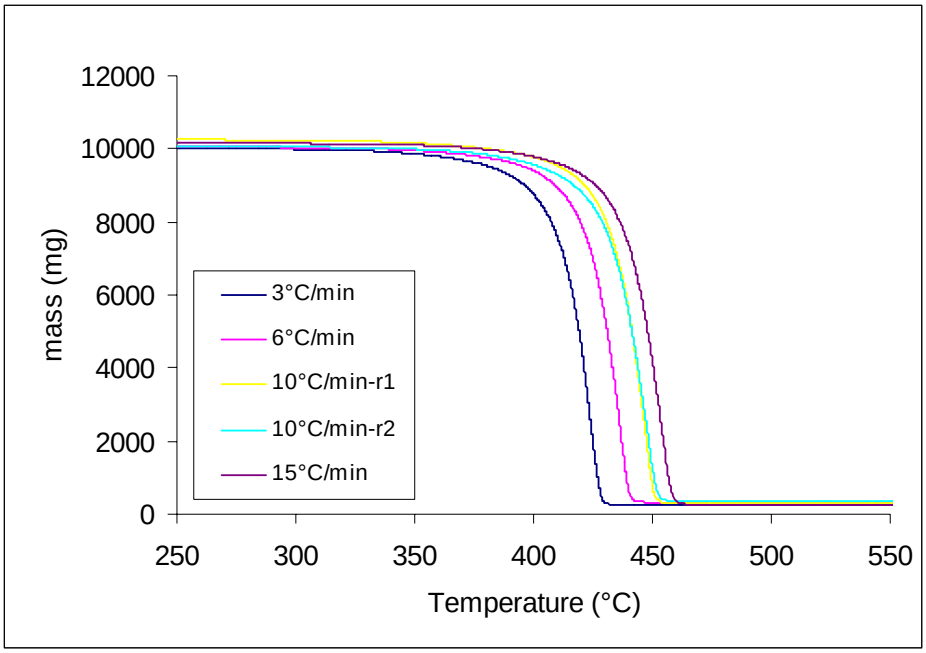

Figure B.10 TG plot for the degradation of PP using 3 wt % S-ECAT

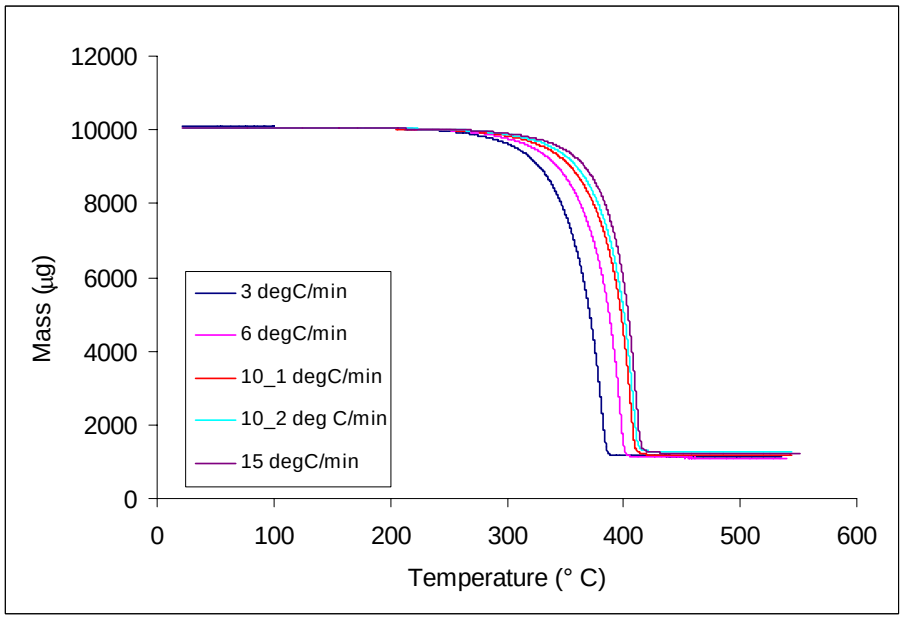

Figure B.11 TG plot for the degradation of PP using 13 wt % S-ECAT

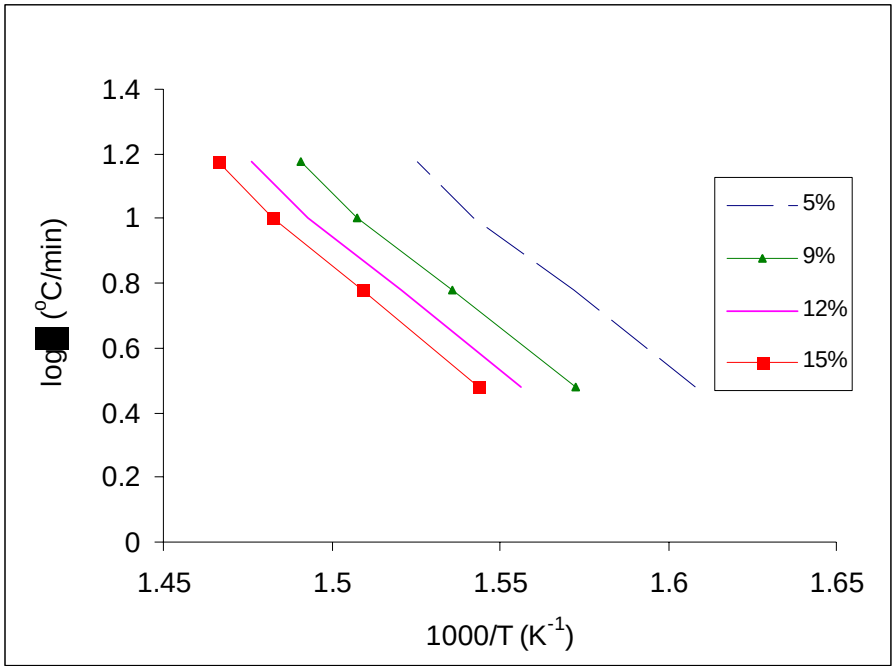

Figure B.12 Isoconversion TG data analysis method. Plot of log β versus T^{-1} for degradation of PP using 8 wt % A-ECAT

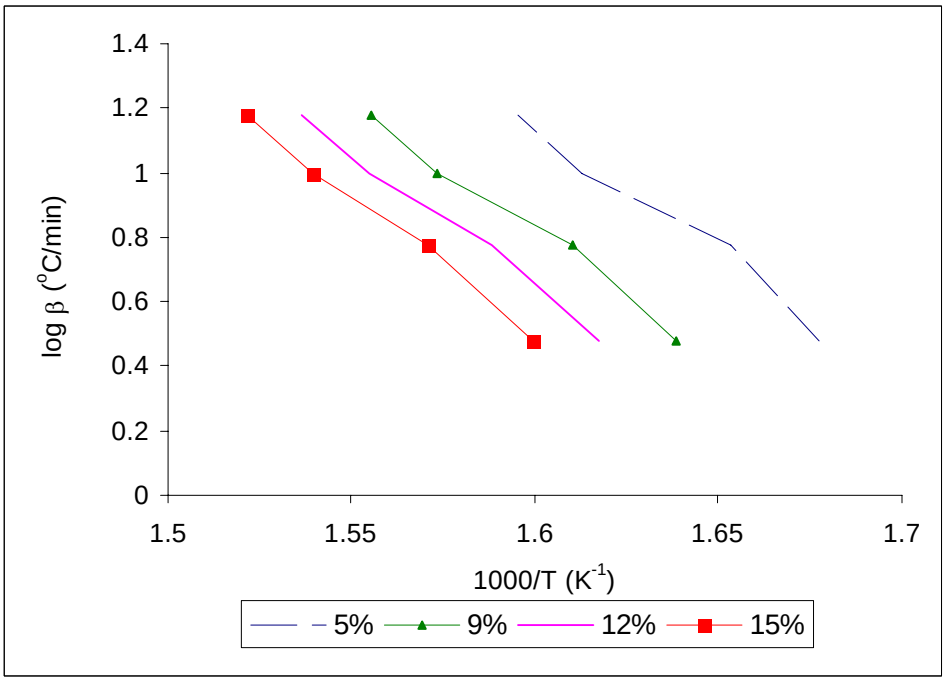

Figure B.13 Isoconversion TG data analysis method. Plot of log β versus T^{-1} for degradation of PP using 8 wt % Fresh CAT

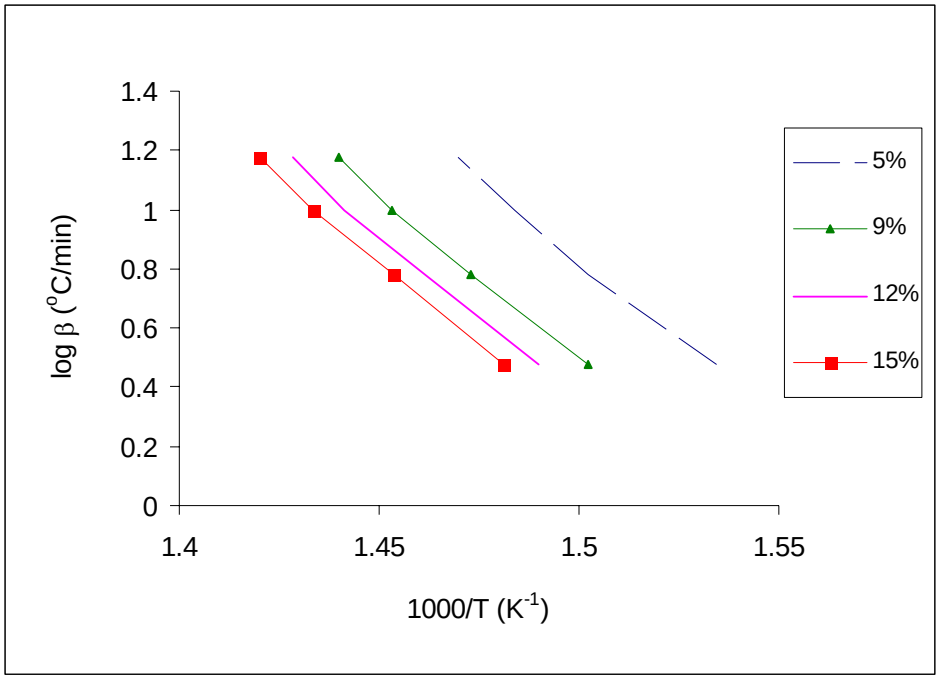

Figure B.14 Isoconversion TG data analysis method. Plot of log β versus T^{-1} for degradation of PP using 3 wt % S-ECAT

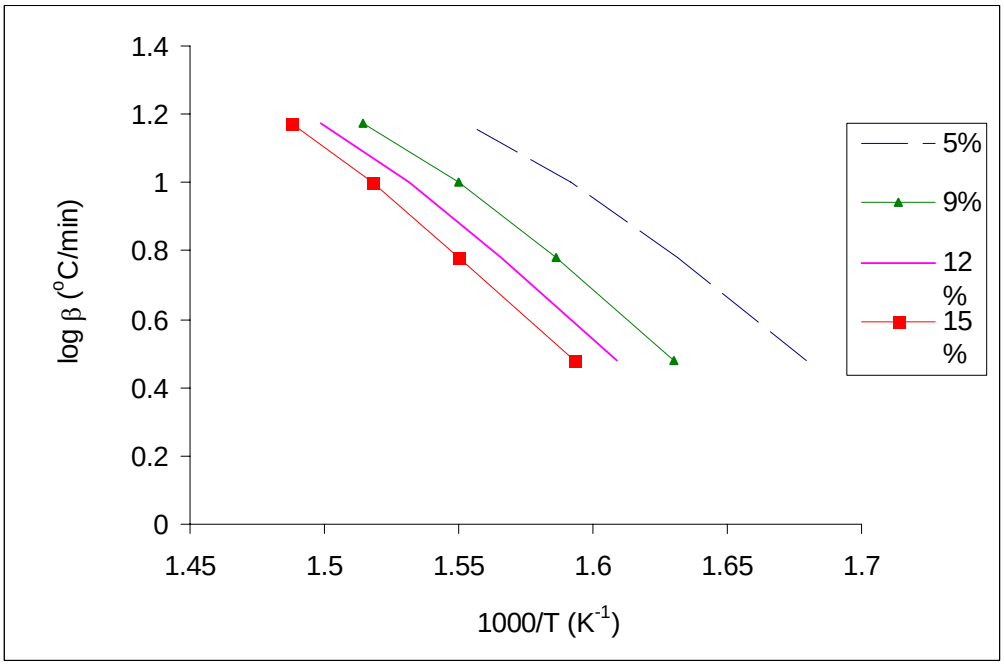

Figure B.15 Isoconversion TG data analysis method. Plot of log β versus T^{-1} for degradation of PP using 8 wt % S-ECAT

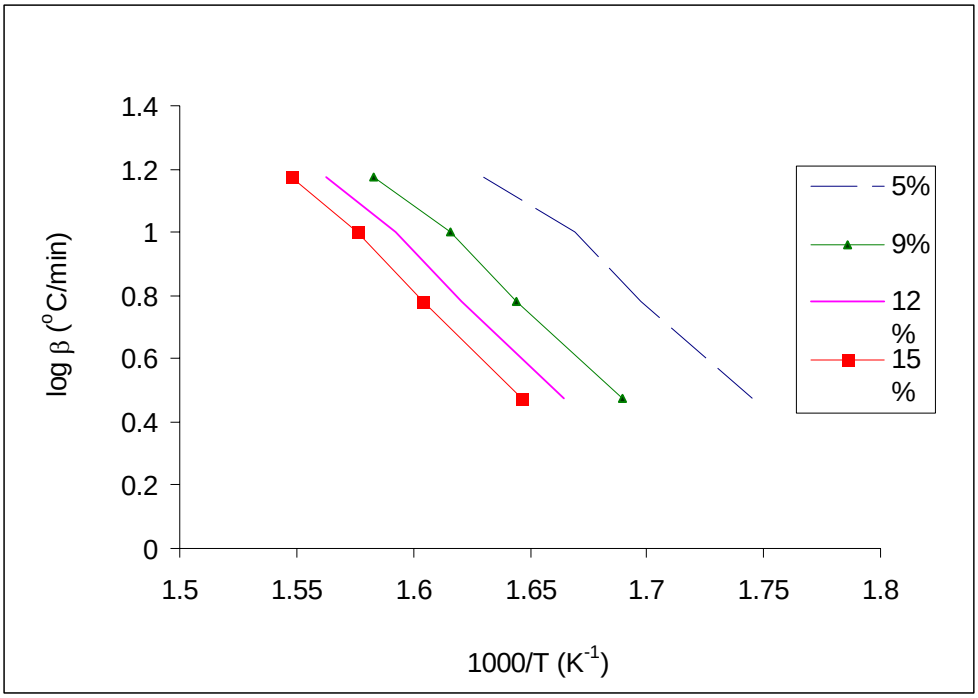

Figure B.16 Isoconversion TG data analysis method. Plot of log β versus T^{-1} for degradation of PP using 13 wt % S-ECAT

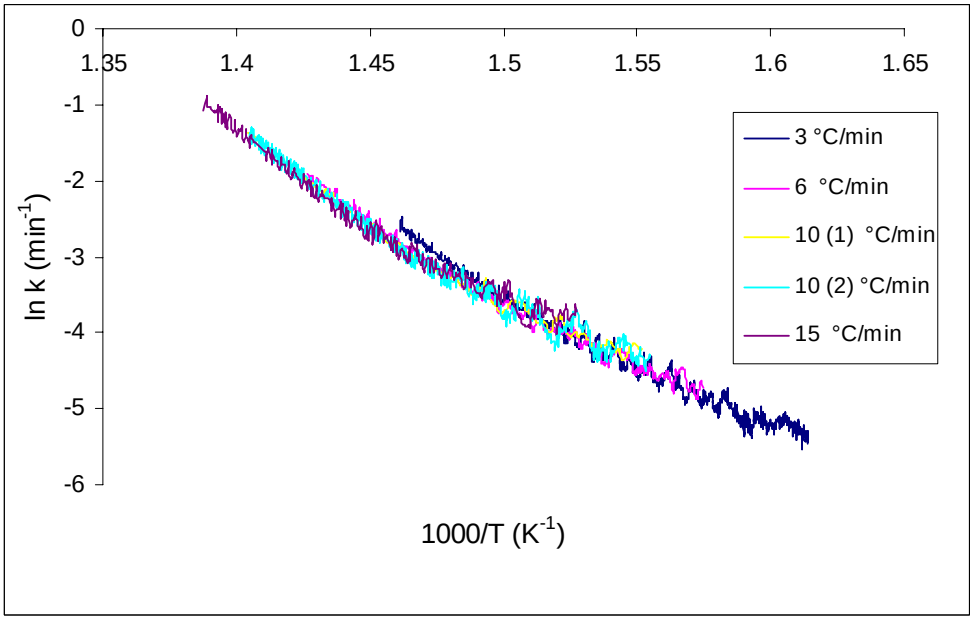

Figure B.17 Arrhenius plot for the catalytic degradation of PE using 8 wt% A-ECAT

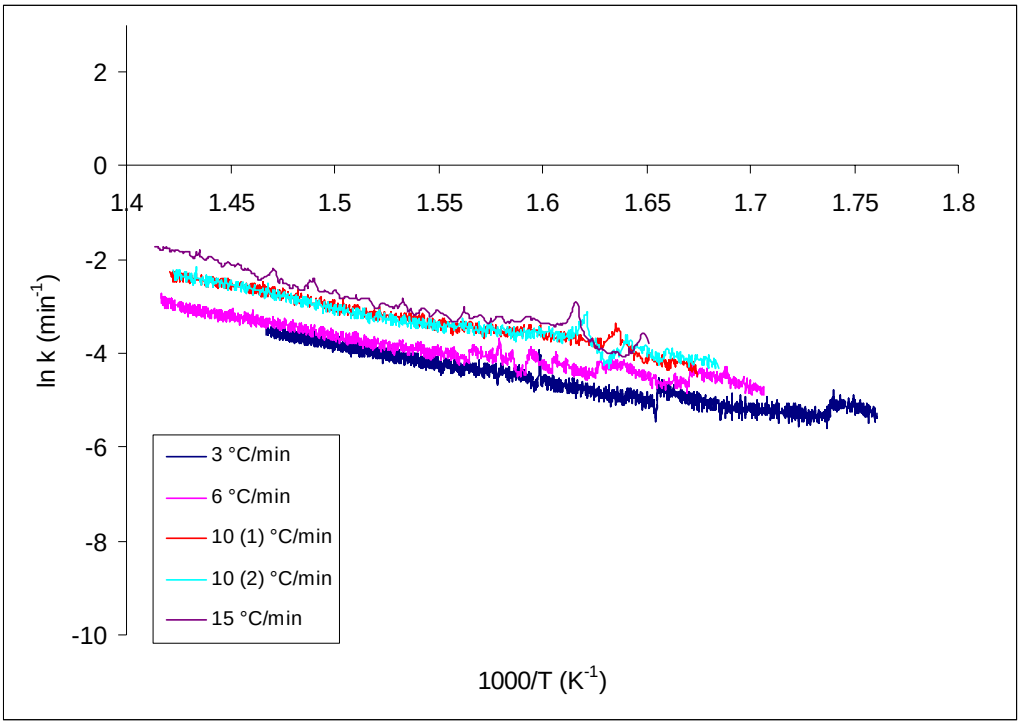

Figure B.18 Arrhenius plot for the catalytic degradation of PE using 8 wt% Fresh CAT

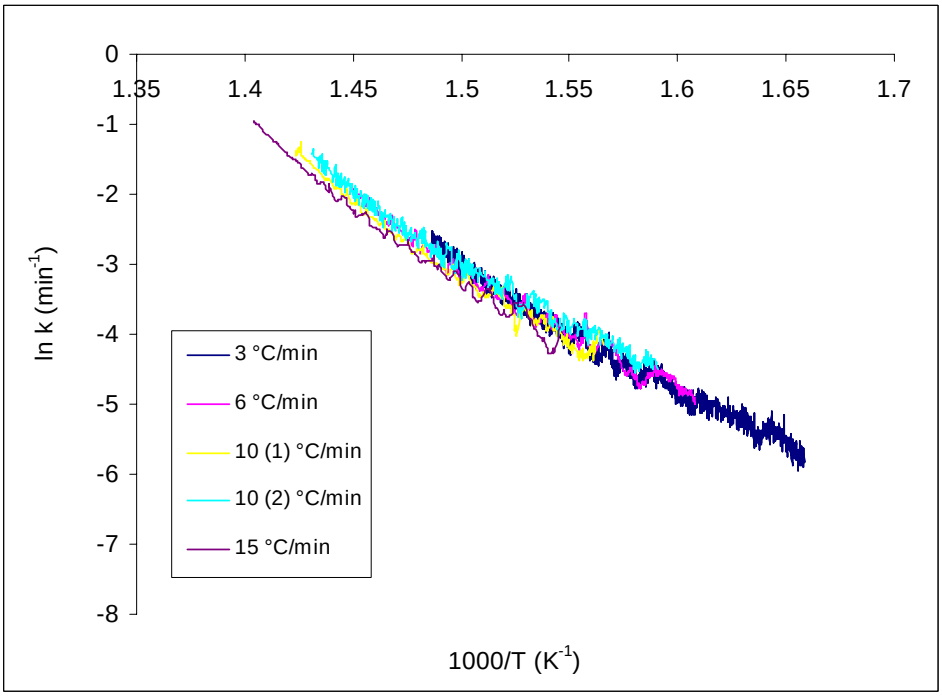

Figure B.19 Arrhenius plot for the catalytic degradation of PE using 8 wt% S-ECAT

Table B.3 Estimation of kinetic parameters for PE pyrolysis using 8 wt % of FCC catalysts. The Arrhenius equation method was applied for a conversion range of 4- 40%
(Some heating rates were repeated)

Catalyst	Catalyst (% w/w)	β (^{o}C/min)	E_a (kJ/mol)	ln A (min^{-1})	r^b
Virgin PE	0	3	357	57	0.98
		6	408	65	0.90
		10-1	383	61	0.99
		10-2	410	65	0.98
		15	409	65	0.99
		Average	393 ± 21	56 ± 3	0.99 ± 0.0
Fresh CAT	8	3	53	7	0.93
		6	50	7	0.94
		10-1	60	8	0.96
		10-2	57	7	0.94
		15	73	11	0.94
		Average	59 ± 8	8 ± 1	0.94 ± 0.0
Fresh Fines	8	3	47	8	0.97
		6	41	9	0.93
		10-1	42	8	0.93
		10-2	42	8	0.96
		15	47	7	0.93
		Average	44 ± 2	8 ± 0.6	0.94 ± 0.0
A-ECAT	8	3	148	23	0.98
		6	158	25	0.98
		10-1	167	27	0.98
		10-2	165	26	0.97
		15	175	28	0.97
		Average	163 ± 9	26 ± 2	0.97 ± 0.01
S-ECAT	8	3	142	23	0.98
		6	150	24	0.98
		10-1	170	27	0.98
		10-2	154	25	0.98
		15	182	30	0.99
		Average	159 ± 14	26 ± 3	0.98 ± 0.0

Appendix C

Table C.1 Physical Properties of Apparent Gaseous Products.
(These hydrocarbons are gases at room temperature)

Compound	Cp° (kJ/kg K)	$\Delta H°_{vap}$ (kJ/kg)	B_p (^oK)	Cp°liq (kJ/kg K)
Butane	1.68	361.32	272.65	2.28
1- Butene	1.53	360.01	266.65	2.30
Ethane	1.75	172.93	185.15	4.53
Ethene	1.53	482.71	169.15	2.40
Methane	2.23	509.91	111.65	2.23
3-Methyl-1-butene	1.69	343.60	293.15	2.23
2-Methylpropane	2.25	332.07	261.45	2.23
Propane	1.67	335.60	231.05	2.71
Propene	1.53	337.45	225.45	2.42

All data are at 298K

Table C.2a Physical Properties of Apparent Liquid Products.
(These hydrocarbons are liquids at room temperature)

Liquid Properties

Compound	Cp° (kJ/kg K)	$\Delta H°_{vap}$ (kJ/kg)	B_p (^oK)
Benzene	1.74	432.72	353.15
Decane	2.21	361.23	447.25
Dodecane	2.21	361.04	489.35
Heptane	2.24	365.23	371.55
1-Heptene	2.14	358.95	366.75
Hexane	2.27	366.67	341.85
1-Hexene	2.18	363.59	336.65
2-Methylbutane	2.28	345.11	300.95
Nonane	2.22	361.77	423.95
Octane	2.23	363.30	398.85
Pentane	2.32	365.90	309.15
1-Pentene	2.20	363.56	303.25
Toluene	1.70	412.42	383.75
Undecane	2.21	360.82	469.15
1,4-Xylene	1.71	399.36	415.00

All data are at 298K

Table C.2b Physical Properties of Apparent Liquid Products.
(These hydrocarbons are liquids at room temperature)

Gas Properties

Compound	Cp° (kJ/kg K)
Decane	nf
Dodecane	1.65
Heptane	1.66
1-Heptene	1.57
Hexane	1.66
1-Hexene	1.57
2-Methylbutane	1.65
Nonane	1.65
Octane	1.65
Pentane	1.67
1-Pentene	1.56
Toluene	1.12
Undecane	nf
1,4-Xylene	1.20

nf- not found and were omitted in all calculations
All data are at 298K

Attachment C.1: MATLAB Function 'inputvar'

This MATLAB file is called multiple times from the other files to output certain parameters and constants.

```
% This function outputs the common input variables for all other pertinent functions: 'f3mod' and
'cost'  THE CASE FOR THE PYROLYSIS OF PP USING A-ECAT IS SHOWN

function input = inputvar()
 % Extruder Geometry
L_D = 52;                   % L/D ratio
Lt = 12;                    % total length of reactor (m)
Z = 0.7;                    % Ds/Db: ratio of screw to barrel diameter
Bw = 1.0;                   % Barrel thickness in inches
D = Lt/L_D;                 % barrel Diameter (m)

% Process conditions
 Ff = 1.894;                % (kg/s)
Fflbhr = Ff*3600*2.205;     % (lb/hr)
 Tin = 25;                  % Temperature of feed melt in Celcius (°C)
capR = 1.894                % Maximum capacity of extruder % (kg/s)

% Feed Properties
 wf = [0.92; 0.08];         % weight fraction of [polymer, wf(1); catalyst, wf(2)]in feed.
Cp = [1.9;1.0];             % (kJ/kgK) % Heat capacity of polymer, Cp(1); catalyst, Cp(2)
RHOm = 769;                 % Polymer melt density (kg/m3)
dHrxnTref = 307;            % Heat of decomposition of polymer @ Trefd (KJ/kg)
Trefs  = 298;               % Reference temperature for other standard parameters (K)
Trefd  = 436 + 273;         % Reference temperature (K)
u = 500;                    % Viscosity kg/m.s
c = 0.6;                    % c: %Crystallinity of polymer, input(17)
dHmref = 60;                % dHm ref: Heat of melting at 100% crystallinity, kJ/kg

% Kinetic Parameters
 lnA = 36;                  % Natural log of Pre-exponenetial factor
PreExp = exp(lnA);          % Pre exponential factor (1/min)
A = PreExp/60;              % (1/sec)- used in calculations
Ea = 215;                   % Activation Energy (KJ/mol)
n = 1;                      % Reaction order
% Scaling Q, the volumetric flow rate to screw speed, N. Based on the volumetric flow rate at
500RPM maximum for the Georgia Tech CRNI extruder

N1 = 500;                   % Base screw speed (RPM)
N2 = 500;                   % Required screw speed (RPM), input(21)
Q1 = Ff/RHOm;               % Volumetric flowrate
Q2 = Q1*(N2/N1);            % Scaling equation (REF: Xanthos 1992)(where diameters in both
                            % extruders are equal)
F2 = RHOm*Q2                % Adjusted initial mass flowrate (kg/s)

input
=[L_D;Lt;Z;Bw;F2;wf(1);wf(2);Cp(1);Cp(2);RHOm;dHrxnTref;Trefs;PreExp;A;E;n;u;Tin;c;dHmr
ef;N1;D;Trefd;capR];
```

Attachment C.2: MATLAB Function 'screw'

This MATLAB file calculates the estimated extruder drive power based on a scale up of a 30 mm NFM twin screw extruder.

```
function mechE = screw()
var = inputvar();                   % Call on function 'inputvar' which outputs the
                                     % required variables
N1 = var(21);                        % RPM
F = var(5);                         % Total mass flowrate (kg/s)
rho = var(10);                      % Density of molten PP @ 180C (kg/m3)
Q = F/rho;                          % Vol flowrate (m3/s)
u = var(17);                        % Viscosity kg/m.s
D2 = var(22);                       % Barrel diameter for current extruder size


% Input geometry for 30mm CRNI Extruder

% length of each segment (inches)
dL=[7.97 6.19 1.77 3.54 1.77 7.96 4.42 1.77 7.97 4.42 1.77 6.2 8 7.2];
L = sum(dL);                %(in)
L = L/39.37;                %(m)

% Diameter of screw in inches (m)
Ds=[.9 1.025 1.12 .96 1.11 .78 .96 1.12 .9 .96 .96 .9 .9 .9]; Ds = mean(Ds)/39.37;
Db =30/1e3;                 % Barrel diameter (m)- single barrel

% Calculate p, # of flights
S = 1.181/39.37;             % pitch, (m)
p = L/S;                     % Number of flights a single screw

% Calculate Vbz, velocity in down channel direction
N = N/60;                           % RPS
pi = 3.141592654;
thetab = atan(S/(pi*Db));           % Helix angle at barrel surface
Vbz = p*N*Db * cos(thetab);

% Calculate Qd, Drag flow
thetas = atan(S/(pi*Ds));                   % Helix angle at screw surface
e = 0.14/39.37;                             % flight thichness, (m)
W = S * cos(thetas)- e;                     % Width of screw channel (m)
H = Db-Ds;                                  % Channel depth (m)
flightd = 1.168/39.37;                      % Flight diam (m)
df = Db -flightd;                           % flight clearance (m)
Qd = (p*Vbz*W*H)/2* [1- (df/H)]^2;          % m3/s

% Calculate f, geometrically determined factor
f = 4 - 3*(cos(thetab))^2*(Q/Qd) + (H/W)*(e/df);                    (1)
```

Attachment C.2: MATLAB Function 'screw' (CONTINUED)

```
% Calculate E: Mechanical input from extruder drive
% Multiplied by 2 for twin screw

E = 2*(p*u*(N*pi*Db)^2*(W/H)*(L/sin(thetab))* f);   % J/s

% Scale up for E
E = E*(D2/Db)^1.5          % (W)

mechE = [E];               % (W; Pa)
```

(2)

C.3: MATLAB Function 'meltzone'

This MATLAB function calculates the temperature change in melting the polymer feed. The outputs are the final temperature of the polymer melt, Tmelt (K) and Polymer feed flowrate.

```
function melt = meltzone()

input = inputvar();                % Call on function 'inputvar' which outputs the required
                                   %variables
% Process Conditions
Tin = input(18);                   % Temperature of feed in Celcius (C)
Ff = input(5);
Fflbhr = Ff*(3600/0.454);          % feed rate in pounds/hr

% Material Properties
Cp = [input(8);input(9)];           % (kJ/kgK) % Heat capacity of polymer, Cp(1);
                                   catalyst, Cp(2)
dHm = input(20);                   % kJ/kg


Tin = Tin + 273;                   % Temperature of feed in Kelvin- should be close to Tm

% Calculation of Reactor Heat Input
      % Mechanical Energy Input from Extruder Drive
         E = screw;                % Calls the function 'screw' (J/s or W)
         Ef = 1;                   % (W) Fraction of E used in the melt zone
         E = (E(1)*Ef)/1e3         % Actual energy supplied by Motor (KW)

% Mass flow energy contribution
          flow = Ff*Cp(1);              %(kJ/K.s)

 % Heat of melting required at Tin
        Qmelt = Ff*(Cp(1)*(Tin-298)+ dHm);  %(kJ/s OR KW)

DT = (E-Qmelt)/flow;               %Temperature difference in melt   %K
Tmelt = Tin + DT;          % Temperature of melt %K
melt = [Tmelt; E; Ff];     %Output : %units = ['K'; 'kW'; /kg/s']
```

Attachment C.4: MATLAB Function 'Diff'

This MATLAB function "Diff" describes the ODEs.

```
function zoneRdiff = Diff (L, z)

%THE CASE FOR PYROLYSIS IN A SINGLE EXTRUDER IS SHOWN
% This function generates differential equations that are typical of a PFR design reactor.
% The PFR equations are used to model the catalytic pyrolysis of polyolefins (PP) in an extruder.
% The dependent variables of the differential equations are defined as follows:
% z(1)= X : Conversion
% z(2)= T: Extruder Temperature
% z(3) = F: Polymer Flow rate
% z(4) = P: Product Flow rate

% The outputs of this function are listed below.
% zoneRdiff= d(X)/dL
% zoneRdiff  = d(T)/dL
% zoneRdiff  = d(F)/dL
% zoneRdiff  = d(P)/dL

% These are simultaneously solved by an odesolver (ODE23s) defined in function "

input = inputvar();          %Calls on function 'inputvar' containing input variables

% Extruder Geometry
L_D = input(1);                    % L/D ratio
Lt = input(2);                     % Total length of reactor (m)
Z = input(3);                      % Ds/Db: ratio of screw to barrel diameter
Bw = input(4);                     % Barrel thickness in inches
Db = input(22);                    % Reactor diameter (m) using L/D ratio = 52
RPM = input(21);

% Process Conditions
Ff = input(5);                     % Initial flowrate of total feed (kg/s)

% Material properties
wf = [input(6);input(7)];          % weight fraction of [polymer, wf(1); catalyst, wf(2)]in feed.
Cp = [input(8);input(9)];           % (kJ/kgK) % Heat capacity of polymer, Cp(1); catalyst,
                                   % Cp(2)

RHOm = input(10);                   % Polymer melt density (kg/m3)

% Heat capacity of product flow
    % Import data from excel file and sheet and assign variables
      M= xlsread('data2.xls');
        % CpGv: Heat capacity of Gaseous products @ room temp in vapor phase
        % CpGl: Heat capacity of Gaseous products @ room tempin liquid phase
        % CpLl: Heat capacity of Liquid products @ room temp in vapor phase
        % CpLv: Heat capacity of Liquid products @ room temp in liquid phase
            CpGv = sum(M(1:9, 5));        % kJ/kgK
            CpGl = sum(M(1:9, 13));       % kJ/kgK
            CpLl = sum(M(10:24,5));       % kJ/kgK
            CpLv = sum(M(25:39,5));       % kJ/kgK
```

Attachment C.4: MATLAB Function 'Diff' (CONTINUED)

```
Fp = wf(1)*Ff;              % Initial polymer (kg/s)
Fplbhr = Fp*7936.64         % Feed rate in pounds/hr

% Kinetic Parameters
PreExp = input(13);         % Pre exponential factor (min^-1)
A = input(14);              % (1/sec)- used in calculations
Ea = input(15);             % Activation Energy (kJ/mol)
n = input(16);               % Rate order

% Constants
R = 0.008314;               % kJ/molK

% Kinetic Equation
Cpo = RHOm;                         % mass concentration of polymer (kg/m^3)
k  = A*exp((-E/(R*z(2))));          % (1/s);
rP = k*Cpo*(1-z(1))^n;              % rate equation (kg/m^3/s)

% Calculation of barrel cs area, Ac through which polymer flows.
% For a twin screw - estimate as the sum of TWO single screws
Ds = Z*Db;
Ac = (2*3.14*((Db^2)-(Ds^2))/4);          % Area of two single screws
residencetime =(Ac*Lt/(Ff/Cpo))/60;       % Residence time of material in the reactor (min)
volume = Ac *Lt;                          % Reaction volume (m^3)

% Calculation of the Heat of Reaction, dHrxnT
DeltaCp = CpGv + CpLv- sum(Cp);       % Overall change in heat capacity (kJ/kgK)

% (KJ/kgK) assuming feed Cp is mainly based on the polymer contribution
FeedCp = wf(1)*Cp(1)+wf(2)*Cp(2);     % Heat capacity of feed (kJ/kgK)
dHrxnTref =  input (11);               % (kJ/kg). Heat of decomposition of polymer
                                       % at Tref = 25°C

Tref  = input(12);                    % Reference temperature (K)
Trefd  = input(23);                   % Reference temperature at polymer degradation
                                      % obtained from DTA (K)

dHrxnT = dHrxnTref + DeltaCp*(z(2)-Trefd);    % (kJ/kg) Heat of reaction at reactor
                                              temperature
```

(2)

Attachment C.4: MATLAB Function 'Diff' (CONTINUED)

```
% Calculation of Reactor Heat Input

 % Mechanical Energy Input from Extruder Drive for the Secondary Reactors in series
E = screw();                        % Calls the function 'screw' (W)
Ef = 1;                             % Contribution to the reaction zones
Etot = (E(1)* Ef)/1e3;              % Energy supplied by the extruder drive in % kW

% Calculation of the overall heat transfer coefficient btw the barrel wall and the polymer melt

lamda = 0.12;                        % Thermal conductivity of polypropylene (W/mK)
                                     % http://www.segerfrojd.se/ppvsmetal.htm
lamdab = 19;                        % Heat conductivity of barrel material (W/mK)
Bw = 0.25;                           % Barrel thickness in inches
Do = Db + 2*(Bw*(2.54*10^(-2)));   % Diameter of outer barrel (m)
Tw = 750 +273;                              %Barrel temperature K

N = RPM/60;                                 % Screw rotation rate in (1/s)
Re = (RHOm*N*Ds)/u;                 % Reynolds number.
Pr = ((Cp(1)*1000)*u)/lamda;        % Prandtl number. NOTE:Cpp in J/kgK

% Calculation of heat transfer coeff btw polymer melt and barrel wall

hi = (lamda/Ds)*(0.94*Re^(0.28)*Pr^(0.33));  % (W/m2K) Check for formula for Cp at T
filmresistance = 1/hi;

% Overall heat transfer coefficient, Uo- based on outer diameter
Uo = (1/((((Db/2)*log((Do/Db)))/lamdab)+(1/hi)))*10^(-3);  % kW/m2K

% Calculation of Electrical Heat flux
 Qw = Uo*(Tw-z(2));                 % Electrical heat flux (kW/m2)

% Next three lines appends the data in Qw in the file 'Qws.txt'
        % for use in the function 'cost.m'

        fid = fopen('Qws.txt','a');
        fprintf(fid,'%6.4f\n',Qw);
        fclose(fid);

Hrxn = rP.*(dHrxnT)                         % (kW/m^3) Heat consumed by decomposition
                                            %reaction
flow = Fp*(FeedCp+ (z(1).*DeltaCp));        % Mass flow energy contribution

% Differential Equations
zoneRdiff(1,:) = rP./(Fp/Ac);       % dX/dL
zoneRdiff(2,:) = (((Ac*Hrxn) + (Qw*2*pi*Db))./flow) + (Erxn/Lt./flow)   % dT/dL
zoneRdiff(3,:) = Ac.*-rP;           % dF/dL :- dPolymer/dL
zoneRdiff(4,:) = Ac.*rP;            % dP/dL :- dProduct/dL
zoneRdiff;                          % Array  of the changes in the values of X, T, F and P
```

Attachment C.5: MATLAB Function 'reactionzone'

This MATLAB function "Extruder" solves the ODEs.

```
% Total of four reaction zones
% Vent after each reaction zone

% Calculation of integration limits for each zone

Ltot = inputvar();                  % calls the script file 'inputvar'
Ltot = Ltot(2);
x = 0.25;                           % fraction of first barrel
y = 0.25;                           % fraction of second barrel
w = 0.25                            % fraction of third barrel
z = 1-(x+y+w);                              % fraction of remainder of extruder reaction zone
Lb = [x*Ltot;y*Ltot;w*Ltot;z*Ltot];      % Total Length of each reaction zone (m)
n = 4;                              % number of integration sections for reactor

% Initialize continuous variables for storing output data

Lt = zeros (1,1);           % Dummy Independent variable, length
zt = zeros (1,4);           % Dummy Dependent variables:
                             %Temp(T), Conversion (X), Product flow(P), Polymer Flow(F)

prod = zeros(1,1);          % Dummy Product flow variable: summation of P


initial = meltzone;          % Calls script 'heat' to input intial values

To = initial(1)             % Temperature (K)at L = 0
Fo = initial(3);             % Feed flowrate (kg/s)
Lo = 0;                      % Defines the beginning of the reactor length
Xo = 0;                     % Conversion at L = 0
Po = 0;                      % Product flow at L = 0

interval = 0.5;

for i = 1:1:n

Lf = Lo + Lb((i-1)+1);


%options = odeset('AbsTol', 1e-12, 'RelTol', 1e-12);
[L,z] = ode23s('Diff', [Lo:interval:Lf], [Xo; To; Fo; Po]);

X = z(:, 1);
T = z(:, 2);
F = z(:, 3);
P = z(:, 4);
```

Attachment C.5: MATLAB Function 'reactionzone' (CONTINUED)

```
%options = odeset('AbsTol', 1e-12, 'RelTol', 1e-12);
[L,z] = ode23s('Diff', [Lo:interval:Lf], [Xo; To; Fo; Po]);

X = z(:, 1);
T = z(:, 2);
F = z(:, 3);
P = z(:, 4);

%Save L and z (X,T,F,P)in variables that are continuous for the total integration

[r,c] = size(L);
[r1, c1] = size (Lt);
rt = r1 + r;
Lt(r1+1:rt,1) =L


[r,c] = size (z);
[r1,c1] = size (zt);
rt = r1+r;
zt(r1+1:rt,:)= z

% Venting volatiles

zo = z(r,:);   %final variables before venting
zo(:,4) = 0;   %vapor flow = o because of vents

%Assign final values to next zone

Xo = zo(:,1)
To = zo(:,2)
Fo = zo(:,3)
Po = zo(:,4)
Lo = Lf;

%store product flows
prod = prod + z(r,4)

end  % ends integration of current zone and begins with next zone

X = zt(2:end, 1);
T = zt(2:end, 2);
F = zt(2:end, 3);
P = zt(2:end, 4);
Lt = Lt(2:end,1);
```

Attachment C.6: MATLAB Function 'cost'

This MATLAB function "cost" estimates the operation costs.

```
Cost Estimation for the catalytic pyrolysis of PP based on a work period
% of 95% of the year (8322 hours/year)
 THE CASE FOR PYROLYSIS IN A SINGLE EXTRUDER IS SHOWN

% Call on function 'inputvar' which outputs the required variables
input = inputvar();

%INPUT VARIABLES
capR = input (25);                  % maximum capacity of extruder (kg/s)
wf = [input(6); input(7)];          % weight fraction of [polymer, wf(1); catalyst, wf(2)]in
                                    feed.
Cp = [input(8);input(9)];           % (KJ/kgK) % Heat capacity of polymer, Cp(1); catalyst,
                                    Cp(2)
Ff = input(5) * (2.205*3600);       % Polymer feed flowrate (lb/hr)
**************************************************************************
% CAPITAL COSTS
      % Cost of Extruder, CostR:
      % Based on capacity of 30mm NGR extruder: six tenths rule
      % capB: Base capacity (lb/hr)
      % capR: Required capacity (lb/hr)
      % costB: Base extruder cost ($)
      % costR: Required extruder cost ($)
         capB = 100;
         costB = 200000;
         capR = capR* (3600* 2.205);  % Conversion from kg/s to lb/hr
         costR = costB* (capR/capB)^0.6;

   % Cost of Pumps and Condensers
    % Sixth-Tenths rule
    costpcB = 3 * 12000; %($) % Three units at $12000 each.
    costpcR = costpcB*(capR/capB)^0.6;  %($)

    %Capital Costs Based On Lang Factor
    CapCost = 3.63*( costpcR+costR);  %($)

% COST OF UTILITIES
Power to drive the Extruder Motor.
      E = screw;                    % Calls the function 'screw'
      Etot = E(1)/1e3;              % KW

% Electrical Heating Costs
% Next three lines appends the data in Qw in the file 'Qws.txt'
% for use in the function 'cost.m'
     Qw_all = load('Qws.txt');
      Qw = sum(Qw_all);
      !del Qws.txt
      D = inputvar();
      Db = D(22);          % Reactor diameter (m) usind L/D ratio = 48
      length = D(2);      %
      Qw = Qw*(2*pi*Db)*length;   %kW                                          (1)
```

Attachment C.6: MATLAB Function 'cost' (CONTINUED)

```
% Total Cost of Electricity Required to Operate Extruder/year
      Celec =0.0475;     %($/KWhr) %www.eia.doe.gov
      %(KJ/s)(1000J/1KJ)(2.778E-7KWh/1J)($0.05/KWh)(3600s/1hr)(8332hr/yr)

 Costelec = (Etot + Qw)*(1000/1)* (2.778E-7/1)*Celec*(3600/1)*(8322/1);  %($/yr)

   % Cost of Cooling Water
      Cwater_b = ((2/(264.17*60))*7)/1000;   %($/s) For NFM extruder
      Cwater_b = (((2/(264.17*60))*7)/1000)*3600*8322;  %($/yr)For NFM extruder
      % Estimation of required cooling water based throughput
      Cwater = Cwater_b* (capR/capB);

   % Total Utitlities Costs
      Cutilities = Costelec + Cwater;      % ($/yr)

*************************************************************************
% MANUFACTURING COSTS

   % Raw Materials Cost
   % Polypropylene
         Pcost = 0;   %($/lb) % Cost of polypropylene.
         %Cost of polymer = unit cost($/lb)* weight fraction *feed flowrate (lb/hr) *
8332hrs/year
         CostP = Pcost * wf(1)* capR * 8322;  %($/yr)

   % FCC catalysts
   % [Albemarle FCC regular; Albemarle FCC fines; Albemarle FCC ECAT; Shell FCC, No
catalyst]
      FCCcost = [0.05; 0.05; 0.05/2; 0.05/2; 0];        %($/lb)

 %Cost of catalyst = unit cost($/lb)* weight fraction *feed flowrate * 8332hrs/year
      CostC = FCCcost(3)* wf(2)* capR * 8322;  %($/yr)

     % Total Manufacturing Costs
      Costmafc = CostC+CostP;   % $/yr
```

(2)

Attachment C.6: MATLAB Function 'cost' (CONTINUED)

```
**********************************************************************
% Labor Costs

   NumOper = 2;              % Estimated number of operators/shift
   NumshiftD = 3;            % Number of shifts/day
   Unitoper = 46000;          % $/operator/yr
   CostLab = NumOper*NumshiftD*Unitoper;  %($/yr)
**********************************************************************

   % TOTAL COSTS
   % Assuming a 3 year capital recovery for the equipments
      Capitalcosts = CapCost/3
      Tcost = CostLab +  Costmafc + Cutilities + CapCost/3 %($/yr)

   % TOTAL CONVERSION COSTS
   Xo
   ConCostF = (Tcost/Ff)*(1/8322)      % $/lb of Feed
   ConCostP = (Tcost/(Ff*Xo))*(1/8322)   % conversion to $/lb of Product
```

(3)

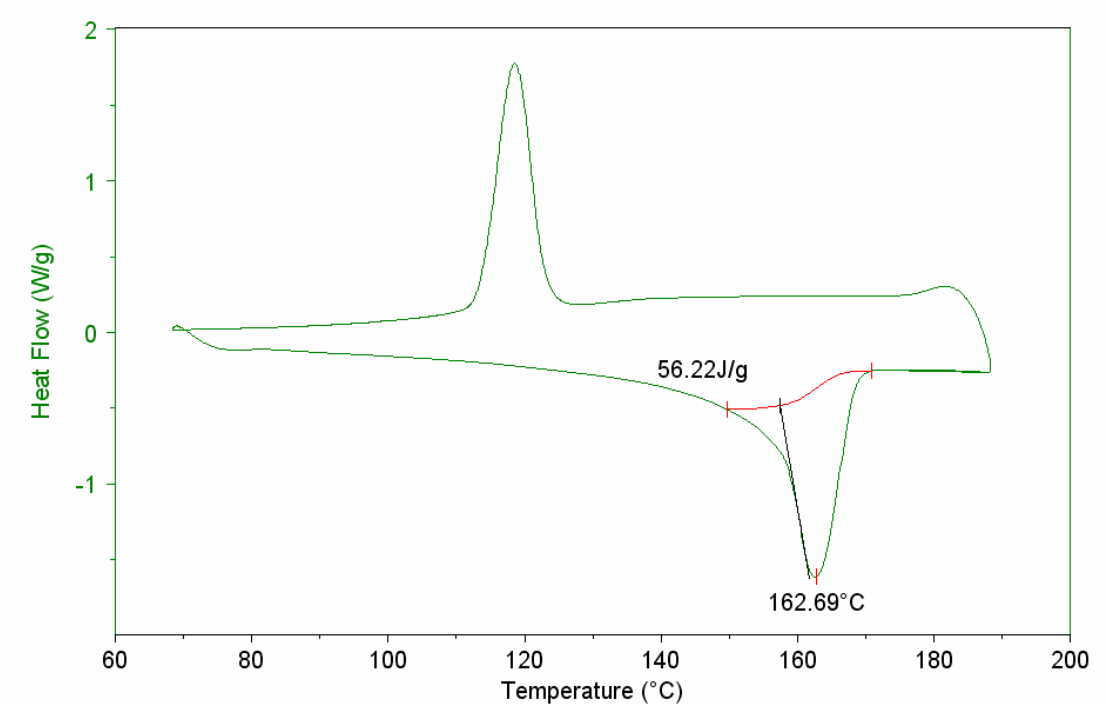

Figure C.1 DSC plot for the non-catalytic pyrolysis of PP

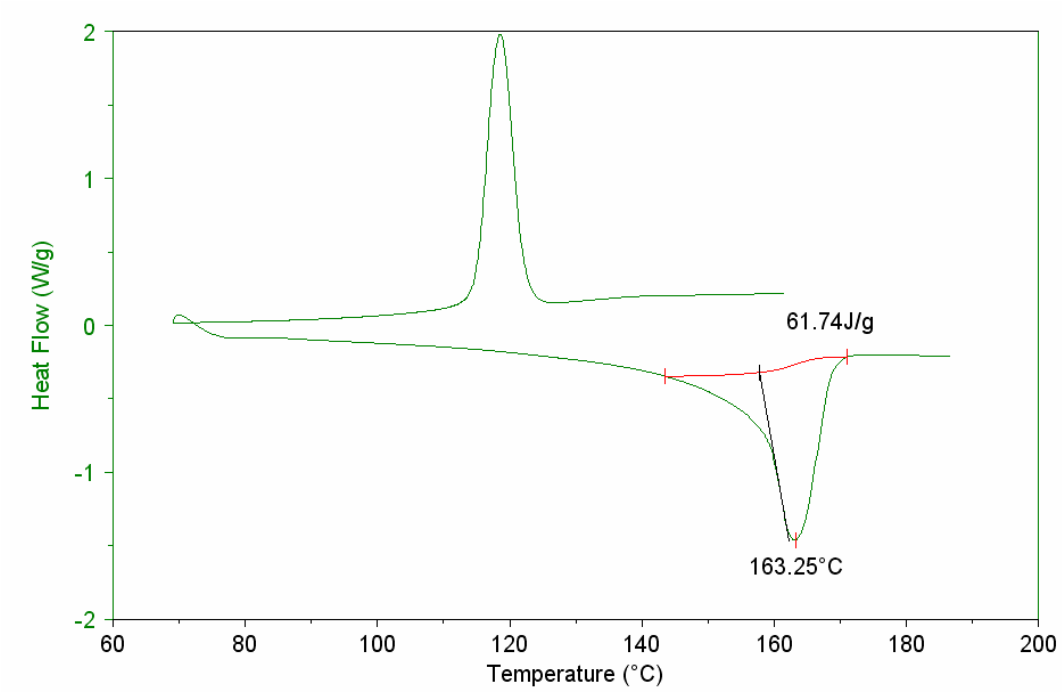

Figure C.2 DSC plot for PP pyrolysis at 3 wt % S-ECAT

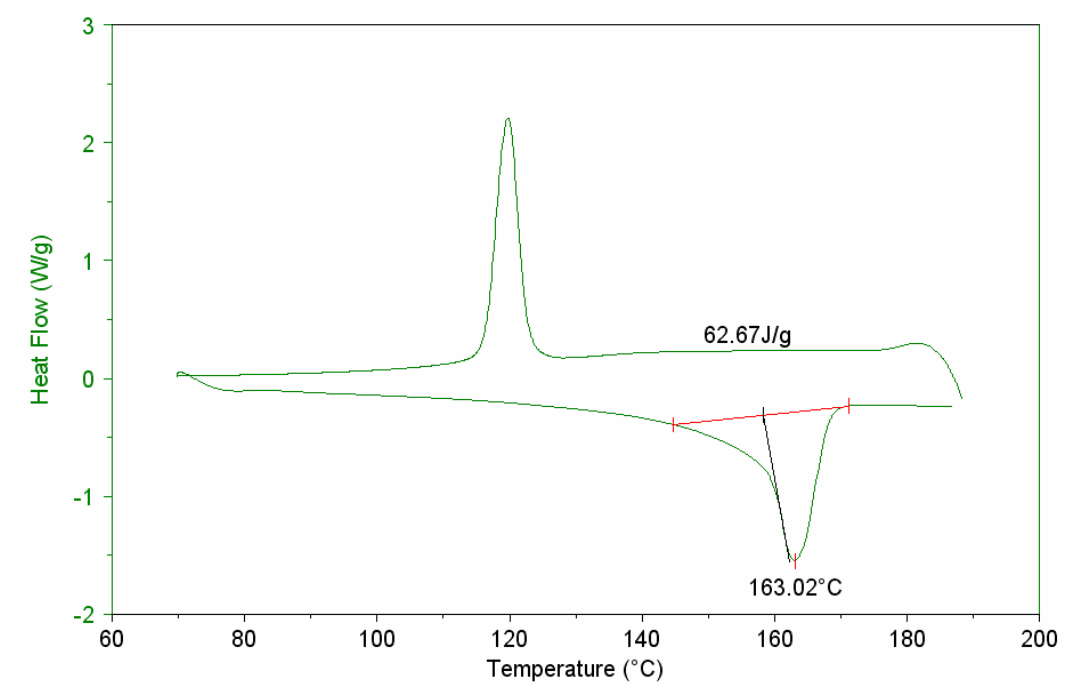

Figure C.3 DSC plot for PP pyrolysis at 8 wt % S-ECAT

REFERENCES

1. Agency, U.E.P., *Municipal Solid Waste in the United States: Facts and Figures.* http://www.epa.gov/epaoswer/non-hw/muncpl/msw99.htm, 2005.
2. Kiran, N., E. Ekinci, and C.E. Snape, *Recyling of plastic wastes via pyrolysis.* Resources, Conservation and Recycling, 2000. **29**(4): p. 273.
3. Marcilla, A., et al., *Kinetic study of polypropylene pyrolysis using ZSM-5 and an equilibrium fluid catalytic cracking catalyst.* Journal Of Analytical And Applied Pyrolysis, 2003. **68-9**: p. 467-480.
4. http://europa.eu.int/comm/energy_transport/atlas/htmlu/lfgmark.html, 2005.
5. Agency, U.E.P., *Landfilling.* http://www.epa.gov/epaoswer/non-hw/muncpl/disposal.htm, 2005.
6. Demirbas, A., *Pyrolysis of municipal plastic waste for recovery of gasoline-range hydrocarbons.* Journal Of Analytical And Applied Pyrolysis, 2004. **72**: p. 97-102.
7. *Pyrolysis.* www.dictionary.com, 2005.
8. Murata, K., K. Sato, and Y. Sakata, *Effect of pressure on thermal degradation of polyethylene.* 2004. **71**(2): p. 569.
9. Sorum, L., M.G. Gronli, and J.E. Hustad, *Pyrolysis characteristics and kinetics of municipal solid wastes.* Fuel, 2001. **80**(9): p. 1217-1227.
10. Faravelli, T., et al., *Thermal degradation of polystyrene.* Journal of Analytical and Applied Pyrolysis, 2001. **60**(1): p. 103.
11. Mastral, F.J., et al., *Pyrolysis of high-density polyethylene in a fluidised bed reactor. Influence of the temperature and residence time.* Journal of Analytical and Applied Pyrolysis, 2002. **63**(1): p. 1.
12. Garforth, A.A., et al., *Production of hydrocarbons by catalytic degradation of high density polyethylene in a laboratory fluidised-bed reactor.* Applied Catalysis A-General, 1998. **169**(2): p. 331-342.
13. Cha, W.S., S.B. Kim, and B.J. McCoy, *Study of polystyrene degradation using continuous distribution kinetics in a bubbling reactor.* Korean Journal Of Chemical Engineering, 2002. **19**(2): p. 239-245.
14. Dolezal, Z., V. Pacakova, and J. Kovarova, *The effects of controlled aging and blending of low- and high-density polyethylenes, polypropylene and polystyrene on their thermal degradation studied by pyrolysis gas chromatography.* Journal of Analytical and Applied Pyrolysis, 2001. **57**(2): p. 177.
15. Kim, S.S. and S. Kim, *Pyrolysis characteristics of polystyrene and polypropylene in a stirred batch reactor.* Chemical Engineering Journal, 2004. **98**(1-2): p. 53-60.
16. Woo, O.S., N. Ayala, and L.J. Broadbelt, *Mechanistic interpretation of base-catalyzed depolymerization of polystyrene.* Catalysis Today, 2000. **55**(1-2): p. 161-171.
17. Woo, O.S. and L.J. Broadbelt, *Recovery of high-valued products from styrene-based polymers through coprocessing: experiments and mechanistic modeling.* Catalysis Today, 1998. **40**: p. 121-140.
18. Chan, J.H. and S.T. Balke, *The thermal degradation kinetics of polypropylene: Part III. Thermogravimetric analyses.* Polymer Degradation and Stability, 1997. **57**(2): p. 135.

19. Hayashi, J., et al., *Pyrolysis of polypropylene in the presence of oxygen.* Fuel Processing Technology, 1998. **55**(3): p. 265-275.
20. Jakab, E., G. Varhegyi, and O. Faix, *Thermal decomposition of polypropylene in the presence of wood-derived materials.* Journal of Analytical and Applied Pyrolysis, 2000. **56**(2): p. 273.
21. Kaminsky, W., *Thermal recycling of polymers.* Journal of Analytical and Applied Pyrolysis, 1985. **8**: p. 439.
22. Kaminsky, W., M. Predel, and A. Sadiki, *Feedstock recycling of polymers by pyrolysis in a fluidised bed.* Polymer Degradation And Stability, 2004. **85**(3): p. 1045-1050.
23. Kiang, J.K.Y., P.C. Uden, and J.C.W. Chien, *Polymer reactions--Part VII: Thermal pyrolysis of polypropylene.* Polymer Degradation and Stability, 1980. **2**(2): p. 113.
24. Lattimer, R.P., *Direct analysis of polypropylene compounds by thermal desorption and pyrolysis--mass spectrometry.* Journal of Analytical and Applied Pyrolysis, 1993. **26**(2): p. 65.
25. Marcilla, A., M. Beltran, and J.A. Conesa, *Catalyst addition in polyethylene pyrolysis - Thermogravimetric study.* Journal Of Analytical And Applied Pyrolysis, 2001. **58**: p. 117-126.
26. Murata, K., et al., *Basic study on a continuous flow reactor for thermal degradation of polymers.* Journal of Analytical and Applied Pyrolysis, 2002. **65**(1): p. 71.
27. Onu, P., et al., *Thermal and catalytic decomposition of polyethylene and polypropylene.* Journal Of Analytical And Applied Pyrolysis, 1999. **49**(1-2): p. 145-153.
28. Ranzi, E., et al., *Kinetic modeling of polyethylene and polypropylene thermal degradation.* Journal of Analytical and Applied Pyrolysis, 1997. **40-41**: p. 305.
29. Seth, D. and A. Sarkar, *Thermal pyrolysis of polypropylene: effect of reflux-condenser on the molecular weight distribution of products.* Chemical Engineering Science, 2004. **59**(12): p. 2433-2445.
30. Tsuchiya, Y. and K. Sumi, *Thermal decomposition products of polypropylene.* Journal of Polymer Science, 1969. **7**: p. 1599 -1607.
31. Bockhorn, H., et al., *Kinetic study on the thermal degradation of polypropylene and polyethylene.* Journal of Analytical and Applied Pyrolysis, 1999. **48**(2): p. 93.
32. Audisio, G., et al., *Catalytic thermal degradation of polymers: Degradation of polypropylene.* Journal of Analytical and Applied Pyrolysis, 1984. **7**(1-2): p. 83.
33. Scott, D.S., et al., *Fast pyrolysis of plastic wastes.* Energy & Fuels, 1990. **4**: p. 407-411.
34. Sakata, Y., et al., *Thermal degradation of polyethylene mixed with poly(vinyl chloride) and poly(ethyleneterephthalate).* Polymer Degradation and Stability, 1996. **53**(1): p. 111.
35. Miskolczi, N., et al., *Thermal degradation of municipal plastic waste for production of fuel-like hydrocarbons.* Polymer Degradation And Stability, 2004. **86**(2): p. 357-366.
36. Cullis, C.F. and M.M. Hirschler, *The Combustion of Organic Polymers*. 1981: Oxford: Clarendon Press.

37. Peterson, J.D., S. Vyazovkin, and C.A. Wight, *Kinetics of the thermal and thermo-oxidative degradation of polystyrene, polyethylene and poly(propylene).* Macromolecular Chemistry And Physics, 2001. **202**(6): p. 775-784.
38. Lin, Y.H. and M.H. Yang, *Catalytic reactions of post-consumer polymer waste over fluidised cracking catalysts for producing hydrocarbons.* Journal Of Molecular Catalysis A-Chemical, 2005. **231**(1-2): p. 113-122.
39. McCaffrey, W.C., M.R. Kamal, and D.G. Cooper, *Thermolysis of polyethylene.* Polymer Degradation and Stability, 1995. **47**(1): p. 133.
40. Songip, A.R., et al., *Test To Screen Catalysts For Reforming Heavy Oil From Waste Plastics.* Applied Catalysis B-Environmental, 1993. **2**(2-3): p. 153-164.
41. Joo, H.S. and J.A. Guin, *Continuous upgrading of a plastics pyrolysis liquid to an environmentally favorable gasoline range product.* Fuel Processing Technology, 1998. **57**: p. 25-40.
42. Serrano, D.P., et al., *Performance of a continuous screw kiln reactor for the thermal and catalytic conversion of polyethylene-lubricating oil base mixtures.* Applied Catalysis B-Environmental, 2003. **44**(2): p. 95-105.
43. Ohkita, H., et al., *Acid Properties Of Silica-Alumina Catalysts And Catalytic Degradation Of Polyethylene.* Industrial & Engineering Chemistry Research, 1993. **32**(12): p. 3112-3116.
44. Ding, W.B., J. Liang, and L.L. Anderson, *Thermal and catalytic degradation of high density polyethylene and commingled post-consumer plastic waste.* Fuel Processing Technology, 1997. **51**(1-2): p. 47-62.
45. Park, D.W., et al., *Catalytic degradation of polyethylene over solid acid catalysts.* Polymer Degradation And Stability, 1999. **65**(2): p. 193-198.
46. Lee, S.Y., et al., *Catalytic degradation of polystyrene over natural clinoptilolite zeolite.* Polymer Degradation And Stability, 2001. **74**(2): p. 297-305.
47. Aguado, J., et al., *Catalytic conversion of low-density polyethylene using a continuous screw kiln reactor.* Catalysis Today, 2002. **75**(1-4): p. 257-262.
48. Park, J.A., et al., *Characteristics of LDPE pyrolysis.* Korean Journal Of Chemical Engineering, 2002. **19**(4): p. 658-662.
49. Hwang, E.Y., et al., *Catalytic degradation of polypropylene I. Screening of catalysts.* Korean Journal Of Chemical Engineering, 1998. **15**(4): p. 434-438.
50. Hwang, E.Y., et al., *Performance of acid treated natural zeolites in catalytic degradation of polypropylene.* Journal Of Analytical And Applied Pyrolysis, 2002. **62**(2): p. 351-364.
51. Bagri, R. and P.T. Williams, *Fluidised-bed catalytic pyrolysis of polystyrene.* Journal Of The Institute Of Energy, 2002. **75**(505): p. 117-123.
52. Kim, J.R., J.H. Yoon, and D.W. Park, *Catalytic recycling of the mixture of polypropylene and polystyrene.* Polymer Degradation And Stability, 2002. **76**(1): p. 61-67.
53. Aguado, J., et al., *Catalytic conversion of polyolefins into fuels over zeolite beta.* Polymer Degradation And Stability, 2000. **69**(1): p. 11-16.
54. Beltrame, P.L., et al., *Catalytic degradation of polymers: Part II--Degradation of polyethylene.* Polymer Degradation and Stability, 1989. **26**(3): p. 209.

55. Sakata, Y., M.A. Uddin, and A. Muto, *Degradation of polyethylene and polypropylene into fuel oil by using solid acid and non-acid catalysts.* Journal Of Analytical And Applied Pyrolysis, 1999. **51**(1-2): p. 135-155.
56. Seo, Y.H., K.H. Lee, and D.H. Shin, *Investigation of catalytic degradation of high-density polyethylene by hydrocarbon group type analysis.* Journal Of Analytical And Applied Pyrolysis, 2003. **70**(2): p. 383-398.
57. Miskolczi, N., et al., *Thermal and thermo-catalytic degradation of high-density polyethylene waste.* Journal Of Analytical And Applied Pyrolysis, 2004. **72**(2): p. 235-242.
58. Herreros, B. *Introduction to Zeolites*. March 1996 [cited.
59. Lónyi, F. and J. Valyon, *On the interpretation of the NH3-TPD patterns of H-ZSM-5 and H-mordenite.* Microporous and Mesoporous Materials, 2001. **47**: p. 293.
60. Armaroli, T., et al., *FTIR study of the interaction of some branched aliphatic molecules with the external and internal sites of H-ZSM5 zeolite.* Chemical Physics Letters and Chemical Physics, 2000. **2**: p. 3341.
61. Cerqueira, H.S., et al., *Influence of coke on the acid properties of a USHY zeolite.* Microporous and Mesoporous Materials, 2000. **38**: p. 197.
62. Topsoe, N.-Y., K. Pedersen, and E.G. Derouane, *Infrared and temperature-programmed desorption study of the acidic properties of ZSM-5-type zeolites.* 1981. **70**(1): p. 41.
63. Venuto, P. and P. Landis, *Zeolite catalysis in synthetic organic chemistry.* Advances in Catalysis, 1968. **18**: p. 259.
64. Karagoz, S., et al., *Catalytic and thermal degradation of high-density polyethylene in vacuum gas oil over non-acidic and acidic catalysts.* Applied Catalysis A-General, 2003. **242**(1): p. 51-62.
65. Luo, G.H., et al., *Catalytic degradation of high density polyethylene and polypropylene into liquid fuel in a powder-particle fluidized bed.* Polymer Degradation And Stability, 2000. **70**(1): p. 97-102.
66. Anders, G., et al., *The influence of HZSM-5 zeolite on the product composition after cracking of high boiling hydrocarbon fractions.* Applied Catalysis A: General, 1990. **62**(1): p. 271.
67. Corma, A., et al., *The role of different types of acid site in the cracking of alkanes on zeolite catalysts.* Journal of Catalysis, 1985. **93**(1): p. 30.
68. Manos, G., A. Garforth, and J. Dwyer, *Catalytic degradation of high-density polyethylene over different zeolitic structures.* Industrial & Engineering Chemistry Research, 2000. **39**(5): p. 1198-1202.
69. Mordi, R.C., R. Fields, and J. Dwyer, *Thermolysis of low density polyethylene catalysed by zeolites.* Journal of Analytical and Applied Pyrolysis, 1994. **29**(1): p. 45.
70. Aguado, J., et al., *Catalytic conversion of polyolefins into liquid fuels over MCM-41: Comparison with ZSM-5 and amorphous Si(O)2-Al2O3.* Energy & Fuels, 1997. **11**(6): p. 1225-1231.
71. Marcilla, A., et al., *Catalytic pyrolysis of polypropylene using MCM-41: kinetic model.* Polymer Degradation And Stability, 2003. **80**(2): p. 233-240.

72. Pierella, L.B., S. Renzini, and O.A. Anunziata, *Catalytic degradation of high density polyethylene over microporous and mesoporous materials.* Microporous And Mesoporous Materials, 2005. **81**(1-3): p. 155-159.
73. Gobin, K. and G. Manos, *Thermogravimetric study of polymer catalytic degradation over microporous materials.* Polymer Degradation and Stability, 2004. **86**(2): p. 225.
74. Scherzer, J., *Octane-Enhancing Zeolite FCC Catalysis*. 1990: Marcel Dekker, Inc. 41-109.
75. Gabova, V., J. Dedecek, and J. Cejka, *Control of Al distribution in ZSM-5 by conditions of zeolite synthesis.* 2003. **10**: p. 1196-1197.
76. Cundy, C.S. and P.A. Cox, *The hydrothermal synthesis of zeolites: Precursors, intermediates and reaction mechanism.* Microporous and Mesoporous Materials, 2005. **82**(1-2): p. 1.
77. Marcilly, C.R., *Where and how shape selectivity of molecular sieves operates in refining and petrochemistry catalytic processes.* Topics In Catalysis, 2000. **13**(4): p. 357-366.
78. http://www.iza-structure.org/databases/, International Zeolite Association, 2005.
79. Degnan, T.F., *Applications of Zeolites in Petroluem Refining.* Topics in Catalysis, 2000. **13**: p. 349-356.
80. Chen, N.Y., W.E. Garwood, and F.G. Dwyer, *Shape Selective Catalysis in Industrial Applications.* 1996.
81. Maxwell, I.E., Studies in Surface Science and Catalysis, 1991. **58**(Ch. 12).
82. Maxwell, I.E., CATTECH, 1997. **1**: p. 5.
83. Chen, N.Y., *Catalysis.* 1988: p. 153.
84. Ahmaruzzaman, M. and D.K. Sharma, *Non-isothermal kinetic studies on co-processing of vacuum residue, plastics, coal and petrocrop.* Journal Of Analytical And Applied Pyrolysis, 2005. **73**(2): p. 263-275.
85. Dwyer, J. and D.J. Rawlence, *Fluid Catalytic Cracking - Chemistry.* Catalysis Today, 1993. **18**(4): p. 487-507.
86. Lin, Y.H., et al., *A combined kinetic and mechanistic modelling of the catalytic degradation of polymers.* Journal Of Molecular Catalysis A-Chemical, 2001. **171**(1-2): p. 143-151.
87. You, Y.S., J.H. Kim, and G. Seo, *Liquid-phase catalytic degradation of polyethylene wax over MFI zeolites with different particle sizes.* Polymer Degradation And Stability, 2000. **70**(3): p. 365-371.
88. Xiao, J. and J. Wei, *Diffusion mechanism of hydrocarbons in zeolites.* Chemical Engineering Science, 1992. **47**: p. 1123.
89. Karger, J. and D. Ruthven, *Diffusion in Zeolites and other Microporous Solids*. 1992, New York: Wiley.
90. Anunziata, O.A. and L.B. Pierella, *Conversion of polyethylene into aromatic hydrocarbons using MEL and BEA zeolites.* Studies in surface science and catalysis, 1999. **125**: p. 481-488.
91. Garforth, A., et al., *Catalytic polymer degradation for producing hydrocarbons over zeolites*, in *Science And Technology In Catalysis 1998*. 1999, Elsevier Science Publ B V: Amsterdam. p. 197-202.

92. Songip, A.R., et al., *Kinetic Studies for Catalytic Cracking of Heavy Oil from Waste Plastics over REY Zeolite.* Energy and Fuels, 1994. **8**: p. 131.
93. You, Y.S., et al., *Liquid-phase degradation of polyethylene wax over mordenite catalysts with different Si Al molar ratios.* Catalysis Letters, 1999. **59**(2-4): p. 221-227.
94. Zhang, Z.B., et al., *Chemical Recycling Of Waste Polystyrene Into Styrene Ever Solid Acids And Bases.* Industrial & Engineering Chemistry Research, 1995. **34**(12): p. 4514-4519.
95. Hernandez, M.D., A.N. Garcia, and A. Marcilla, *Study of the gases obtained in thermal and catalytic flash pyrolysis of HDPE in a fluidized bed reactor.* Journal Of Analytical And Applied Pyrolysis, 2005. **73**(2): p. 314-322.
96. Lin, Y.H. and H.Y. Yen, *Fluidised bed pyrolysis of polypropylene over cracking catalysts for producing hydrocarbons.* Polymer Degradation And Stability, 2005. **89**(1): p. 101-108.
97. Zhou, Q., et al., *Catalytic degradation of low-density polyethylene and polypropylene using modified ZSM-5 zeolites.* Polymer Degradation And Stability, 2004. **84**(3): p. 493-497.
98. Kokotailo, G.T., et al., *Structure of synthetic zeolite ZSM-5.* Nature, 1978. **272**: p. 437.
99. Aguado, J., et al., *Influence of the operating variables on the catalytic conversion of a polyolefin mixture over HMCM-41 and nanosized HZSM-5.* Industrial & Engineering Chemistry Research, 2001. **40**(24): p. 5696-5704.
100. den Hollander, M.A., et al., *Gasoline conversion: reactivity towards cracking with equilibrated FCC and ZSM-5 catalysts.* Applied Catalysis A-General, 2002. **223**(1-2): p. 85-102.
101. Ali, S., et al., *Polymer waste recycling over "used" catalysts.* Catalysis Today, 2002. **75**(1-4): p. 247-255.
102. Manos, G., A. Garforth, and J. Dwyer, *Catalytic degradation of high-density polyethylene on an ultrastable-Y zeolite. Nature of initial polymer reactions, pattern of formation of gas and liquid products, and temperature effects.* Industrial & Engineering Chemistry Research, 2000. **39**(5): p. 1203-1208.
103. Cardona, S.C. and A. Corma, *Tertiary recycling of polypropylene by catalytic cracking in a semibatch stirred reactor - Use of spent equilibrium FCC commercial catalyst.* Applied Catalysis B-Environmental, 2000. **25**(2-3): p. 151-162.
104. Lee, K.H. and D.H. Shin, *Catalytic degradation of waste HDPE over acidic catalysts with different pore sizes.* Journal Of Industrial And Engineering Chemistry, 2003. **9**(5): p. 584-589.
105. Habib, E.T., Jr., et al., *Advances in fluid catalytic cracking.* Catalytic Science Series, 2002. **3**(Zeolites for Cleaner Technologies): p. 105-130.
106. Sivasanker, S., *Catalysis in petroleum refining.* Catalysis, 2002: p. 362-376.
107. de la Puente, G., et al., *The influence on selectivity of the aluminum content in the matrix of FCC catalysts.* Applied Catalysis, A: General, 2003. **242**(2): p. 381-391.
108. Costa, A.F., et al., *Performance of FCC catalysts prepared with sub-micron Y zeolite.* Studies in Surface Science and Catalysis, 2004. **154C**(Recent Advances in the Science and Technology of Zeolites and Related Materials): p. 2296-2301.

109. Marcilla, A., et al., *Study of the catalytic pyrolysis behaviour of polyethylene-polypropylene mixtures.* Journal of Analytical and Applied Pyrolysis, 2005. **74**(1-2): p. 387.
110. Bagri, R. and P.T. Williams, *Catalytic pyrolysis of polyethylene.* Journal Of Analytical And Applied Pyrolysis, 2002. **63**(1): p. 29-41.
111. Park, S.K., et al., *Regeneration of Spent Resid Fluidized Catalytic Cracking Catalyst by Removing Metal Poisons Such as V, Ni, and Fe.* Industrial & Engineering Chemistry Research, 2003. **42**(4): p. 736-742.
112. de la Puente, G. and U. Sedran, *Recycling polystyrene into fuels by means of FCC: performance of various acidic catalysts.* Applied Catalysis B-Environmental, 1998. **19**(3-4): p. 305-311.
113. Lee, K.H. and D.H. Shin, *Catalytic degradation of waste polyolefinic polymers using spent FCC catalyst with various experimental variables.* Korean Journal Of Chemical Engineering, 2003. **20**(1): p. 89-92.
114. Schuurman, Y., et al., *Effect of coke deposition on transport and sorption in FCC catalysts studied by temporal analysis of products.* Chemical Engineering Science, 2005. **60**(4): p. 1007-1017.
115. Jentoft, F.C. and B.C. Gates, *Solid-acid-catalyzed alkane cracking mechanisms: evidence from reactions of small probe molecules.* Topics in Catalysis, 1997. **4**(1 - 2): p. 1.
116. Xu, M., et al., *Study of coked commercial FCC catalysts by a novel microreactor GC system and its characterization by 129Xe NMR.* China Petroleum Processing and Petrochemical Technology, 2004(1): p. 37-42.
117. He, M.-Y., *The development of catalytic cracking catalysts: acidic property related catalytic performance.* Catalysis Today, 2002. **73**(1-2): p. 49-55.
118. Marcilla, A., et al., *HZSM5 and HUSY deactivation during the catalytic pyrolysis of polyethylene.* Applied Catalysis A-General, 2004. **278**(1): p. 37-43.
119. Zaggout, F.R., A.R. Al Mughari, and A. Garforth, *Catalytic degradation of High Density Polyethylene using zeolites.* Journal Of Environmental Science And Health Part A-Toxic/Hazardous Substances & Environmental Engineering, 2001. **36**(2): p. 163-175.
120. Yaluris, G., et al., *Mechanism of fluid cracking catalysts deactivation by Fe.* Studies in Surface Science and Catalysis, 2004. **149**: p. 139-163.
121. Bayraktar, O. and E.L. Kugler, *Visualization of the Equilibrium FCC Catalyst Surface by AFM and SEM-EDS.* Catalysis Letters, 2003. **90**(3-4): p. 155-160.
122. Bayraktar, O. and E.L. Kugler, *Coke content of spent commercial fluid catalytic cracking (FCC) catalysts. Determination by temperature-programmed oxidation.* Journal of Thermal Analysis and Calorimetry, 2003. **71**(3): p. 867-874.
123. Guisnet, M., *"Coke" molecules trapped in the micropores of zeolites as active species in hydrocarbon transformations.* Journal Of Molecular Catalysis A-Chemical, 2002. **182**(1): p. 367-382.
124. Lee, K.H., D.H. Shin, and Y.H. Seo, *Liquid-phase catalytic degradation of mixtures of waste high-density polyethylene and polystyrene over spent FCC catalyst. Effect of mixing proportions of reactants.* Polymer Degradation And Stability, 2004. **84**(1): p. 123-127.

125. Lee, K.H., et al., *Comparison of plastic types for catalytic degradation of waste plastics into liquid product with spent FCC catalyst.* Polymer Degradation And Stability, 2002. **78**(3): p. 539-544.
126. Marcilla, A., et al., *Kinetic study of the catalytic decomposition of different commercial polyethylenes over an MCM-41 catalyst.* Journal Of Analytical And Applied Pyrolysis, 2002. **64**(1): p. 85-101.
127. Mertinkat, J., K. Predel, and W. Kaminsky, *Cracking catalysts used as fluidized bed material in Hamburg pyrolysis process.* Journal of Analytical and Applied pyrolysis, 1999. **49**: p. 87-95.
128. De la Puente, G., J.M. Arandes, and U. Sedran, *Recycled Plastics in FCC feedstocks: Specific Contributions.* Industrial and Engineering Chemistry Research, 1997. **36**: p. 4530-4534.
129. Serrano, D.P., et al., *Nanocrystalline ZSM-5: a highly active catalyst for polyolefin feedstock recycling*, in *Studies In Surface Science and Catalysis*. 2002, Elsevier Science Bv: Amsterdam. p. 77-84.
130. Tonetto, G., J. Atias, and H. de Lasa, *FCC catalysts with different zeolite crystallite sizes: acidity, structural properties and reactivity.* Applied Catalysis A: General, 2004. **270**(1-2): p. 9.
131. Takuma, K., et al., *A novel technology for chemical recycling of low-density polyethylene by selective degradation into lower olefins using h-borosilicate as a catalyst.* Chemistry Letters, 2001(4): p. 288-289.
132. De Lasa, H.I., *Riser simulator.* US Patent 5,102,628, 1992.
133. de la Puente, G., C. Klocker, and U. Sedran, *Conversion of waste plastics into fuels - Recycling polyethylene in FCC.* Applied Catalysis B-Environmental, 2002. **36**(4): p. 279-285.
134. Mahgoub, K.A. and S. Al-Khattaf, *Catalytic cracking of hydrocarbons in a riser simulator: The effect of catalyst accessibility and acidity.* Energy & Fuels, 2005. **19**(2): p. 329-338.
135. Buekens, A.G. and H. Huang, *Catalytic plastics cracking for recovery of gasoline-range hydrocarbons from municipal plastic wastes.* Resources Conservation And Recycling, 1998. **23**(3): p. 163-181.
136. Aguado, R., et al., *Kinetics of polystyrene pyrolysis in a conical spouted bed reactor.* Chemical Engineering Journal, 2003. **92**(1-3): p. 91-99.
137. Huffman, G.P. and N. Shah, *Can waste plastics and tires be recycled economically?* Chemtech, 1998. **28**(12): p. 34-43.
138. Kaminsky, W. and H. Rossler, *Olefins From Wastes.* Chemtech, 1992. **22**(2): p. 108-113.
139. Walendziewski, J., *Engine fuel derived from waste plastics by thermal treatment.* Fuel, 2002. **81**(4): p. 473-481.
140. Pinto, F., P. Costa, and G. Cabrita, *Pyrolysis of plastic wastes 2. Effect of catalyst on product yield.* Journal Of Analytical And Applied Pyrolysis, 1999. **51**: p. 57-71.
141. Miranda, R., et al., *Vacuum pyrolysis of commingled plastics containing PVC - I. Kinetic study.* Polymer Degradation And Stability, 2001. **72**(3): p. 469-491.

142. Heinzel, A., T.C. Keener, and S.-J. Khang, *The pyrolysis behavior of mixtures of commodity plastics with polyvinyl chloride in a thermogravimetric analyzer.* Archiwum Ochrony Srodowiska, 2001. **27**(3): p. 11-33.
143. Bockhorn, H., A. Hornung, and U. Hornung, *Mechanisms and kinetics of thermal decomposition of plastics from isothermal and dynamic measurements.* Journal Of Analytical And Applied Pyrolysis, 1999. **50**(2): p. 77-101.
144. Heikkinen, J.M., et al., *Thermogravimetry as a tool to classify waste components to be used for energy generation.* Journal Of Analytical And Applied Pyrolysis, 2004. **71**(2): p. 883-900.
145. Sharypov, V.I., et al., *Co-pyrolysis of wood biomass and synthetic polymer mixtures. Part I: influence of experimental conditions on the evolution of solids, liquids and gases.* Journal of Analytical and Applied Pyrolysis, 2002. **64**(1): p. 15.
146. Senneca, O., et al., *A thermogravimetric study of nonfossil solid fuels. 1. Inert pyrolysis.* Energy & Fuels, 2002. **16**(3): p. 653-660.
147. Serrano, D.P., et al., *Feedstock recycling of agriculture plastic film wastes by catalytic cracking.* Applied Catalysis B-Environmental, 2004. **49**(4): p. 257-265.
148. Ciliz, N., E. Ekinci, and C. Snape, *Pyrolysis of virgin and waste polypropylene and its mixtures with waste polyethylene and polystyrene.* Waste management, 2004. **24**(2): p. 173-181.
149. Wong, H.W. and L.J. Broadbel, *Tertiary resource recovery from waste polymers via pyrolysis: Neat and binary mixture reactions of polypropylene and polystyrene.* Industrial & Engineering Chemistry Research, 2001. **40**(22): p. 4716-4723.
150. Bhaskar, T., et al., *Pyrolysis studies of PP/PE/PS/PVC/HIPS-Br plastics mixed with PET and dehalogenation (Br, Cl) of the liquid products.* Journal Of Analytical And Applied Pyrolysis, 2004. **72**(1): p. 27-33.
151. Faravelli, T., et al., *Kinetic modeling of thermal degradation of polyethylene and polystyrene mixtures.* Journal Of Analytical And Applied Pyrolysis, 2003. **70**: p. 761-777.
152. Delattre, C., et al., *Improvement of the microactivity test for kinetic and deactivation studies involved in catalytic cracking.* Chemical Engineering Science, 2001. **56**(4): p. 1337.
153. Mastellone, M.L., et al., *Fluidized bed pyrolysis of a recycled polyethylene.* Polymer Degradation And Stability, 2002. **76**(3): p. 479-487.
154. Zeng, G.M., et al., *Manufacture of liquid fuel by catalytic cracking waste plastics in a fluidized bed.* Energy Sources, 2003. **25**(6): p. 577-590.
155. Murata, K., K. Sato, and Y. Sakata, *Effect of pressure on thermal degradation of polyethylene.* Journal of Analytical and Applied Pyrolysis, 2004. **71**(2): p. 569.
156. Liu, Y., J. Qian, and J. Wang, *Pyrolysis of polystyrene waste in a fluidized-bed reactor to obtain styrene monomer and gasoline fraction.* Fuel Processing Technology, 2000. **63**(1): p. 45.
157. Akpanudoh, N.S., K. Gobin, and G. Manos, *Catalytic degradation of plastic waste to liquid fuel over commercial cracking catalysts: Effect of polymer to catalyst ratio/acidity content.* Journal of Molecular Catalysis A: Chemical, 2005. **235**(1-2): p. 67.

158. Li, X.-G. and M.-R. Huang, *Thermal decomposition kinetics of thermotropic poly(oxybenzoate-co-oxynaphthoate) Vectra copolyester.* Polymer Degradation and Stability, 1999. **64**(1): p. 81.
159. Nam, J.D. and J.C. Seferis, *Generalized composite degradation kinetics for polymeric systems under isothermal and nonisothermal conditions.* Journal of Polymer Science Part B: Polymer Physics, 1992. **30**: p. 455-463.
160. Price, D.M., D.J. Hourston, and F. Dumont, *Thermogravimetry of Polymers.* Encyclopedia of Analytical Chemistry. R.A. Meyers (Ed.), 2000: p. 8094-8105.
161. Ozawa, T., *A New Method of Analyzing Thermogravimetric Data.* Bulletin of the Chemical Society of Japan, 1965. **38**: p. 1881-1886.
162. Flynn, J.H. and L.A. Wall, *A Quick and Direct Method for the Determination of Activation Energy from Thermogravimetric Data.* Polymer Letters, 1966. **4**: p. 323-328.
163. Kissinger, H.E., *Reaction Kinetics in Differential Thermal Analysis.* Journal of Analytical Chemistry, 1957. **29**: p. 1702.
164. E1641, A.t.M., *Standard Test Method for Decomposition Kinetics by Thermogravimetry, ASTM Book of Standards 14.02.* American Society for Testing and Materials, 1994: p. 1042-1046.
165. Opfermann, J. and E. Kaisersberger, *An Advantageous Variant of the Ozawa-Flynn-Wall Analysis.* Thermochim Acta, 1992. **203**: p. 167-175.
166. Kanungo, S.B., *Kinetics of solid state reactions under isothermal and non-isothermal conditions.* Journal Of The Indian Chemical Society, 2005. **82**(4): p. 315-328.
167. Mamleev, V., et al., *Three model-free methods for calculation of activation energy in TG.* Journal Of Thermal Analysis And Calorimetry, 2004. **78**(3): p. 1009-1027.
168. Simon, P., *Isoconversional methods - Fundamentals, meaning and application.* Journal Of Thermal Analysis And Calorimetry, 2004. **76**(1): p. 123-132.
169. Minying, L., et al., *Thermal degradation process and kinetics of poly(dodecamethyleneisopphthalamide).* www.chemistrymag.org/cji/2003/056043pe.htm, 2003.
170. Flynn, J.H., Journal of Research of the National Bureau of Standards, A, 1966. **70**: p. 487.
171. Flynn, J.H., Thermochim Acta, 1980. **37**: p. 225.
172. Kim, S. and J.K. Park, *Characterization of thermal reaction by peak temperature and height of DTG curves.* Thermochim Acta, 1995. **264**: p. 137-156.
173. Murray, P. and J. White, *Kinetics of thermal dehydrogenation of clays.* British Ceramic Transactions, 1955. **54**: p. 204.
174. Ozawa, T., Journal of Thermal Analysis, 1976. **2**: p. 301.
175. Kim, S., et al., *Using peak properties of a DTG curve to estimate kinetic parameters of the pyrolysis reaction: application to high density polyethylene.* Polymer Degradation and Stability, 2004. **85**: p. 799-805.
176. Freeman, E.S. and B. Caroll, Journal of Physical Chemistry, 1958. **62**: p. 394.
177. Sharp, J.H. and S.A. Wentworth, *Kinetic analysis of thermogravimetric data.* Journal of Analytical Chemistry, 1969. **41**: p. 2060.

178. Coats, A.W. and J.P. Redfern, *Kinteic parameters from thermogravimetric data.* Journal of Polymer Science. Polymer Letters Edition, 1965. **3**: p. 917.
179. Ceamanos, J., et al., *Kinetics of pyrolysis of high density polyethylene. Comparison of isothermal and dynamic experiments.* Journal Of Analytical And Applied Pyrolysis, 2002. **65**(2): p. 93-110.
180. Araujo, A.S., et al., *Kinetic evaluation of the pyrolysis of high density polyethylene over H-AlMCM-41 material*, in *Nanoporous Materials Iii*. 2002, Elsevier Science Bv: Amsterdam. p. 473-478.
181. Park, Y.K., et al., *Effect of MCM-41 preparation methods on the kinetics of catalytic pyrolysis of linear low density polyethylene.* Polymer-Korea, 2005. **29**(2): p. 122-126.
182. Kim, S.-S., C.J. Park, and S.H. Kim, *Isothermal and non-isothermal pyrolysis characteristics of polypropylene in stirred batch reactor.* Hwahak Konghak, 2001. **39**(6): p. 757-762.
183. Bockhorn, H., et al., *Modelling of isothermal and dynamic pyrolysis of plastics considering non-homogeneous temperature distribution and detailed degradation mechanism.* Journal Of Analytical And Applied Pyrolysis, 1999. **49**(1-2): p. 53-74.
184. Feng, W., E. Vynckier, and O.F. Froment, *Single-event kinetics of catalytic cracking.* Industrial & Engineering Chemistry Research, 1993. **32**: p. 2997.
185. Liguras, D.K. and D.T. Allen, *Structural models for catalytic cracking. 1. Model compound reactions.* Industrial & Engineering Chemistry Research, 1989. **28**(6): p. 665.
186. Johannes, I., H. Tamvelius, and L. Tiikma, *A step-by-step model for pyrolysis kinetics of polyethylene in an autoclave under non-linear increase of temperature.* Journal Of Analytical And Applied Pyrolysis, 2004. **72**(1): p. 113-119.
187. Kruse, T.M., H.W. Wong, and L.J. Broadbelt, *Mechanistic modeling of polymer pyrolysis: Polypropylene.* Macromolecules, 2003. **36**(25): p. 9594-9607.
188. Kruse, T.M., et al., *Mechanistic modeling of polymer degradation: A comprehensive study of polystyrene.* Macromolecules, 2002. **35**(20): p. 7830-7844.
189. Poutsma, M.L., *Reexamination of the pyrolysis of polyethylene: Data needs, free-radical mechanistic considerations, and thermochemical kinetic simulation of initial product-forming pathways.* Macromolecules, 2003. **36**(24): p. 8931-8957.
190. Mehta, K. and G. Madras, *Dynamics of molecular weight distributions for polymer scission.* AICHE Journal, 2001. **47**(11): p. 2539-2547.
191. Sterling, W.J. and B.J. McCoy, *Distribution kinetics of thermolytic macromolecular reactions.* Aiche Journal, 2001. **47**(10): p. 2289-2303.
192. Kodera, Y. and B.J. McCoy, *Distribution kinetics of plastics decomposition.* Journal Of The Japan Petroleum Institute, 2003. **46**(3): p. 155-165.
193. Kumar, G.S., V.R. Kumar, and G. Madras, *Continuous distribution kinetics for the thermal degradation of LDPE in solution.* Journal Of Applied Polymer Science, 2002. **84**(4): p. 681-690.
194. Cardona, S.C. and A. Corma, *Kinetic study of the catalytic cracking of polypropylene in a semibatch stirred reactor.* Catalysis Today, 2002. **75**(1-4): p. 239-246.

195. Kruse, T.M., et al., *Binary mixture pyrolysis of polypropylene and polystyrene: A modeling and experimental study.* Journal Of Analytical And Applied Pyrolysis, 2005. **73**(2): p. 342-354.
196. Bryson, L., *Monomer Recovery from Nylon Carpets by Reactive Extrusion*. 2003-present, Georgia Tech.
197. http://www.carpetbuyershandbook.com/pile_fibers.htm, *Carpet Pile Fibers.* 2005.
198. Wang, Y.E., *Recycling technologies for fibrous textile and carpet waste and research activities at Georgia Tech. Bolton, UK.* 1998.
199. Jin, K., *Processing Characteristics and Properties of Glass Fiber Reinforced Composites from Post Consumer Carpets*, in *School of Polymer, Textile and Fiber Engineering*. 2003, Georgia Institute of Technology: Atlanta. p. 68.
200. Van Grieken, R., et al., Microporous Mesoporous Matter, 2000. **39**: p. 135-147.
201. http://www.chem.binghamton.edu/chem445/zsm5/zsm5.htm, *Synthesis of ZSM-5: A Size/Shape-Selective Zeolite Catalyst for Xylene Isomerization.* 2005.
202. Jones, C.W., *Conversation*. 2005.
203. Eibling, R.E. and T.H. Lorier, *Thermal analysis of simulated slurry mix eveaporator samples.* sti.srs.gov/fulltext/tr2004506/tr2004506.pdf, 2004.
204. ASTM, *Standard Test Method for Decomposition Kinetics by Thermogravimetry.* ASTM E 1641 -99.
205. Instruments, S., *EXSTAR6000 System Optional Software Series TG/DTA Kinetics Software "TG/DTA Kinet" Operation Manual*. 1995.
206. Ortega, A., *The Kinetics of Solid-State Reactions Toward Consensus, Part 2: Fitting Kinetics Data in Dynamic Conventional Thermal Analysis.* International Journal of Chemical Kinetics, 2002. **34**: p. 193-208.
207. Durmus, A., et al., *Thermal-catalytic degradation kinetics of polypropylene over BEA, ZSM-5 and MOR zeolites.* Applied Catalysis B: Environmental, 2005. **61**(3-4): p. 316.
208. www.fccnetwork.com, 2002.
209. Gao, Z., et al., *A kinetic study of thermal degradation of polypropylene.* Polymer Degradation and Stability, 2003. **80**(2): p. 269.
210. McCaffrey, W.C., D.G. Cooper, and M.R. Kamal, *Tertiary recycling of polyethylene: mechanism of liquid production from polyethylene by thermolysis reactive distillation.* Polymer Degradation And Stability, 1998. **62**(3): p. 513-521.
211. Lattimer, R.P., *Pyrolysis field ionization mass spectrometry of polyolefins.* Journal of Analytical and Applied Pyrolysis, 1995. **31**: p. 203.
212. Koga, N. and J. Sestak, *Kinetic compensation effect as a mathematical consequence of the exponential rate constant.* Thermochimica Acta, 1991. **182**(2): p. 201.
213. http://www.polymerprocessing.com/operations/tscrew/. *Twin Screw Extrusion*. [cited 2005.
214. Rauwendaal, C., *Polymer extrusion*. 4th ed. 2001, Cincinati: Hanser publishers.
215. Janseen, L.P.B.M., *Reactive Extrusion Systems*. 2004, New York: Marcel Dekker, Inc.
216. Murata, K. and Y.Hirano, *Basic study on a continuous flow reactor for the thermal degradation of polymers.* Journal Of Analytical And Applied Pyrolysis, 2002. **65**(1): p. 71.

217. Serrano, D.P. and J. Aguado, *Conversion of low density polyethylene into petrochemical feedstocks using a continuous screw kiln reactor.* Journal Of Analytical And Applied Pyrolysis, 2001. **58**: p. 789-801.
218. Lin, Y.H. and M.H. Yang, *Catalytic reactions of post-consumer polymer waste over fluidised cracking catalysts for producing hyrdocarbons.* Journal of Molecular Catalysis, 2005. **231**: p. 113-122.
219. Dean, J.A., ed. *Lange's Handbook of Chemistry (15th Edition).* 1999, McGraw-Hill.
220. Martin, C. *Counter- Rotating Twin -Screw Extruders*. www.4spe.org/training/products/0392sampbk4counter.pdf [cited.
221. Janseen, L.P.B.M., *Figure 2.22*, in *Reactive Extrusion Systems*. 2004, Marcel Dekker, Inc.: New York. p. 36.
222. Beyler, C.L. and M.M. Hirschler, *Thermal Decomposition of Polymers.* **Chapter 7**.
223. Fogler, S., *Elements of Chemical Reaction Engineering 3rd Edition.* 2002.
224. http://www.engr.utk.edu/mse/pages/Textiles/Olefin%20fibers.htm, *Olefin Fiber.* 2005.
225. www.goodfellow.com, 2005.
226. Tadmor, Z., and Imrich Klein, *Engineering Principles of Plasticating Extrusion*. 1970, New York: van Nostrand Reinhold.
227. Xanthos, M., ed. *Reactive Extrusion: Principle and Practice*. Polymer Processing Institute, ed. J.A. Biesenberger. 1992, Hanser: New York.
228. White, J.L., *Twin Screw Extrusion*. 1991, New York: Hanser.
229. Turton, R., Richard C. Baile, Wallace B. Whiting, Joseph A. Shaewitz, *Analysis, Synthesis and Design of Chemical Process*. 1998, Upper Saddle River, NJ: Prentice Hall, PTR.
230. Albemarle-employee, *Conversation: Fresh FCC Catalyst Pricing*. September 2005.
231. Sichina, W.J., *DSC as Problem Solving Tool: Measurement of Percent Crystallinity of Thermoplastics.* las.perkinelmer.com/content/ ApplicationNotes/TA%20PETech-40.pdf, 2000.
232. http://www.nfm.net/technologies/devolatilization.aspx, *NFM/Welding Engineers.* 2005.
233. Schirmer, J., J.S. Kim, and E. Klemm, *Catalytic degradation of polyethylene using thermal gravimetric analysis and a cycled-spheres-reactor.* Journal Of Analytical And Applied Pyrolysis, 2001. **60**(2): p. 205-217.
234. Ukei, H., et al., *Catalytic degradation of polystyrene into styrene and a design of recyclable polystyrene with dispersed catalysts.* Catalysis Today, 2000. **62**(1): p. 67-75.
235. Takuma, K., et al., *Production of aromatic hydrocarbons by catalytic degradation of polyolefins over H-gallosilicate.* Industrial & Engineering Chemistry Research, 2001. **40**(4): p. 1076-1082.
236. Williams, P.T. and R. Bagri, *Hydrocarbon gases and oils from the recycling of polystyrene waste by catalytic pyrolysis.* International Journal Of Energy Research, 2004. **28**(1): p. 31-44.

237. Vasile, C., et al., *Thermal and catalytic decomposition of mixed plastics.* Journal of Analytical and Applied Pyrolysis, 2001. **57**(2): p. 287.